A NOVEL TECHNIQUE FOR STRUCTURAL HEALTH ASSESSMENT IN THE PRESENCE OF NONLINEARITY

by

Abdullah Abdulamir Al-Hussein

A Dissertation Submitted to the Faculty of the

DEPARTMENT OF CIVIL ENGINEERING AND ENGINEERING MECHANICS

In Partial Fulfillment of the Requirements
For the Degree of

DOCTOR OF PHILOSOPHY

In the Graduate College

THE UNIVERSITY OF ARIZONA

2 0 1 5

THE UNIVERSITY OF ARIZONA
GRADUATE COLLEGE

As members of the Dissertation Committee, we certify that we have read the dissertation prepared by Abdullah Abdulamir Al-Hussein

entitled A Novel Technique for Structural Health Assessment in the Presence of Nonlinearity

and recommend that it be accepted as fulfilling the dissertation requirement for the Degree of Doctor of Philosophy.

_____ Date: (11/12/2014)
Dr. Achintya Haldar

_____ Date: (11/12/2014)
Dr. Tribikram Kundu

_____ Date: (11/12/2014)
Dr. Chandrakant Desai

_____ Date: (11/12/2014)
Dr. Lianyang Zhang

Final approval and acceptance of this dissertation is contingent upon the candidate's submission of the final copies of the dissertation to the Graduate College.

I hereby certify that I have read this dissertation prepared under my direction and recommend that it be accepted as fulfilling the dissertation requirement.

_____ Date: (11/12/2014)
Dissertation Director: Dr. Achintya Haldar

STATEMENT BY AUTHOR

This dissertation has been submitted in partial fulfillment of requirements for an advanced degree at The University of Arizona and is deposited in the University Library to be made available to borrowers under rules of the Library.

Brief quotations from this dissertation are allowable without special permission, provided that an accurate acknowledgment of source is made. Requests for permission for extended quotation from or reproduction of this manuscript in whole or in part may be granted by the head of the Graduate College when in his or her judgment the proposed use of the material is in the interests of scholarship. In all other instances, however, permission must be obtained from the author.

SIGNED: ___Abdullah Al-Hussein___

ACKNOWLEDGEMENTS

I would like to express my deep and sincere gratitude to my advisor, Prof. Achintya Haldar, for his supervision, guidance, and advice as well as his continuous encouragement and momentum to carry out my research work successfully. His professional and energetic support has helped me in writing this dissertation, a task which I could not have achieved alone. In particular, I am grateful for enlightening me the first glance of research in the area of structural health assessment.

I am also grateful to Prof. Tribikram Kundu, Prof. Chandrakant Desai, and Dr. Lianyang Zhang for serving on my dissertation committee. Their time and recommendations are acknowledged and greatly appreciated.

I would like to acknowledge Dr. Ajoy Kumar Das, my co-researcher and friend, for his valuable help and useful discussions about my research. I really appreciate his time and constructive suggestions. I am also thankful to Dr. Giovanni Federico for helping me with ANSYS software.

I would like to express appreciation to my undergraduate teachers and my present colleagues, Dr. Mohamad Alyounis and Mr. Khalid Al-Asadi, for their help and support. I would also like to thank Dr. Alyounis for making my life easy right from my first day in Tucson.

My special gratitude goes to my close friends, Dr. Ehsan Mahmoudabadi, Dr. Umar Amjad, and Mr. Ismail Bahadir, for their support and for the good times that we shared. I also would like to extend my thanks to Dr. Richard Kaiser, Mr. Anshul Agarwal, Mr. Jose Ramon Gaxiola, and the rest of my friends for their support.

Most importantly, I would like to express my deep appreciation to my beloved parents, brothers, and sisters for all their love and support through my entire life. I also would like to thank my fiancé for her consistent moral support.

Finally, thanks to All Mighty God for giving me the ability, mindset, and perseverance to be where I am now.

DEDICATIONS

"In the Name of God, the Most Gracious, the Most Merciful"

Dedicated to
the memory of my father,
my mother,
my brothers,
and my sisters
for their love, endless support,
and encouragement

TABLE OF CONTENTS

Page

TABLE OF CONTENTS - *Continued*

Page

TABLE OF CONTENTS - *Continued*

Page

TABLE OF CONTENTS - *Continued*

Page

TABLE OF CONTENTS - *Continued*

Page

LIST OF FIGURES

Page

LIST OF FIGURES - *Continued*

Page

LIST OF FIGURES - *Continued*

Page

LIST OF TABLES

Page

LIST OF TABLES - *Continued*

Page

ABSTRACT

A novel structural health assessment (SHA) technique is proposed. It is a finite element-based time domain nonlinear system identification technique. The procedure is developed in two stages to incorporate several desirable features and increase its implementation potential. First, a weighted global iteration with an objective function is introduced in the unscented Kalman filter (UKF) procedure in order to obtain stable, convergent, and optimal solution. Furthermore, it also improves the capability of the UKF procedure to identify a large structural system using only a short duration of responses measured at a limited number of dynamic degrees of freedom (DDOFs). The combined procedure is denoted as unscented Kalman filter with weighted global iteration (UKF-WGI).

Then, UKF-WGI is integrated with iterative least-squares with unknown input (ILS-UI) in order to increase its implementation potential. The substructure concept is also incorporated in the procedure. The integrated procedure is denoted as unscented Kalman filter with unknown input and weighted global iteration (UKF-UI-WGI). The two most important features of the method are that it does not need information on input excitation and uses only limited number of noise-contaminated response information to identify structural systems. Also, the method is able to identify the defects at the local element level by tracking the changes in the stiffness of the structural elements in the finite element representation.

The UKF-UI-WGI procedure is implemented in two stages. In Stage 1, based on the location of input excitation, the substructure is selected. Using only responses at all DDOFs in the substructure, ILS-UI can identify the input excitation time-histories,

stiffness parameters of all the elements in the substructure, and two Rayleigh damping coefficients. The outcomes of the first stage are necessary to initiate UKF-WGI. Using the information from Stage 1, the stiffness parameters of all the elements in the structure are identified using UKF-WGI in Stage 2.

To demonstrate the effectiveness of the procedure, health assessment of relatively large structural systems is presented. Small and relatively large defects are introduced at different locations in the structure and the capability of the method to detect the health of the structure is examined. The optimum number and location of measured responses are also investigated. It is demonstrated that the method is capable of identifying defect-free and defective states of the structures using minimum information. Furthermore, it can locate defect spot within a defective element accurately.

The comparative studies are also conducted between the proposed methods and available methods in the literature. First, it is between the UKF-WGI and extended Kalman filter with weighted global iteration (EKF-WGI) procedure. Then, it is between UKF-UI-WGI and generalized iterative least-squares extended Kalman filter with unknown input (GILS-EKF-UI) procedure, developed earlier by the research team. It is demonstrated that the proposed UKF-based procedures are superior to the EKF-based procedures for SHA.

CHAPTER 1

INTRODUCTION

1.1 Statement of the Problem

Civil infrastructure systems play important role in economic vitality of a community. They are designed to have long life spans. Unfortunately, they deteriorate with time and continuously accumulate damage throughout their service life due to the natural aging process, overloading, and/or lack of adequate maintenance. They may also experience sudden damage due to natural hazards such as earthquakes, storms, etc., or manmade events such as blasts, explosions, etc. If damage is left undetected and unmitigated, it could potentially cause more damage and eventually lead to catastrophic structural failure with loss of human life and severe economic consequences. Even if there is no loss of life, communities suffer if the structure is partially or completely out of service even for a limited period. In order to ensure the serviceability and safety of structures, structural damage detection is necessary at the earliest possible stage.

Many civil infrastructure systems all over the world are in service for an extended period of time and some of their operating periods have exceeded their design lives. Most of them were built conforming to old design standards; they are not expected to satisfy up-to-date design guidelines and other safety requirements. Based on the American Society of Civil Engineers ASCE's 2013 Report Card for America's Infrastructure, the nation's infrastructure received an overall grade of D+ and estimated investment needed to bring them up to the current standard would be $3.6 trillion by 2020. And based on statistics of 2013 by the U.S. Department of Transportation Federal Highway Administration (U.S.D.O.T. FHWA), more than 30% of existing bridges have exceeded

their 50-year design life. In Canada, more than 40% of the bridges currently in use were built over 50 years ago (Bisby and Briglio, 2004) and a significant number of these structures need strengthening, rehabilitation, or replacement. The large amount of the cost to rehabilitate the infrastructures underlines the importance of developing reliable and cost effective methods in the near future.

The deterioration process of a structure is expected to be different depending on the environment where it is located or the functionality for which it was built. The challenge is how to assess the rate of deterioration; how to locate defect spots and severity in a structure; decide whether the structure will remain safe during its expected design life; and who will decide if the structure is safe or unsafe, influencing economic activities of the region.

1.2 Damage in Structure

The definition of damage is difficult to conceptualize in a general and widely accepted manner. In general, damage can be defined as changes within a structural system which adversely affect its current and future performance (Farrar et al., 2001). Accordingly, structural damage is usually associated with changes to geometric and material properties of the structure, such as the occurrence of cracks in structural components, gradual deterioration of Young's modulus of the structural materials and the yielding of some structural components.

There are different types of damage simulation considered in this study. By reviewing the numerical or experimental studies in damage detection or assessment, the simulations of structural damage are classified into the following categories (Vo, 2003; Martinez-Flores, 2005; Bandara, 2013);

a) Reduction of thickness or cross section of the element;

b) Reduction of Young's modulus of the element; and

c) Loss of stiffness of the structural element.

1.3 Structural Health Assessment Methods

The primary purposes of structural health monitoring and assessment are to ensure longevity and safety of the structures and to optimize the maintenance cost. The damage detection methods can be classified into four levels, as follows (Rytter, 1993):

Level 1: Detection of damage

Level 2: Location of damage

Level 3: Evaluation of the severity of damage

Level 4: Determination of the remaining service life of the structure due to damage

The damage detection methods increase in robustness as the level of damage evaluation increases. In this way, level 1 methods consider only the determination whether the structure presents damage or not. Level 2 methods consider whether the structure is damaged and its location. In level 3 methods, the detected and located damage must be quantified in extension and severity, and finally, in level 4, the remaining service life of the structure needs to be determined considering the quantified damage. It is related to the fields of fracture mechanics, fatigue life analysis, or structural design assessment.

The most widely used method for detecting structural damage is visual inspection. As the name implies, visual inspection requires personnel to physically observe damage and document its location and severity. However, this method can locate the damage only if it is so severe that its effects can be easily seen. Another drawback of visual inspection

is that often nonstructural elements must be removed or destroyed in order to uncover potentially damaged areas. For example, severe damages (fractures) at joints of steel structures after the 1994 Northridge earthquake were not found until removing fire-protection coatings on beam-column joints.

Alternative methods are local nondestructive evaluation (NDE), often used as a secondary step once suspected areas of damage have been identified. Some examples of these methods are acoustic emissions or ultrasonic methods, magnetic field methods, and radiography. The local NDE methods have been proven inefficient for a large structural system, as they require the vicinity of damage to be known a *priori* and the portion of structures inspected to be readily accessible. Furthermore, execution of these methods in such situations is expensive, time consuming, and labor intensive. The most significant challenge for any local NDE technologies is the difficulty in directly relating the test results to the health condition of the whole structural system.

The need for cost-effective damage detection methods suitable for a large structural system has led to development of several structural health assessment techniques. Among various damage detection methods, the system identification (SI)-based methods are the most widely studied.

1.4 System Identification Concept

System identification (SI) is based on determining the underlying physical system from a given set of input/output relationships. The concept of SI is not new. It started evolving in structural engineering in the early 1970s. A considerable amount of work has been reported in the last decades. Doebling et. al (1996) and Kerschen et. al (2006) summarized the state-of-the-art in the related areas that used the concept of SI.

A typical SI technique has three components: input, system to be identified, and output, as shown in Figure 1.1. For structural system applications, the input is a loading that excites the system. The system is a mathematical model of the structure. It can be represented by a series of equations or represented in algorithmic form, e.g., in a finite element representation in terms of mass, stiffness, and damping properties of each element. The output is the response of a structural system due to the input excitation, reflecting the current state of the structure. Knowing the input excitation and the output response information, the third component (i.e., the system) can be identified.

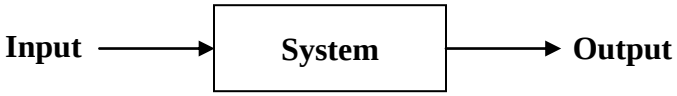

Figure 1.1 Concept of system identification

1.5 Structural Health Assessment Based on SI

Various structural health assessment (SHA) using SI techniques are currently available. Among them, methods based on vibration-based SHA have received great attention due to advancements in computing power, sensor, and data acquisition hardware. The basic premise of vibration-based SHA methods is that structural damage will alter the structural stiffness, mass, and/or energy dissipation, which in turn change the dynamic behaviors of structures. Thus, by tracking these changes, SHA methods can detect the occurrence of structural damages, and even locate and quantify them.

In general, the vibration-based SHA can be classified into two categories: frequency and time domain. Since frequency domain modal properties represent global properties, it

may not be efficient to locate defects at the local element level. This leads to the conclusion that a time domain approach will be more appropriate.

In time domain approach, using information on the excitation and responses, the dynamic properties of each element in the structure in terms of mass, stiffness, and damping can be identified. In most studies, the masses of all structural members are considered to be known. Since the changes in damping of defective structure as compared to defect-free structure are not completely understood or correlated at present, the identified damping parameters cannot be effectively utilized for the defect identification purpose. In most cases, the stiffness parameters of elements in the finite element representation are used to identify a structural system. By comparing the identified stiffness properties with the expected values; reference values obtained from the design drawings; changes from the previous values if inspections are carried out periodically; or variations from one member to another with similar sectional properties, the location(s), number, and severity of defects can be established. The same procedure can also be applied to evaluate rehabilitated structures indicating the effectiveness of the rehabilitation and whether all the defects are properly identified and repaired or not.

1.6 Challenges in SHA

One of the major challenges in SHA using SI concept is the collection of input excitation information (Wang and Haldar, 1994; Lourens et. al., 2012). Outside the highly controlled laboratory environment, input excitations may come from different sources. Their types and magnitude are usually unknown. The information on input excitation may contain so much error that it compromises the fundamental concept of SI. The desirability of SI will be significantly improved if the system can be identified using

only output response information. The problem is mathematically more challenging since two of three components of a SI approach are unknown.

Furthermore, measured response information is expected to contain noise even when it is recorded by smart sensors. For large complicated structural systems, it may not be possible or economical to instrument sensors at all dynamic degrees of freedom (DDOFs). The response information may be available only at a small part of the structure where sensors are placed.

The structural model used should accurately represent a real structure. Some of SHA approaches applied only to shear buildings, the simplest structural model. The simplified models may not exactly describe the realistic behavior of the actual structure.

Most structural system behaves nonlinearly; therefore, an ideal SHA should be based on the nonlinear SI concept. Also if the structural system is assumed to be a linear, the system identification procedure is nonlinear. In other words, the state vector of the system, which needs to be identified, includes system parameters and nonlinear dynamic responses and this makes the structural system identification nonlinear. However, nonlinear SI is not easy. The research team at the University of Arizona has developed several procedures based on extended Kalman filter for nonlinear system identification; however, these procedures can be used to identify the structure in the presence of mild nonlinearity. The nonlinearity in the structural behavior is expected to be high if the structure has severe defects. Since the level of nonlinearity is expected to be unknown at the initiation of the inspection, it is necessary to develop a SHA procedure capable of identifying a system in the presence of high nonlinearity.

To the best of the author's knowledge, there is not an all-in-one solution to all the challenges mentioned above. Many researchers have proposed some new techniques, trying to solve one or several above problems and increase the implementation potential of SHA methods.

1.7 Objectives of the Research

The primary goal of the proposed research is to develop a robust yet simple and economical nondestructive health assessment procedure for large real structural systems at the local element level. The primary objective is met with the help of the following five objectives:

Objective 1: Develop a novel finite element-based time domain nonlinear-SI procedure for large real structural systems using responses at a minimum number of DDOFs, denoted as unscented Kalman filter with weighted global iteration (UKF-WGI).

Objective 2: Develop a novel finite element-based time domain nonlinear-SI procedure for large real structural systems using responses at a minimum number of DDOFs and without using information on input excitation, denoted as unscented Kalman filter with unknown input and weighted global iteration (UKF-UI-WGI).

Objective 3: Verify the proposed procedures to identify defects in large real structural systems at the local element level and also defect spots within a defective element.

Objective 4: Investigate how the uncertain factors required to implement the procedures will influence the accuracy of the identification process.

Objective 5: Compare the capability of the proposed procedures for structural health assessment with the available procedures in the literature.

1.8 Scope of the Research

The primary focus of this research is to develop and verify the novel approach described in the objectives. First, a weighted global iteration procedure with an objective function is incorporated with the unscented Kalman filter (UKF) algorithm in order to obtain stable, convergent, and optimal solution to the identification process. Then, iterative least-squares with unknown input (ILS-UI) is integrated with the UKF procedure in order to identify the structure without using input excitation. The integrated procedure is verified analytically. Numerical simulation of the structures are developed in the commercial software ANSYS (ver. 15) to collect noise-free time-history of dynamic response. Both types of structural behavior (linear and nonlinear) are considered. The structure is excited by different types of loadings such as sinusoidal, blast, and seismic loading. After the responses are generated, the information on the input excitation(s) is completely ignored. Noise-free responses are then contaminated with various levels of noises. The defects are modeled by reducing cross-sectional properties of the member. The integrated procedure to identify the structural system is developed in FORTRAN computer language.

1.9 Significance of the Research

This research is significant as its outcomes contribute towards the safe and efficient performance of realistic civil structures and result in reducing loss of lives and property when subjected to long term deterioration under service load or extreme events such as earthquake and impact loads. This research has a direct impact on developing an efficient damage identification and condition assessment strategy for civil structures, using

unscented Kalman filter. The outcome of the present study contributes towards the safety of structures and prevents unexpected structural failures.

1.10 Layout of the Thesis

This dissertation comprises seven chapters, and is organized as follows.

Chapter 1 introduces the background of health assessment of civil structural systems, the issues to be addressed and the objectives, scope, significance, and layout of this dissertation.

Chapter 2 contains a literature review on the available SHA approaches with emphasis on the research work of vibration-based SHA. The positive and negative aspects of the available approaches are identified. Finally, a summary of the literature review findings related to the selection of damage detection methodologies and their limitations are presented.

Chapter 3 develops the mathematical concept of the proposed procedure (UKF-WGI) to identify large structural systems using responses at a minimum number of DDOFs.

Chapter 4 verifies UKF-WGI for health assessment of large real structures exhibiting linear and nonlinear behavior using a limited number of noise free and noise-contaminated responses.

Chapter 5 develops the mathematical concept of the proposed procedure (UKF-UI-WGI) to identify large structural systems using responses at a minimum number of DDOFs and without using information on input excitation.

Chapter 6 verifies UKF-UI-WGI for health assessment of large real structures in presence of different defect scenarios. The structures are excited by different types of

excitation. The parametric study of uncertain variables required to implement the procedure is presented. The optimum number and location of measured responses for SHA are also studied.

Chapter 7 summarizes the contributions, findings, and conclusions achieved from the research in this dissertation. Recommendations for future work are also presented.

CHAPTER 2

LITERATURE REVIEW

2.1 Introduction

Structural health assessment (SHA) and damage detection have been hot research topics for several decades; hundreds of approaches have been proposed using various hardware and algorithms. This chapter reviews the most significant works on the topic of SHA. Only important works related to the current study are emphasized; extensive reviews can be found in Doebling et al. (1996, 1998), Salawu (1997), Chang et al. (2003), Carden and Fanning (2004), Sohn et al. (2004), Kerschen et al. (2006), Montalvo et al. (2006), Fan and Qiao (2011), Farrar and Worden (2011), Haldar and Das (2012a, b), and Haldar et al. (2013). In this study, the merits and demerits of the major works have been identified. The discussions will identify the major additional challenges in developing the framework for the present research.

2.2 Non-Model-Based SHA Methods

Visual inspection is the oldest and most commonly used inspection method in civil engineering, and it will probably never be abandoned. However, a visual inspection can only reveal defects at or close to accessible surfaces. This indicates that the method has to be supplemented with other inspection methods.

Early evolutions in instruments helped in developing several nondestructive evaluation (NDE) techniques, including acoustic emission, ultrasonic wave, radiography imagining, eddy current detection, and many other methods (Chang et al., 2003).

NDE methods typically require carrying out some experiment near the damage location to test the physical properties of the structural materials in order to detect the presence and severity of damage inside the structure. For example, ultrasonic methods will generate incident ultrasonic sound waves on the surface of a structural component and will measure the reflective waves. If there are cracks inside the structure, additional reflective waves will be produced and captured by sensors. Therefore, analysis of reflective waves allows detection of hidden structural damage.

Successful implementation of the NDE methods usually requires prior knowledge of the defect location and at the same time, ready access for physical inspection. Defect hidden behind obstructions is generally not detectable using these methods. Subject to such limitations, these local methods can detect damage on or near the surface of the structure. In addition, such methods are generally costly, time consuming, and ineffective when applied to large and complex structural systems.

2.3 Model-Based SHA Methods

The basic idea of model-based SHA methods is determining the underlying physical system from a given set of input/output relationships. They use the system identification concept. For non-model SHA methods, the physical system can be viewed as a “black box”; thus, no inherent knowledge of the structure of the system is required.

The fundamental axiom of model-based SHA methods is that global level structural responses are altered by defects presented at the local level, i.e., in structural members. Thus, tracking the signature embedded in the measured responses, the information on the locations of defects and their severity can be obtained. According to the type of

measurement data used, damage detection methods can also be classified as either static-based SHA methods or vibration-based SHA methods.

2.4 Static-Based SHA Methods

Static-based methods for damage detection are based on the premise that changes in the stiffness of a structure will give rise to changes in displacements or strains of the structure. Monitoring and measuring these changes under designated loading cases allow the evaluation of changes in structural stiffness. Since the static equilibrium equation is solely related to structural stiffness, and accurate static displacement and strain data can be obtained rapidly, the static damage identification methods have received considerable interest by the researchers. Problems of damage detection using displacements could be found in (Sanayei and Onipede, 1991; Banan et al., 1994a, b; Hjelmstad and Shin, 1997; Yeo et al., 2000; Nasrellah, 2009) and using strains could be found in (Sanayei and Saletnik, 1996a, b; Liu and Chian, 1997; Mehrabi et al., 1998; Nasrellah, 2009).

Static-based SHA methods have several advantages, including that the amount of data needed to be stored is relatively small and simple, and no assumption on the mass or damping characteristics is required. Thus, fewer errors and uncertainties are introduced into the model. However, several challenges remain which prevent the widespread use of static-based methods including the means of measuring static response data. Deflection measurements can be obtained easily on scale models by means of displacement dial gauges. However, the same measurement devices cannot be used on full scale structures. The static strain measurements are often easier to obtain and less susceptible to noise. Strain gauges can be mounted at several points on a structure to monitor the structural response. The main drawback with strain data is the large cost due to the high level of

technical knowledge required when mounting each device. Faulty installation during construction can render a device or group of devices inoperable, and repair or replacement can be costly.

Another challenge facing static-based SHA is the issue of measurement errors. As evidenced by the previous research results, measurement noise can significantly affect the accuracy of static-based methods (Aditya and Chakraborty, 2008; Anh, 2009). The number of measurement points required to identify the structure should be larger than the number of unknown parameters (Haldar and Al-Hussein, 2014). Civil engineering structures are generally large and complex with extremely high overall stiffness; therefore, it may require extremely large static load to obtain measurable deflections.

2.5 Vibration-Based SHA Methods

Vibration-based SHA methods have been receiving increased attention in recent years due to their significant advantages such as; it is possible to excite a structure with a small amplitude dynamic load relative to the required magnitude of the static load. In some circumstances, natural sources such as wind and earthquakes and human-made sources such as moving vehicles can be used. The use of acceleration responses eliminates the need for a fixed physical reference such as that required by the measurement of deflection. Vibration-based methods can accommodate higher levels of measurement error compared to static-based methods.

The available vibration-based methods can be broadly divided into two categories; frequency domain SHA and time domain SHA.

2.5.1 Frequency Domain SHA

Frequency domain methods are the most widely used in many disciplines. These methods typically use structural modal parameters, such as natural frequency, damping, and mode shape, to detect the damage in the structure.

The underlying premise of damage detection methods in the frequency domain is that modal parameters of a structure are functions of its physical parameters (mass, damping, and stiffness). As a result, changes in these physical parameters, such as reduction in stiffness resulting from the onset of cracks or loosening of a connection, will cause changes in vibration characteristics of the structure such as modal properties. Therefore, measuring and monitoring these changes allows the evaluation of occurrence, localization, and severity of structural damage.

The frequency domain methods can be classified as forward and inverse methods. For the forward methods, the patterns of measured structural modal parameters changes are compared with those of analytical structural modal parameters changes for all possible damage cases. Then the damage case which produces the best match to the measured structural modal parameters changes is regarded as the suspect one. These types of methods take the advantage that some patterns of measured structural modal parameters changes are a function of damage location only. The inverse methods typically use the structural modal parameters as the prediction model; by solving some inverse problems, the parameters of the physical structural model (like stiffness) are estimated. Hence, inverse methods can provide information about the presence of the damage.

2.5.1.1 Methods Based on Natural Frequency Shifts

The most common and earliest approaches for vibration-based damage detection have implemented either the natural or the resonant frequencies of the structure to evaluate the existence of damage. The tangible relation between the changes of structural stiffness and the changes of structural natural frequency makes it a natural choice to use the estimated structural frequencies to identify damage. Salawu (1997) presented an extensive review on identifying structural damage using natural frequencies.

An early study that treated damage detection as a forward problem was presented by Cawley and Adams (1979). They demonstrated that the ratio of the frequency changes in two modes is only a function of damage location. A collection of possible damage points was considered, and an error term was constructed that related the measured frequency shifts to predicted local stiffness reductions. A number of mode pairs were considered for each potential damage location, and the pair that gave the lowest error indicated the location of the damage. Penny et al. (1993) and Friswell et al. (1994) attempted to improve this method by using a least-squares fitting technique.

The forward methods require the computation of modal frequency changes for all possible damage cases. Therefore, they are impractical for detection of damage in large structures. They become more complicated if multiple-damage cases existing in the structure.

Lifshitz and Rotem (1969) were among the first to propose damage detection via modal frequency as an inverse problem. They looked at the change in the dynamic modulus, which can be related to shifts in natural frequencies, to detect damage in particle-filled elastomers. Stubbs and Osegueda (1990 a, b) developed a damage

detection method using the sensitivity of modal frequency changes, which relates changes in modal frequencies to changes in member stiffness. This method is essentially a sensitivity-based finite element model updating technique, and its accuracy, as most damage detection methods based on model updating, depends on the quality of the finite element model used to compute the modal sensitivities.

Further examples of inverse methods for examining changes in modal frequencies for indications of damage have been presented by Adams, et al. (1978), Wang and Zhang (1987), Stubbs, et al. (1990), Hearn and Testa (1991), Richardson and Mannan (1992), Sanders, et al. (1992), Narkis (1994), Brincker, et al. (1995), Balis Crema, et al. (1995), and Skjaerbaek, et al. (1996).

Frequency-based damage detection approaches have many desirable features. They are easy to implement and relatively inexpensive because modal frequency can be measured using very few sensors. However, the disadvantages seem to overwhelm their merits. Modal frequency is a global parameter and is insensitive to local damage. The damage that creates low frequency requires precise measurements (Doebling et al., 1998). Significant damage may cause very small changes in natural frequencies particularly for larger structures; these small changes may be undetected due to measurement errors. For example, tests conducted on the I-40 Bridge over the Rio Grande in Albuquerque, New Mexico (Farrar et al., 1994) also demonstrated this point. When the cross-sectional stiffness at the centre of a main plate girder had been reduced by 96%, reducing the bending stiffness of the overall bridge cross section by 21%, no significant reductions in the modal frequencies were observed.

Furthermore, frequency-based methods cannot distinguish damage at symmetrical locations in a symmetric structure. Another drawback is that natural frequencies are easily affected by environmental changes such as temperature or humidity fluctuations. Therefore, the natural frequencies alone are not sufficient to predict the damage (Maeck and De Roeck, 2002).

2.5.1.2 Methods Based on Damping

The damping properties have not been used as extensively as natural frequencies and mode shapes for damage diagnosis. Crack detection in a structure based on damping, however, has the advantage over detection schemes based on frequencies and mode shapes in that damping changes have the ability to detect the nonlinear, dissipative effects that cracks produce.

Adams et al. (1975) found that, with fiber-reinforced plastics, a state of damage could be detected by a reduction in the stiffness and an increase in damping, whether this damage was localized, as in a crack, or distributed through the bulk of the specimen as in the case of many micro cracks.

Modena et al. (1999) showed that visually undetectable cracks cause very little change in resonant frequencies and require higher mode shapes to be detected, while these same cracks cause larger changes in the damping. In some cases, damping changes on the order of 50% are observed. Their study focuses on identifying manufacturing defects or structural damage in precast reinforced concrete elements.

Panteliou et al. (2001) showed analytically and experimentally that the damping factor increases with increasing the crack depth. They found that the identification of

crack by using change in damping factor has the advantage that it is relatively insensitive to boundary conditions in comparison to the shifts in natural frequencies.

Yamaguchi et al. (2013) studied damage detection in steel and concrete bridges based on the identification of changes in their modal damping. They demonstrated that the energy-based damping analysis can be a powerful tool for the damage detection of bridges in the vibration-based SHM. They also noticed that the modal damping is very sensitive indictor against corrosion-induced damage in the reinforced concrete beams. Even at very small damage level without any visible crack, it was possible to detect this damage with damping identification, indicating that the local corrosion level might be detectable by measuring the modal damping ratio of reinforced concrete structure.

2.5.1.3 Methods Based on Change of Mode Shapes

(a) Direct change in mode shape

Since the structural modal shapes are more sensitive to the damage than the natural frequency and damping ratios, researchers turned to use the mode shape to detect the damage.

Two most commonly used methods to compare two sets of measured mode shapes are the modal assurance criterion (MAC) (Allemeng et al., 1982) and the coordinate modal assurance criterion (COMAC) (Lieven et al., 1988) where one set of data is measured from the intact structure and the other is measured after the structure is damaged. MAC indicates the correlation between two sets of mode shapes and COMAC indicates the correlation between the mode shapes at a selected measurement point on the structure.

West (1984) first demonstrated the possibility of using mode shape information for locating structural damage. The modal assurance criterion (MAC) was used to determine the correlation of the modes before and after damage. The mode shape was partitioned using various schemes and the change in the MAC across the different partitioning techniques was used to localize the structural damage.

Srinivasan and Kot (1992) found that changes in mode shapes were a more sensitive indicator of damage than changes in resonant frequencies for a shell structure. These changes were quantified using changes in the MAC values comparing the damaged and undamaged mode shapes.

Salawu and Williams (1995) conducted modal tests of a full-scale bridge before and after rehabilitation. They concluded that natural frequencies of the bridge did not change significantly as a result of structural repairs, and both MAC and COMAC were able to give good indications of the presence and location of the repairs. It was also concluded that the performance of MAC and COMAC depends on the modes and measurement locations used for damage localization.

In the literatures, there are many other assurance criteria proposed to assess the consistence of modal shapes and other structural dynamic properties like frequency response function as well. These methods include partial modal assurance criterion (Heylen and Janter, 1990), modal assurance criterion using reciprocal modal vectors (Wei et al., 1990), coordinate orthogonality check (Avitabile and Pechinsky, 1994), the frequency response assurance criterion (Heylen and Lammens, 1996), scaled modal assurance criterion (Brechlin et al., 1998), coordinate modal error function (Catbas et al., 1998), and frequency scaled modal assurance criterion (Fotsch and Ewins, 2001).

(b) Change in mode shape curvature

An alternative to using mode shapes to obtain spatial information regarding the damage location is to utilize the mode shape derivatives, such as mode shape curvature. Derivatives of mode shapes are sensitive to small damages, so they can be used to detect damage. The curvature mode shapes are derived from the measured displacement mode shapes using a central difference approximation.

Pandey et al. (1991) presented a method to detect damage in a beam structure by using absolute changes in mode shape curvatures. The curvature values were computed from the displacement mode shape using a central difference approximation. They demonstrated that absolute changes in mode shape curvature can be a good indicator of damage for beam structures. They also found that the modal curvature was a far more sensitive damage indicator than the MAC or COMAC values.

Abdul Wahab and De Roeck (1999) successfully applied a modal curvature based method to the Z24 Bridge in Switzerland. They introduced a damage indicator which is determined by the difference in curvature before and after damage averaged over a number of modes. Also if the structure contained several damages, the method gave a clear identification of these locations. They concluded that the use of modal curvature to locate damage in civil engineering structures seems promising.

Dutta and Talukdar (2004) investigated the change in mode shape curvature in more detail to detect and localize multiple damages in simply supported and continuous bridge structures. They noticed the higher peaks in modal curvature changes at damage location along the beam, both in longitudinal and transverse directions. They also showed that the

modal curvatures of the lower modes are in general more accurate than those of the higher modes.

Despite the advantage of using the mode shapes and their derivatives to identify the damage, they suffer from several limitations in application (Hua, 2006): 1) dense array of measurement points is required for an accurate configuration of mode shapes and curvature mode shapes; 2) the mode shape has larger statistical variation than does modal frequency; 3) the mode shape based methods, especially the curvature mode shape based methods, are not readily applicable for structures with complex configuration; and 4) it is required to select a mode shape, yet it is a *priori* unknown which mode suffers from significant change due to particular structural damage.

(c) Change of modal strain energy (damage index method)

When a particular vibration mode stores a large amount of strain energy in some structural members, the frequency and shape of that mode are highly sensitive to the changes in those structural members. Some studies indicated that modal strain energy is useful in localizing structural damage.

Stubbs et al. (1992) was the first introduced the concept of modal strain energy-based damage detection. They developed a method based on the decrease in modal strain energy caused by damage in a region located between two structural degrees of freedom, as derived from the curvature of the measured mode shapes. This method is referred to in the literature as the damage index method.

Kim and Stubbs (1995) applied the method to a model plate girder. It was observed that damage can be confidently located with a relatively small localization error and a relatively small false-negative (i.e., missing detection of true damage locations) error but

a relatively large false-positive (i.e., prediction of locations that are not damaged) error. It is also observed that severity of damage can be estimated with a relatively large error.

Li et al. (2006) introduced a modal strain energy decomposition method for damage location identification of three-dimensional (3D) frame structures. This method was based on decomposing the modal strain energy of each structural member (or element). Axial damage indicator and transverse damage indicator were calculated for each member to perform the identification of damage location analysis. The method required only a small number of mode shapes of damaged and baseline structures. A 3D five-story frame structure was studied numerically. The results showed that the axial damage indicator was able to locate damage occurring in horizontal elements, and that the transverse damage indicator was able to locate damage occurring in vertical elements. However, false positive error was generated and damage severity was not identified well.

Wang et al. (2010) presented an improved modal strain energy correlation method (MSEC) where the prediction of modal strain energy change vector was differently obtained by running the eigen-solutions on-line in optimization iterations. A genetic algorithm was used to operate the iterative searching process. The results demonstrate that the improved MSEC method sufficed to meet the demand in detecting the damage of truss bridge structures, even when noisy measurement is considered.

2.5.1.4 Methods Based on Dynamically Measured Flexibility Matrix

Another class of damage identification methods uses the dynamically measured flexibility matrix. The modal flexibility matrix includes the influence of both the mode shapes and the natural frequencies. It is defined as the accumulation of the contributions from all available mode shapes and corresponding natural frequencies (Huth et al., 2005).

Berman and Flannelly (1971) showed that higher modes contribute more to stiffness matrix than lower modes based on the governing equation of structural dynamics. Therefore, to obtain a good estimate of stiffness matrix or its change as required for damage localization, one needs to measure all the modes of a structure, especially the higher modes. Due to practical limitations, it is extremely difficult to measure higher frequency response data, and this presents a severe constraint to the accuracy of stiffness difference methods. Therefore, to avoid this difficulty, dynamically measured flexibility matrix was used to estimate the change in structural stiffness.

Pandey and Biswas (1994, 1995) presented a method based on changes in the measured flexibility of the structure to detect and localize the damage. This method was applied to several numerical examples and to an actual spliced beam where the damage was linear in nature. Results of the numerical and experimental examples showed that estimates of the damage condition and the location of the damage could be obtained from just the first two measured modes of the structure.

Zhao and Dewolf (1999) presented a theoretical sensitivity study comparing the use of natural frequencies, mode shapes, and modal flexibility for damage detection. The differences in sensitivities were evaluated for a spring-mass system. The results demonstrate that modal flexibility is more likely to indicate damage than the other two.

Salehi et al. (2011) presented a method to localize the structural damage based on dynamically measured flexibility matrix. The method was successfully implemented on uniform beam structures. The method was verified via numerical as well as experimental case studies. They showed that the results in both cases are satisfactory and could be used for damage detection of real life structures. The main advantage of the method was that it

did not require theoretical model or baseline information about the intact state of the structure.

2.5.1.5 Methods Based on Model Updating

Another class of damage identification techniques is based on the modification of structural model matrices such as mass, stiffness, and damping to reproduce as closely as possible the measured static or dynamic response. These methods solve for the updated matrices by forming a constrained optimization problem based on the structural equations of motion, the nominal model, and the measured data. Comparisons of the updated matrices to the original correlated matrices provide an indication of damage and can be used to quantify the location and extent of damage.

Liu (1995) presented an optimal updating technique for computing the elemental stiffness and mass parameters for a truss structure from measured modal frequencies and mode shapes. The method minimized the norm of the modal force error. The author demonstrated that if sufficient modal data were available, the elemental properties could be directly computed using the measured modal frequencies, measured mode shapes, and two matrices which represented the elemental orientations in space and the global connectivity of the truss. The method was able to locate a damaged member using the first four measured modes in sets of three at a time.

Hu et al. (2001) developed two identification algorithms for assessing structural damages using the modal test data which were not strongly dependent on analytical models. For the first algorithm, they used a special perturbation technique which led to approximate estimation of the damage state and avoided the analytical evaluation of the global stiffness and mass matrices. In the second method, only the information on

analytically derived mass matrix was used to predict the extent of damage. These approaches first locate the damages using a special subspace rotation algorithm, and then identify the magnitude of damage using the quadratic programming technique. A ten-bay planar truss and two fixed ended beams were used to verify these algorithms. They modeled the damage states by reducing the modulus of elasticity by 10% and 50%.

Teughels and De Roeck (2005) successfully applied the finite element model updating method to assess damage in a number of structures. The method was applied in two steps. In the first, the initial finite element model was tuned to the undamaged state to obtain a reference model, which was used afterwards in the second step, when the reference model was updated to the damaged state. The method was illustrated on prestressed and reinforced concrete beams, tested in laboratory, and on a prestressed concrete bridge. In all examples, the damage could be clearly identified.

The frequency domain methods have several advantages. They are relatively simple approaches and the modal information can be expressed in countable forms in terms of frequencies and mode shape vectors instead of using enormous amount of response data. The changes in the modal information can be used to detect defects in structures. In this approach, the effect of noise in the responses is reduced due to an averaging effect. Despite these advantages, there are many disadvantages or deficiencies in these methods. Commonly used methods for damage detection, such as structural natural frequency, mode shape and so forth, are not very sensitive to local structural damage (Farrar et al., 1994; Haldar et al., 1998; Katkhuda, 2004; Zhang, 2010). As a result, small or moderate structural damage are very difficult, if at all possible, to detect. In addition, other factors (like environmental temperature) may often lead to larger changes in the structural

frequency and mode shape than those caused by the damage, making the damage detection even more difficult. The modal parameters are not reliable if only the first few modes are measured (Raghavendrachar and Aktan, 1992). The information on higher modes is required. However, the higher order modes are very difficult to identify and they are considered extremely unreliable for large complicated structural systems (Oh and Jung, 1998). The minimum number of modes required to identify defects is not yet addressed in the literature (Ko et al., 1994; Salawu and Williams, 1994; Beck and Yuen, 2004).

2.5.2 Time Domain SHA

Time domain SHA here refer to the methods that directly make use of the response time-histories to detect structural damage. These methods typically first select a mathematical model to represent the structure; then, the parameters of the model are identified by minimizing the difference between the measured structural responses and that predicted by the model. Although the time domain approach is better to locate and quantify defects at the local level, it is not widely used. Recent advances in the technology of the sensors, computers, and data acquisition systems are expected to make this approach more desirable than the modal approaches in the near future.

In the past decades, a number of time domain techniques have been developed in civil engineering for structural system identification, including auto regressive moving average method (Shinozuka et al., 1982; Pandit and Wu, 1993), least-squares estimation (Smyth et al., 1999; Chen and Li, 2004; Yang and Lin, 2005; Xu et al., 2012), H_∞ filter (Sato and Qi, 1998, 1999), sequential Monte Carlo methods (Yoshida and Sato, 2002; Chen et al., 2005; Nasrellah and Manohar, 2011; Chatzi and Smyth, 2013), extended

Kalman filter (Yun and Shinozuka, 1980; Hoshiya and Saito, 1984; Loh and Tsaur, 1988; Yang et al., 2006), ensemble Kalman filter (Ghanem and Ferro, 2006; Khalil et al., 2007), unscented Kalman filter (Mariani and Ghisi, 2007; Wu and Smyth, 2007; Chatzi and Smyth, 2009; Chatzi et al., 2010) and genetic algorithms (Udwadia and Proskurowski, 1998; Koh et al., 1999, 2000, 2003; Perry et al., 2006)

Further reviews on available time domain methods were presented by Wang (1995), Katkhuda (2004) and Martinez-Flores (2005). The following section will focus on the time domain methods related to the proposal research.

2.5.2.1 Least-Squares Based Methods

The least-squares based methods are one of the most widely used in structural SI. In this approach, the unknown parameters of structural systems are estimated by minimizing the sum of squared errors between the predicted and the measured outputs. Caravani et al. (1977) were among the first to carry out SI study by means of a recursive least-squares algorithm. He used it to directly identify the stiffness and damping parameters of shear-type structures. Torkamani and Ahmadi (1988a, b, c) estimated the stiffness using known frequencies and mode shapes identified in frequency domain. Here, the mode shapes and frequencies were expanded as functions of stiffness in a Taylor series. The least-squares, weighted least-squares and statistical SI techniques were used to identify the stiffness parameters of shear-type structures. A large number of extracted mode shapes and frequencies produces better estimates. However, this generally is difficult to achieve. Moreover, the identification of damping coefficients was not considered in these methods. Agbabian et al. (1991) used the least-squares method to identify stiffness and damping coefficients of a three DDOFs structural system. Yang and Lin (2005) presented

adaptive tracking technique, which was based on the least-squares estimation approach, to identify the time-varying structural parameters during a severe event, such as the earthquake. The method was applied to linear structures (Phase I ASCE structural health monitoring benchmark building) and a nonlinear elastic structure.

Based on the least-squares method, other time domain SI techniques were developed such as and maximum likelihood method (DiPasquale and Cakmak, 1988; Imai et al., 1989). They identified unknown parameters by maximizing the probability of the measured data. This probability is referred to as the likelihood function of the measurements. As the logarithm is monotonic, maximizing the likelihood function is usually replaced by maximizing its logarithm. Shinozuka et al. (1982) applied the maximum likelihood method to identify the parameters of a two-dimensional model of a suspension bridge. Shao et al. (1985) used the maximum likelihood method for parameter identification of a vibrating system. The instrumental variable method (Eykhoff, 1982) which utilizes a coefficient matrix, also known as the instrumental variable matrix, was used to identify a structure using the least-squares method. It is important to note that all the above mentioned methods require the information of the input excitation.

To improve the application of least-squares based methods, the research team at the University of Arizona developed a number of least-squares based methods to identify the health of the structure without using input excitation. Wang and Haldar (1994) developed iterative least-squares with unknown input (ILS-UI) procedure. The procedure can identify the structural parameters, i.e., stiffness and damping at the local level using responses measured at all DDOFs and without using input excitation information. The structural damping is assumed to be viscous. Ling and Haldar (2004) improved the

efficiency of the method by introducing Rayleigh-type proportional damping and they called modified ILS-UI or MILS-UI. The method was further improved by Katkhuda et al. (2005) and it was called as generalized ILS-UI or GILS-UI. All these methods were applied for two dimensional structures. Later, the method was also further enhanced by Das and Haldar (2010a, 2010b) for 3D structures and it was called as 3D-GILS-UI. All of these methods were verified numerically using measured responses generated by commercially available finite element software. They also added artificially white noises to numerically generated noise-free responses. They verified the methods for shear-type buildings, trusses, and frames and showed that the methods could assess health of the structure for both noise-free and noisy responses (Wang and Haldar, 1994; Ling and Haldar, 2004; Katkhuda et al., 2005; Katkhuda and Haldar, 2006; Haldar and Das, 2010).

After the effectiveness of the ILS-UI procedure and its variants demonstrated analytically, the research team at the University of Arizona verified them experimentally. Vo (2003) and Vo and Haldar (2004, 2008) tested one dimensional beams (simply supported and fixed ended beams) and Martinez-Flores and Haldar (2007) and Martinez-Flores et al. (2008) tested a two dimensional frame built to one-third scaled three-story steel structure in the laboratory. They used actual experimental response information to identify the structural parameters of defect-free and defective structure without using the information on the input excitation. Both studies conclusively confirmed the validity of the procedure to assess the health of the structure.

For the sake of completeness, recently available least-squares based methods with unknown input for SHA are reviewed briefly here. Smyth et al. (1999) presented least-squares based adaptive identification algorithm to identify both the single degree of

freedom (SDOF) and multiple degrees of freedom (MDOF) nonlinear hysteretic systems under arbitrary dynamic environments. They showed that the method successfully tracked the restoring force corresponding to the experimental data from a reinforced concrete structural member.

Chen and Li (2004) presented an iterative identification procedure consisting of the least-squares technique and a modification process between each recursive step. They verified the procedure using shear-type buildings and truss bridges. The results demonstrated that the method could accurately identify both the structural parameters and the input time-history when the responses are noise-free or slightly contaminated with noise. However, the identification accuracy of the damping coefficients was broadly acceptable at low noise level, and became relatively poor at high noise level.

Yang et al. (2007) proposed a recursive least-squares estimation with unknown inputs (RLSE-UI) approach to identify the structural parameters, such as the stiffness, damping, and other nonlinear parameters, as well as the unmeasured excitations. It was used to identify abrupt changes in the stiffness and/or damping. Simulation results based on an ASCE benchmark building for structural health monitoring and nonlinear structures demonstrated that the proposed adaptive approach was quite effective and accurate.

Xu et al. (2012) proposed weighted adaptive iterative least-squares estimation with incomplete measured excitations (WAILSE-IME) approach to identify the structural parameters and external loading. The performance of the proposed approach was verified by numerical simulation on a six-story shear model structure with noise-free measurement and noise-polluted simulation data and dynamic tests on a four-story frame structure built in the lab. They showed that the approach accurately identified the

structural parameters and unknown excitation. They also showed its robustness when noise-polluted structural response measurements are employed.

2.5.2.2 Kalman Filter-Based Methods

The Kalman filter (KF) was proposed in 1960 (Kalman, 1960) and has won wide acclamation among engineers, scientists, and managers. Since the time of its introduction, the Kalman filter has been the subject of extensive research and application. This is likely due in large part to advances in digital computing that made the use of the filter practical, but also to the relative simplicity and robust nature of the filter itself. The filter is an optimal recursive data-processing algorithm, such that all previous data, except the most recent, need not be kept in storage at the time when a new measurement is taken. The technique can process noisy measurement data.

The Kalman filter (KF) is a linear filter that can be applied to a linear system. Unfortunately, linear structural systems may not exist - all structural systems possess some degree of nonlinearity. Moderate to high level of excitation may force the structure to behave nonlinearly. Presence of defects may also cause nonlinearity, even when the excitation is at the low level. Also if the structural system is linear, the estimation of the unknown parameters jointly with the state is a nonlinear estimation problem. Therefore, nonlinear system identification techniques need to be used to identify the structural system. In order to apply the mechanics of the Kalman filter to nonlinear problem, the extended Kalman filter, ensemble Kalman filter, and unscented Kalman filter were developed.

(a) Extended Kalman filter (EKF)

The extended Kalman filter (EKF) is originally developed by Kalman and Bucy (1961) and Jazwinski (1970). The principle of the EKF is that it linearises all nonlinear models so that the basic Kalman filter can be applied. The EKF has been one of the most widely used tools for nonlinear state estimation and parameter identification based on vibration measurements in civil engineering.

Carmichael (1979) incorporated the model parameter estimation by the EKF within the state estimation problem by suitably augmenting the state vector of dynamic behavior of the model. The method was verified using a single degree-of-freedom system. The adaptability of the reference state vector was not markedly stable due to the finite difference approximation.

Yun and Shinozuka (1980) applied EKF to identify a nonlinear multiple degree-of-freedom model of an offshore tower in which the response of each mass was observed. Analytical simulation studies were performed for structural systems on the basis of artificially generated input and output observations under the various output noise conditions. They showed that the EKF yielded good estimates even under the conditions of fairly large amounts of output noise.

Hoshiya and Saito (1984) introduced a weighted global iteration (WGI) procedure with an objective function in the EKF algorithm in order to obtain stable solutions as well as their fast convergency to the optimal ones. The procedure is denoted as EKF-WGI. The weight factor is incorporated along with the initial covariance matrix in order to accelerate the EKF processing, while the stability might be sacrificed to some extent. When the algorithm tends to diverge, the best estimated values are obtained

corresponding to the minimum objective function. They reported that the weight seems to play an important role in the promotion of convergency. EKF-WGI was verified extensively by identifying structural parameters (Hoshiya and Saito, 1984; Hoshiya and Maruyama, 1987; Toki et al., 1989; Koh et al., 1991; Oreta and Tanabe, 1993, 1994; Lin and Zhang, 1994).

The shortcoming of the EKF-WGI is that it requires the information of input excitation. As mentioned earlier, to improve implementation potential of the procedure, it should be able to identify the structural system without using the input excitation information. To overcome this challenge, the research team at the University of Arizona developed a two-stage approach by combining ILS-UI and its variants and EKF-WGI procedures. Based on the location of input excitation and available measured responses, a substructure can be selected that will satisfy all the requirements of the ILS-UI procedure in Stage 1. At the completion of Stage 1, the information on the unknown excitation and the damping and stiffness parameters of all the elements in the substructure will be available. The identified damping can be assumed to be applicable for the whole structure. The identified stiffness parameters will provide information on the initial values of the state vector required to implement EKF-WGI. With the information on initial state vector and excitation information, the EKF-WGI procedure can be initiated to identify the whole structure in Stage 2. Wang and Haldar (1997) were among the first developed a two-stage procedure and they denoted it as iterative least-squares extended Kalman filter with unknown input (ILS-EKF-UI) method. Then, Ling and Haldar (2004) modified the procedure and called it as MILS-EKF-UI. Later, Katkhuda and Haldar (2008) generalized the procedure to be applied for a different type of structural system

and it is known as GILS-EKF-UI. Finally, Das and Haldar (2012a) extended the procedure further to be applied to three-dimensional structural system and they named it as 3D GILS-EKF-UI. These procedures were successfully verified using analytically generated responses (Wang, 1995; Ling, 2000; Katkhuda, 2004; Das and Haldar, 2011a, b; Das et al., 2012; Das and Haldar, 2012a, b, c; Das, 2012). Then, the GILS-EKF-UI was verified experimentally in the laboratory for a two dimensional frame (Martinez-Flores, 2005; Martinez-Flores et al., 2008). They considered defect-free and several defective states with different levels of severities, including broken members, loss of cross sectional area over the entire length of members, loss of area over small length of a member, presence of one or multiple cracks in a member, etc.

For the sake of completeness, other recently proposed EKF-based SHA methods with unknown input for SHA are reviewed briefly.

Ma and Ho (2004) proposed an inverse method, which comprises two parts; the extended Kalman filter and a recursive least-squares estimator. The method was used to identify input forces of nonlinear structural systems. The estimation performance of the proposed method was evaluated through numerical experiments of nonlinear lumped-mass systems. They demonstrated that the inverse method successfully applied to identify the excitation forces.

Yang et al. (2007) proposed EKF with unknown inputs (EKF-UI) to identify the structural parameters, such as the stiffness, damping, and nonlinear parameters, as well as the unmeasured excitations. They verified the approach to linear and nonlinear structures and demonstrated that the approach successfully identified the structural parameters, their variations due to damages, and unknown excitations.

(b) Ensemble Kalman filter (EnKF)

The ensemble Kalman filter (EnKF) concept is a sophisticated sequential data assimilation method. It is a Monte Carlo approximation of the Kalman filter (KF), where the true covariance matrix in the KF is replaced by the sample covariance matrix computed from the ensemble. The EnKF propagates the samples using the full nonlinear model. It has been shown in many applications that EnKF resolves the issue of poor error covariance evolution associated with EKF. This method was first introduced by Evensen (1994)

Although the EnKF has been applied extensively in recent years in various geophysical areas, its application to structural health assessment is very limited. The EnKF has just recently been introduced as a parameter identification tool by Ghanem and Ferro (2006). They presented approach combining the ensemble Kalman filter and non-parametric modeling techniques to tackle structural health monitoring for nonlinear systems. Both location and time of occurrence of damage were accurately detected in spite of measurement and modeling noise. A comparison between ensemble and extended Kalman filters was also presented and they showed that the robustness of the EnKF with respect to severe nonlinearities.

Khalil et al. (2007) explored the capabilities of the EKF, EnKF, and particle filter (PF) for joint state-parameter estimation for a simple nonlinear structural dynamical system. It was demonstrated that the EKF failed to track the true state of the system due to the highly non-Gaussian nature of the state variables, caused by the presence of strong nonlinearities. The EnKF and PF performed well in tracking the true state of the system. They also showed that even in the presence of relatively large model and measurement

noise, the estimates of the nonlinear stiffness coefficients given by the EnKF and PF matched reasonably well with the true values.

(c) Unscented Kalman filter (UKF)

Unscented Kalman filter (UKF) is a nonlinear filter, and was first proposed by Julier (Julier et al., 1995; Julier and Uhlmann, 1997; Julier et al., 2000) and further enhanced (Wan and van der Merwe, 2000; van der Merwe and Wan, 2001a; van Zandt, 2001; Julier, 2002; Julier and Uhlmann, 2002; Julier, 2003; Tenne and Singh, 2003). Unlike the extended Kalman filter (EKF), which is based on the linearizing the nonlinear function by using Taylor series expansions, UKF uses the true nonlinear models and approximates a Gaussian distribution of the state random variable. The principle of UKF is to generate a number of sampling points (sigma points) around the current state estimate based on its covariance. Then, these points are explicitly propagated through the nonlinear system equations to get more accurate estimation of the mean and covariance of the mapping results.

The UKF concept has been shown to be a superior alternative to the EKF in a variety of applications in the areas of nonlinear state estimation and parameter identification including nonlinear dynamical system identification (Sitz et al., 2002; Popescu and Wong, 2003; Voss et al., 2004), navigation and tracking (Chen et al., 2003; Crassidis and Markley, 2003; van der Merwe et al., 2004; Lee and Alfriend, 2004; Julier and Uhlmann, 2004), chemical engineering estimation (Romanenko and Castro, 2004; Romanenko et al., 2004), visual tracking (Li et al., 2004), and neural network training (Wan and van der Merwe, 2000; van der Merwe and Wan, 2001b; Choi et al., 2004, 2005). Despite the fact

that UKF apparently surpasses EKF, UKF has not been used widely in the field of civil engineering.

Mariani and Ghisi (2007) applied EKF and UKF to a case of softening single degree-of-freedom (SDOF) structural system. They showed that the performance of UKF, in terms of state tracking and model calibration, was significantly superior to that of EKF.

Wu and Smyth (2007) compared the performance of EKF and UKF to nonlinear structural system identification problems. A single-degree of freedom nonlinear hysteretic dynamic system, a 2-DDOF linear structural system, and a two-story nonlinear elastic system were considered. The authors showed that the results of UKF were more accurate than EKF in highly nonlinear system and UKF was at least as good as EKF for weakly nonlinear systems. They also demonstrated that UKF was more robust to the measurement noise level than EKF and UKF could be applied to non-differentiable functions.

Chatzi and Smyth (2009) presented a comparison on performance of UKF and two particle filter (PF)-based methods for unmeasured state and model parameter identification of 3-DDOF system with Bouc-Wen oscillator. The authors proved that UKF and Gaussian mixture sigma-point particle filter (GMSPPF) are the most efficient ones for identifying the final system parameters and as far as the computational cost is concerned the UKF method is considerably faster.

Chatzi et al. (2010) presented a method for the on-line identification of nonlinear hysteretic systems where the nature of the analytical model describing the system is not clearly established. It was a Bayesian approach based on the UKF method in order to

investigate the effects of model complexity and parameterization. The capability of the method was demonstrated through validation tests using the experimental data sets.

2.5.2.3 Substructure Methods

A localized structural identification procedure often referred to as substructuring approach. The localized substructuring procedure has the advantage that identification of input excitation is not necessary if the node of excitation does not belong to the substructure under consideration. However, multiple substructures will be necessary for complete structural identification.

Koh et al. (1991) first proposed a substructure system identification method in the time domain. A large structure is divided into many smaller substructures and EKF-WGI was used to identify the unknown structural parameters (stiffness and damping coefficients) of each substructure separately. Numerical simulation studies were performed for three types of structures, namely a shear building, a plane frame building and a plane truss bridge.

Oreta and Tanabe (1993) presented a procedure for localized identification of structural parameters using EKF-WGI. The concept of primary-secondary system was applied. A structure was decomposed into two substructures (primary and secondary system) which were attached at a common boundary (boundary system). The response at the boundary DDOFs in the substructure must be available as input so that the identification could be implemented. The procedure was numerically verified for a shear building.

Oreta and Tanabe (1994) identified structural parameters of a frame element isolated from the complete structure using substructuring procedure. The EKF-WGI procedure

was used to estimate the physical characteristics of a frame element; the axial rigidity, flexural rigidity, and damping parameters. Numerical simulation studies were performed on two-story plane frames.

Law and Yong (2011) presented two substructural damage detection methods to identify external excitations and local damages in a substructure. In the first method, the finite element model of the whole structure was required and a selected substructure was assessed for its structural conditions. In the second method, the finite element model of the selected substructure was only required with both the dynamic measurement and excitation conducted within the same substructure. Numerical studies with a planar truss structure showed that both methods could fairly accurately identify the local damages with 10% noise in the measured responses.

As mentioned earlier, the research team at the University of Arizona presented a substructure approach. The iterative least-squares with unknown input procedure was used to identify the input excitation and structural parameters (stiffness and damping coefficients). The information of response was only required to implement the procedure. They verified the procedure for different types of excitation; impulsive, sinusoidal, and irregular earthquake loading.

2.6 Challenges for SHA

Although many vibration-based SHA methods in the time domain have been developed so far, no method could be regarded sufficiently accurate, efficient, and robust for broader applications to assess health of real structures. The reasons are discussed below.

The LS-based approach is one of the most widely used in the identification of structural systems. However, it can be used only if the responses are available at all DDOFs in the structure. Therefore, its implementation can be limited; primarily it is applicable to relatively small structural systems (Haldar and Al-Hussein, 2015).

The widely used EKF approach provides only an approximation to the optimal nonlinear estimation and it has three well-known drawbacks (Julier et al., 1995);

(a) Linearisation can produce highly unstable filter performance if the timestep intervals are not sufficiently small.

(b) The derivation of the Jacobian matrices is nontrivial in most applications and often lead to significant implementation difficulties.

(c) Sufficiently small timestep intervals usually imply high computational overhead as the number of calculations demanded for the generation of the Jacobian and the predictions of state estimate and covariance are large.

For strongly nonlinear structural systems, EnKF can be expected to have superior performance over EKF. However, since EnKF used Monte Carlo approximation, it often requires a very large number of sample points and is therefore very computationally expensive and practically inapplicable when dimension of the problem is large. Therefore, it is impractical for large structural systems.

UKF has the advantage over the classical EKF of being able to handle any functional nonlinearity and it does not require the calculation of Jacobians. Furthermore, UKF is much more computationally efficient than EnKF and it can be applied for large structural systems.

The author observed that the UKF concept has been successfully applied to numerous practical estimation problems, mentioned earlier, and shown to be a powerful filter in many cases (Al-Hussein and Haldar, 2014). However, its uses for the health assessment of civil infrastructures are very limited and there are several shortcomings to its application including (Al-Hussein and Haldar, 2015a, b, d):

(a) It was applied to simple structures represented by shear building with a small number of DDOFs, typically not greater than three.

(b) The identification of the defective state of a structure was not considered in these studies.

(c) The input excitation was assumed to be known in all of its applications.

(d) At least one response time-histories (acceleration, velocity, or displacement) were assumed to be available at all DDOFs.

(e) Relatively a large duration of response histories is needed.

The most important challenge in the vibration-based SHA is to measure both the excitation and the response time-histories simultaneously at high sampling rates. The collection of input excitation information is not simple. As structural systems get larger and complicated, the identification of their health becomes increasingly challenging and the author observed that the traditional concept of UKF may not be able to identify them (Al-Hussein and Haldar, 2015e). In addition, for large complicated structural systems, it may not be possible or economical to measure responses at all DDOFs. For this class of systems, the response time-histories will be measured only at small part(s) of the structure, i.e., at a limited number of DDOFs. This will require a substructure approach. Also, it is difficult to confirm after the identification process whether or not the estimated

parameters are stable and convergent to the expected values. To overcome this challenge, additional mathematical sophistication is required. The use of a large duration of response histories may contaminate the responses from other sources of excitation during field investigations.

Observing these deficiencies prompted the author to propose a comprehensive improvement of the UKF concept for the structural health assessment of real large structural systems. The new approach is a combination of LS and UKF-based approach and it uses the concept of substructure. Furthermore, the weighted global iteration with an objective function is incorporated with the UKF algorithm to obtain stable and convergent solution. The advantage of new integrated approach is that it can assess health of large structures at the local element level using only noise-contaminated responses at a limited number of DDOFs and without using excitation information. In addition, it uses small response time-histories; often fractions of a second.

CHAPTER 3

THEORY OF IDENTIFICATION OF LARGE STRUCTURAL SYSTEMS USING LIMITED RESPONSE INFORMATION

3.1 Introduction

As mentioned in the previous chapter, the applications of UKF in civil engineering area are very limited and in all these applications there are some deficiencies. It was pointed out that the UKF procedure was applied for simple structural systems (shear-type building) with a small number of DDOFs and at least one response time-histories (acceleration, velocity, or displacement) with a relatively large duration were assumed to be available at all DDOFs. Therefore, this chapter aims to develop an approach to overcome these deficiencies. In this approach, a weighted global iteration procedure with an objective function (Hoshiya and Saito, 1984) is incorporated with the UKF algorithm in order to obtain optimal, stable, and convergent solutions for the identification process. The approach is denoted as unscented Kalman filter with weighted global iteration (UKF-WGI). The procedure is a time-domain nonlinear system identification technique where the structure is represented by finite elements. The desirable features of the proposed approach are that it can identify a large real structural system at a local element level using a limited number of noise-contaminated responses. The methodology of the UKF-WGI procedure is presented in this chapter. For the sake of completeness, the main differences in mathematical formation of the UKF-WGI and EKF-WGI are also presented.

3.2 The Concept behind Kalman Filter

Kalman filter (KF) is an optimal recursive data processing algorithm. One aspect of this optimality is that KF incorporates all information that can be provided to it. It processes all available measurements, regardless of their precision, to estimate the current value of the variables of interest. It is recursive because not all previous data need to be kept in storage and reprocessed every time a new measurement is taken. Information gained in successive steps is all incorporated into the latest result. It is a data processing algorithm or filter, which is useful for the reason that only knowledge about system inputs and outputs is available for estimation purposes. Variables of interest cannot be measured directly, but have to somehow be generated using the available data. A filter tries to obtain an optimal estimate of variables from data coming from a noisy environment (Maybeck, 1979).

The basic concept of Kalman filter is shown in Figure 3.1. The concept can be summarized in three steps: (1) the prediction is obtained based on initial conditions and mathematical model; the uncertainty in the prediction is expected to be high, (2) the measurements are collected to enhance the prediction confidence, and (3) the corrected optimal estimate is obtained based on the prediction and measurement resulting in an improved identification.

3.3 Mathematical Formulation of UKF-WGI

In order to implement the UKF-WGI procedure, it is necessary to describe the dynamic system by a set of nonlinear differential equations. Assuming the governing differential equation of motion represents the dynamic system perfectly; the mathematical model does not include any process noise and can be written as:

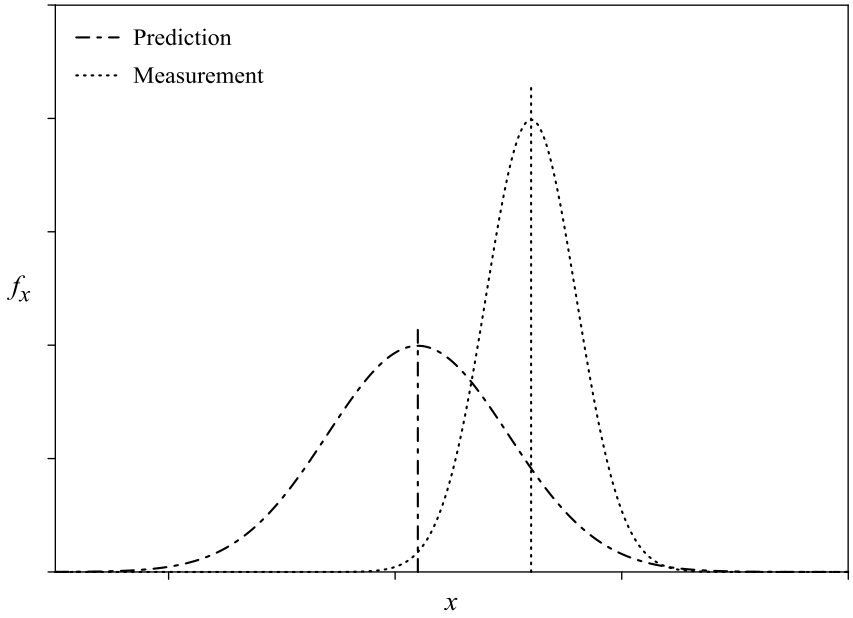

(a)

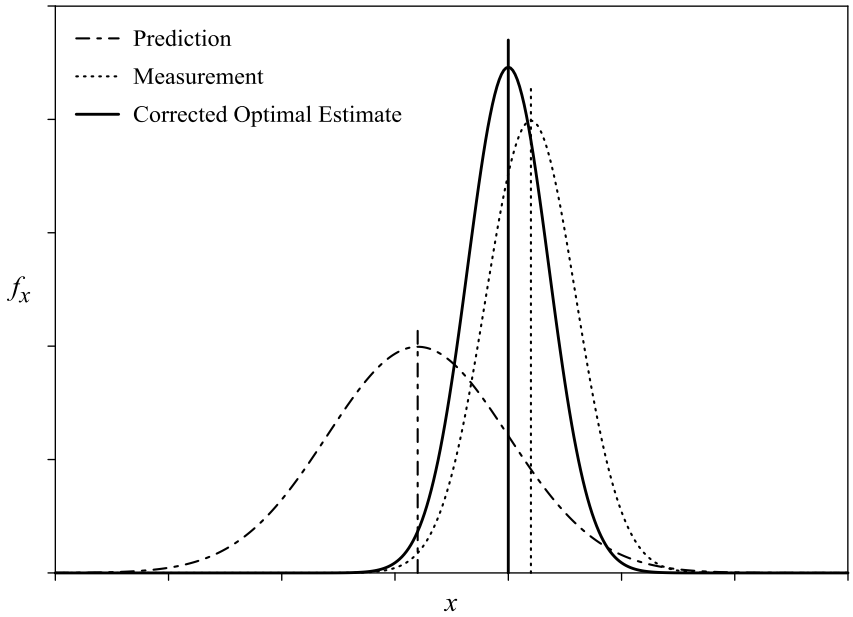

(b)

Figure 3.1 Kalman filter concept

$$\mathbf{M}\ddot{\mathbf{X}}(t) + \mathbf{C}\dot{\mathbf{X}}(t) + \mathbf{K}\mathbf{X}(t) = \mathbf{f}(t) \tag{3.1}$$

It can be expressed in a state-space form by a set of first-order nonlinear differential equations as:

$$\dot{\mathbf{Z}}_t = f(\mathbf{Z}_t, t) \tag{3.2}$$

where $\mathbf{Z}_t$ is the state vector at time *t*; $\dot{\mathbf{Z}}_t$ is the derivative of the state vector with respect to time *t*; f is a nonlinear function of the state.

For a structure with *N* degrees of freedom and *L* elements, an augment state vector can be defined as:

$$\mathbf{Z}_t = \begin{bmatrix} \mathbf{X}(t) \\ \dot{\mathbf{X}}(t) \\ \widetilde{\mathbf{K}} \end{bmatrix} \tag{3.3}$$

where $\mathbf{X}(t)$ and $\dot{\mathbf{X}}(t)$ are the *N*×1 vectors of displacement and velocity, respectively, for all DDOFs of the structure; $\widetilde{\mathbf{K}}$ is the *L*×1 vector of the element stiffness parameters of the whole structure that needs to be identified. Therefore, the size of $\mathbf{Z}_t$ is (*2N*+*L*)×1.

For instance, $\mathbf{X}(t)$, $\dot{\mathbf{X}}(t)$, and $\widetilde{\mathbf{K}}$ vectors for a two dimensional frame elements can be expressed as:

$$\mathbf{X}(t) = \begin{bmatrix} x_1(t) \\ y_1(t) \\ \theta_1(t) \\ x_2(t) \\ y_2(t) \\ \theta_2(t) \\ \vdots \\ \vdots \\ x_N(t) \\ y_N(t) \\ \theta_N(t) \end{bmatrix}, \quad \dot{\mathbf{X}}(t) = \begin{bmatrix} \dot{x}_1(t) \\ \dot{y}_1(t) \\ \dot{\theta}_1(t) \\ \dot{x}_2(t) \\ \dot{y}_2(t) \\ \dot{\theta}_2(t) \\ \vdots \\ \vdots \\ \dot{x}_N(t) \\ \dot{y}_N(t) \\ \dot{\theta}_N(t) \end{bmatrix}, \quad \widetilde{\mathbf{K}} = \begin{bmatrix} k_1 \\ k_2 \\ \vdots \\ \vdots \\ k_L \end{bmatrix} \tag{3.4}$$

where k_i is the unknown stiffness parameter of the i^{th} frame element and it is assumed to

be invariant with time during the identification. k_i is generally defined as E_iI_i/L_i, where E_i, I_i, and L_i are the Young's modulus of the material, moment of inertia, and length of the i^{th} element.

Equation 3.2 can be rewritten as

$$\dot{\mathbf{Z}}_t = \begin{bmatrix} \dot{\mathbf{X}}(t) \\ \ddot{\mathbf{X}}(t) \\ 0 \end{bmatrix} = \begin{bmatrix} \dot{\mathbf{X}}(t) \\ -\mathbf{M}^{-1}\left[\mathbf{K}\mathbf{X}(t) + \mathbf{C}\dot{\mathbf{X}}(t) - \mathbf{f}(t)\right] \\ 0 \end{bmatrix} \tag{3.5}$$

where $\ddot{\mathbf{X}}(t)$ is the $N\times1$ vector of acceleration for all DDOFs of the structure; **M**, **K**, and **C** are the $N\times N$ global mass, stiffness, and damping matrices of the whole structure, respectively; and $\mathbf{f}(t)$ is the $N\times1$ input excitation force vector.

Since the changes in damping of defective structure as compared to defect-free structure are not completely understood or correlated at present, the identified damping parameters cannot be effectively utilized for the defect identification purpose. Therefore, to improve the efficiency of the UKF-WGI algorithm, Rayleigh-type mass and stiffness damping is used. For Rayleigh damping, matrix **C** in Equation (3.5) becomes:

$$\mathbf{C} = a\mathbf{M} + b\mathbf{K} \tag{3.6}$$

where a and b are the mass and stiffness proportional damping coefficients, respectively. These constants have close-form relationship with the first two natural frequencies, f_1 and f_2, of a structure. Knowing f_1 and f_2 and assuming the damping ratios are same for the first two natural modes, a and b can be estimated using analytical expressions (Clough and Penzien, 2003) as:

$$\begin{bmatrix} a \\ b \end{bmatrix} = \frac{2\xi}{\omega_m + \omega_n} \begin{bmatrix} \omega_m\omega_n \\ 1 \end{bmatrix} \tag{3.7}$$

where ξ is the damping ratio; and ω_m and ω_n are the first two natural circular frequencies.

Equation 3.5 can be rewritten as:

$$\dot{\mathbf{Z}}_t = \begin{bmatrix} \dot{\mathbf{X}}(t) \\ \ddot{\mathbf{X}}(t) \\ 0 \end{bmatrix} = \begin{bmatrix} \dot{\mathbf{X}}(t) \\ -\mathbf{M}^{-1}\left[\mathbf{K}\mathbf{X}(t) + (a\mathbf{M} + b\mathbf{K})\dot{\mathbf{X}}(t) - \mathbf{f}(t)\right] \\ 0 \end{bmatrix} \tag{3.8}$$

The discrete time measurements with additive noise at $t = k\Delta t$ can be expressed as:

$$\mathbf{Y}_k = h(\mathbf{Z}_k, t) + \mathbf{V}_k \tag{3.9}$$

where $\mathbf{Y}_k$ is the measurement vector at $t = k\Delta t$; h is the nonlinear function that relates the state to the measurement; $\mathbf{Z}_k$ is the state vector at $t = k\Delta t$; Δt is the constant time increment; and $\mathbf{V}_k$ is a measurement noise vector of zero mean white noise Gaussian processes with covariance matrix $\mathbf{R}_k$.

For the measurement model, acceleration responses will be measured at B number of DDOFs, where B is smaller than the total number of DDOFs N for the whole structure. Then the acceleration time-histories will be successively integrated to obtain the velocity and displacement time-histories (Vo and Haldar, 2003; Das, 2012; Das et al., 2013). Therefore, the discrete time measurement model can be expressed in a linear form as (Al-Hussein et al., 2013; Al-Hussein and Haldar, 2015f, g, h):

$$\mathbf{Y}_k = \mathbf{H} \cdot \mathbf{Z}_k + \mathbf{V}_k \tag{3.10}$$

where $\mathbf{Y}_k$ is the measurement vector comprising of the measured displacement and velocity at $t = k\Delta t$; $\mathbf{Y}_k$ and $\mathbf{V}_k$ are vectors of size $(2B\times1)$; and $\mathbf{H}$ is the $2B\times(2N+L)$ measurement matrix. For measured responses, their corresponding elements in matrix $\mathbf{H}$ have unit values.

To implement the filtering process, the initial values of the state vector are assumed to be Gaussian random variable. The initial mean of the state vector $\hat{\mathbf{Z}}_{0|0}$ is:

$$\hat{\mathbf{Z}}_{0|0} = \begin{bmatrix} \hat{\mathbf{X}}(0|0) \\ \hat{\dot{\mathbf{X}}}(0|0) \\ \tilde{\mathbf{K}}(0|0) \end{bmatrix} \tag{3.11}$$

The initial value of the displacement and velocity not measured at DDOFs in the state vector can be assumed to be zero.

The uncertainty in the assumption of the initial mean of the displacement, velocity, and stiffness parameters is considered by the initial error covariance matrix $\mathbf{P}_{0|0}$. It is generally assumed to be a diagonal matrix and can be expressed as:

$$\mathbf{P}_{0|0} = \begin{bmatrix} \mathbf{P}_x(0|0) & 0 \\ 0 & \mathbf{P}_s(0|0) \end{bmatrix} \tag{3.12}$$

where $\mathbf{P}_x(0|0)$ is the initial error covariance matrix of the displacement and velocity responses of size ($2N \times 2N$) and $\mathbf{P}_s(0|0)$ is the initial error covariance matrix of the stiffness parameters. $\mathbf{P}_s(0|0)$ is a diagonal matrix of size ($L \times L$) containing large positive numbers to accelerate the convergence of the local iteration process (Al-Hussein and Haldar, 2015c, e). Its value depends on the magnitude of the stiffness parameters.

After assigning the initial values for the state vector and its error covariance matrix, the filtering process of UKF-WGI is initiated to estimate the state mean vector and its error covariance matrix at time step k+1 using the following three steps:

a. Sigma point calculation step

To implement UKF-WGI, sets of 2n+1 sampling points or so-called sigma points will be generated around the current state vector (k) based on its covariance as:

$$\boldsymbol{\chi}_{0,k|k} = \hat{\mathbf{Z}}_{k|k} \tag{3.13}$$

$$\boldsymbol{\chi}_{i,k|k} = \hat{\mathbf{Z}}_{k|k} + \sqrt{(\lambda + n)}\, \mathbf{C}_{col.i} \qquad i = 1, \dots, n \tag{3.14}$$

$$\boldsymbol{\chi}_{i+n,k|k} = \hat{\mathbf{Z}}_{k|k} - \sqrt{(\lambda + n)}\,\mathbf{C}_{col.i} \qquad i = 1, \dots, n \tag{3.15}$$

where

$$\lambda = \alpha^2(n + \kappa) - n \tag{3.16}$$

in which $\mathbf{C}$ is a square root of the covariance matrix such that $\mathbf{P}_k = \mathbf{C}\mathbf{C}^{\mathbf{T}}$; $\mathbf{C}_{col.i}$ is the i^{th} column of $\mathbf{C}$'s matrix; n is the dimension of the state vector ($n = 2N + L$), and α and κ are tuning parameters. The value of κ can be $(3 - n)$ or 0. In fact, parameter κ can be used to reduce the higher order errors of the mean and the covariance approximations. The parameter α controls the size of the sigma point distribution and it should ideally be a small positive number ($0 \leq \alpha \leq 1$).

Note that sigma points are a set of vectors whose components are real numbers. The Cholesky decomposition method should be used for the calculation of the matrix square root because this method is numerically efficient and stable.

b. Prediction step

The sigma points are propagated through the nonlinear dynamic equation as:

$$\boldsymbol{\chi}_{i,k+1|k} = \boldsymbol{\chi}_{i,k|k} + \int_{k\Delta t}^{(k+1)\Delta t} f(\mathbf{Z}_t, t)dt \qquad i = 0, \dots, 2n \tag{3.17}$$

The predicted state vector $\hat{\mathbf{Z}}_{k+1|k}$ can be shown to be:

$$\hat{\mathbf{Z}}_{k+1|k} = \sum_{i=0}^{2n} W_i\,\boldsymbol{\chi}_{i,k+1|k} \tag{3.18}$$

and its predicted error covariance matrix $\mathbf{P}_{k+1|k}$ can be expressed as:

$$\begin{aligned}\mathbf{P}_{k+1|k} = \sum_{i=0}^{2n} W_i \left(\boldsymbol{\chi}_{i,k+1|k} - \hat{\mathbf{Z}}_{k+1|k}\right)\left(\boldsymbol{\chi}_{i,k+1|k} - \hat{\mathbf{Z}}_{k+1|k}\right)^T \\ + (1 - \alpha^2 + \beta)\left(\boldsymbol{\chi}_{0,k+1|k} - \hat{\mathbf{Z}}_{k+1|k}\right)\left(\boldsymbol{\chi}_{0,k+1|k} - \hat{\mathbf{Z}}_{k+1|k}\right)^T\end{aligned} \tag{3.19}$$

where β is a parameter added to the weight on the zeroth sigma point of the calculation of the covariance. The value of β is greater than 0 and the best value is 2 for Gaussian distribution. The weight factor W_i can be shown to be:

$$W_0 = \frac{\lambda}{\lambda + n} \qquad i = 0 \tag{3.20}$$

$$W_i = \frac{1}{2(\lambda + n)} \qquad i = 1, \dots, 2n \tag{3.21}$$

Since the measurement model is linear as mentioned earlier, Kalman filter (KF) will be used to compute the predicted measurement vector, its error covariance, and cross correlation matrix as suggested by Hao et al. (2007) instead of using the sigma points used in UKF.

The predicted measurement vector $\widehat{\mathbf{Y}}_{k+1|k}$ can be expressed as:

$$\widehat{\mathbf{Y}}_{k+1|k} = \mathbf{H}\widehat{\mathbf{Z}}_{k+1|k} \tag{3.22}$$

and its error covariance matrix $\mathbf{P}^{YY}_{k+1|k}$ as:

$$\mathbf{P}^{YY}_{k+1|k} = \mathbf{H}\mathbf{P}_{k+1|k}\mathbf{H}^T + \mathbf{R}_{k+1} \tag{3.23}$$

and the cross correlation matrix $\mathbf{P}^{ZY}_{k+1|k}$ can be estimated as:

$$\mathbf{P}^{ZY}_{k+1|k} = \mathbf{P}_{k+1|k}\mathbf{H}^T \tag{3.24}$$

c. Updating step:

The state vector and the error covariance matrix are updated using the available measurements at time k+1 as follows:

$$\mathbf{K}_{k+1} = \mathbf{P}^{ZY}_{k+1|k}(\mathbf{P}^{YY}_{k+1|k})^{-1} \tag{3.25}$$

$$\widehat{\mathbf{Z}}_{k+1|k+1} = \widehat{\mathbf{Z}}_{k+1|k} + \mathbf{K}_{k+1}\left(\mathbf{Y}_{k+1} - \widehat{\mathbf{Y}}_{k+1|k}\right) \tag{3.26}$$

$$\mathbf{P}_{k+1|k+1} = \mathbf{P}_{k+1|k} - \mathbf{K}_{k+1}\mathbf{P}_{k+1|k}^{YY}\mathbf{K}_{k+1}^{T} \tag{3.27}$$

in which $\mathbf{K}_{k+1}$ is the Kalman gain matrix; $\hat{\mathbf{Z}}_{k+1|k+1}$ is the updated state vector; and $\mathbf{P}_{k+1|k+1}$ is the updated error covariance matrix.

The three steps of the UKF (sigma point, prediction and updating operations), described by Equation (3.13) through Equation (3.27), are carried out for all q time points. The iteration process at each time point is generally denoted as the local iteration. When the local iteration is carried out for all the time points, it is termed as the global iteration. The identified parameters obtained through local iteration may not be stable and convergent.

From the literature, the author observed that the traditional UKF method successfully identified small defect-free structural systems consisting of very few DDOFs just by implementing local iterations assuming response time-histories are available over long time periods, sometimes 40 s (Wu and Smyth, 2007), and at least one response time-histories (acceleration, velocity, or displacement) were assumed to be available at all DDOFs. Some of these assumptions make UKF-based method difficult to implement for the structural health assessment purpose. For large structural systems, it will be impractical to collect the response information at all DDOFs and collecting responses over a long period of time will make them vulnerable to contamination caused by multiple sources of excitation. The author experienced non-convergence problem with the traditional UKF when dealing with large systems. It is important to repeat the global iteration procedure until the two successive states are essentially identical. However, the author noted that the error covariance matrix of the stiffness parameters reduced significantly during the successive global iterations and the identified stiffness values

sometimes converge to the wrong values particularly when the initial values are far from the expected values representing defective states. This prompted the author to introduce a weighted global iteration (WGI) factor, *w*, to the error covariance matrix after the first global iteration, as discussed below, so that the algorithm can converge to the correct values of the stiffness parameters representing the current state of the structure. The concept of WGI was first introduced by Hoshiya and Saito (1984) to improve the performance of the EKF procedure. In the present study, the same concept is incorporated to the UKF algorithm in order to obtain optimal, stable, and convergent solutions for the identification process. If no weight is used in the UKF procedure, the reduction in the stiffness covariance will continue as the global iteration progresses. This will cause a small change in the identified stiffness parameter between the initial and the end of a global iteration, i.e., it will satisfy the convergence tolerance before the stiffness parameter reaches to its correct value. Amplifying the stiffness covariance at the beginning of each global iteration helps the iterations to continue until the stiffness parameter converges to the correct value. It is an important step in implementing UKF-WGI.

After the completion of the first global iteration, the state vector and its error covariance matrix are initialized for the second global iteration in the following manner:

$$\hat{\mathbf{Z}}_{0|0}^{(2)} = \begin{bmatrix} \hat{\mathbf{X}}^{(2)}(0|0) \\ \hat{\dot{\mathbf{X}}}^{(2)}(0|0) \\ \tilde{\mathbf{K}}^{(2)}(0|0) \end{bmatrix} = \begin{bmatrix} \hat{\mathbf{X}}^{(1)}(0|0) \\ \hat{\dot{\mathbf{X}}}^{(1)}(0|0) \\ \tilde{\mathbf{K}}^{(1)}(q|q) \end{bmatrix} \tag{3.28}$$

$$\mathbf{P}_{0|0}^{(2)} = \begin{bmatrix} \mathbf{P}_x^{(1)}(0|0) & 0 \\ 0 & w\mathbf{P}_s^{(1)}(q|q) \end{bmatrix} \tag{3.29}$$

Following the same procedure, global iterations are continued until all the structural parameters converge within a predetermined convergence criterion or tolerance level, ε_s, i.e.,

$$\left|(\mathrm{K}_{q|q}^{(i)} - \mathrm{K}_{q|q}^{(i-1)})/(\mathrm{K}_{q|q}^{(i)})\right| \leq \varepsilon_s \tag{3.30}$$

where *i* represents the i^{th} global iteration. ε_s is considered to be 1% in this study.

Although the weighted global iteration plays an important role in the later stage to assure convergence, the global iteration procedure does not guarantee the convergence of the iteration scheme. In fact, it may diverge because of the incorrect assumption of the initial state vector, modeling error, and the specified numerical precision. When the identified system parameters tend to diverge, the best estimated values are obtained corresponding to the minimum objective function. The objective function is calculated in the following manner (Hoshiya and Saito, 1984):

$$\delta_{ik} = \mathrm{y}_{i,k} - \mathrm{H}_i \hat{\mathbf{Z}}_{k|k} \tag{3.31}$$

$$\gamma_i = \sum_{k=1}^{q} \delta_{ik}^2 \Big/ \sum_{k=1}^{q} \mathrm{y}_{i,k}^2 \tag{3.32}$$

$$\bar{\beta} = \frac{1}{B}\sum_{i=1}^{B} \gamma_i \tag{3.33}$$

$$\bar{\theta} = \left[\sum_{i=1}^{B} \left(\gamma_i - \bar{\beta}\right)^2\right]^{1/2} \tag{3.34}$$

in which *B* is the size of the measurement vector, $\mathbf{Y}_k$; γ_i is the normalized mean-square of the difference between the i^{th} measurement y_i and the corresponding estimate $\hat{z}_i$ where $\hat{z}_i$ and y_i are the i^{th} elements of the vectors $\mathbf{Z}_k$ and $\mathbf{Y}_k$, respectively; $\bar{\beta}$ is the average of γ_i. The objective function, $\bar{\theta}$, shows the scatterness in the root mean-square of each γ_i from

the central value $\bar{\beta}$. Therefore, minimum $\bar{\theta}$ indicates that the difference between each measurement and the corresponding estimate becomes totally minimum and thus keeping their balance.

3.4 Implementation of the UKF-WGI Procedure

The UKF-WGI procedure can be implemented using the following steps:

1. Develop the initial state vector $\hat{\mathbf{Z}}_{0|0}$ and error covariance matrix $\mathbf{P}_{0|0}$ for the whole structure.
2. Carry out the local iterations in the UKF procedure, i.e., generation of sigma point, prediction, and updating operations, for all the time points (q), completing the first global iteration and producing the updated state vector $\hat{\mathbf{Z}}_{q|q}^{(1)}$ and error covariance matrix $\mathbf{P}_{q|q}^{(1)}$.
3. Define the initial state vector $\hat{\mathbf{Z}}_{0|0}^{(2)}$ and error covariance matrix $\mathbf{P}_{0|0}^{(2)}$ for the second global iteration using the system parameters and their covariance values obtained in step 2 by scaling up the covariance values by a weight factor (w).
4. Carry out the local iteration steps of the UKF procedure within the second global iteration to obtain $\hat{\mathbf{Z}}_{q|q}^{(2)}$ and $\mathbf{P}_{q|q}^{(2)}$.
5. Continue the iterative process until a predetermined convergence criterion (ε_s), which is considered to be 1% in this study, is satisfied for all system parameters. Otherwise, the best estimated values are obtained corresponding to the minimum objective function ($\bar{\theta}$).

A flow chart for the UKF-WGI procedure is shown in Figure 3.2.

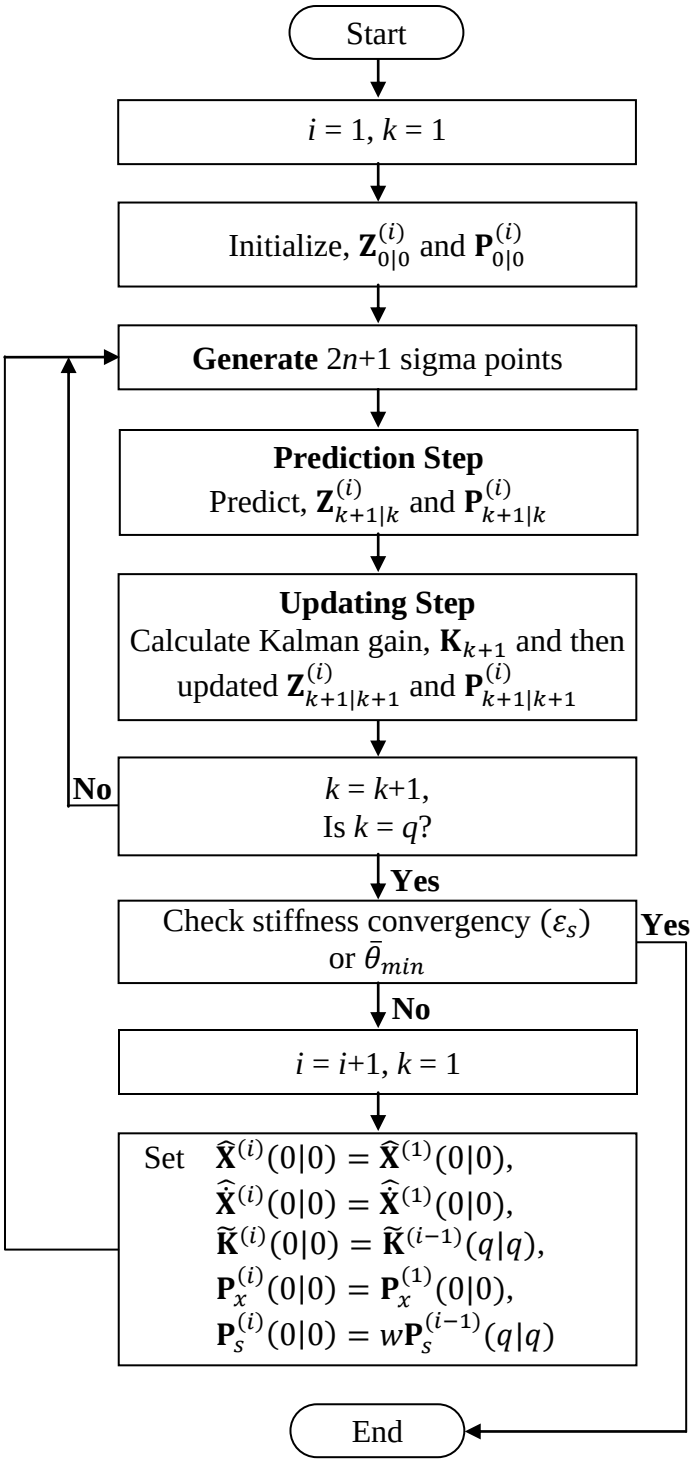

Figure 3.2 Flow chart for the UKF-WGI procedure

3.5 Finite Element Formulations for a Plane Frame

In this section, the finite element formulations for a two dimensional frame is presented. This type of structure has three DDOFs at each node. Two of them are translational DDOFs; one is along the length of the element and the other is perpendicular to it, and the third one is the rotation as shown in Figure 3.3. This figure also shows the local and global coordinate system for a two dimensional frame element.

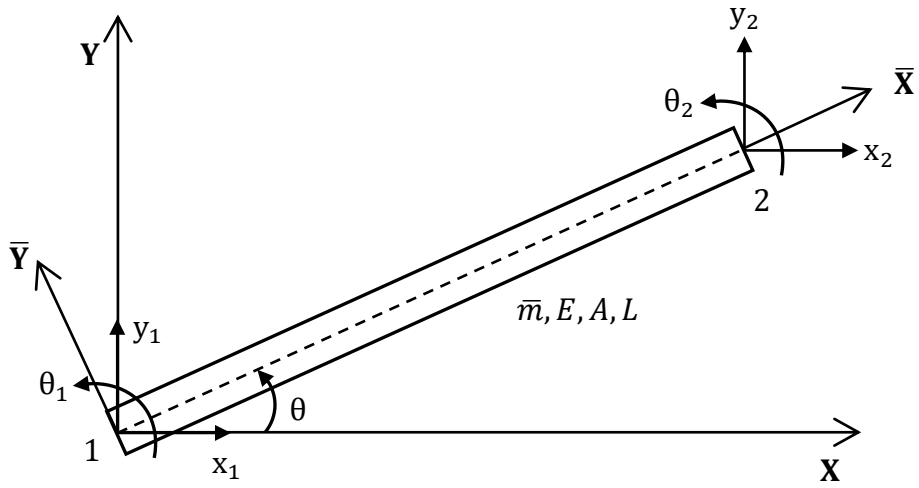

Figure 3.3 Local and global coordinate system for a two dimensional frame element

The consistent mass matrix $\bar{\mathbf{M}}_i$ and stiffness matrix $\bar{\mathbf{K}}_i$ for the i^{th} element of uniform cross section in the local coordinate system $(\bar{X}, \bar{Y})$, shown in Figure 3.3, can be represented as (Cook et al., 2002; Logan, 2007):

$$\bar{\mathbf{M}}_i = \frac{\bar{m}_i L_i}{420}\begin{bmatrix} 140 & & & & & \\ 0 & 156 & & & \text{Sym.} & \\ 0 & 22L_i & 4L_i^2 & & & \\ 70 & 0 & 0 & 140 & & \\ 0 & 54 & 13L_i & 0 & 156 & \\ 0 & -13L_i & -3L_i^2 & 0 & -22L_i & 4L_i^2 \end{bmatrix} \tag{3.35}$$

$$\bar{\mathbf{K}}_i = \frac{E_i I_i}{L_i}\begin{bmatrix} \frac{A_i}{I_i} & & & & & \\ 0 & \frac{12}{L_i^2} & & & \text{Sym.} & \\ 0 & \frac{6}{L_i} & 4 & & & \\ -\frac{A_i}{I_i} & 0 & 0 & \frac{A_i}{I_i} & & \\ 0 & -\frac{12}{L_i^2} & -\frac{6}{L_i} & 0 & \frac{12}{L_i^2} & \\ 0 & \frac{6}{L_i} & 2 & 0 & -\frac{6}{L_i} & 4 \end{bmatrix} = k_i \bar{\mathbf{S}}_i \tag{3.36}$$

where $\bar{m}_i$ is the mass per unit length of the i^{th} element; $\bar{\mathbf{S}}_i$ is the stiffness coefficients within the square bracket in Equation (3.36) for the i^{th} element in the local coordinate system.

The local mass and stiffness matrices can be transformed to the global coordinate system as:

$$\mathbf{M}_i = \mathbf{T}_i^T \bar{\mathbf{M}}_i \mathbf{T}_i \tag{3.37}$$

$$\mathbf{K}_i = \mathbf{T}_i^T \bar{\mathbf{K}}_i \mathbf{T}_i \tag{3.38}$$

where $\mathbf{M}_i$ and $\mathbf{K}_i$ are the mass and stiffness matrices, respectively, for the i^{th} element in the global coordinate system (X, Y), shown in Figure 3.3. $\mathbf{T}_i$ is the transformation matrix and can be written for the i^{th} two dimensional frame element as:

$$\mathbf{T}_i = \begin{bmatrix} cos\theta & sin\theta & 0 & 0 & 0 & 0 \\ -sin\theta & cos\theta & 0 & 0 & 0 & 0 \\ 0 & 0 & 1 & 0 & 0 & 0 \\ 0 & 0 & 0 & cos\theta & sin\theta & 0 \\ 0 & 0 & 0 & -sin\theta & cos\theta & 0 \\ 0 & 0 & 0 & 0 & 0 & 1 \end{bmatrix} \tag{3.39}$$

where θ is the angle between the global and local axis of the element as shown in Figure 3.3.

Equation (3.38) can be rewritten as:

$$\mathbf{K}_i = k_i \mathbf{T}_i^T \bar{\mathbf{S}}_i \mathbf{T}_i = k_i \mathbf{S}_i \tag{3.40}$$

The mass matrix $\mathbf{M}_i$ for the i^{th} element in the global coordinate system can be evaluated from Equation (3.37) as:

$$\mathbf{M}_i = \frac{\bar{m}_i L_i}{420}\begin{bmatrix} 140c^2+156s^2 & & & & & \\ -16cs & 140s^2+156c^2 & & & \text{Sym.} & \\ -22L_i s & 22L_i c & 4L_i^2 & & & \\ 70c^2+54s^2 & 16cs & -13L_i s & 140c^2+156s^2 & & \\ 16cs & 70s^2+54c^2 & 13L_i c & -16cs & 140s^2+156c^2 & \\ 13L_i s & -13L_i c & -3L_i^2 & 22L_i s & -22L_i c & 4L_i^2 \end{bmatrix} \tag{3.41}$$

and the stiffness matrix $\mathbf{K}_i$ for the i^{th} element in the global coordinate system can be evaluated from Equation (3.40) as (Logan, 2007):

$$\mathbf{K}_i = \frac{E_i I_i}{L_i}\begin{bmatrix} \frac{A_i}{I_i}c^2+\frac{12}{L_i^2}s^2 & & & & & \\ \left(\frac{A_i}{I_i}-\frac{12}{L_i^2}\right)cs & \frac{A_i}{I_i}s^2+\frac{12}{L_i^2}c^2 & & & \text{Sym.} & \\ -\frac{6}{L_i}s & \frac{6}{L_i}c & 4 & & & \\ -\left(\frac{A_i}{I_i}c^2+\frac{12}{L_i^2}s^2\right) & -\left(\frac{A_i}{I_i}-\frac{12}{L_i^2}\right)cs & \frac{6}{L_i}s & \frac{A_i}{I_i}c^2+\frac{12}{L_i^2}s^2 & & \\ -\left(\frac{A_i}{I_i}-\frac{12}{L_i^2}\right)cs & -\left(\frac{A_i}{I_i}s^2+\frac{12}{L_i^2}c^2\right) & -\frac{6}{L_i}c & \left(\frac{A_i}{I_i}-\frac{12}{L_i^2}\right)cs & \frac{A_i}{I_i}s^2+\frac{12}{L_i^2}c^2 & \\ -\frac{6}{L_i}s & \frac{6}{L_i}c & 2 & \frac{6}{L_i}s & -\frac{6}{L_i}c & 4 \end{bmatrix} \tag{3.42}$$

where $s = sin\theta$ and $c = cos\theta$

3.6 Main Differences in Mathematical Formulations of EKF and UKF Procedures

The main differences between the EKF and UKF procedure is in the prediction step, i.e., prediction of state vector and its error covariance using mathematical model of the system. However, they are the same in updating step, i.e., updating the predicted state vector and its error covariance using available measurements.

In the prediction step of EKF, Jacobian matrices are used to linearize the nonlinear equations so that the linear KF can be used. However, in the prediction step of UKF, a number of state vectors or so-called sigma points is generated and then propagated through the nonlinear equations to get more accurate estimate.

Thus, to implement the EKF procedure, instead of using Equation (3.13) through Equation (3.21) of the UKF procedure, the following equations are necessary.

The nonlinear dynamic equation is expanded as a Taylor series about the estimate $\hat{\mathbf{Z}}_{k|k}$. By neglecting second and higher order terms, the predicted state vector $\hat{\mathbf{Z}}_{k+1|k}$ and its error covariance matrix $\mathbf{P}_{k+1|k}$ can be estimated as:

$$\hat{\mathbf{Z}}_{k+1|k} = \hat{\mathbf{Z}}_{k|k} + \int_{k\Delta t}^{(k+1)\Delta t} f\left(\hat{\mathbf{Z}}_{t|k}, t\right) dt \tag{3.43}$$

and

$$\mathbf{P}_{k+1|k} = \mathbf{\Phi}_{k+1|k}\, \mathbf{P}_{k|k}\, \mathbf{\Phi}_{k+1|k}^{\mathrm{T}} \tag{3.44}$$

where $\mathbf{\Phi}_{k+1|k}$ is the Jacobian matrix of the state transition of the system and can be written in an approximate form as:

$$\mathbf{\Phi}_{k+1|k} = \mathbf{I} + \Delta \mathrm{t} \left[\frac{\partial f(\mathbf{Z}_t, \mathrm{t})}{\partial \mathbf{Z}_t}\right]_{\mathbf{Z}_t = \hat{\mathbf{Z}}_{k|k}} \tag{3.45}$$

in which **I** is a unit matrix.

It is important to point out here that in this study the measurement model is linear and linear KF is used to predict the measurement vector and its error covariance matrix. Therefore, Equation (3.22) to Equation (3.24) will be used for prediction of the measurement in the EKF procedure.

3.7 Illustrative Example

Before verifying the proposed UKF-WGI method in evaluating structural health, it will be informative to demonstrate the implications of using UKF and EKF-based procedures for nonlinear system identification. A simple example is presented below to demonstrate the effect of nonlinearity on the state estimation using these procedures. The following nonlinear function is considered:

$$y = f(x) = 100\sin(x) \tag{3.46}$$

Suppose that *x* is a normal random variable with mean of 1.1 *rad* and variance P_x of 0.16 $(rad)^2$. The mean and variance of *y* are needed to be estimated.

The true mean $\bar{y}_T$ and variance $P_{y,T}$ can be calculated using the following equations as:

$$\bar{y}_T = E[f(x)] = \int_{-\infty}^{\infty} f(x) \cdot \frac{1}{\sigma_x\sqrt{2\pi}} e^{-\frac{1}{2}\left(\frac{x-\bar{x}}{\sigma_x}\right)^2} dx \tag{3.47}$$

and

$$P_{y,T} = E[(f(x) - E[f(x)])^2] \tag{3.48}$$

For UKF, three sigma points are propagated through the nonlinear function and the mean and variance of *y* are calculated as a weighted average using the sigma points. The mean and variance of *y* using EKF, denoting them as $\bar{y}_E$ and $P_{y,E}$, respectively, can be shown to be:

$\bar{y}_E = f(\bar{x}) = 100\sin(\bar{x})$

$P_{y,E} = (\nabla f)P_x(\nabla f)^T = [100\cos(\bar{x})](0.16)[100\cos(\bar{x})]$

True mean and variance of *y* along with values obtained by UKF and EKF are shown in Table 3.1. The propagations of uncertainties using UKF and EKF are shown in Figure 3.4. It can be observed that UKF approximates the propagation of the uncertainty in terms of the probability density function (PDF) through the nonlinearity more accurately than EKF. Since in general $\bar{y} \neq f(\bar{x})$, the mean value obtained by EKF introduces significant error. The superiority of UKF over EKF in propagating uncertainty for a highly nonlinear function can be clearly seen in Figure 3.4.

Table 3.1 Comparison between true and predicted mean and variance of $y = 100\sin(x)$

	True	UKF	EKF
Mean of *y*	82.27	82.09	89.12
Variance of *y*	368.54	411.00	329.20

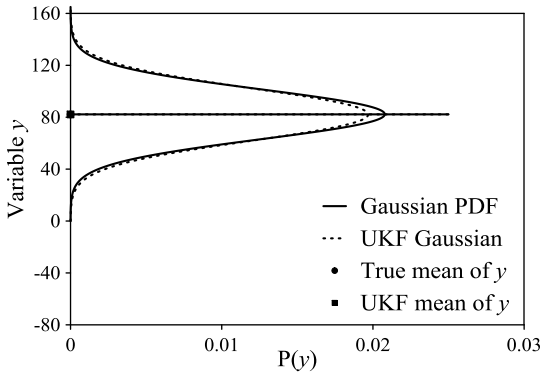

(i) Gaussian PDF of y

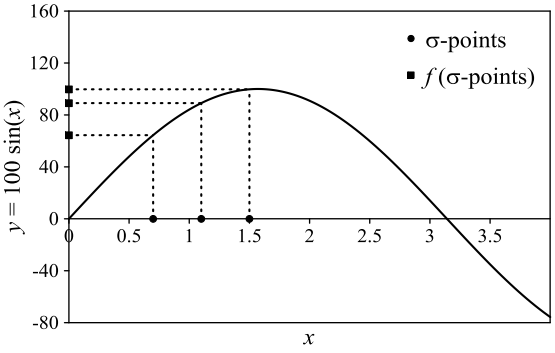

(ii) Sigma points

(a) Propagation of uncertainty using UKF

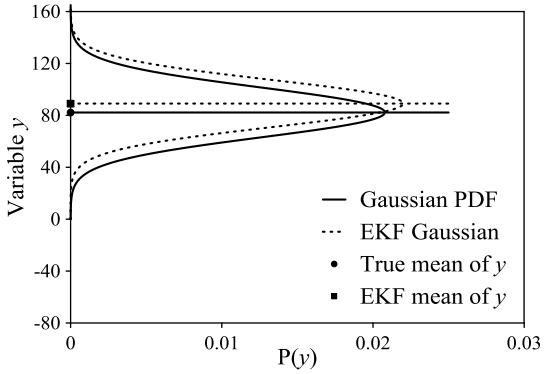

(i) Gaussian PDF of y

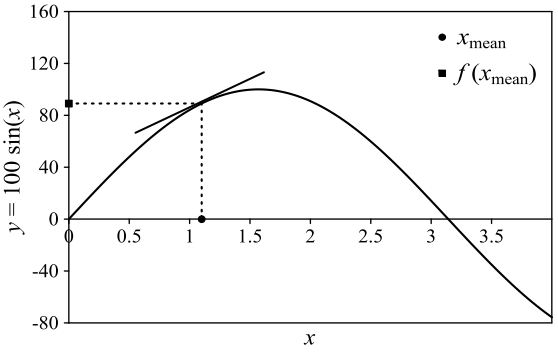

(ii) Linearization

(b) Propagation of uncertainty using EKF

Figure 3.4 Propagation of uncertainties using UKF and EKF

CHAPTER 4

VERIFICATION OF UKF-WGI TO HEALTH ASSESSMENT OF LARGE STRUCTURAL SYSTEMS

4.1 Introduction

In this chapter, the accuracy and effectiveness of the UKF-WGI procedure are demonstrated with the help of health assessment problems for relatively large realistic structural systems. The capability of the procedure for health assessment of structural systems exhibiting nonlinear behavior is also investigated. An attempt is made to identify the structures using absolute minimum number of measured responses, collected only over a short period of time. Both noise-free and noise-contaminated response information is considered. For appropriate verification, both defect-free and defective states of the structure are considered. Different defect scenarios of the structure are considered including small and relatively large defects introduced at single or multiple member(s) in the structure. Then, the capability of the method to detect the health of the structure is examined.

To demonstrate the superiority of the proposed UKF-WGI method, it is compared with the EKF-WGI procedure.

4.2 Health Assessment of Structural System

4.2.1 Description of the Frame

A one-bay three-story steel frame, as shown in Figure 4.1, is considered. The same frame was tested in the laboratory by the research team at the University of Arizona (Martinez-Flores and Haldar, 2007). To fit the testing facilities, the frame was scaled to

one-third of its actual dimensions. The scaled frame has a bay width of 3.05 m and story height of 1.22 m. The frame consists of 9 members; 6 columns and 3 beams. Steel section of size S4x7.7 was used for all the beams and columns in order to minimize the effects of fabrication defects and differences in material properties. The frame is represented by the finite element (FE) with 9 elements and 8 nodes. Each node has three DDOFs; two translational and one rotational. The support condition at the bases is considered to be fixed. Therefore, the total number of DDOFs for the frame is 18. The actual stiffness parameters k_i, defined in terms of (E_iI_i/L_i), for the beam and column are estimated to be 96500 N-m and 241250 N-m, respectively. The first two natural frequencies of the defect-free frame are estimated to be f_1 = 9.8985 Hz and f_2 = 34.767 Hz. Then, the two Rayleigh damping coefficients a and b are estimated using the procedure suggested by Clough and Penzien (2003). The value of a and b is found to be 1.1628328 and 0.00008559, respectively corresponding to 1.201% of the modal critical damping ratio.

In this example, the frame is considered to behave linearly. As discussed earlier, although the structural system is linear, the estimation of the unknown parameters jointly with nonlinear dynamic responses in the state is a nonlinear estimation problem. The frame is excited by the same excitation load used during testing (Martinez-Flores, 2005). The sinusoidal excitation is $f(t) = 1.4 \sin(58.23t)$ N applied at node 1 as shown in Figure 4.2. The responses are generated numerically using commercial software ANSYS (ver. 15). The responses in terms of displacement, velocity, and acceleration time-histories are recorded at 9 DDOFs (nodes 1, 2, and 3) from 0.02 to 0.32 s with sampling interval of 0.00025 s providing 1201 time points. The horizontal and vertical responses of defect-

free frame at node 1 for the duration of 0.5 s are shown in Figures 4.3 and 4.4, respectively.

In practical inspections, the measured excitation load and responses are expected to be noise-contaminated. To explore the capability of the proposed procedure for structural identification in the presence of noise, numerically generated zero-mean additive Gaussian white noise with intensity of 5%, 10%, and 20% of the root mean square (RMS) values of the simulated load and responses (acceleration, velocity, and displacement) at each DDOF are added separately to the corresponding load and responses.

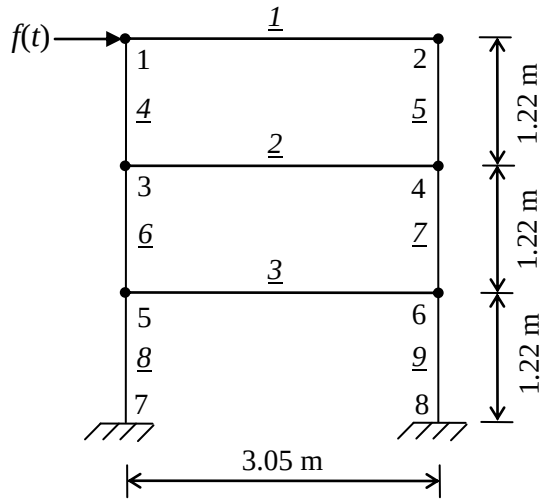

Figure 4.1 Finite element representation of one-bay three-story frame

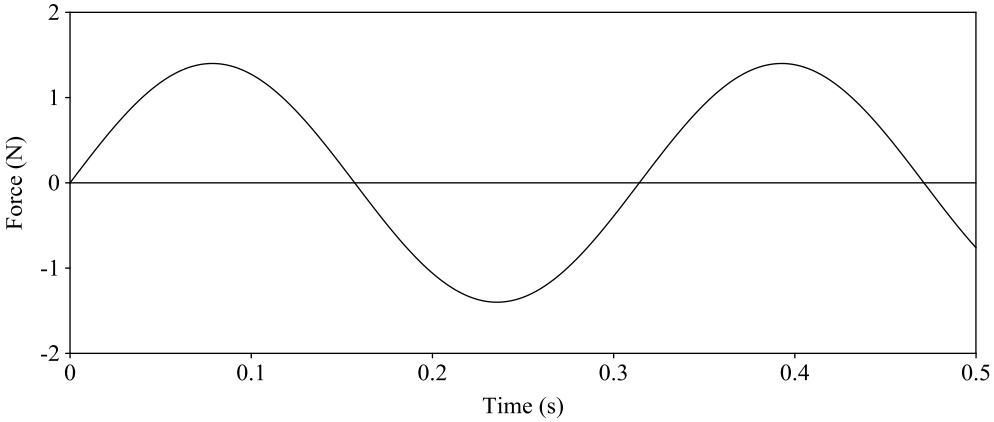

Figure 4.2 Sinusoidal force applied horizontally at node 1

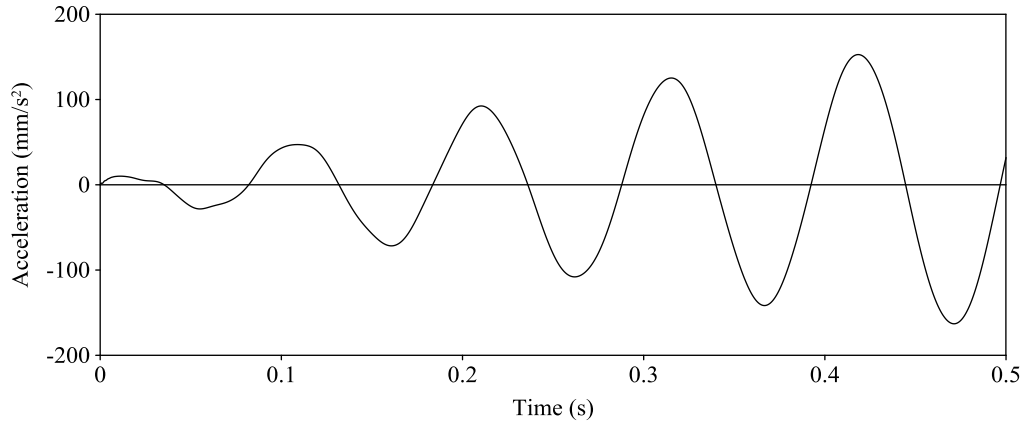

(a)

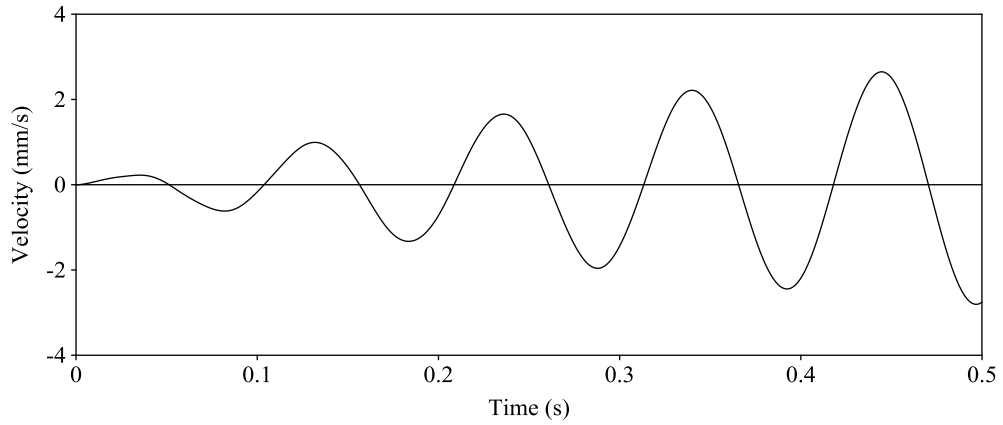

(b)

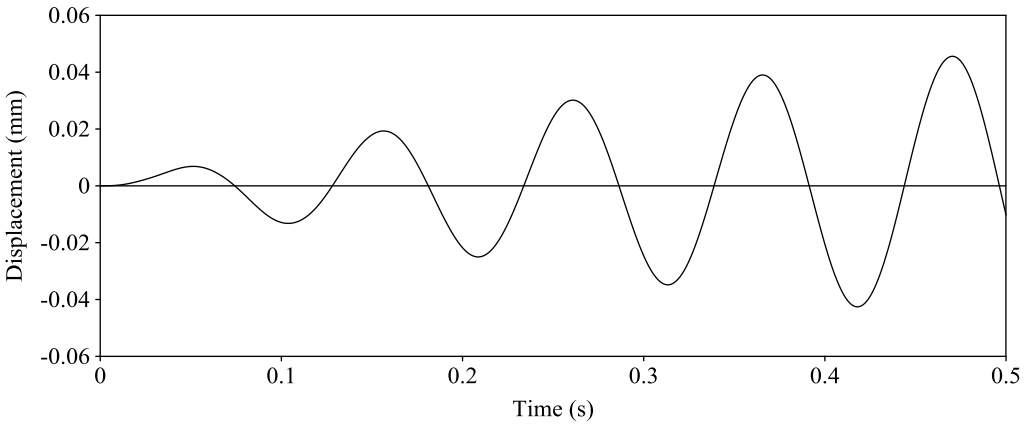

(c)

Figure 4.3 Horizontal responses at node 1; (a) Acceleration; (b) Velocity; and (c) Displacement

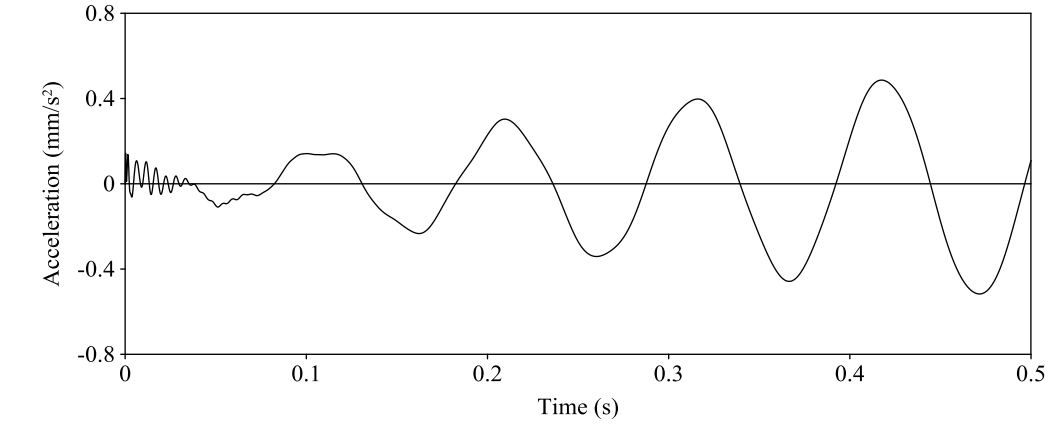

(a)

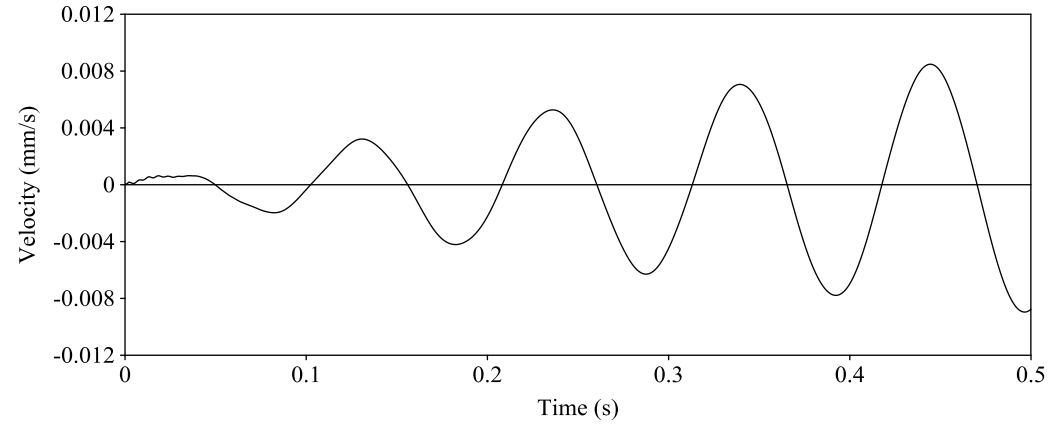

(b)

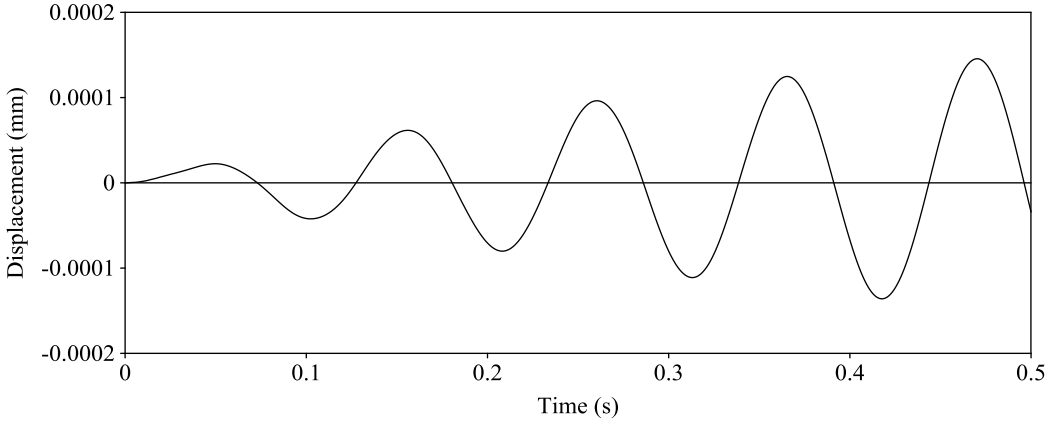

(c)

Figure 4.4 Vertical responses at node 1; (a) Acceleration; (b) Velocity; and (c) Displacement

4.2.2 Health Assessment of Frame

The effectiveness of the proposed UKF-WGI procedure for structural health assessment in the presence of different levels of noise is examined by considering different state of the structure. Then, in order to demonstrate its superiority, the results of the UKF-WGI procedure are compared with the results of the EKF-WGI procedure. The following cases are considered:

1. Defect-free frame
2. Defect 1: defect in a single member
3. Defect 2: defects in multiple members

4.2.2.1 Health Assessment of Defect-Free Frame

Initially the procedures are verified by identifying the defect-free frame. The number of responses used to identify the frame is only 9; responses at nodes 1, 2, and 3. The initial values of the stiffness parameters for all the elements in the frame are considered to be the nominal values. The diagonal of the initial error covariance of the displacement and velocity, $\mathbf{P}_x(0|0)$, and the initial error covariance matrix of the stiffness parameters, $\mathbf{P}_s(0|0)$, are considered to be 10^{-3} and 10^{3}, respectively. The dynamic responses generated theoretically from ANSYS are assumed to have a very small amount of noise. Accordingly, a value of 10^{-4} is considered in the diagonal of the covariance matrix of measurement noise vector, $\mathbf{R}_k$. A value of 10^{-2} is considered to $\mathbf{R}_k$ for all the other three noise cases (5%, 10%, and 20%) since the level of noises in the responses are expected to be unknown during the inspection. A value of 10 for the weight factor, *w*, has been used in this example.

Using the above information, the stiffness parameters of all the elements in the structure are identified for all noise level cases using the UKF-WGI procedure. The results of the identification are presented in Table 4.1. The error is defined as percentage change in identified stiffness parameter with respect to the actual value. The acceptable error in the identification process was reported to be about 10% (Hoshiya and Saito 1984; Toki et al., 1989; Koh et al., 1991). For all four noise cases, the errors in the identification are much smaller than the acceptable error. It can be observed that the error in identification increases as noise level increase as expected. Since the changes in stiffness parameter identification for all four cases are very small among the members, it is clear that the algorithm identified the state of the frame as defect free accurately.

The same frame is then identified using the EKF-WGI procedure and the results of identified stiffness parameters are summarized in Table 4.2. The maximum error in the identification is still within the acceptable level but the results are less accurate than that of the proposed method. For this case also, the defect-free state can be predicted.

Table 4.1 Stiffness parameter (*EI/L*) identification using UKF-WGI for defect-free

Member	Nominal (N-m)	RMS noise intensity							
		0%		5%		10%		20%	
		Identified (N-m)	Change (%)	Identified (N-m)	Change (%)	Identified (N-m)	Change (%)	Identified (N-m)	Change (%)
(1)	(2)	(3)	(4)	(5)	(6)	(7)	(8)	(9)	(10)
k_1	96500	96505	0.01	96410	-0.09	96362	-0.14	96293	-0.21
k_2	96500	96513	0.01	96305	-0.20	96191	-0.32	96049	-0.47
k_3	96500	96491	-0.01	96333	-0.17	96046	-0.47	95418	-1.12
k_4	241250	241318	0.03	241186	-0.03	241088	-0.07	240874	-0.16
k_5	241250	241321	0.03	241198	-0.02	241098	-0.06	240894	-0.15
k_6	241250	241443	0.08	241227	-0.01	241163	-0.04	241058	-0.08
k_7	241250	241269	0.01	241239	0.00	241234	-0.01	241261	0.00
k_8	241250	241223	-0.01	241264	0.01	241258	0.00	241199	-0.02
k_9	241250	241240	0.00	241269	0.01	241262	0.00	241166	-0.03
Note:	$P_x(0\|0) = 10^{-3}$; $P_s(0\|0) = 10^3$; $w = 10$								

Table 4.2 Stiffness parameter (*EI/L*) identification using EKF-WGI for defect-free

Member	Nominal (N-m)	RMS noise intensity							
		0%		5%		10%		20%	
		Identified (N-m)	Change (%)	Identified (N-m)	Change (%)	Identified (N-m)	Change (%)	Identified (N-m)	Change (%)
(1)	(2)	(3)	(4)	(5)	(6)	(7)	(8)	(9)	(10)
k_1	96500	96485	-0.02	96343	-0.16	96166	-0.35	95817	-0.71
k_2	96500	96686	0.19	96220	-0.29	95930	-0.59	95386	-1.15
k_3	96500	96308	-0.20	96388	-0.12	96223	-0.29	95895	-0.63
k_4	241250	241069	-0.07	241314	0.03	241387	0.06	241493	0.10
k_5	241250	239295	-0.81	241251	0.00	241051	-0.08	239893	-0.56
k_6	241250	241445	0.08	241229	-0.01	241181	-0.03	241103	-0.06
k_7	241250	240793	-0.19	241230	-0.01	241149	-0.04	240849	-0.17
k_8	241250	241795	0.23	241249	0.00	241227	-0.01	241159	-0.04
k_9	241250	241533	0.12	241286	0.01	241334	0.03	241377	0.05
Note:	$P_x(0\|0) = 10^{-3}$; $P_s(0\|0) = 10^3$; $w = 10$								

4.2.2.2 Health Assessment of Defective Frame - Defect 1

After successfully assessing structural health of the defect-free frame, the defective state of the frame is considered. In Defect 1, member 3 connecting nodes 5 and 6, is considered to be defective. The moment of inertia of the member over the entire length is considered to be reduced by 20% of the defect-free value. The values of the parameters required to initiate the procedure, i.e., $P_x(0|0)$, $P_s(0|0)$, and w are indicated at the bottom of Table 4.3 and the value of R_k is considered to 10^{-4} for noise free and 10^{-2} for all the noise cases. The responses are considered to be available at 9 DDOFs.

First, the UKF-WGI procedure is implemented to identify the health of the frame using noise-free excitation load and responses. The identified stiffness parameters and corresponding changes in identification are shown in Columns 3 and 4 of Table 4.3, respectively. The bold values in the table represent the reduction in the identified stiffness parameter of defective member. The maximum reduction in stiffness parameters is about 20% for member 3 indicating UKF-WGI accurately identified the location and the severity of the defects.

Then, the procedure is implemented to identify the frame using noise-contaminated load and responses with different level of noises, i.e., 5%, 10%, and 20% RMS. The results are summarized in Columns 5-10 of Table 4.3. For all cases, the maximum reductions in stiffness parameters are in member 3 indicating that it is defective. It can be seen that as the levels of noise increase the errors in the identification also increase. However, it is still within the acceptable errors.

The EKF-WGI procedure is then used to identify the frame considering the same information considered above. The results of identification are shown in Table 4.4. For

noise-free case, EKF-WGI is capable of identifying the defect but not as accurate as UKF-WGI. However, the results of all three noise cases show that the reduction in stiffness parameters is not only at defective member 3 but also in other members indicating erroneously there are more than one defective member. For an example, for 5% RMS noise case, in addition to 23.65% reduction in the stiffness parameter of member 3, the stiffness parameter of member 8 is also reduced by 17.54%. Moreover, the stiffness parameter of member 9 is increased by 31.31%. Similar observations can be made for the other two noise cases. Therefore, the EKF-WGI procedure failed to identify the state of each member in the frame in the presence of noise.

This example clearly shows the superiority of the UKF-WGI over the EKF-WGI procedure for structural system identification in the presence of noise.

Table 4.3 Stiffness parameter (*EI/L*) identification using UKF-WGI for Defect 1

Member	Nominal (N-m)	RMS noise intensity							
		0%		5%		10%		20%	
		Identified (N-m)	Change (%)	Identified (N-m)	Change (%)	Identified (N-m)	Change (%)	Identified (N-m)	Change (%)
(1)	(2)	(3)	(4)	(5)	(6)	(7)	(8)	(9)	(10)
k_1	96500	96263	-0.25	96919	0.43	97038	0.56	97032	0.55
k_2	96500	96969	0.49	95024	-1.53	94227	-2.36	93429	-3.18
k_3	96500	76627	**-20.59**	78683	**-18.46**	79683	**-17.43**	80639	**-16.44**
k_4	241250	240682	-0.24	240698	-0.23	241604	0.15	241906	0.27
k_5	241250	239884	-0.57	240962	-0.12	241026	-0.09	240925	-0.13
k_6	241250	244157	1.20	238680	-1.07	238975	-0.94	238838	-1.00
k_7	241250	241268	0.01	241130	-0.05	240614	-0.26	238902	-0.97
k_8	241250	241649	0.17	239461	-0.74	237193	-1.68	235022	-2.58
k_9	241250	242302	0.44	239286	-0.81	236086	-2.14	231637	-3.98
Note:	$P_x(0\|0) = 10^{-3}$; $P_s(0\|0) = 10^3$; $w = 10$								

Table 4.4 Stiffness parameter (*EI/L*) identification using EKF-WGI for Defect 1

Member	Nominal (N-m)	RMS noise intensity							
		0%		5%		10%		20%	
		Identified (N-m)	Change (%)	Identified (N-m)	Change (%)	Identified (N-m)	Change (%)	Identified (N-m)	Change (%)
(1)	(2)	(3)	(4)	(5)	(6)	(7)	(8)	(9)	(10)
k_1	96500	94945	-1.61	96411	-0.09	97187	0.71	94996	-1.56
k_2	96500	99304	2.91	96772	0.28	93366	-3.25	89659	-7.09
k_3	96500	74172	**-23.14**	73675	**-23.65**	80781	**-16.29**	83675	**-13.29**
k_4	241250	235757	-2.28	239274	-0.82	247353	2.53	250808	3.96
k_5	241250	229016	-5.07	229140	-5.02	218309	-9.51	213968	-11.31
k_6	241250	253566	5.10	236950	-1.78	238643	-1.08	237288	-1.64
k_7	241250	235208	-2.50	218070	-9.61	228426	-5.32	231908	-3.87
k_8	241250	247922	2.77	198924	-17.54	219542	-9.00	226070	-6.29
k_9	241250	244776	1.46	316792	31.31	257691	6.81	247382	2.54
Note:	$P_x(0\|0) = 10^{-3}$; $P_s(0\|0) = 10^3$; $w = 10$								

4.2.2.3 Health Assessment of Defective Frame - Defect 2

In Defect 2, two members at a time in the frame are considered to be defective. The moment of inertia of the members 1 and 2 over the entire length is considered to be reduced by 20% and 10%, respectively of the defect-free value. The value of parameters required to initiate the procedure is the same as that in the previous example. The results of identification for noise free and three noise levels using the UKF-WGI and EKF-WGI procedure are shown in Tables 4.5 and 4.6, respectively. All the observations made for Defect 1 in the previous section are also applicable for this defective state. However, for this example of multiple defects, the EKF-WGI also failed to identify the state of each member in the frame for noise free case.

Table 4.5 Stiffness parameter (*EI/L*) identification using UKF-WGI for Defect 2

Member	Nominal (N-m)	RMS noise intensity							
		0%		5%		10%		20%	
		Identified (N-m)	Change (%)	Identified (N-m)	Change (%)	Identified (N-m)	Change (%)	Identified (N-m)	Change (%)
(1)	(2)	(3)	(4)	(5)	(6)	(7)	(8)	(9)	(10)
k_1	96500	77203	**-20.00**	77721	**-19.46**	78301	**-18.86**	80423	**-16.66**
k_2	96500	86919	**-9.93**	86741	**-10.11**	86520	**-10.34**	86181	**-10.69**
k_3	96500	96360	-0.15	94311	-2.27	93410	-3.20	92307	-4.35
k_4	241250	241318	0.03	239346	-0.79	237507	-1.55	235219	-2.50
k_5	241250	241238	0.00	239937	-0.54	237433	-1.58	233405	-3.25
k_6	241250	242274	0.42	241893	0.27	242571	0.55	242798	0.64
k_7	241250	241388	0.06	243410	0.90	245494	1.76	246269	2.08
k_8	241250	241236	-0.01	246172	2.04	247880	2.75	249293	3.33
k_9	241250	241333	0.03	246211	2.06	246695	2.26	244809	1.48
Note:	$P_x(0\|0) = 10^{-3}$; $P_s(0\|0) = 10^3$; $w = 10$								

Table 4.6 Stiffness parameter (*EI/L*) identification using EKF-WGI for Defect 2

Member	Nominal (N-m)	RMS noise intensity							
		0%		5%		10%		20%	
		Identified (N-m)	Change (%)	Identified (N-m)	Change (%)	Identified (N-m)	Change (%)	Identified (N-m)	Change (%)
(1)	(2)	(3)	(4)	(5)	(6)	(7)	(8)	(9)	(10)
k_1	96500	74638	**-22.65**	77078	**-20.13**	79073	**-18.06**	81938	**-15.09**
k_2	96500	92335	**-4.32**	88454	**-8.34**	85913	**-10.97**	86821	**-10.03**
k_3	96500	88342	-8.45	86693	-10.16	94015	-2.58	92705	-3.93
k_4	241250	231541	-4.02	238114	-1.30	238663	-1.07	241588	0.14
k_5	241250	217217	-9.96	229054	-5.06	216972	-10.06	212742	-11.82
k_6	241250	266857	10.61	241230	-0.01	240846	-0.17	239025	-0.92
k_7	241250	219562	-8.99	218247	-9.53	231592	-4.00	232941	-3.44
k_8	241250	259686	7.64	213427	-11.53	238268	-1.24	240506	-0.31
k_9	241250	252736	4.76	330462	36.98	263757	9.33	253145	4.93
Note:	$P_x(0\|0) = 10^{-3}$; $P_s(0\|0) = 10^3$; $w = 10$								

4.3 Health Assessment of Geometrically Nonlinear Structural System

4.3.1 Description of the Problem

The frame shown in Figure 4.1 is considered again; however, it is considered to behave geometrically nonlinear in this example. The frame is considered to be excited by similar excitation load conducted experimentally by Martinez-Flores (2005) but with much higher amplitude to force the frame to behave nonlinear. The excitation is $f(t) = 1.4 \sin(58.23t)$ kN applied at node 1 as shown in Figure 4.5. For the theoretical verification of the methods, the responses of the frame in the presence of geometric nonlinearity are generated numerically using commercial software ANSYS (ver. 15). The responses in terms of displacement, velocity, and acceleration time-histories are recorded at 9 DDOFs (nodes 1, 2, and 3) from 0.02 to 0.32 s with sampling interval of 0.00025 s providing 1201 time points. The horizontal and vertical responses of defect-free frame at node 1 for duration of 0.5 s are shown in Figures 4.6 and 4.7, respectively.

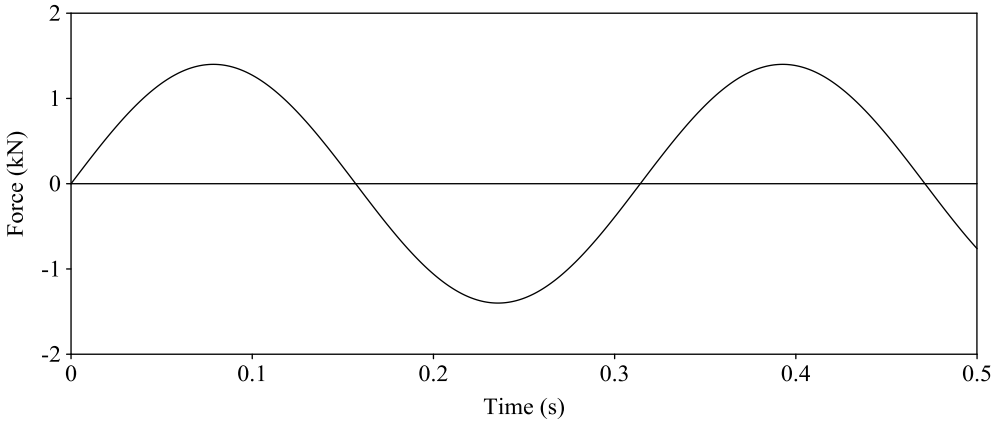

Figure 4.5 Sinusoidal force applied horizontally at node 1

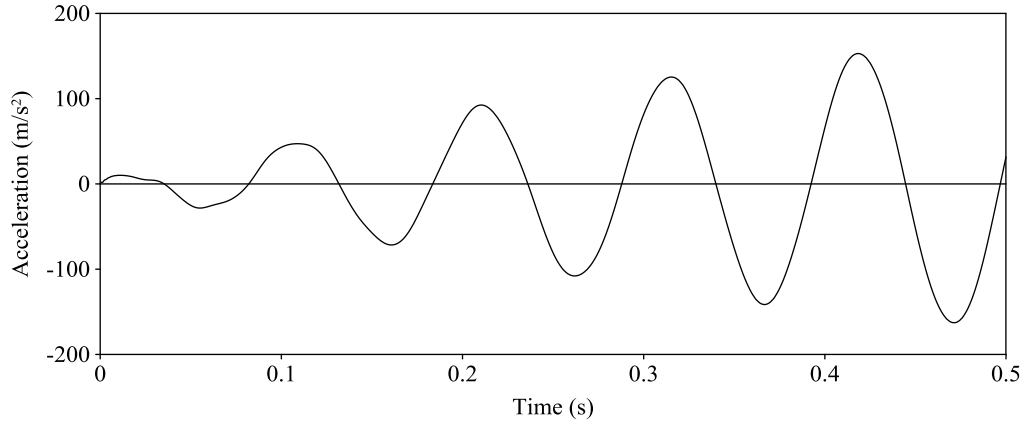

(a)

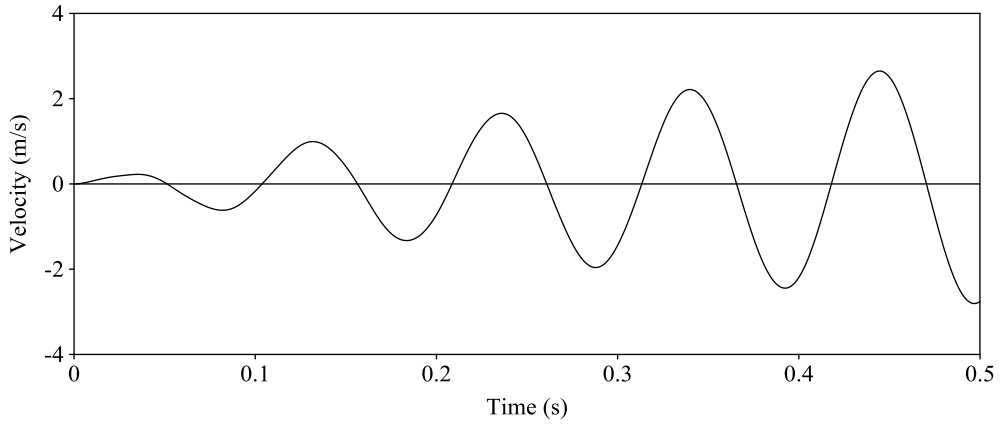

(b)

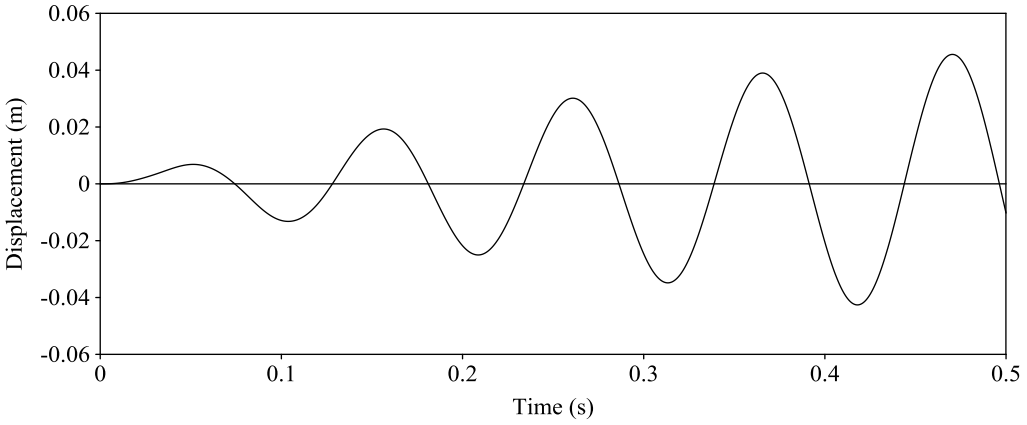

(c)

Figure 4.6 Horizontal responses at node 1; (a) Acceleration; (b) Velocity; and (c) Displacement

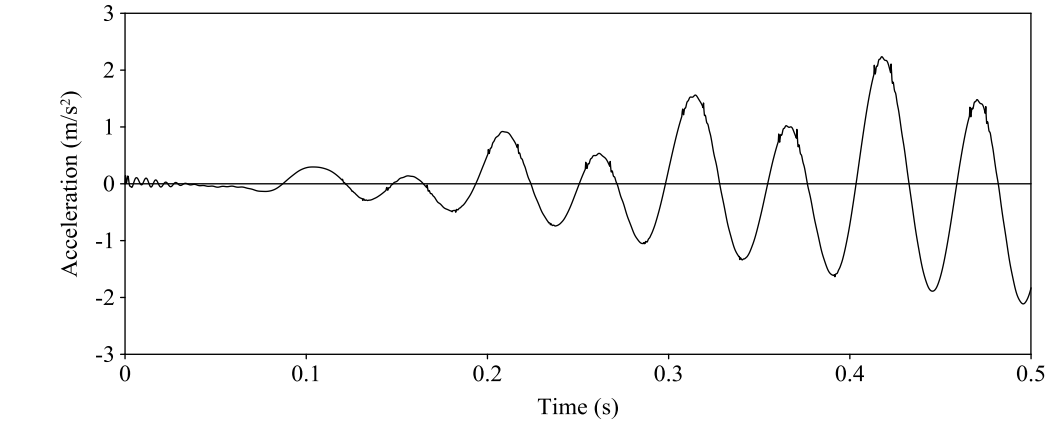

(a)

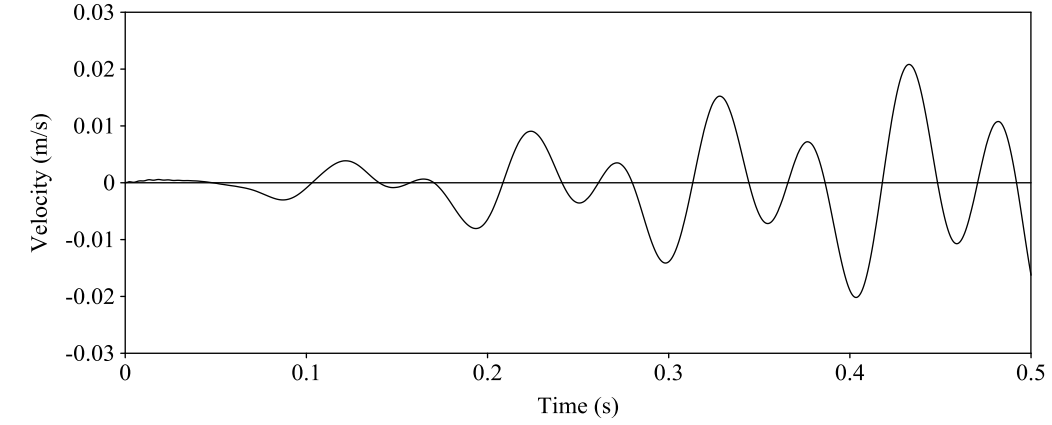

(b)

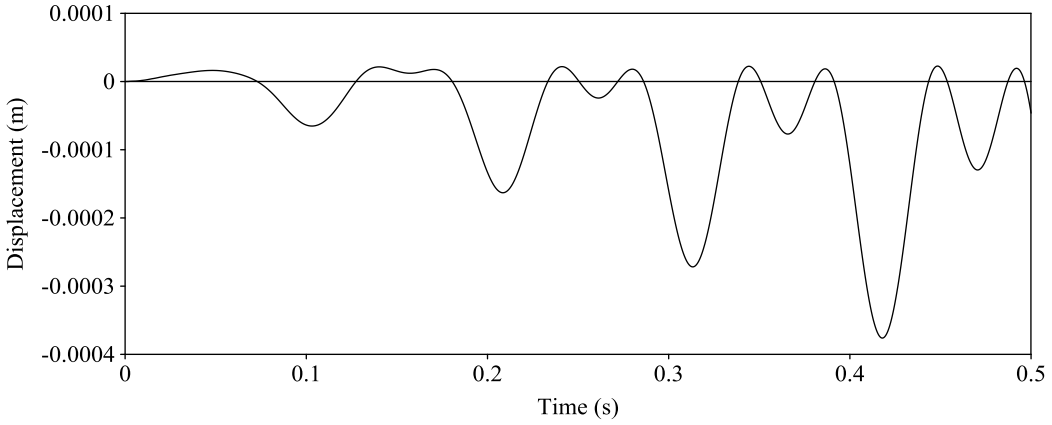

(c)

Figure 4.7 Vertical responses at node 1; (a) Acceleration; (b) Velocity; and (c) Displacement

4.3.2 Health Assessment of Frame

The capabilities of the proposed UKF-WGI procedure are examined and compared with the EKF-WGI procedure in the presence of geometric nonlinearity by considering the following cases:

1. Defect-free and a small defect in a single member
2. Moderate to severe defect in a single member
3. Defects in multiple members

4.3.2.1 Defect-Free and a Small Defect in a Single Member

Initially the frame is considered to be defect-free. The number of responses used to identify the frame is 9 as mentioned in the previous example. The diagonal of the covariance matrix of measurement noise vector, $\mathbf{R}_k$, the initial error covariance of the displacement and velocity, $\mathbf{P}_x(0|0)$, the initial error covariance matrix of the stiffness parameters, $\mathbf{P}_s(0|0)$, and the weight factor, *w*, are considered to be 10^{-4}, 10^{-3}, 10^{3}, and 10, respectively.

Using only responses at 9 DDOFs (nodes 1, 2, and 3), the stiffness parameters of all the members in the frame are identified for the defect-free state using UKF-WGI. The results of identified stiffness parameters are summarized in Column 3 of Table 4.7 and the errors in identification are summarized in Column 4 of Table 4.7. The maximum error in the identification is 0.08%. Obviously, the proposed UKF-WGI is very accurate. Since the identified stiffness parameters did not vary significantly from one member to another and from the expected values, the proposed method correctly identified the defect-free state of the frame.

The same frame is then identified using the EKF-WGI procedure and the results of identified stiffness parameters and corresponding errors are summarized in Columns 3 and 4, respectively of Table 4.8. The maximum error in the identification is 0.81%. It is still within the acceptable level but not as good as the proposed method.

After the successful verification of the defect-free state, the following two defect scenarios are considered:

a. Defect 1 - loss of cross-sectional area over a finite length in member 3
b. Defect 2 - reduction in stiffness of member 3 by 10%

For Defect 1, the cross-sectional area of member 3 is considered to be corroded over a length of 20 cm, located at a distance of 0.5 m from node 5, as shown in Figure 4.8. The web and flange thicknesses are considered to be reduced by 40% of their original values. The loss of thicknesses will result in the reduction of the cross-sectional area by 38.70% and the moment of inertia by 35.46% from the nominal values. For Defect 2, the moment of inertia of member 3 over the entire length is considered to be reduced by 10% of the defect-free value.

Using only responses at 9 DDOFs (nodes 1, 2, and 3), the stiffness parameters of all members in the frame are identified for the two defective cases using both UKF-WGI and EKF-WGI procedures. The results of UKF-WGI and EKF-WGI are summarized in Tables 4.7 and 4.8, respectively. The bold values in the table represent the reduction in the identified stiffness parameter of defective member. The results indicate that both procedures identified the location and severity of defects correctly.

It can be concluded that both methods are capable of identifying the state of the frame if it is defect-free or having a small defect in a single member.

As mentioned earlier, defects are assessed by tracking the changes in the responses. To show those changes, the responses, i.e., acceleration, velocity, and displacement, along horizontal direction at node 1 are compared in Figure 4.9 among defect-free and Defects 1 and 2.

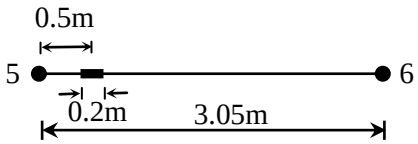

Figure 4.8 Defect 1 representation

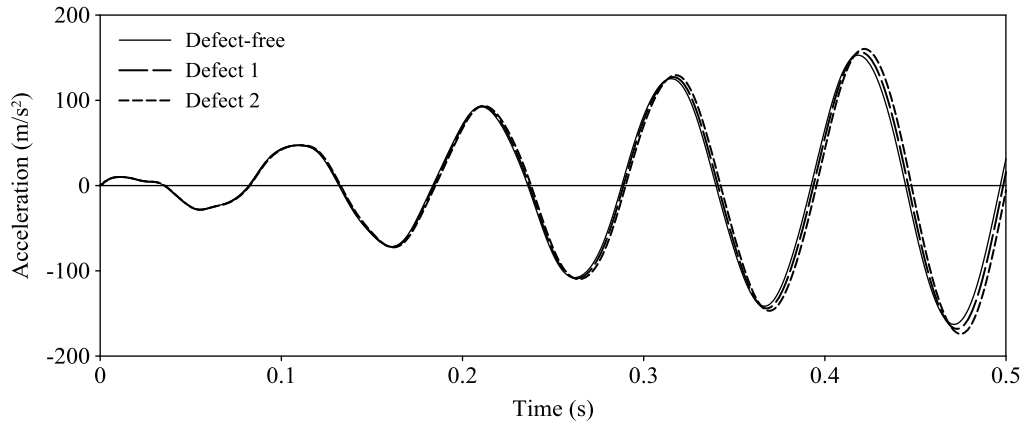

(a)

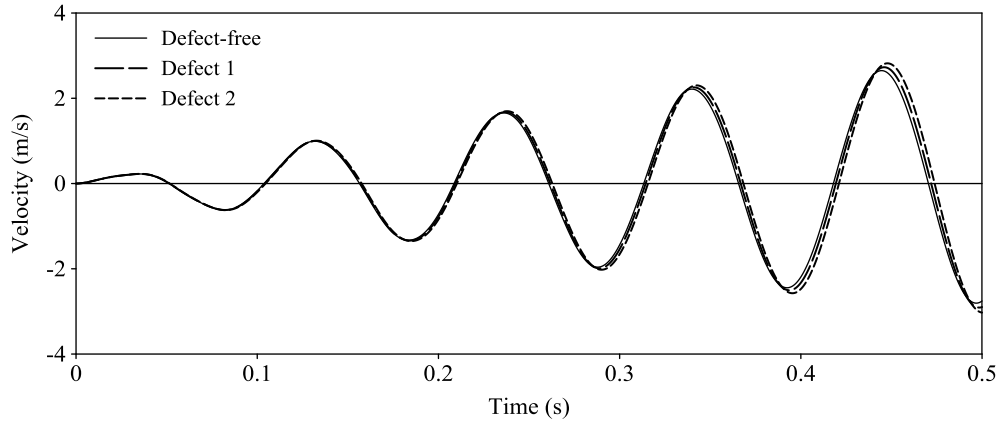

(b)

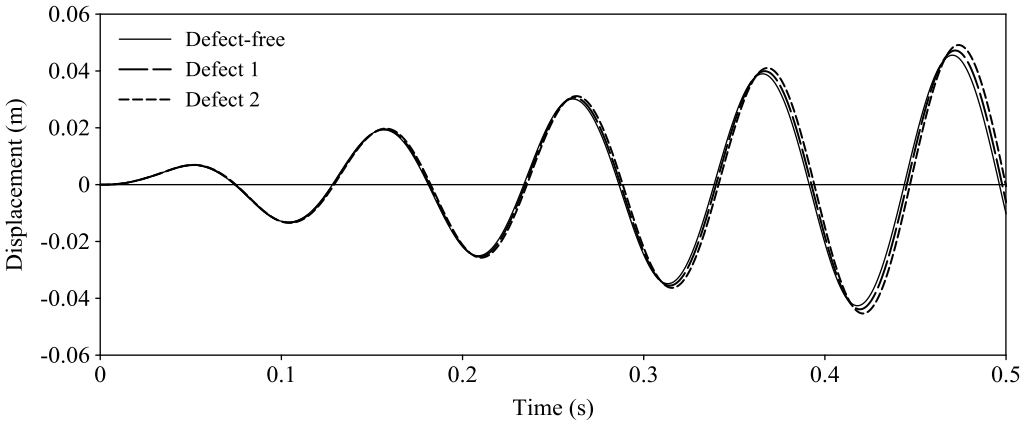

(c)

Figure 4.9 Horizontal responses at node 1 for defect-free and Defects 1 and 2;

(a) Acceleration; (b) Velocity; and (c) Displacement

Table 4.7 Stiffness parameter (*EI/L*) identification for defect-free and small defect using UKF-WGI

Member	Theoretical (N-m)	Defect-Free		Defect 1		Defect 2	
		Identified (N-m)	Change (%)	Identified (N-m)	Change (%)	Identified (N-m)	Change (%)
(1)	(2)	(3)	(4)	(5)	(6)	(7)	(8)
k_1	96500	96505	0.01	96435	-0.07	96571	0.07
k_2	96500	96513	0.01	96580	0.08	96390	-0.11
k_3	96500	96491	-0.01	92386	**-4.26**	87241	**-9.59**
k_4	241250	241318	0.03	241460	0.09	241726	0.20
k_5	241250	241321	0.03	241084	-0.07	241851	0.25
k_6	241250	241443	0.08	240817	-0.18	241557	0.13
k_7	241250	241269	0.01	241217	-0.01	241365	0.05
k_8	241250	241223	-0.01	240459	-0.33	240032	-0.50
k_9	241250	241240	0.00	240436	-0.34	240290	-0.40
Note:	$R_k = 10^{-4}$; $P_x(0\|0) = 10^{-3}$; $P_s(0\|0) = 10^3$; $w = 10$						

Table 4.8 Stiffness parameter (*EI/L*) identification for defect-free and small defect using EKF-WGI

Member	Theoretical (N-m)	Defect-Free		Defect 1		Defect 2	
		Identified (N-m)	Change (%)	Identified (N-m)	Change (%)	Identified (N-m)	Change (%)
(1)	(2)	(3)	(4)	(5)	(6)	(7)	(8)
k_1	96500	96485	-0.02	96453	-0.05	96706	0.21
k_2	96500	96686	0.19	96582	0.09	95978	-0.54
k_3	96500	96308	-0.20	92334	**-4.32**	87766	**-9.05**
k_4	241250	241069	-0.07	241065	-0.08	241035	-0.09
k_5	241250	239295	-0.81	239424	-0.76	240099	-0.48
k_6	241250	241445	0.08	240990	-0.11	240826	-0.18
k_7	241250	240793	-0.19	240699	-0.23	240443	-0.33
k_8	241250	241795	0.23	240960	-0.12	240061	-0.49
k_9	241250	241533	0.12	240726	-0.22	239880	-0.57
Note:	$R_k = 10^{-4}$; $P_x(0\|0) = 10^{-3}$; $P_s(0\|0) = 10^3$; $w = 10$						

4.3.2.2 Moderate to Severe Defect in a Single Member

In this case, the following three defective scenarios are considered:

a. Defect 3 - reduction in stiffness of member 3 by 20%
b. Defect 4 - reduction in stiffness of member 2 by 30%
c. Defect 5 - reduction in stiffness of member 1 by 80%

In these defects, the moment of inertia of the member over the entire length is considered to be reduced by the specified percentage from the defect-free value. The horizontal responses at node 1 are compared in Figure 4.10 among defect-free and Defects 3, 4, and 5. The results of all three defects using UKF-WGI and EKF-WGI are summarized in Tables 4.9 and 4.10, respectively. For Defect 3 with 20% reduction, both procedures appear to locate the defective member correctly. However, in detecting the severity of the defect, EKF-WGI is less accurate. Also, by considering the changes in the stiffness parameter of all the members, EKF-WGI is less conclusive. Differences of the two approaches become very significant for Defects 4 and 5.

In fact, one can conclude that EKF-WGI failed to identify the defective states. Changes in the stiffness parameter of defect-free members for Defect 4 are higher than the defective member. For Defect 5, one can erroneously conclude that more than one member are defective. An inspector should not have any such assessment difficulties if UKF-WGI is used. The proposed method is accurate and superior to EKF-WGI in every aspect.

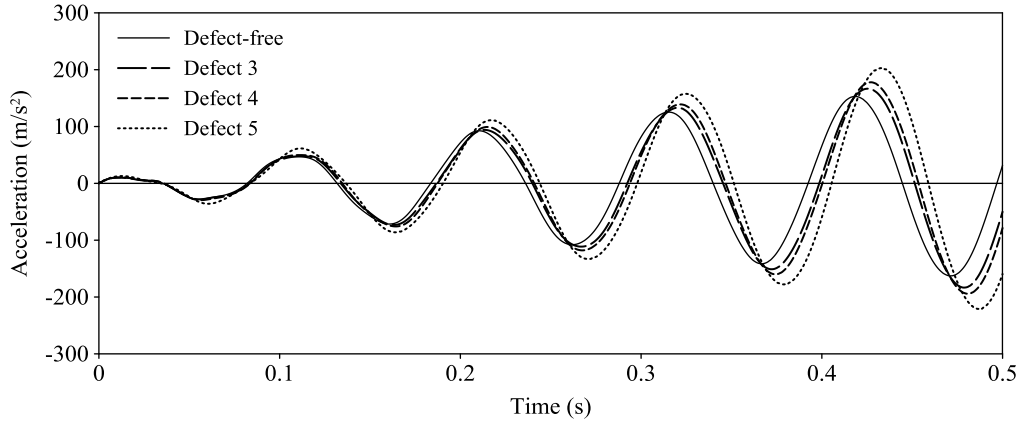

(a)

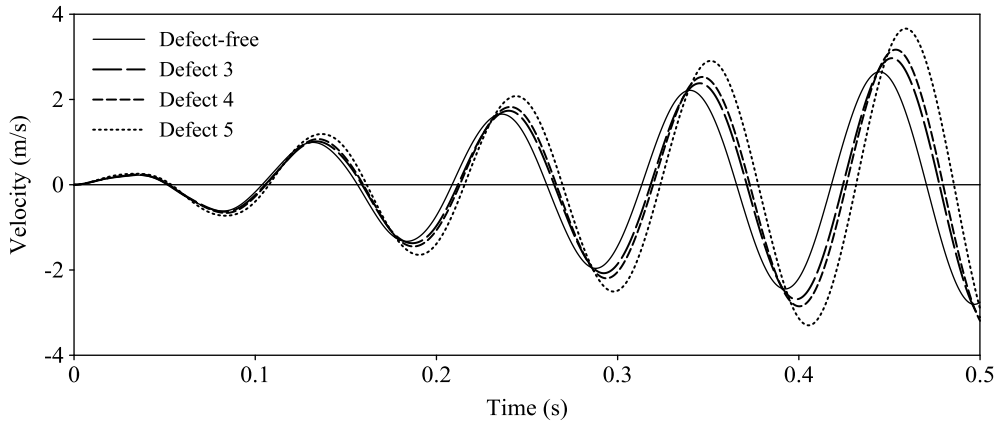

(b)

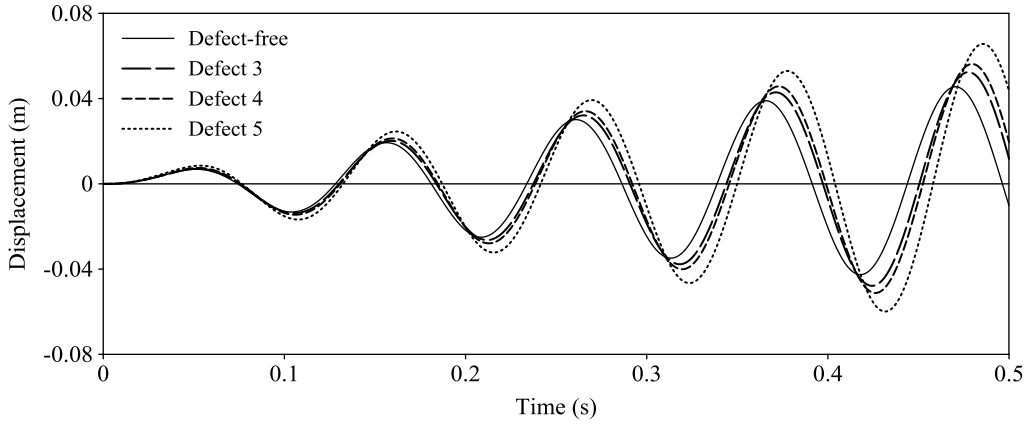

(c)

Figure 4.10 Horizontal responses at node 1 for defect-free and Defects 3, 4, and 5; (a) Acceleration; (b) Velocity; and (c) Displacement

Table 4.9 Stiffness parameter (*EI/L*) identification for moderate to severe defect using UKF-WGI

Member	Theoretical (N-m)	Defect 3		Defect 4		Defect 5	
		Identified (N-m)	Change (%)	Identified (N-m)	Change (%)	Identified (N-m)	Change (%)
(1)	(2)	(3)	(4)	(5)	(6)	(7)	(8)
k_1	96500	96703	0.21	95988	-0.53	19369	**-79.93**
k_2	96500	96129	-0.38	68224	**-29.30**	96065	-0.45
k_3	96500	78082	**-19.09**	95416	-1.12	97182	0.71
k_4	241250	242146	0.37	240138	-0.46	241213	-0.02
k_5	241250	242487	0.51	238831	-1.00	243095	0.76
k_6	241250	240756	-0.20	245811	1.89	239939	-0.54
k_7	241250	241487	0.10	238192	-1.27	245577	1.79
k_8	241250	239065	-0.91	239795	-0.60	238505	-1.14
k_9	241250	239076	-0.90	245816	1.89	240982	-0.11
Note:	$R_k = 10^{-4}$; $P_x(0\|0) = 10^{-3}$; $P_s(0\|0) = 10^3$; $w = 10$						

Table 4.10 Stiffness parameter (*EI/L*) identification for moderate to severe defect using EKF-WGI

Member	Theoretical (N-m)	Defect 3		Defect 4		Defect 5	
		Identified (N-m)	Change (%)	Identified (N-m)	Change (%)	Identified (N-m)	Change (%)
(1)	(2)	(3)	(4)	(5)	(6)	(7)	(8)
k_1	96500	94914	-1.64	89596	-7.15	18926	**-80.39**
k_2	96500	99334	2.94	77319	**-19.88**	102977	6.71
k_3	96500	74190	**-23.12**	79365	-17.76	80227	-16.86
k_4	241250	235770	-2.27	227074	-5.88	240830	-0.17
k_5	241250	229060	-5.05	205014	-15.02	203276	-15.74
k_6	241250	252869	4.82	283547	17.53	277569	15.05
k_7	241250	234577	-2.77	176189	-26.97	210000	-12.95
k_8	241250	246939	2.36	353955	46.72	356277	47.68
k_9	241250	245965	1.95	217192	-9.97	199653	-17.24
Note:	$R_k = 10^{-4}$; $P_x(0\|0) = 10^{-3}$; $P_s(0\|0) = 10^3$; $w = 10$						

4.3.2.3 Defects in Multiple Members

In this case, the following three defective scenarios are considered:

a. Defect 6 - reductions in stiffness of members 1 and 2 by 60% and 30%, respectively
b. Defect 7 - reductions in stiffness of members 2 and 3 by 25% and 15%, respectively
c. Defect 8 - reductions in stiffness of members 1, 2, and 3 by 30%, 20%, and 10%, respectively

In these defect scenarios, the moment of inertia of more than one member over the entire length is considered to be reduced by the specified percentage from the defect-free value. The horizontal responses at node 1 are compared in Figure 4.11 among defect-free and Defects 6, 7, and 8. The identified stiffness parameters of all the members for all the defect scenarios using UKF-WGI and EKF-WGI are summarized in Tables 4.11 and 4.12, respectively. All the observations made for Defects 3-5 in the previous section are also applicable for these defective states. The proposed UKF-WGI not only identified the defective members correctly, it also estimated the severity of the defects accurately. On the other hand, EKF-WGI failed to identify the frame and cannot be used for the SHA of the frame under consideration.

From the examples given, it can be concluded that the applicability of the two procedures will depend on the level of nonlinearity, which depends on the severity of the defects and the level of geometric nonlinearity. Both methods will be appropriate for weakly nonlinear cases, i.e., for identifying the defect-free structure and structure with a small defect in a single member. However, the EKF-WGI method failed to identify the structure for highly nonlinear cases, i.e., structure with moderate to severe defect and also small defects in multiple members. Since the level of nonlinearity is expected to be

unknown at the initiation of the inspection, to be on the safe side, the proposed UKF-WGI method should be used to assess structural health.

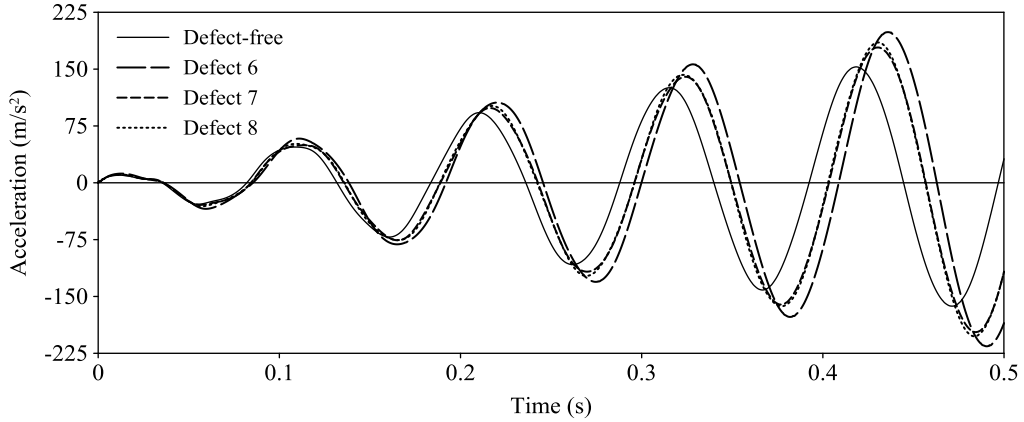

(a)

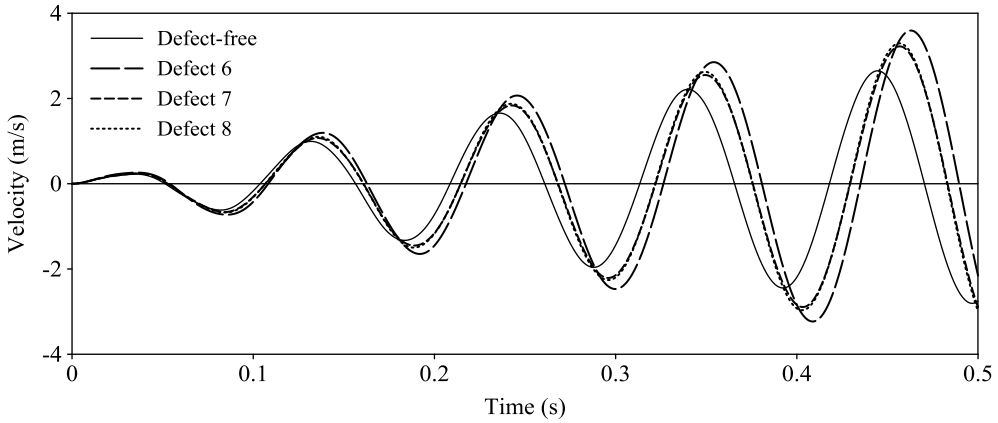

(b)

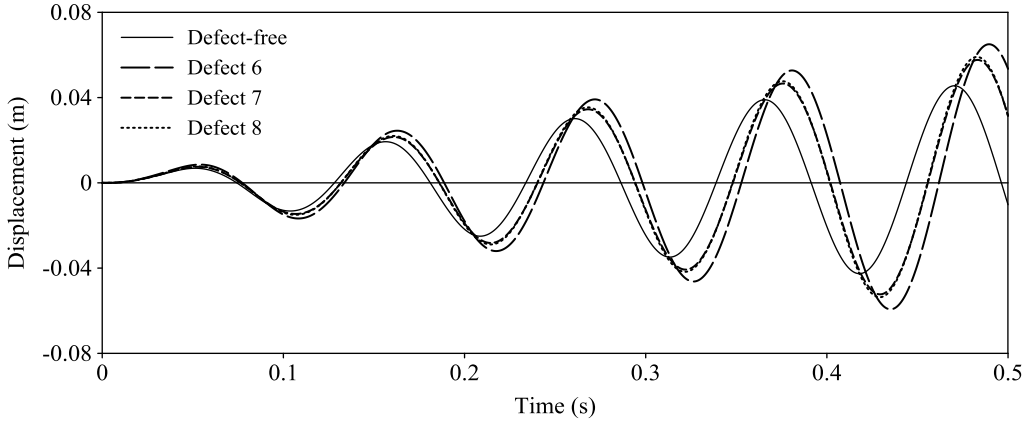

(c)

Figure 4.11 Horizontal responses at node 1 for defect-free and Defects 6, 7, and 8; (a) Acceleration; (b) Velocity; and (c) Displacement

Table 4.11 Stiffness parameter (*EI/L*) identification for multiple defects using UKF-WGI

Member	Theoretical (N-m)	Defect 6		Defect 7		Defect 8	
		Identified (N-m)	Change (%)	Identified (N-m)	Change (%)	Identified (N-m)	Change (%)
(1)	(2)	(3)	(4)	(5)	(6)	(7)	(8)
k_1	96500	38536	**-60.07**	96309	-0.20	67598	**-29.95**
k_2	96500	67827	**-29.71**	72603	**-24.76**	77190	**-20.01**
k_3	96500	95684	-0.85	82011	**-15.01**	86952	**-9.89**
k_4	241250	240686	-0.23	240994	-0.11	241600	0.15
k_5	241250	239772	-0.61	240726	-0.22	241747	0.21
k_6	241250	243545	0.95	242901	0.68	241928	0.28
k_7	241250	240320	-0.39	240310	-0.39	241243	0.00
k_8	241250	241987	0.31	240294	-0.40	240420	-0.34
k_9	241250	243079	0.76	241164	-0.04	241000	-0.10
Note:	$R_k = 10^{-4}$; $P_x(0\|0) = 10^{-3}$; $P_s(0\|0) = 10^3$; $w = 10$						

Table 4.12 Stiffness parameter (*EI/L*) identification for multiple defects using EKF-WGI

Member	Theoretical (N-m)	Defect 6		Defect 7		Defect 8	
		Identified (N-m)	Change (%)	Identified (N-m)	Change (%)	Identified (N-m)	Change (%)
(1)	(2)	(3)	(4)	(5)	(6)	(7)	(8)
k_1	96500	36633	**-62.04**	89300	-7.46	63048	**-34.67**
k_2	96500	74140	**-23.17**	82816	**-14.18**	86999	**-9.85**
k_3	96500	80688	-16.39	65454	**-32.17**	69909	**-27.56**
k_4	241250	231775	-3.93	225094	-6.70	227146	-5.85
k_5	241250	205656	-14.75	203039	-15.84	202774	-15.95
k_6	241250	286954	18.94	287864	19.32	288914	19.76
k_7	241250	188708	-21.78	190159	-21.18	191787	-20.50
k_8	241250	348092	44.29	332438	37.80	330295	36.91
k_9	241250	211515	-12.33	233682	-3.14	234084	-2.97
Note:	$R_k = 10^{-4}$; $P_x(0\|0) = 10^{-3}$; $P_s(0\|0) = 10^3$; $w = 10$						

4.4 Observations and Discussions

The proposed UKF-WGI procedure is verified to assess the health of a relatively large realistic structure. It is a two-dimensional three-story frame. The procedure is verified for both linear and geometrically nonlinear structural systems. Different damage scenarios are considered to demonstrate the effectiveness of the proposed procedure. Small, moderate, and severe defect(s) in single or multiple members in the structure are considered. For verification purposes, both noise-free and noise-contaminated input excitation and output response information are used for identification. Three levels of noise (5, 10, and 20% of RMS values) are considered. The absolute minimum number of measured responses, collected only over a short period of time is used to identify the structures.

The numerical examples demonstrated that the proposed procedure is capable of identifying the health of both linear and geometrically nonlinear structural systems using minimum number of response information. Furthermore, the procedure is able to identify the location and severity of defects at the local element level accurately. The examples also showed the robustness of procedure in the presence of noise. Even if the levels of noises in excitation and response information are high, the procedure is still able to identify the structure very well at the element level.

The capabilities of UKF-WGI and EKF-WGI are also studied. It confirmed the superiority of UKF-WGI over EKF-WGI in all aspects.

CHAPTER 5

THEORY OF IDENTIFICATION OF LARGE STRUCTURAL SYSTEMS USING LIMITED RESPONSE INFORMATION WITH UNKNOWN INPUT

5.1 Introduction

The UKF-WGI procedure, presented in Chapter 3, has been developed to assess health of a large structural system using a limited number of noise-contaminated responses. The UKF-WGI procedure, however, can be implemented only if the input excitation is known. The collection of input excitation information is not simple. Outside the control laboratory environment, the measurements of excitation information could be very expensive, troublesome and so error-prone that the SI concept may not be applicable. In many cases, e.g., after an earthquake, the excitation time-history may not be available for a structure under investigation. It will be extremely desirable if a large system can be identified using only response information completely ignoring the excitation information. This will make the SI-based concept mathematically more challenging since two of the three components of SI will be unknown.

The other drawback of UKF-WGI is that the initial value of the state vector must be known to implement the procedure. However, it is unknown at the beginning of the inspection. To address the challenges, a novel approach is proposed in this study. The approach integrates the UKF-WGI concept with an iterative least-squares technique. In addition, to increase implementation of the approach, a substructure concept is also used. The integrated approach denoted as unscented Kalman filter with unknown input and weighted global iteration (UKF-UI-WGI).

5.2 The Concept behind UKF-UI-WGI

To incorporate all the desirable features discussed earlier, the proposed UKF-UI-WGI procedure requires a two-stage. In Stage 1, iterative least-squares with unknown input (ILS-UI), developed by the research team at the University of Arizona, is used. Then, the unscented Kalman filter with weighted global iteration (UKF-WGI) procedure is implemented in Stage 2.

To implement the UKF-UI-WGI concept, the system is represented by finite elements and the mass of all the elements is assumed to be known, as is commonly considered in other studies. Rayleigh-type mass and stiffness proportional damping is considered to improve the efficiency of the algorithm.

Based on the location of the input excitation(s) and available measured response information, substructure(s) need to be introduced in Stage 1. The responses at all DDOFs of the substructure(s) must be available so that ILS-UI can be used to identify it. ILS-UI identifies the time-history of unknown input excitation(s), stiffness parameters of all the elements in the substructure(s), and the two Rayleigh damping coefficients. The information on damping is assumed to be applicable to the whole structure. Initial unknown state vector containing information on stiffness parameters of all the elements in the whole structure can be generated judicially considering the identified stiffness parameters for the substructure as will be discussed later in detail.

At the completion of Stage 1, all the required information to implement the UKF-WGI procedure is available and the whole structure can be identified in Stage 2. In this way, the health of the whole system can be assessed using only noise-contaminated responses measured at a limited number of DDOFs completely ignoring the excitation

information. By tracking the stiffness properties of all the elements, in the finite element representation, identified by the proposed method, the location and severity of defect(s) in any element can be assessed as will be clarified in more details later.

5.3 Substructure Concept

The first step in the proposed procedure is to select the substructure. Some of the terminologies, used in this section for selection of substructure, are needed to be introduced first. They are:

(a) Substructure: a small part of the structure.

(b) Key nodes (*kn*): nodes where the unknown input excitations are applied. A substructure is defined around the key nodes at which the equilibrium equations are satisfied.

For earthquake excitation, since the inertia forces due to seismic excitation act at all the nodes of the structure, any nodes in the structure can be considered as key nodes.

(c) Related elements (*re*): elements connecting directly to key nodes. They contribute to the equilibrium equations at the key nodes.

(d) Related nodes (*rn*): nodes attached to the related elements other than the key nodes. They also contribute to the equilibrium equations.

(e) Total number of nodes in the substructure (*nsub*): summation of the number of key nodes and related nodes; $nsub = kn + rn$.

(f) Support conditions (*sc*): number of constraints to dynamic degrees of freedom at the external support in the substructure. For example for a plane framed structure, *sc* = 3, 2, and 1 for a fixed, hinged, and roller support, respectively.

(g) Total number of DDOFs in the substructure (*dsub*): total number of nodes in the substructure times the number of DDOFs at a node (*ddof*) subtracting the number of support conditions; $dsub = nsub \times ddof - sc$.

5.3.1 Substructure Selection Steps

The steps required to define the substructure are mentioned below and they are clarified using a frame shown in Figure 5.1, where the substructure is shown in double lines.

Step 1: identify the key node(s), *kn*. For the substructure shown in Figure 5.1, $kn = 1$.

Step 2: Determine the number of DDOFs at key node(s), *dkn*. For the substructure shown in Figure 5.1, $dkn = 3$; two translational along horizontal and vertical axis and one rotational.

Step 3: Determine the number of related elements, *re*. For the substructure shown in Figure 5.1, the related elements are 1 and 5. Thus, $re = 2$.

Step 4: Determine the number of related nodes, *rn*. For the substructure shown in Figure 5.1, the related nodes are 2 and 3. Thus, $rn = 2$.

Step 5: Determine the total number of nodes in the substructure, *nsub*. For the substructure shown in Figure 5.1, $nsub = 1+2 = 3$.

Step 6: Determine the total number of support conditions in the substructure, *sc*. For the substructure shown in Figure 5.1, $sc = 0$.

Step 7: Determine the total number of DDOFs in the substructure, *dsub*. For the substructure shown in Figure 5.1, $dsub = 3\times3 - 0 = 9$.

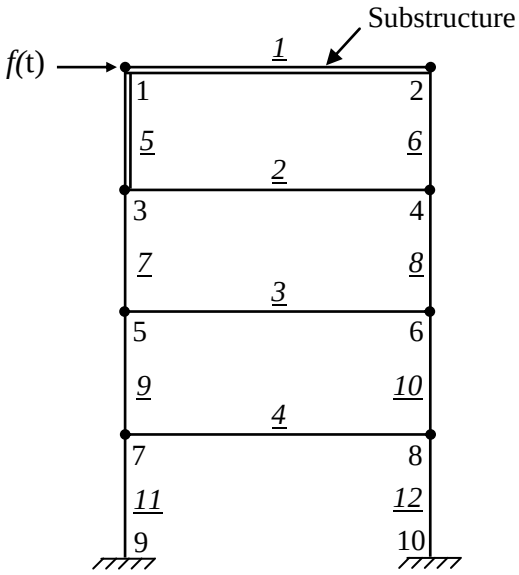

Figure 5.1 Finite element representation of a four-story frame

5.3.2 Substructure Selection Examples

The selection of substructure is considered for different types and locations of loading in this section. The four-story frame shown in Figure 5.1 is considered to demonstrate the substructure selection process. Five different cases are considered. They are:

1. One unknown input excitation applied horizontally at node 1.
2. Two unknown input excitations applied horizontally at node 1 and 3.
3. Two unknown input excitations applied horizontally at node 1 and 5.
4. Two unknown input excitations applied horizontally at node 1 and 7.
5. Unknown earthquake excitation.

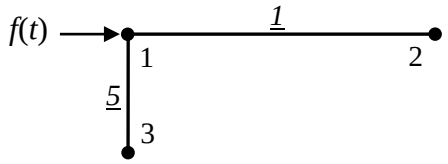

kn = 1
dkn = 3
re = 2
rn = 2
nsub = 3
sc = 0
dsub = 9

Figure 5.2 Substructure needed for loading case 1

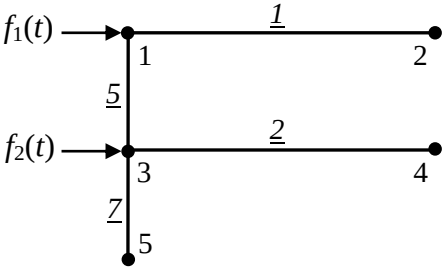

kn = 1, 3
dkn = 6
re = 4
rn = 3
nsub = 5
sc = 0
dsub = 15

Figure 5.3 Substructure needed for loading case 2

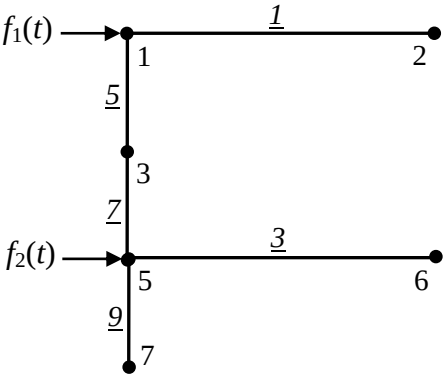

kn = 1, 5
dkn = 6
re = 5
rn = 4
nsub = 6
sc = 0
dsub = 18

Figure 5.4 Substructure needed for loading case 3

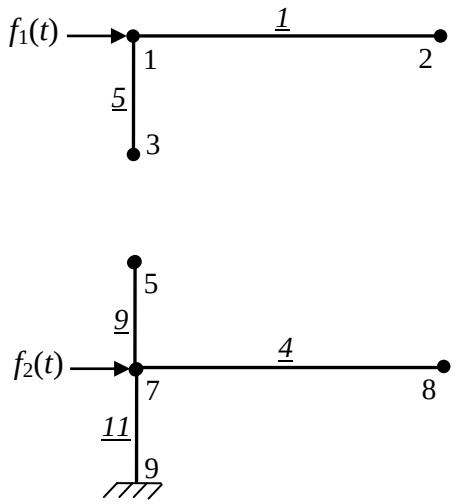

kn = 1, 7
dkn = 6
re = 5
rn = 5
nsub = 7
sc = 3
dsub = 18

Figure 5.5 Substructure needed for loading case 4

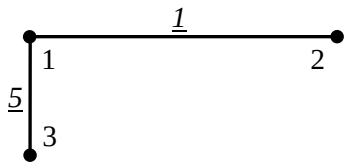

kn = 1
dkn = 3
re = 2
rn = 2
nsub = 3
sc = 0
dsub = 9

Figure 5.6 Substructure needed for loading case 5

5.4 The UKF-UI-WGI Procedure

The mathematical formulations of the two-stage procedure of UKF-UI-WGI are presented in this section.

5.4.1 Stage 1 - Substructure Identification Using ILS-UI

The governing differential equation of motion for the key node(s) in the substructure in the presence of Rayleigh damping can be expressed as:

$$\mathbf{M}_{kn,sub}\ddot{\mathbf{X}}_{sub}(t) + \left(a\mathbf{M}_{kn,sub} + b\mathbf{K}_{kn,sub}\right)\dot{\mathbf{X}}_{sub}(t) + \mathbf{K}_{kn,sub}\mathbf{X}_{sub}(t) = \mathbf{f}_{kn}(t) \qquad (5.1)$$

where $\mathbf{M}_{kn,sub}$ and $\mathbf{K}_{kn,sub}$ are the *dkn*×*dsub* global mass and stiffness matrices, respectively, related to the key nodes and they can be constructed by taking all the components of rows related to the key nodes from the global mass and stiffness matrices of the substructure; $\ddot{\mathbf{X}}_{sub}(t)$, $\dot{\mathbf{X}}_{\text{sub}}(t)$, and $\mathbf{X}_{sub}(t)$ are *dsub*×1 vectors containing the dynamic responses, in terms of acceleration, velocity, and displacement at time *t*, respectively, of all DDOFs in the substructure; $\mathbf{f}_{kn}(t)$ is the *dkn*×1 input excitation vector at time *t*; and *a* and *b* are the mass and stiffness proportional Rayleigh damping coefficients, respectively. The subscript 'sub' is used to denote substructure.

The mass matrix $\mathbf{M}_{kn,sub}$ is generally assumed to be known (Wang and Haldar, 1994). The input excitation vector $\mathbf{f}_{kn}(t)$ is considered to be unknown. The parameters to be identified are the stiffness parameter of each element in the substructure and the Rayleigh damping coefficients *a* and *b*. To identify the unknown parameters, Equation (5.1) can be reorganized as:

$$\left(a\mathbf{M}_{kn,sub} + b\mathbf{K}_{kn,sub}\right)\dot{\mathbf{X}}_{sub}(t) + \mathbf{K}_{kn,sub}\mathbf{X}_{sub}(t) = \mathbf{f}_{kn}(t) - \mathbf{M}_{kn,sub}\ddot{\mathbf{X}}_{sub}(t) \qquad (5.2)$$

The global stiffness matrix for the i^{th} element can be written as:

$$\mathbf{K}_i = k_i \mathbf{S}_i \tag{5.3}$$

where k_i is the stiffness parameter of i^{th} element defined as E_iI_i/L_i for a frame element and E_iA_i/L_i for a truss element. L_i, A_i, I_i, and E_i are the length, cross-sectional area, moment of inertia, and modulus of elasticity, respectively of the i^{th} element. $\mathbf{S}_i$ is the *dsub*×*dsub* global stiffness coefficient left after taking k_i out from the i^{th} stiffness matrix.

The global mass and stiffness matrices for the substructure can be assembled from the mass and stiffness matrices of all the elements in the substructure as:

$$\mathbf{M}_{sub} = \sum_{i=1}^{esub} \mathbf{M}_i \tag{5.4}$$

$$\mathbf{K}_{sub} = \sum_{i=1}^{esub} \mathbf{K}_i \tag{5.5}$$

where *esub* is the total number of elements in the substructure and it is equal to the related elements; *esub* = *re*.

Using Equations (5.3) to (5.5), Equation (5.2) can be rearranged as:

$$\begin{aligned}(k_1\mathbf{S}_1 + k_2\mathbf{S}_2 + \cdots + k_{esub}\mathbf{S}_{esub})_{kn}\,\mathbf{X}_{sub}(t) \\ + b(k_1\mathbf{S}_1 + k_2\mathbf{S}_2 + \cdots + k_{esub}\mathbf{S}_{esub})_{kn}\,\dot{\mathbf{X}}_{sub}(t) \\ + a\mathbf{M}_{kn,sub}\dot{\mathbf{X}}_{sub}(t) = \mathbf{f}_{kn}(t) - \mathbf{M}_{kn,sub}\ddot{\mathbf{X}}_{sub}(t)\end{aligned} \tag{5.6}$$

or,

$$\begin{aligned}[\mathbf{S}_1\mathbf{X}_{sub}(t)\ \ \mathbf{S}_2\mathbf{X}_{sub}(t) \ldots \mathbf{S}_{esub}\mathbf{X}_{sub}(t)\ \mathbf{S}_1\dot{\mathbf{X}}_{sub}(t)\ \ \mathbf{S}_2\dot{\mathbf{X}}_{sub}(t) \ldots \mathbf{S}_{esub}\dot{\mathbf{X}}_{sub}(t) \\ \mathbf{M}_{sub}\dot{\mathbf{X}}_{sub}(t)]_{kn}\,\mathbf{P}_{sub} = \mathbf{f}_{kn}(t) - \mathbf{M}_{kn,sub}\ddot{\mathbf{X}}_{sub}(t)\end{aligned} \tag{5.7}$$

Equation (5.7) can be rearranged in matrix form as:

$$\mathbf{A}_{kn}(t)\mathbf{P}_{sub} = \mathbf{F}_{kn}(t) \tag{5.8}$$

Considering that the responses are measured at all q time points, Equation (5.8) can

be reorganized with *dkn*×*q* equilibrium equations at the key node(s) in a matrix form as:

$$\mathbf{A}_{kn}\mathbf{P}_{sub} = \mathbf{F}_{kn} \tag{5.9}$$

where

$$\mathbf{A}_{kn} = [\mathbf{A}_{dkn\times usub}(1) \quad \mathbf{A}_{dkn\times usub}(2) \quad \cdots \quad \mathbf{A}_{dkn\times usub}(q)]^T \tag{5.10}$$

$$\mathbf{P}_{sub} = [k_1 \;\; k_2 \ldots k_{esub} \;\; bk_1 \;\; bk_2 \;\; \ldots \;\; bk_{esub} \;\; a]^T \tag{5.11}$$

$$\mathbf{F}_{kn} = \begin{bmatrix} \mathbf{f}_{dkn\times 1}(1) - \mathbf{M}_{dkn\times dsub}\ddot{\mathbf{X}}_{dsub\times 1}(1) \\ \mathbf{f}_{dkn\times 1}(2) - \mathbf{M}_{dkn\times dsub}\ddot{\mathbf{X}}_{dsub\times 1}(2) \\ \vdots \\ \mathbf{f}_{dkn\times 1}(q) - \mathbf{M}_{dkn\times dsub}\ddot{\mathbf{X}}_{dsub\times 1}(q) \end{bmatrix} \tag{5.12}$$

in which $\mathbf{P}_{sub}$ is the *usub*×1 vector composed of unknown system parameters (stiffness and damping coefficients) that need to be identified; $\mathbf{F}_{kn}$ is the (*dkn*×*q*)×1 vector composed of unknown input excitations and inertia forces at all time points; $\mathbf{A}_{kn}$ is the (*dkn*×*q*)×*usub* matrix composed of measured responses in terms of displacement and velocity at all time points; and $\mathbf{A}_{kn}(t)$ is the *dkn*×*usub* matrix at time point *t*.

It is important to note that only acceleration time-histories of all DDOFs of the substructure will be measured for *q* time points. Then, the velocity and displacement time-histories required to implement UKF-UI-WGI will be obtained by successive integration of the acceleration time-histories as discussed in more detail by Vo and Haldar (2003) and Das (2012).

In Equation (5.9), the number of equations are greater than the number of unknowns (*dkn*×*q* > *usub*) indicating an over-determined system of equations. The least-squares technique is used to solve for the unknown system parameter vector $\mathbf{P}_{sub}$. It leads to the following expression:

$$\mathbf{P}_{sub} = (\mathbf{A}_{kn}^T\mathbf{A}_{kn})^{-1}\mathbf{A}_{kn}^T\mathbf{F}_{kn} \tag{5.13}$$

If all elements of the matrix $\mathbf{A}_{kn}$ and the force vector $\mathbf{F}_{kn}$ are known, the unknown parameter vector $\mathbf{P}_{sub}$ can be straightforwardly evaluated using Equation (5.13). However, since the input excitation is not known, the force vector $\mathbf{F}_{kn}$ in Equation (5.9) becomes partially unknown. The method proposed by Wang and Haldar (1994) and modified by Katkhuda et al. (2005) is used to solve for vector $\mathbf{P}_{sub}$ by starting an iteration process where it is assumed that the unknown input forces to be zero at all time points since they are not known. It is observed that the proposed method is not sensitive to this initial assumption. The iteration process continues until a predetermined convergence tolerance level (ε_f) on the input excitation at all time points is obtained. The convergence requires $\left|\mathbf{f}_{kn}^{i+1} - \mathbf{f}_{kn}^{i}\right| < \varepsilon_f$ where $\mathbf{f}_{kn}^{i+1}$ and $\mathbf{f}_{kn}^{i}$ are the forces estimated in two consecutive time steps.

5.4.1.1 Implementation of Stage 1 – ILS-UI Procedure

The basic steps required to implement the ILS-UI procedure are as follows:

Step 1: Considering the location of the input excitation and available response information, select the most appropriate substructure(s).

Step 2: Develop matrix $\mathbf{A}_{kn}$ in Equation (5.10) and assume the unknown input excitation vector to be zero at all time points $\mathbf{f}_{kn} = \mathbf{0}$.

$$\mathbf{f}_{kn} = \begin{bmatrix} \mathbf{f}_{kn}(1) \\ \mathbf{f}_{kn}(2) \\ \vdots \\ \mathbf{f}_{kn}(q) \end{bmatrix} = \begin{bmatrix} \mathbf{0} \\ \mathbf{0} \\ \vdots \\ \mathbf{0} \end{bmatrix} \tag{5.14}$$

Step 3: Using Equation (5.13), the first estimation of the system parameter vector $\mathbf{P}_{sub}$ can be obtained.

Step 4: Substitute estimated system parameters $\mathbf{P}_{sub}$ in step 3 into Equation (5.1) to

obtain unknown input excitation vector $\mathbf{f}_{kn}$ at all q time points.

Step 5: Apply force constraints to the input excitation $\mathbf{f}_{kn}$, obtained in step 4. If the input excitation is zero at the jth DDOF, the constraint $\mathbf{f}_j(t) = \mathbf{0}$ at all q time points, needs to be introduced.

Step 6: Update $\mathbf{P}_{sub}$ using Equation (5.13), then update $\mathbf{f}_{kn}$ using Equation (5.1) and then update $\mathbf{P}_{sub}$ again.

Continue the iteration procedure until a predetermined convergence level (ε_f) on the input excitation at all time points is satisfied. The tolerance level ε_f is considered to be 10^{-8} in this study.

The flow chart for Stage 1 is shown in Figure 5.7.

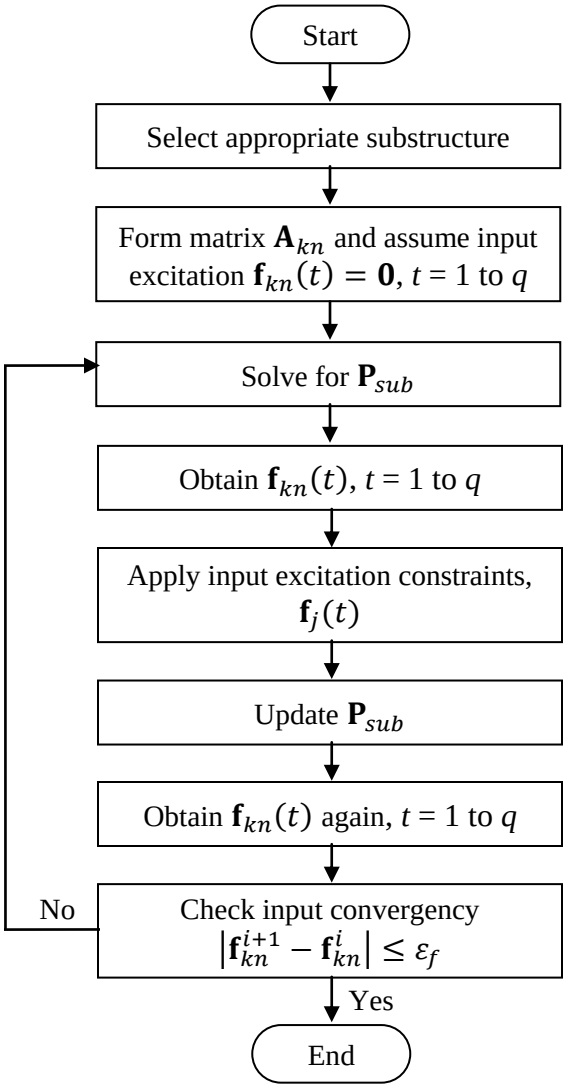

Figure 5.7 Flow chart for Stage 1 of UKF-UI-WGI procedure

5.4.1.2 Application of ILS-UI Approach for a Plane Frame

In this section, the general concept of the ILS-UI approach is applied to a two dimensional frame. This type of structure has three DDOFs at each node. Two of them are translational DDOFs; one is along the length of the element and the other is perpendicular to it, and the third one is the rotation as shown in Figure 3.3.

The mass matrix and stiffness matrix for each element in the global coordinate system can be evaluated from Equation (3.41) and Equation (3.42), respectively. The global mass matrix $\mathbf{M}_{sub}$ and stiffness matrix $\mathbf{K}_{sub}$ for the substructure can be assembled from the mass and stiffness matrices of all the elements in the substructure using Equation (5.4) and Equation (5.5), respectively.

Let's consider the substructure shown in Figure (5.2). The substructure consists of three nodes (*nsub* = 3) with nine DDOFs (*dsub* = 9) and two elements (*esub* = 2). For convenience, the number of element 5 will be changed to 2.

The next step is to develop $\mathbf{A}_{sub}(t)$ matrix at time point *t*, which is expressed as:

$$\mathbf{A}_{sub}(t) = [\mathbf{S}_1\mathbf{X}_{sub}(t) \quad \mathbf{S}_2\mathbf{X}_{sub}(t) \quad \mathbf{S}_1\dot{\mathbf{X}}_{sub}(t) \quad \mathbf{S}_2\dot{\mathbf{X}}_{sub}(t) \quad \mathbf{M}_{sub}\dot{\mathbf{X}}_{sub}(t)] \qquad (5.15)$$

For element 1, the local and global coordinates coincide, i.e., $\theta = 0$. Thus, $sin\theta = 0$ and $cos\theta = 1$, $\mathbf{S}_1\mathbf{X}_{sub}(t)$ is formed in the following way:

$$\mathbf{S}_1\mathbf{X}_{sub}(t) = \begin{bmatrix} \frac{A_1}{I_1} & 0 & 0 & -\frac{A_1}{I_1} & 0 & 0 & 0 & 0 & 0 \\ 0 & \frac{12}{L_1^2} & \frac{6}{L_1} & 0 & -\frac{12}{L_1^2} & \frac{6}{L_1} & 0 & 0 & 0 \\ 0 & \frac{6}{L_1} & 4 & 0 & -\frac{6}{L_1} & 2 & 0 & 0 & 0 \\ -\frac{A_1}{I_1} & 0 & 0 & \frac{A_1}{I_1} & 0 & 0 & 0 & 0 & 0 \\ 0 & -\frac{12}{L_1^2} & -\frac{6}{L_1} & 0 & \frac{12}{L_1^2} & -\frac{6}{L_1} & 0 & 0 & 0 \\ 0 & \frac{6}{L_1} & 2 & 0 & -\frac{6}{L_1} & 4 & 0 & 0 & 0 \\ 0 & 0 & 0 & 0 & 0 & 0 & 0 & 0 & 0 \\ 0 & 0 & 0 & 0 & 0 & 0 & 0 & 0 & 0 \\ 0 & 0 & 0 & 0 & 0 & 0 & 0 & 0 & 0 \end{bmatrix} \begin{Bmatrix} x_1(t) \\ y_1(t) \\ \theta_1(t) \\ x_2(t) \\ y_2(t) \\ \theta_2(t) \\ x_3(t) \\ y_3(t) \\ \theta_3(t) \end{Bmatrix} \tag{5.16}$$

and $\mathbf{S}_1\dot{\mathbf{X}}_{sub}(t)$ is formed in the following way:

$$\mathbf{S}_1\dot{\mathbf{X}}_{sub}(t) = \begin{bmatrix} \frac{A_1}{I_1} & 0 & 0 & -\frac{A_1}{I_1} & 0 & 0 & 0 & 0 & 0 \\ 0 & \frac{12}{L_1^2} & \frac{6}{L_1} & 0 & -\frac{12}{L_1^2} & \frac{6}{L_1} & 0 & 0 & 0 \\ 0 & \frac{6}{L_1} & 4 & 0 & -\frac{6}{L_1} & 2 & 0 & 0 & 0 \\ -\frac{A_1}{I_1} & 0 & 0 & \frac{A_1}{I_1} & 0 & 0 & 0 & 0 & 0 \\ 0 & -\frac{12}{L_1^2} & -\frac{6}{L_1} & 0 & \frac{12}{L_1^2} & -\frac{6}{L_1} & 0 & 0 & 0 \\ 0 & \frac{6}{L_1} & 2 & 0 & -\frac{6}{L_1} & 4 & 0 & 0 & 0 \\ 0 & 0 & 0 & 0 & 0 & 0 & 0 & 0 & 0 \\ 0 & 0 & 0 & 0 & 0 & 0 & 0 & 0 & 0 \\ 0 & 0 & 0 & 0 & 0 & 0 & 0 & 0 & 0 \end{bmatrix} \begin{Bmatrix} \dot{x}_1(t) \\ \dot{y}_1(t) \\ \dot{\theta}_1(t) \\ \dot{x}_2(t) \\ \dot{y}_2(t) \\ \dot{\theta}_2(t) \\ \dot{x}_3(t) \\ \dot{y}_3(t) \\ \dot{\theta}_3(t) \end{Bmatrix} \tag{5.17}$$

For element 2, the angle between the local and global coordinates θ is -90^o. Thus, $sin\theta = -1$ and $cos\theta = 0$, $\mathbf{S}_2\mathbf{X}_{sub}(t)$ is formed in the following way:

$$\mathbf{S}_2\mathbf{X}_{sub}(t) = \begin{bmatrix} \frac{12}{L_2^2} & 0 & \frac{6}{L_2} & 0 & 0 & 0 & -\frac{12}{L_2^2} & 0 & \frac{6}{L_2} \\ 0 & \frac{A_2}{I_2} & 0 & 0 & 0 & 0 & 0 & -\frac{A_2}{I_2} & 0 \\ \frac{6}{L_2} & 0 & 4 & 0 & 0 & 0 & -\frac{6}{L_2} & 0 & 2 \\ 0 & 0 & 0 & 0 & 0 & 0 & 0 & 0 & 0 \\ 0 & 0 & 0 & 0 & 0 & 0 & 0 & 0 & 0 \\ 0 & 0 & 0 & 0 & 0 & 0 & 0 & 0 & 0 \\ -\frac{12}{L_2^2} & 0 & -\frac{6}{L_2} & 0 & 0 & 0 & \frac{12}{L_2^2} & 0 & -\frac{6}{L_2} \\ 0 & -\frac{A_2}{I_2} & 0 & 0 & 0 & 0 & 0 & \frac{A_2}{I_2} & 0 \\ \frac{6}{L_2} & 0 & 2 & 0 & 0 & 0 & -\frac{6}{L_2} & 0 & 4 \end{bmatrix} \begin{Bmatrix} x_1(t) \\ y_1(t) \\ \theta_1(t) \\ x_2(t) \\ y_2(t) \\ \theta_2(t) \\ x_3(t) \\ y_3(t) \\ \theta_3(t) \end{Bmatrix} \tag{5.18}$$

and $\mathbf{S}_2\dot{\mathbf{X}}_{sub}(t)$ is formed in the following way:

$$\mathbf{S}_2\dot{\mathbf{X}}_{sub}(t) = \begin{bmatrix} \frac{12}{L_2^2} & 0 & \frac{6}{L_2} & 0 & 0 & 0 & -\frac{12}{L_2^2} & 0 & \frac{6}{L_2} \\ 0 & \frac{A_2}{I_2} & 0 & 0 & 0 & 0 & 0 & -\frac{A_2}{I_2} & 0 \\ \frac{6}{L_2} & 0 & 4 & 0 & 0 & 0 & -\frac{6}{L_2} & 0 & 2 \\ 0 & 0 & 0 & 0 & 0 & 0 & 0 & 0 & 0 \\ 0 & 0 & 0 & 0 & 0 & 0 & 0 & 0 & 0 \\ 0 & 0 & 0 & 0 & 0 & 0 & 0 & 0 & 0 \\ -\frac{12}{L_2^2} & 0 & -\frac{6}{L_2} & 0 & 0 & 0 & \frac{12}{L_2^2} & 0 & -\frac{6}{L_2} \\ 0 & -\frac{A_2}{I_2} & 0 & 0 & 0 & 0 & 0 & \frac{A_2}{I_2} & 0 \\ \frac{6}{L_2} & 0 & 2 & 0 & 0 & 0 & -\frac{6}{L_2} & 0 & 4 \end{bmatrix} \begin{Bmatrix} \dot{x}_1(t) \\ \dot{y}_1(t) \\ \dot{\theta}_1(t) \\ \dot{x}_2(t) \\ \dot{y}_2(t) \\ \dot{\theta}_2(t) \\ \dot{x}_3(t) \\ \dot{y}_3(t) \\ \dot{\theta}_3(t) \end{Bmatrix} \tag{5.19}$$

$\mathbf{M}_{sub}\dot{\mathbf{X}}_{sub}(t)$ is formed in the following way:

$$\mathbf{M}_{sub}\ddot{\mathbf{X}}_{sub}(t) = \left(\frac{\bar{m}_1 L_1}{420} \begin{bmatrix} 140 & 0 & 0 & 70 & 0 & 0 & 0 & 0 & 0 \\ 0 & 156 & 22L_1 & 0 & 54 & -13L_1 & 0 & 0 & 0 \\ 0 & 22L_1 & 4L_1^2 & 0 & 13L_1 & -3L_1^2 & 0 & 0 & 0 \\ 70 & 0 & 0 & 140 & 0 & 0 & 0 & 0 & 0 \\ 0 & 54 & 13L_1 & 0 & 156 & -22L_1 & 0 & 0 & 0 \\ 0 & -13L_1 & -3L_1^2 & 0 & -22L_1 & 4L_1^2 & 0 & 0 & 0 \\ 0 & 0 & 0 & 0 & 0 & 0 & 0 & 0 & 0 \\ 0 & 0 & 0 & 0 & 0 & 0 & 0 & 0 & 0 \\ 0 & 0 & 0 & 0 & 0 & 0 & 0 & 0 & 0 \end{bmatrix} \right.$$

$$\left. + \frac{\bar{m}_2 L_2}{420} \begin{bmatrix} 156 & 0 & 22L_2 & 0 & 0 & 0 & 54 & 0 & -13L_2 \\ 0 & 140 & 0 & 0 & 0 & 0 & 0 & 70 & 0 \\ 22L_2 & 0 & 4L_2^2 & 0 & 0 & 0 & 13L_2 & 0 & -3L_2^2 \\ 0 & 0 & 0 & 0 & 0 & 0 & 0 & 0 & 0 \\ 0 & 0 & 0 & 0 & 0 & 0 & 0 & 0 & 0 \\ 0 & 0 & 0 & 0 & 0 & 0 & 0 & 0 & 0 \\ 54 & 0 & 13L_2 & 0 & 0 & 0 & 156 & 0 & -22L_2 \\ 0 & 70 & 0 & 0 & 0 & 0 & 0 & 140 & 0 \\ -13L_2 & 0 & -3L_2^2 & 0 & 0 & 0 & -22L_2 & 0 & 4L_2^2 \end{bmatrix} \right) \begin{Bmatrix} \dot{x}_1(t) \\ \dot{y}_1(t) \\ \dot{\theta}_1(t) \\ \dot{x}_2(t) \\ \dot{y}_2(t) \\ \dot{\theta}_2(t) \\ \dot{x}_3(t) \\ \dot{y}_3(t) \\ \dot{\theta}_3(t) \end{Bmatrix} \tag{5.20}$$

Then, $\mathbf{A}_{kn}(t)$ matrix is constructed by taking all the components of the first three rows of $\mathbf{A}_{sub}(t)$ matrix, which is related to the key node.

The $\mathbf{P}_{sub}$ vector in Equation (5.8) is defined as:

$$\mathbf{P}_{sub} = \begin{bmatrix} k_1 \\ k_2 \\ bk_1 \\ bk_2 \\ a \end{bmatrix} \tag{5.21}$$

The $\mathbf{F}_{kn}(t)$ vector in Equation (5.8) is expressed as:

$$\mathbf{F}_{kn}(t) = \mathbf{f}_{kn}(t) - \mathbf{M}_{kn,sub}\ddot{\mathbf{X}}_{sub}(t) \tag{5.22}$$

where $\mathbf{f}_{kn}(t)$ vector at time point *t* contains the input excitation force at all DDOFs of the key node and it is defined as:

$$\mathbf{f}_{kn}(t) = \begin{bmatrix} f_{1x}(t) \\ f_{1y}(t) \\ f_{1\theta}(t) \end{bmatrix} \tag{5.23}$$

and $\ddot{\mathbf{X}}_{sub}(t)$ vector at time point *t* contains the acceleration responses at all DDOFs in the substructure and it is defined as:

$$\ddot{\mathbf{X}}_{sub}(t) = \begin{bmatrix} \ddot{x}_1(t) \\ \ddot{y}_1(t) \\ \ddot{\theta}_1(t) \\ \ddot{x}_2(t) \\ \ddot{y}_2(t) \\ \ddot{\theta}_2(t) \\ \ddot{x}_3(t) \\ \ddot{y}_3(t) \\ \ddot{\theta}_3(t) \end{bmatrix} \tag{5.24}$$

Although nine equations are developed for all DDOFs of the substructure, only three equilibrium equations at three DDOFs of the key node are considered to identify the structure. Considering that the responses are measured at all q time points, the matrix $\mathbf{A}_{kn}$ in Equation (5.9) can be formed using Equation (5.10) where the size of $\mathbf{A}_{kn}(t)$ is 3×5 and thus the size of $\mathbf{A}_{kn}$ is 3q×5.

The $\mathbf{F}_{kn}$ vector is formed in the following way:

$$\mathbf{F}_{kn} = \begin{bmatrix} \mathbf{F}_{kn}(1) \\ \mathbf{F}_{kn}(2) \\ \vdots \\ \mathbf{F}_{kn}(q) \end{bmatrix} \tag{5.25}$$

where the size of $\mathbf{F}_{kn}(t)$ is 3×1 and thus the size of $\mathbf{F}_{kn}$ is 3q×1.

5.4.2 Stage 2 - Complete Structural Identification Using UKF-WGI

The outcomes of Stage 1 will be used to implement UKF-WGI. They are the time-history of unknown input excitation(s), stiffness parameters of all the elements in the substructure(s), and the two Rayleigh damping coefficients. The information on damping will be assumed to be applicable to the whole structure. Initial unknown state vector containing information on stiffness parameters of all the elements in the whole structure can be generated judicially considering the identified stiffness parameters for the

substructure. Since all the beams and all the columns in a structure are expected to have respective similar stiffness parameters. All the beam elements will be assigned the same stiffness value obtained for beam element(s) in the substructure. Similarly, all the column elements will be assigned the same stiffness value of the column element(s) in the substructure. Therefore, all the required information to implement the UKF-WGI procedure will be available and the whole structure can be identified using the formulations mentioned in Chapter 3. A flow chart for implementation of a two-stage of the UKF-UI-WGI procedure is shown in Figure 5.8.

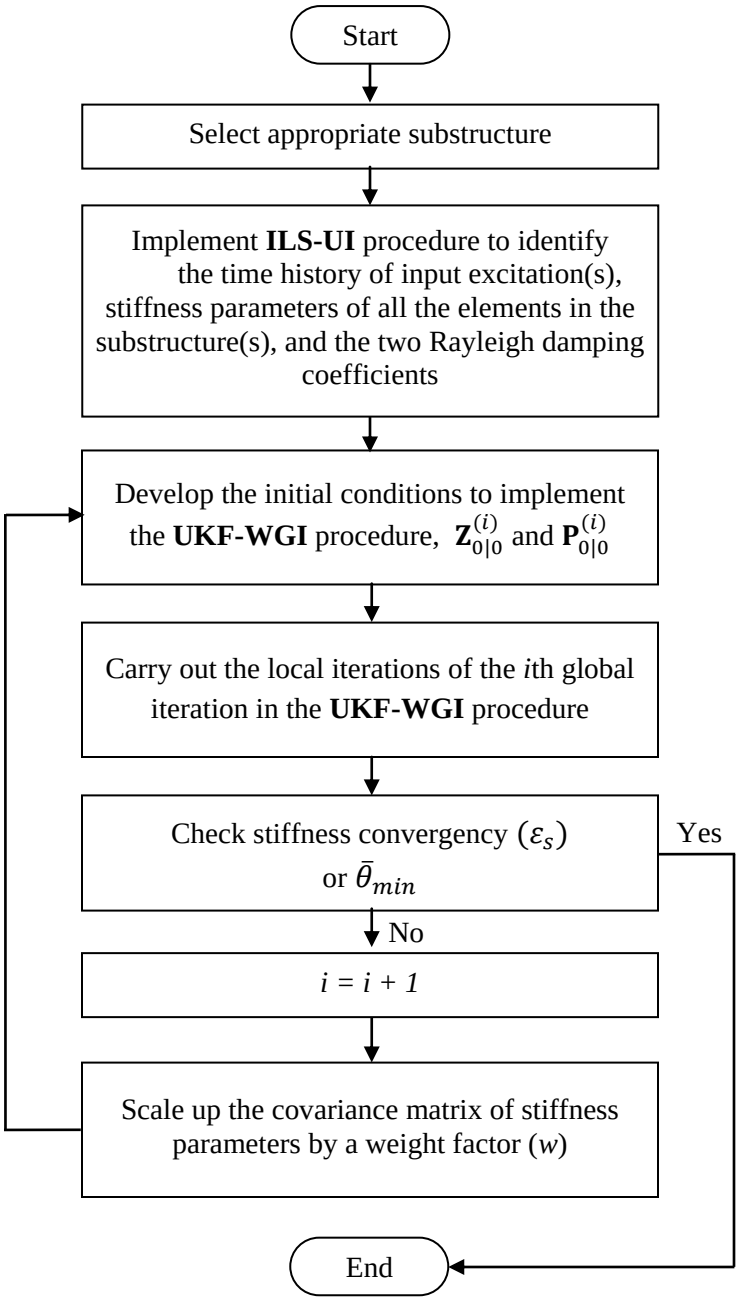

Figure 5.8 Flow chart of the UKF-UI-WGI procedure

CHAPTER 6

VERIFICATION OF UKF-UI-WGI TO HEALTH ASSESSMENT OF LARGE STRUCTURAL SYSTEMS

6.1 Introduction

This chapter aims to verify the performance, efficiency, and accuracy of the proposed procedures for health assessment of large structural systems. The verification will be based upon a variety of combinations of simulation with respect to input excitation, the configuration of an analytical model, number of measured responses and their location, sampling rates, and so on. Different type of input excitations is considered including impulsive, harmonic, and earthquake excitation. Single and multiple loading(s) are used to excite the structure. Different damage scenarios in the structures are considered including small and large defect in single and multiple member(s). The capability of the procedure is also examined to identify the defect spot in the defective element. The minimum number of measured responses required to implement the procedure is explored and the best locations of the measured responses are also investigated. Different sampling rates of responses are used. The stability and convergence characteristics of the proposed procedure are studied comprehensively. To demonstrate the effectiveness of the proposed procedure, it is compared with the basic UKF procedure and also with the EKF-based procedure.

6.2 Health Assessment of One-Bay Five-Story Frame

6.2.1 Description of the Frame

A two-dimensional one-bay five-story steel frame, shown in Figure 6.1, is considered. The frame consists of 15 members; 5 beams and 10 columns. The bay width is 9.14 m and the story height is 3.66 m. The beams and columns are made of W21×68 and W14×61 sections, respectively of Grade 50 steel. The frame is represented by the finite element (FE) with 15 elements and 12 nodes. Each node has three DDOFs; two translational and one rotational. The support at the bases is considered to be fixed. Therefore, the total number of DDOFs for the frame is 30. The nominal stiffness parameters k_i, defined in terms of (E_iI_i/L_i), for the beam and column are estimated to be 13476 kN-m and 14553 kN-m, respectively. The Rayleigh-damping coefficients a and b can be estimated using a procedure suggested by Clough and Penzien (2003). In this procedure, the damping ratios are assumed to be the same for the first two natural frequencies. The first two natural frequencies of the defect-free frame are estimated to be f_1 = 3.6973 Hz and f_2 = 11.715 Hz, respectively. The corresponding Rayleigh damping coefficients a and b are calculated to be 1.0594748 and 0.000619589, respectively, equivalent to 3% of the modal critical damping ratio. The frame is excited by a harmonic force f(t) = 10sin(20t) kN, shown in Figure 6.2, applied horizontally at the top floor at node 1.

For a theoretical verification of the proposed method, responses in terms of displacements, velocities, and accelerations are numerically generated using a commercial software ANSYS (ver. 14.0). The responses generated from 0.02 to 0.32 s with sampling time interval of 0.00025 s providing 1201 time points are used in the

subsequent health assessment process. The responses of defect-free frame at node 1 for duration of 0.5 s are shown in Figures 6.3 through 6.5. After the responses are obtained, the information on input excitation is completely ignored.

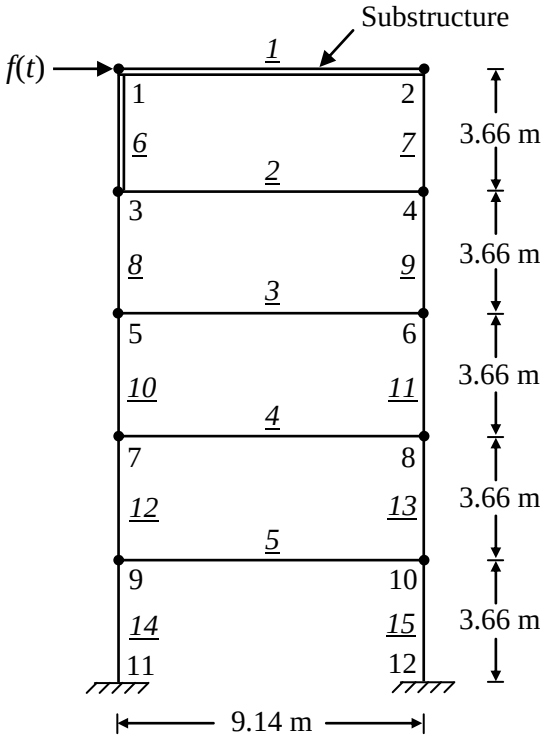

Figure 6.1 Finite element representation of a five-story frame

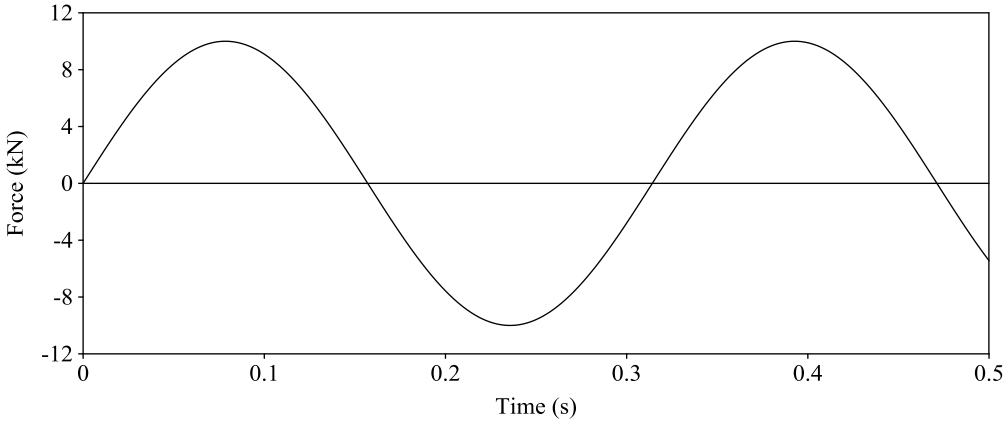

Figure 6.2 Sinusoidal force applied horizontally at node 1

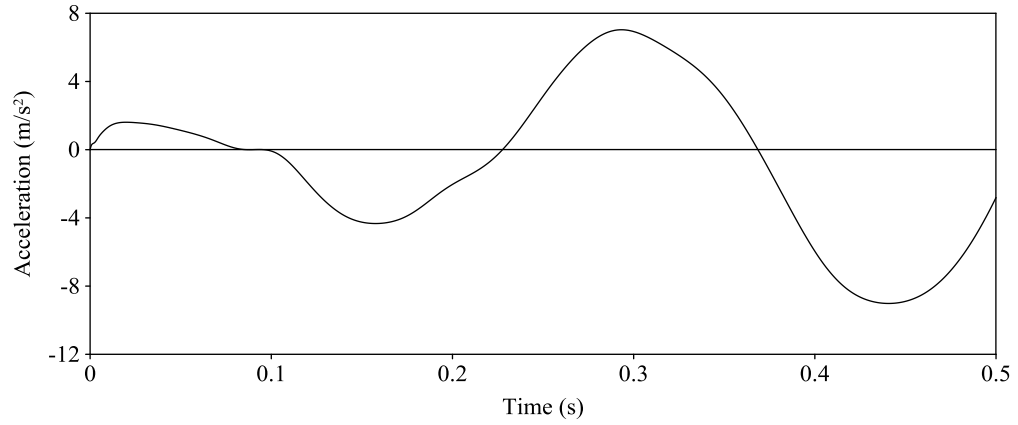

(a)

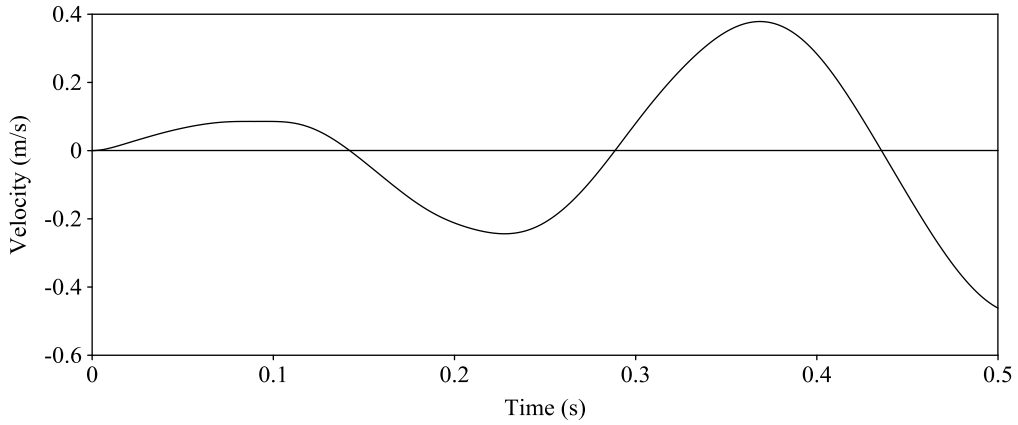

(b)

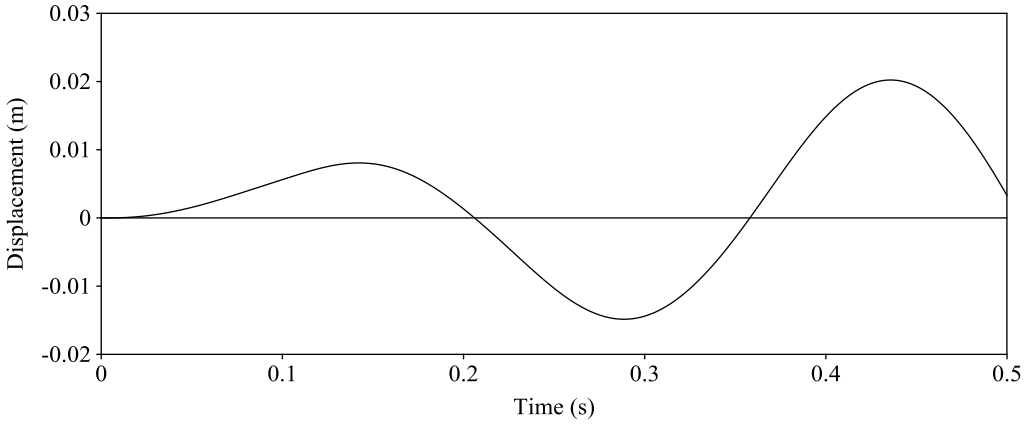

(c)

Figure 6.3 Horizontal responses at node 1; (a) Acceleration; (b) Velocity; and (c) Displacement

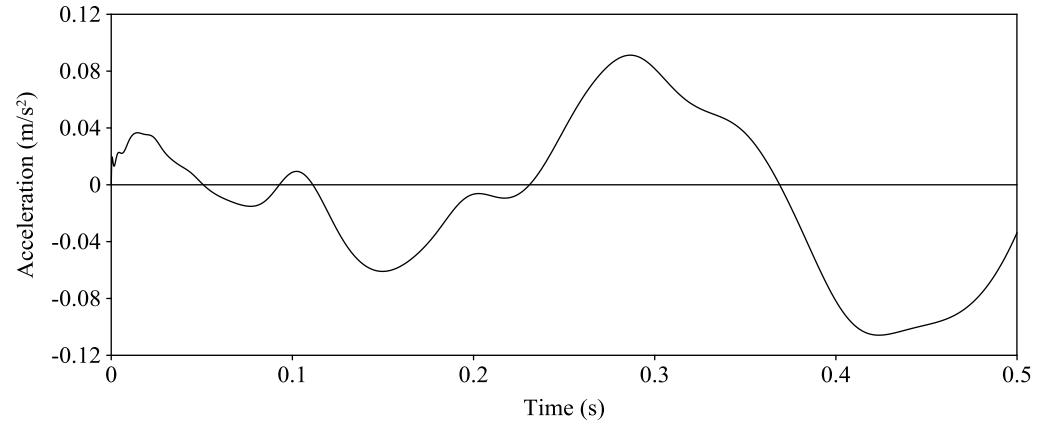

(a)

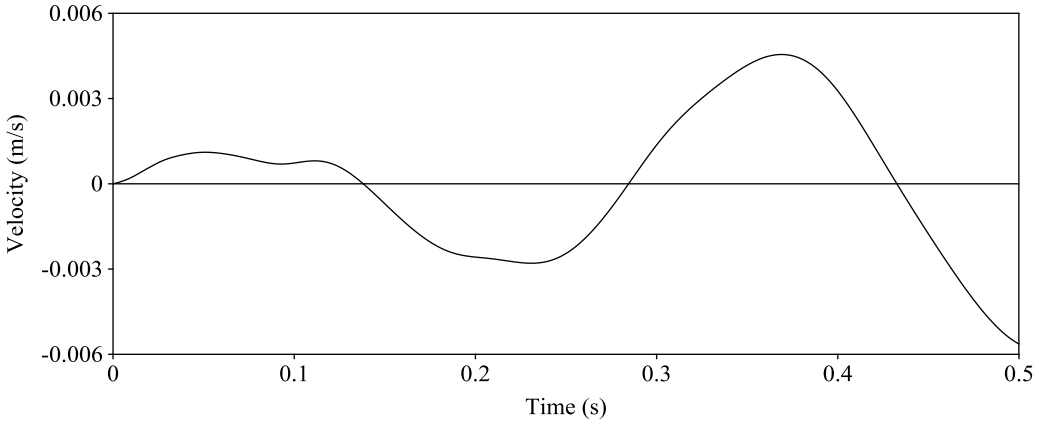

(b)

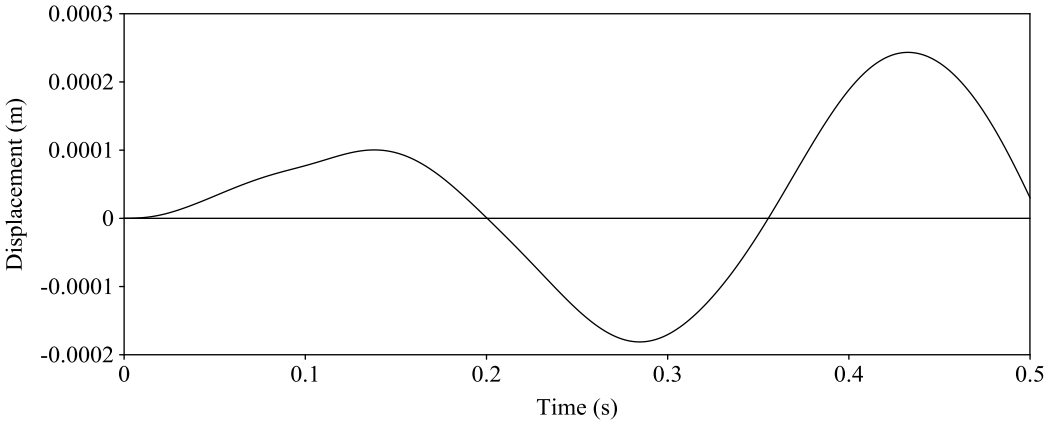

(c)

Figure 6.4 Vertical responses at node 1; (a) Acceleration; (b) Velocity; and (c) Displacement

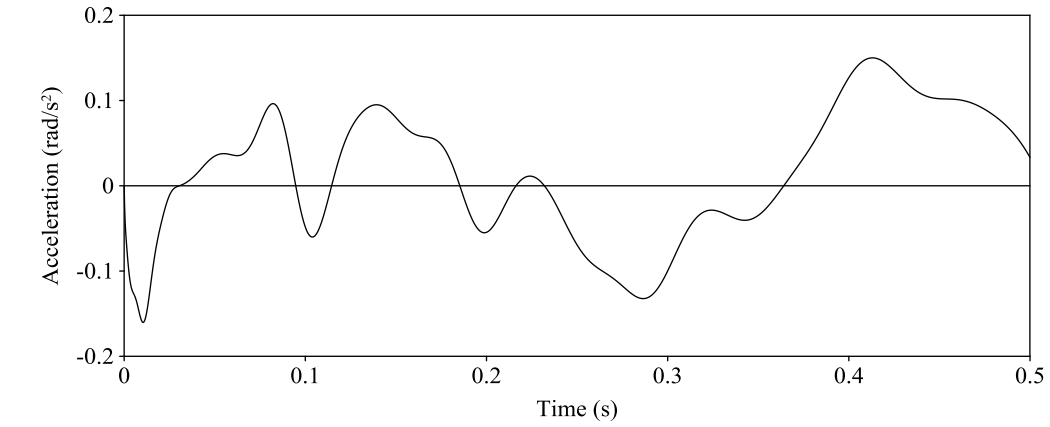

(a)

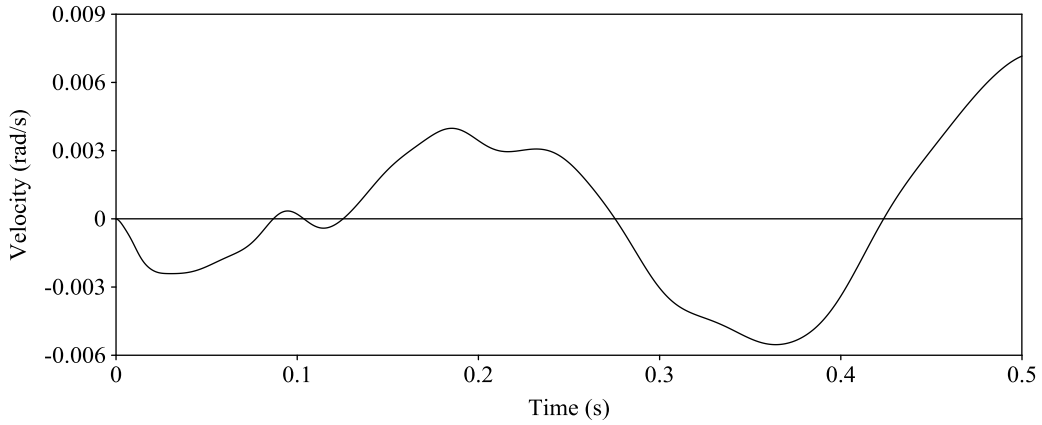

(b)

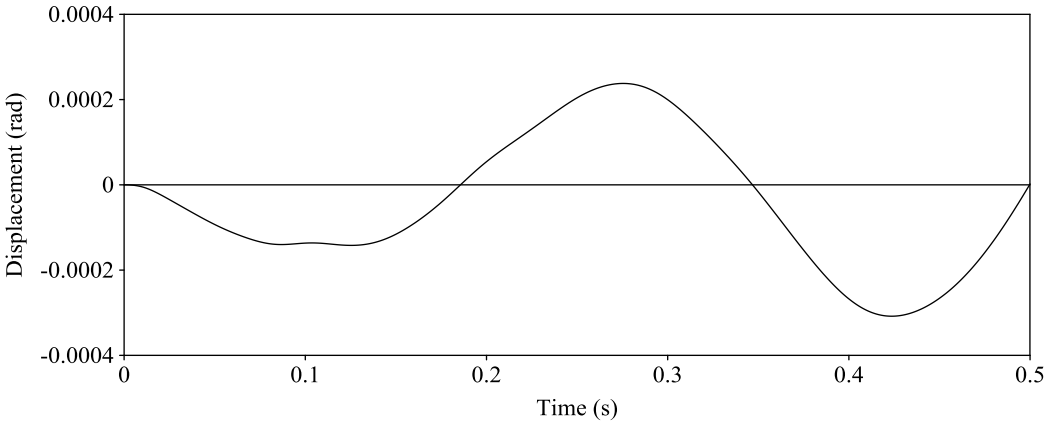

(c)

Figure 6.5 Rotation responses at node 1; (a) Acceleration; (b) Velocity; and (c) Displacement

6.2.2 Substructure Selection

The first step is to select an appropriate substructure to implement Stage 1 of the UKF-UI-WGI procedure. The substructure for this example is shown in double lines in Figure 6.1 and the information required about the substructure is summarized in Figure 6.6. At the minimum, responses at 9 DDOFs (nodes 1, 2, and 3) must be available to implement the ILS-UI procedure. The same substructure is used for all cases including defect-free and defective states in the subsequent sections for this frame.

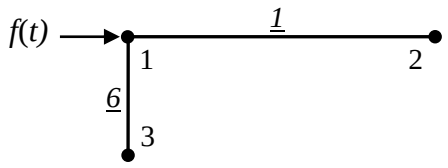

kn = 1
dkn = 3
re = 2
rn = 2
nsub = 3
sc = 0
dsub = 9

Figure 6.6 Substructure needed to implement Stage 1 of UKF-UI-WGI

6.2.3 Health Assessment of Defect-Free Frame

Initially, the frame is considered to be defect-free. In Stage 1, using responses analytically generated at 9 DDOFs, the time-history of the unknown input excitation is identified accurately as shown in Figure 6.7. The stiffness parameters of elements 1 and 6 are identified as summarized in Column 3 of Table 6.1a-i and the two Rayleigh damping coefficients *a* and *b* are identified as summarized in Column 3 of Table 6.1a-ii. The error in the identification of stiffness parameters is only 0.001%. As commonly used in the literature, the errors are defined as the percentage deviation of identified values,

representing the current state, with respect to the initial theoretical values. In actual field inspections, the information on the initial theoretical values can be obtained from design drawings, or from previous inspections, if available. The acceptable error in identification is about 10% as mentioned earlier. The error in identified damping coefficients *a* and *b* are 0.01% and 1.91%, respectively.

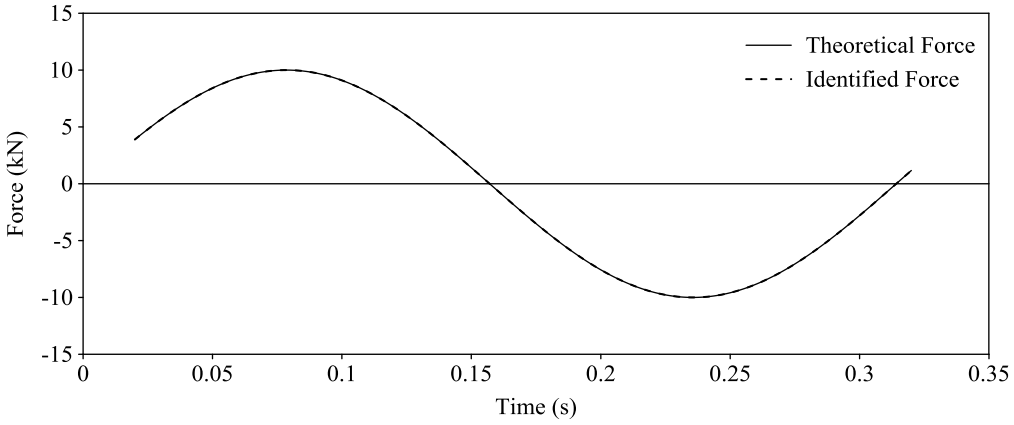

Figure 6.7 Theoretical and identified sinusoidal force at node 1

In Stage 2, the initial state vector $\hat{\mathbf{Z}}_{0|0}$ and its error covariance matrix $\mathbf{P}_{0|0}$ need to be developed. The initial state vector can be expressed as:

$$\hat{\mathbf{Z}}_{0|0}^{(1)} = \begin{bmatrix} \hat{\mathbf{X}}^{(1)}(0|0) \\ \hat{\dot{\mathbf{X}}}^{(1)}(0|0) \\ \tilde{\mathbf{K}}^{(1)}(0|0) \end{bmatrix}$$

The initial value of the displacement $\hat{\mathbf{X}}^{(1)}(0|0)$ and velocity $\hat{\dot{\mathbf{X}}}^{(1)}(0|0)$ for measured DDOFs, i.e., responses at nodes 1, 2, and 3, is assumed to have the same corresponding measured values and for not measured DDOFs is assumed to be zero. The initial value of stiffness parameters $\tilde{\mathbf{K}}^{(1)}(0|0)$ is developed judiciously using the information of

identified stiffness parameters in the substructure. The initial values of all the 5 beams and 10 columns in the frame are 13476 and 14553 kN-m, respectively.

The diagonal of the covariance matrix of measurement noise vector, $\mathbf{R}_k$, the initial error covariance of the displacement and velocity, $\mathbf{P}_x(0|0)$, the initial error covariance matrix of the stiffness parameters, $\mathbf{P}_s(0|0)$, and the weight factor, *w*, are considered to be 10^{-4}, 0.1, 10^3, and 10, respectively as summarized at the bottom of Table 6.1b.

The whole frame is then identified using UKF-WGI. The identified stiffness parameters of all the elements and the corresponding errors in identification are presented in Columns 3 and 4, respectively of Table 6.1b. The maximum error in the identified stiffness parameter is 0.25% when only responses at 9 DDOFs are used. The error in identification is very small. Moreover, if more response information is used in the UKF-WGI algorithm, the errors are expected to decrease. To show that, assume the responses are available at 12 DDOFs (9 DDOFs in the substructure plus 3 DDOFs at node 5). The results are shown in Columns 3 and 4 of Table 6.2. The maximum error in the identified stiffness parameter is 0.20%. It is obvious that the results based on 12 DDOFs are better than that of using 9 DDOFs indicating the value of additional response information. This is expected. Since the identified stiffness parameter of the members did not significantly change from the expected values, the frame can be correctly identified as defect-free.

6.2.4 Health Assessment of Defective Frame

After the successful verification of the defect-free state, defects at different locations and severity are introduced in the members and the efficiency of the proposed procedure is examined. The following three defect scenarios are considered:

(i) Defect 1 - stiffness of member 3 is reduced by 20% from the defect-free value.

(ii) Defect 2 - stiffness of member 4 is reduced by 50% from the defect-free value.

(iii) Defect 3 - stiffness of members 2 and 4 are reduced by 50% and 30%, respectively, from the defect-free value.

Obviously, the location and severity of defects will be unknown at the beginning of the inspection, but the measured responses should reflect their presence, if there are any. For this illustrative example, the responses are analytically generated by appropriately modeling the location, nature, and extent of defects.

In Stage 1, considering only the responses at 9 DDOFs in the substructure, the input excitation time-history, the two Rayleigh damping coefficients and the stiffness parameter of elements 1 and 6 are identified for each defective state. The identified stiffness parameters for all three defect scenarios are summarized in Columns 5, 7, and 9 and the corresponding errors in identification (percentage changes in identified stiffness parameters with respect to the actual values) are summarized in Columns 6, 8, and 10 of Table 6.1a-i. The errors in the identified damping coefficients are shown in Columns 5, 7, and 9 of Table 6.1a-ii. As in the defect-free case, the substructure is identified very accurately for all 3 defective states. Then, the information obtained from Stage 1 is used to initiate UKF-WGI in Stage 2 to assess the health of the whole frame. In Stage 2, using only the responses at 9 DDOFs in the substructure, the whole frame is identified and the results are summarized in Columns 5, 7, and 9 of Table 6.1b. The values of all the parameters to initiate Stage 2, i.e., R_k, $P_x(0|0)$, $P_s(0|0)$, and w are indicated at the bottom of Table 6.1b. UKF-WGI identified locations and severity of defects correctly for all cases. However, for Defect 3, member 11 is also reduced by 12.32% incorrectly indicating that it may also be defective. The error in identification should go down if

more responses are used. At this time, the absolute minimum number of responses required to implement the proposed method is still under development. The frame is again identified considering responses at 12 DDOFs, i.e., 9 DDOFs in the substructure and 3 DDOFs at node 5. The results are summarized in Columns 5-10 of Table 6.2. It is clear from the results that UKF-UI-WGI successfully identified all defect scenarios. The maximum error in the identification went down significantly when the frame is identified with responses at 12 DDOFs. This improvement is much more noticeable than that of defect-free case. Results also indicate that the identifications of the defective states are more challenging than the defect-free state. In any case, it can be concluded that the UKF-UI-WGI procedure can assess health of defect-free and defective structure very well.

Table 6.1 Structural parameter identification

(a) Stage 1: Identification of substructure using ILS-UI

(i) Stiffness parameter (*EI/L*) identification

Member	Nominal (kN-m)	Defect-Free		Defect 1		Defect 2		Defect 3	
		Identified (kN-m)	Change (%)	Identified (kN-m)	Change (%)	Identified (kN-m)	Change (%)	Identified (kN-m)	Change (%)
(1)	(2)	(3)	(4)	(5)	(6)	(7)	(8)	(9)	(10)
k_1	13476	13476	0.001	13476	0.001	13476	0.001	13476	0.001
k_6	14553	14553	0.001	14553	0.001	14553	0.001	14553	0.001

(ii) Damping coefficient identification

Damping Coefficients	Defect-Free		Defect 1		Defect 2		Defect 3	
	Nominal (kN-m)	Change (%)	Nominal (kN-m)	Change (%)	Nominal (kN-m)	Change (%)	Nominal (kN-m)	Change (%)
(1)	(2)	(3)	(4)	(5)	(6)	(7)	(8)	(9)
a	1.05947	-0.01	1.04472	-0.01	1.00177	-0.02	0.99955	-0.01
$b \times 10^{-4}$	6.19589	-1.91	6.28260	-1.88	6.30317	-1.86	6.62649	-1.80

(b) Stage 2: Identification of whole structure using UKF-WGI with 9 DDOFs

Member	Nominal (kN-m)	Defect-Free		Defect 1		Defect 2		Defect 3	
		Identified (kN-m)	Change (%)	Identified (kN-m)	Change (%)	Identified (kN-m)	Change (%)	Identified (kN-m)	Change (%)
(1)	(2)	(3)	(4)	(5)	(6)	(7)	(8)	(9)	(10)
k_1	13476	13477	0.01	13475	-0.01	13477	0.01	13460	-0.12
k_2	13476	13488	0.09	13502	0.19	13499	0.17	6755	**-49.88**
k_3	13476	13510	0.25	10755	**-20.19**	13376	-0.74	13304	-1.28
k_4	13476	13482	0.04	13725	1.84	6964	**-48.33**	10032	**-25.56**
k_5	13476	13456	-0.15	13223	-1.88	13090	-2.87	12712	-5.67
k_6	14553	14554	0.01	14551	-0.02	14551	-0.01	14527	-0.18
k_7	14553	14553	0.00	14539	-0.10	14544	-0.06	14490	-0.43
k_8	14553	14567	0.10	14742	1.30	14922	2.53	15369	5.61
k_9	14553	14562	0.06	14695	0.98	14787	1.61	14739	1.28
k_{10}	14553	14557	0.03	14298	-1.75	14033	-3.57	14142	-2.83
k_{11}	14553	14558	0.04	14192	-2.48	13619	-6.42	12759	-12.32
k_{12}	14553	14550	-0.02	14612	0.41	14506	-0.32	13897	-4.50
k_{13}	14553	14550	-0.02	14258	-2.03	14388	-1.13	14349	-1.40
k_{14}	14553	14543	-0.07	14593	0.28	14744	1.32	15053	3.43
k_{15}	14553	14543	-0.07	14925	2.55	15105	3.79	15635	7.43

Note: $R_k = 10^{-4}$; $P_x(0|0) = 0.1$; $P_s(0|0) = 10^3$; $w = 10$

Table 6.2 Identification of whole structure using UKF-WGI with 12 DDOFs

Member	Nominal (kN-m)	Defect-Free		Defect 1		Defect 2		Defect 3	
		Identified (kN-m)	Change (%)	Identified (kN-m)	Change (%)	Identified (kN-m)	Change (%)	Identified (kN-m)	Change (%)
(1)	(2)	(3)	(4)	(5)	(6)	(7)	(8)	(9)	(10)
k_1	13476	13482	0.04	13476	0.00	13478	0.01	13471	-0.04
k_2	13476	13487	0.08	13480	0.03	13481	0.04	6747	**-49.93**
k_3	13476	13493	0.12	10809	**-19.79**	13506	0.22	13509	0.24
k_4	13476	13497	0.16	13416	-0.45	6744	**-49.96**	9444	**-29.92**
k_5	13476	13450	-0.20	13502	0.20	13433	-0.32	13446	-0.23
k_6	14553	14557	0.03	14556	0.02	14555	0.02	14548	-0.03
k_7	14553	14557	0.02	14546	-0.05	14549	-0.03	14527	-0.18
k_8	14553	14553	0.00	14558	0.04	14560	0.05	14578	0.17
k_9	14553	14548	-0.04	14497	-0.38	14523	-0.20	14451	-0.70
k_{10}	14553	14581	0.20	14771	1.50	14695	0.98	14696	0.98
k_{11}	14553	14574	0.14	14692	0.96	14718	1.13	14724	1.17
k_{12}	14553	14550	-0.02	14591	0.26	14300	-1.74	14218	-2.30
k_{13}	14553	14552	-0.01	14608	0.38	14620	0.46	14582	0.20
k_{14}	14553	14541	-0.08	14445	-0.74	14685	0.91	14732	1.23
k_{15}	14553	14540	-0.09	14490	-0.43	14442	-0.76	14438	-0.79

Note: $R_k = 10^{-4}$; $P_x(0|0) = 0.1$; $P_s(0|0) = 10^3$; $w = 10$

6.2.5 Robustness, Convergence, and Stability of UKF-UI-WGI

To successfully implement a new concept for wider applications, its robustness, convergence, and stability characteristics need further consideration. Since the proposed method incorporates several important features, their relevance in improving some of these characteristics are specifically discussed in the following sections.

6.2.5.1 Effect of Weighted Global Iteration

As mentioned earlier, one of the most important features of UKF-UI-WGI is the introduction of weight factor, *w*, before initiating the second and subsequent global iterations. Since identification of the defective states is more challenging, the convergence characteristics of the algorithm to identify all three defective states with different weight factors are studied in this section.

For Defect 1, the process of convergence of the stiffness parameter of defective member 3, a beam, is studied first. The nominal stiffness parameter of defective member 3 is 10781 kN-m. In Stage 1, the stiffness parameter of the defect-free beam element in the substructure is identified as 13476 kN-m. As discussed earlier, to define the initial state vector of the whole frame, required to initiate UKF-WGI, the stiffness parameter of all beam elements are considered to be 13476 kN-m. Obviously, for defective member 3, it will be incorrect. It will be interesting to know the optimum value of *w* that will help UKF-WGI to converge to the real value. At the end of the first global iteration, the identified stiffness parameter of member 3 is 12331 kN-m, as shown in Table 6.3; essentially this value would have been obtained by the traditional UKF method using only one global iteration. The result clearly indicates that the traditional UKF cannot identify a large structural system using short response time-histories. The accuracy of the

identification may be slightly improved by using longer response time-histories but it still cannot identify the structure correctly. The identified stiffness parameter of defective member 3 for various weight factors are summarized in Table 6.3. When w =1, i.e., no weight is used, the algorithm converged after 4^{th} global iteration satisfying 1% convergence criterion, as discussed in Equation (3.30), but the error in the identification is 9.45%, i.e., the stiffness parameter did not converge to the nominal or expected value. When w is considered to be 10, 50, 100, and 1000, it needed 6, 5, 4, and 3 global iterations, respectively, to converge to the expected value with very small errors. The convergence behavior as a function of w is also plotted in Figure 6.8a.

The reason for this beneficial effect of the weight factor is examined further with the help of Figure 6.9. As can be seen from Figure 6.9a with w = 1, the variance of the stiffness parameter of member 3 went down to 386 after 4^{th} global iteration; however, it is 16752 after the same global iteration with w = 10. Low variance will cause a small change in the stiffness parameter between the initial and the end of each global iteration. This may satisfy the convergence tolerance criterion (ε_s) before the stiffness parameter reaches to its correct value and the algorithm will stop. As shown in Figure 6.9b for w = 10, the amplified variance facilitates the iteration to continue without satisfying the convergence criterion but ultimately it converges to the correct value.

To study the significance of w further, the author reduced the convergence criterion from 1% to 0.1% with w =1 to identify the stiffness parameter of member 3. The algorithm converged to 11289 kN-m after 21 global iterations with 4.71% error in the identification. The error is still higher than that of the weighted global iteration procedure, i.e., when w is greater than 1. It can also be seen from Table 6.3 and Figure

6.8a that the total number of global iterations required to identify the stiffness parameter decreases with the increase in the weight factor. It is also important to note that the use of a very large value of *w* may compromise the convergence.

For Defect 2, the stiffness parameter of defective member 4 is reduced by 50% indicating that it should be around 6738 kN-m. For this defect scenario with *w* = 50 and 100, the algorithm converged for the defective member but did not converge satisfying the 1% convergence criterion for other defect-free members. Obviously, the convergence criterion must be satisfied for all members; defect-free and defective. Therefore, in this situation the use of the objective function becomes necessary. At end of each global iteration, the corresponding objective function is also evaluated. Then, the stiffness parameters for all the members at a specific global iteration corresponding to the minimum objective function, $\bar{\theta}_{min}$, are used to assess the structural health. As shown in Table 6.4 with *w* = 50, the objective function is minimum at the 7th global iteration; therefore, the identified stiffness parameters at this global iteration are used to assess the structural health. The bold values in Table 6.4 represent the minimum objective function. When *w* = 1, the algorithm converged after 6th global iteration to 8917 kN-m with 32.34% error in the identification and the objective function became minimum at the same time, indicating that when *w* =1, the $\bar{\theta}_{min}$ concept cannot be used as an alternative solution to identify the system. When *w* = 10 and 1000, the algorithm converged to the correct value and the objective function also became minimum at the same global iteration. From this example, it can be concluded that the weighted global iteration concept with objective function will be appropriate to assess health of large structural systems with reasonable accuracy. As expected, by comparing results in Tables 6.3 and

6.4, one can observe that to identify a more severe defective state, i.e., a large difference between the initial assumed and correct values, will require more global iterations. The convergence behavior as a function of *w* is also plotted in Figure 6.8b.

For Defect 3, members 2 and 4 are considered to be defective. The convergence behavior for members 2 and 4 are shown in Figures 6.8c and 6.8d, respectively. All the observations made earlier for the two defective states are applicable here also. With *w* =1, the algorithm also failed to identify the defective states correctly. This example shows that the weighted global iteration procedure is also capable of locating multiple defects and their severity accurately.

Table 6.3 Identified stiffness parameter (*EI/L*) of member 3 for Defect 1

NGI*	Nominal (kN-m)	*w* = 1	*w* = 10	*w* = 50	*w* = 100	*w* = 1000
(1)	(2)	(3)	(4)	(5)	(6)	(7)
0	10781	13476	13476	13476	13476	13476
1	10781	12331	12331	12331	12331	12331
2	10781	12070	11445	11108	11022	10894
3	10781	11911	11030	10857	10823	10811
4	10781	11800	10890	10804	10795	
5	10781		10829	10797		
6	10781		10809			
Error % at convergence		9.45	0.26	0.15	0.13	0.28
Note: $R_k = 10^{-4}$; $P_x(0\|0) = 0.1$; $P_s(0\|0) = 10^3$						
*NGI: number of global iterations						

Table 6.4 Identified stiffness parameter (*EI/L*) of member 4 for Defect 2 and objective function

NGI	Nominal (kN-m)	*w* = 1		*w* = 10		*w* = 50		*w* = 100		*w* = 1000	
		EI/L	$\bar{\theta}*10^{-5}$	*EI/L*	$\bar{\theta}*10^{-5}$	*EI/L*	$\bar{\theta}*10^{-5}$	*EI/L*	$\bar{\theta}*10^{-5}$	*EI/L*	$\bar{\theta}*10^{-5}$
(1)	(2)	(3)	(4)	(5)	(6)	(7)	(8)	(9)	(10)	(11)	(12)
0	6738	13476		13476		13476		13476		13476	
1	6738	9715	1331	9715	1331	9715	1331	9715	1331	9715	1331
2	6738	9437	619.1	8644	390.5	8284	203.3	8189	151.3	7665	53.99
3	6738	9243	538.3	8197	96.60	7515	23.23	7369	16.25	6990	6.01
4	6738	9103	477.9	7648	35.01	7112	7.82	6993	5.17	6742	**4.29**
5	6738	8998	431.8	7292	28.78	6885	3.92	6795	4.07		
6	6738	8917	**395.2**	7102	11.50	6765	3.86	6723	**4.05**		
7	6738			6962	4.04	6722	**3.85**	6727	4.14		
8	6738			6862	3.28	6722	3.91	6720	4.19		
9	6738			6800	3.45	6717	3.98	6726	4.12		
10	6738			6764	3.34	6725	3.91	6717	4.05		
11	6738			6744	**3.25**	6718	3.89	6727	4.10		
12	6738					6725	3.90	6717	4.06		
13	6738					6718	3.90	6726	4.10		
Error % at $\bar{\theta}_{min}$		32.34		0.09		-0.23		-0.22		0.06	
Note: $R_k = 10^{-4}$; $P_x(0\|0) = 0.1$; $P_s(0\|0) = 10^3$											

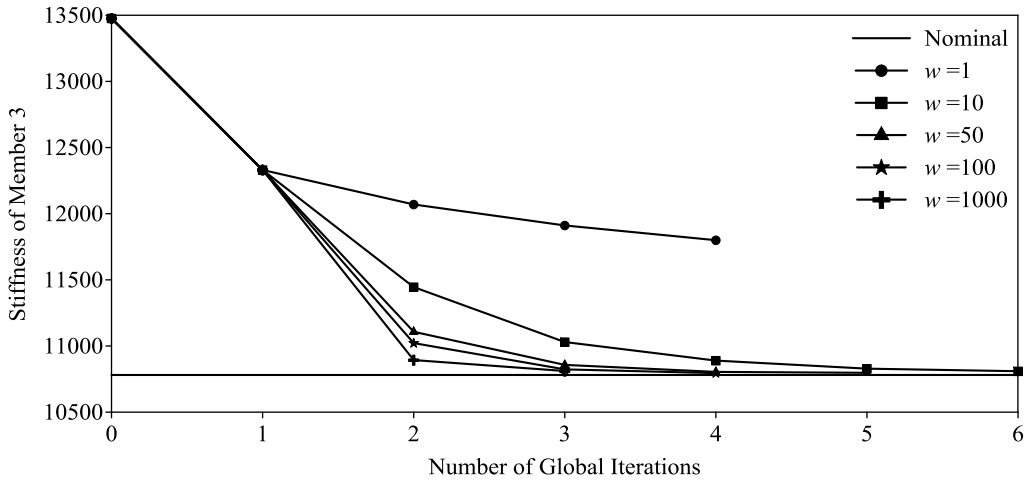

(a) Member 3 of Defect 1

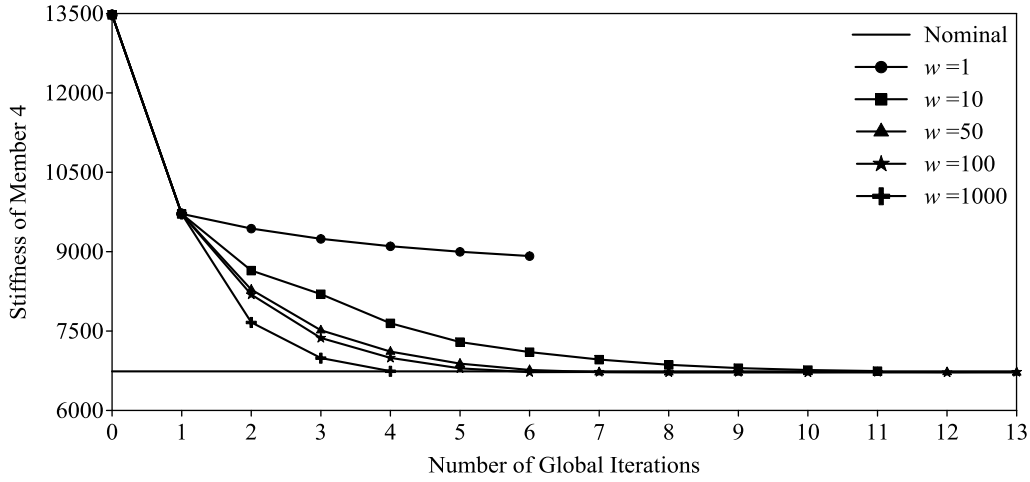

(b) Member 4 of Defect 2

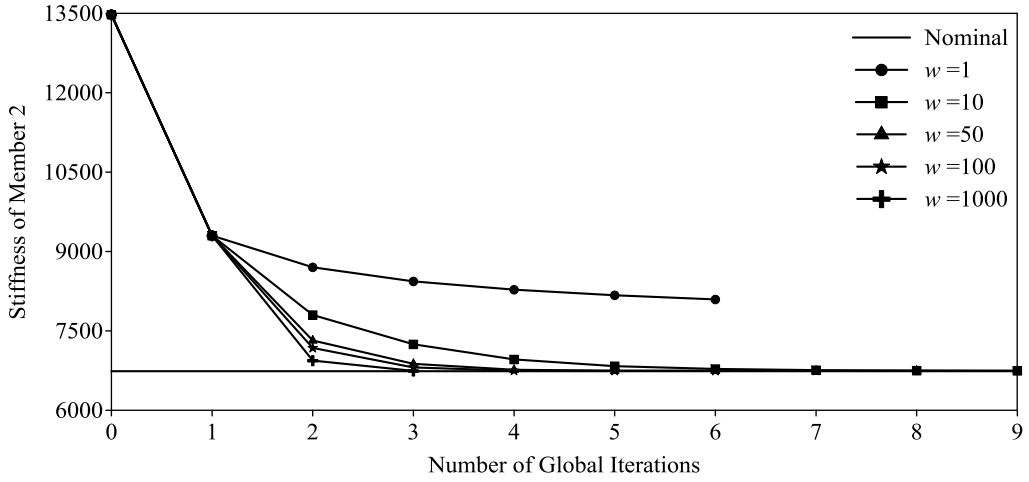

(c) Member 2 of Defect 3

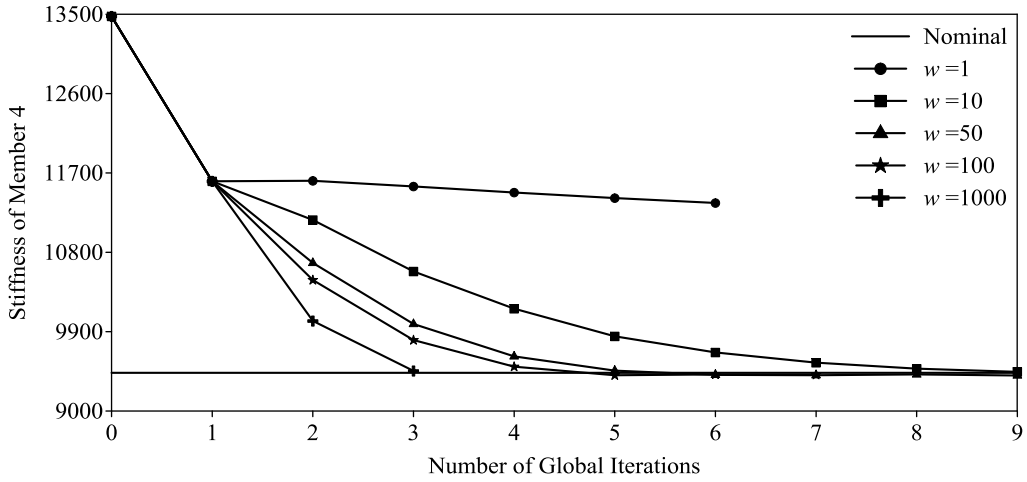

(d) Member 4 of Defect 3

Figure 6.8 Convergence behaviors using different weight factor

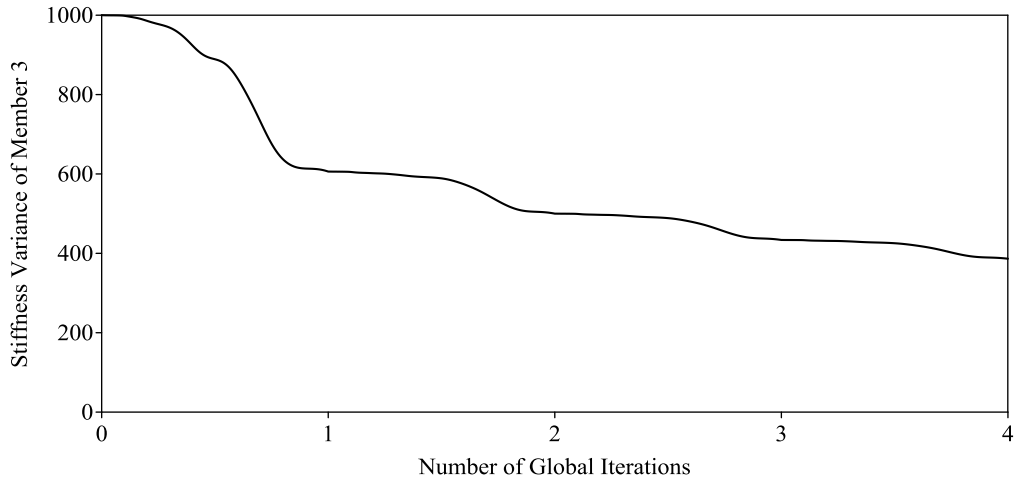

(a) w = 1

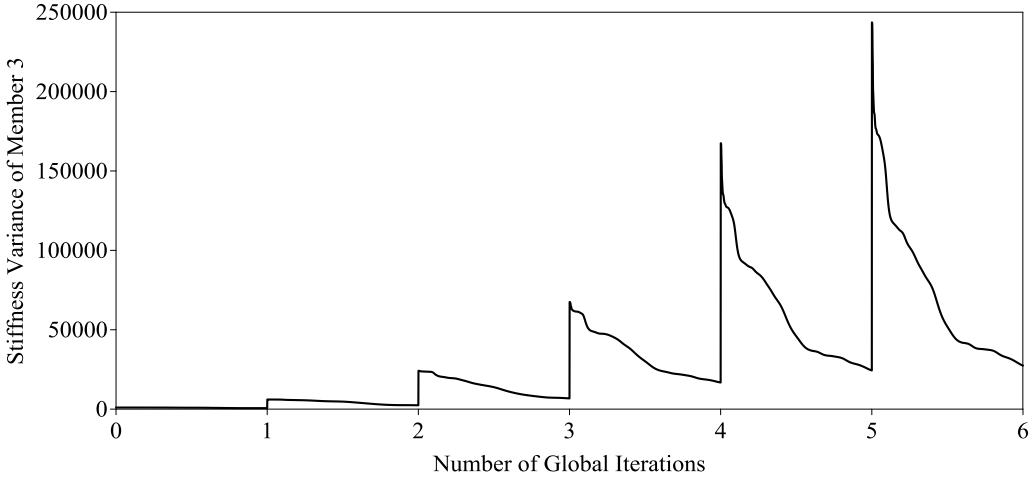

(b) w = 10

Figure 6.9 Stiffness variance behavior of member 3 for Defect 1 with w = 1 and 10

6.2.5.2 Effect of Value of Initial Stiffness Covariance

The value of initial stiffness covariance $P_s(0|0)$ is one of the important factors in the identification process. The value of $P_s(0|0)$ depends on the magnitudes of the stiffness parameters of the structural elements. For the frame under consideration, the defect-free stiffness parameter for a beam and a column are estimated to be 13476 and 14553 kN-m, respectively. To study the convergence behavior, the covariance of the initial stiffness is considered to be 10^3, 10^4, 10^5, and 10^6 for all three defective cases. For this example, the covariance of magnitude 10^3 and 10^4 are relatively small. The convergence characteristics are shown in Figure 6.10 for w = 10 and R_k = 10^{-4}. The results show that faster convergence can be obtained by using a large value of $P_s(0|0)$. The results also demonstrate the robustness of the UKF-WGI procedure. Even with relatively smaller value of $P_s(0|0)$, the stiffness parameter converges to the nominal value with the help of the weight factor. Defect 2 can be considered further to clarify the above statement. In this example, the initial value of the stiffness parameter of defective member is assumed to be 13476 kN-m instead of 6738 kN-m, but the algorithm still converged to the real value even when $P_s(0|0)$ is assumed to be 10^3 and 10^4, using weighted global iteration. It can be concluded from above observation that the large initial covariance is desirable to accelerate the UKF-WGI processing. However, its value should not be very large so that the stability might be compromised in some cases.

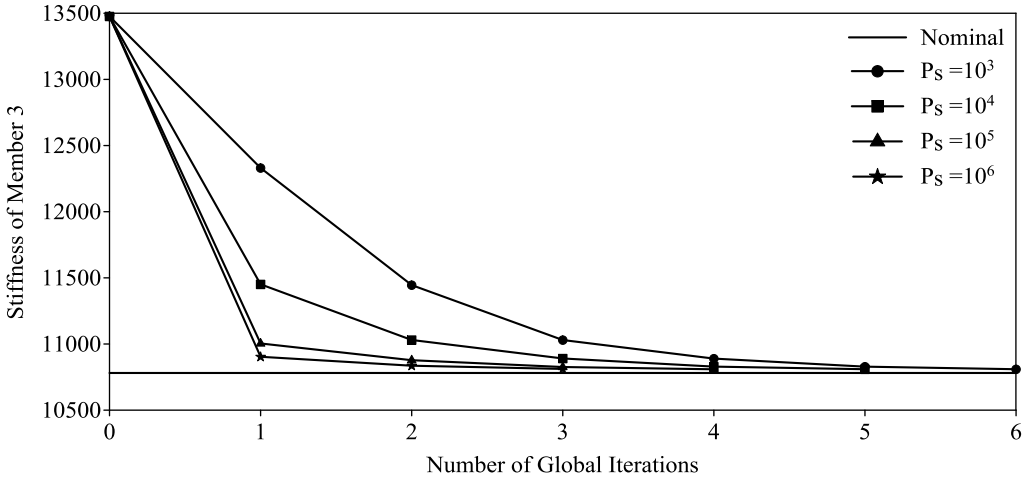

(a) Member 3 of Defect 1

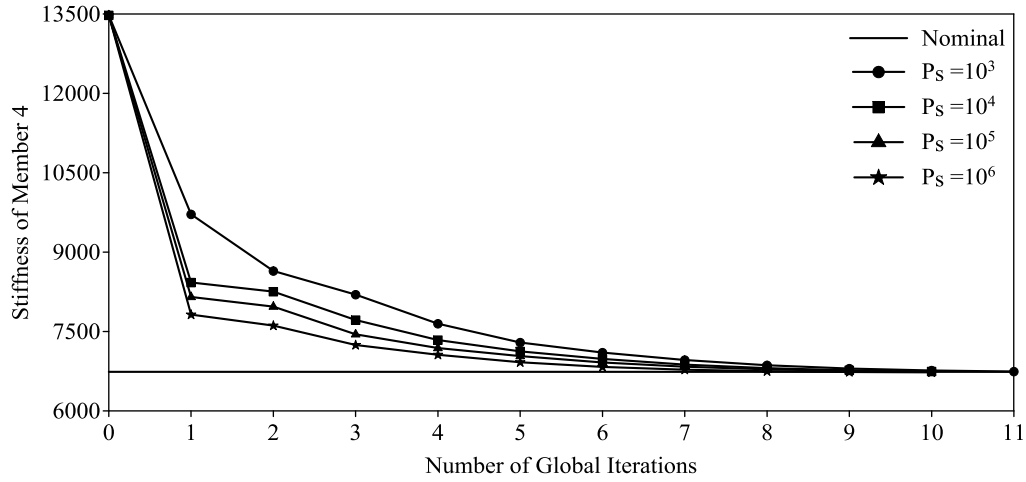

(b) Member 4 of Defect 2

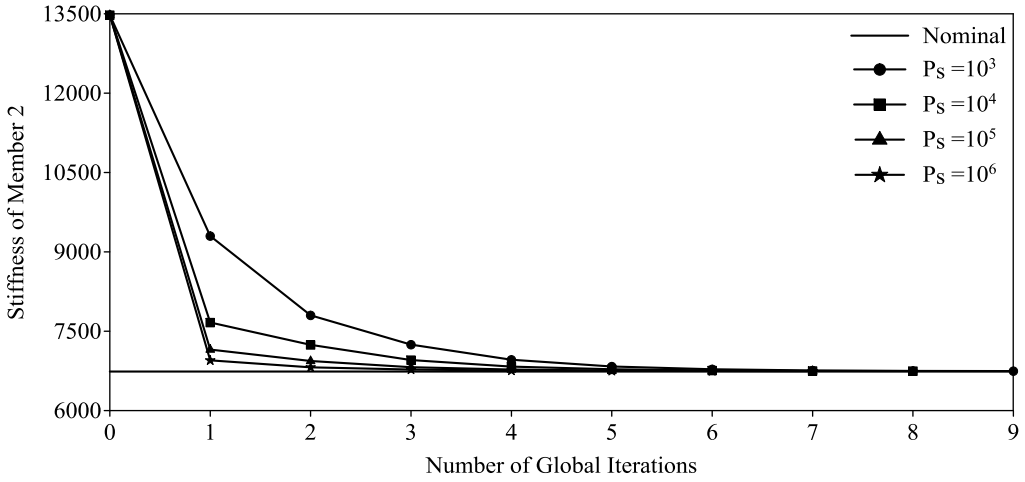

(c) Member 2 of Defect 3

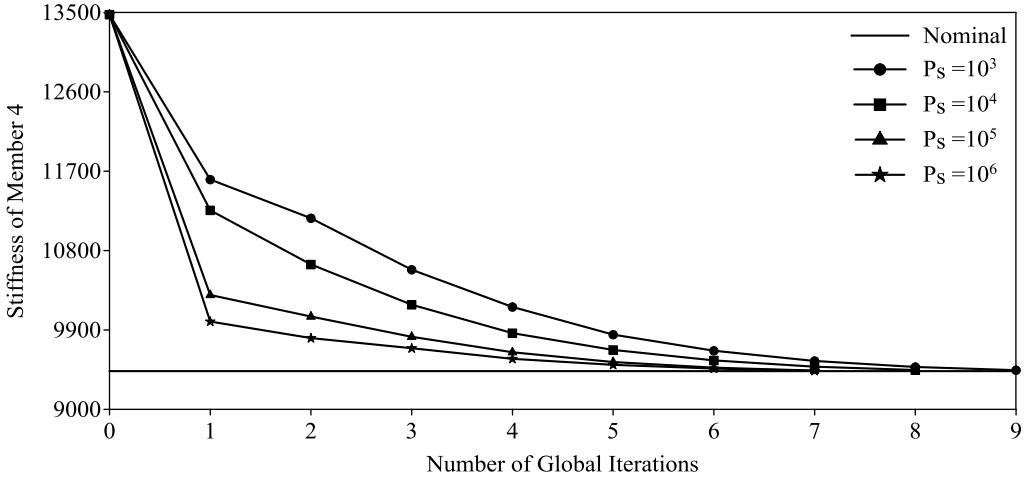

(d) Member 4 of Defect 3

Figure 6.10 Convergence behaviors using different value of initial stiffness covariance

6.2.5.3 Effect of Covariance of Measurement Noise

Another important factor to implement UKF-WGI needs further consideration is the covariance of measurement noise (R_k). The convergence characteristics of the algorithm are studied by considering R_k to be 10^{-2}, 10^{-3}, 10^{-4}, 10^{-5}, and 10^{-6} for all three defective cases. The larger value of R_k indicates the poor quality of measured responses. The filter will be slower to respond to the response data and the algorithm will converge slowly requiring more global iteration. The total numbers of global iteration required to identify the structures in all three defect scenarios are plotted in Figure 6.11 for w = 10 and $P_s(0|0) = 10^3$. The figures clearly indicate that the UKF-WGI procedure correctly identified the locations and the severity of defects, even when the quality of the measured responses is not good.

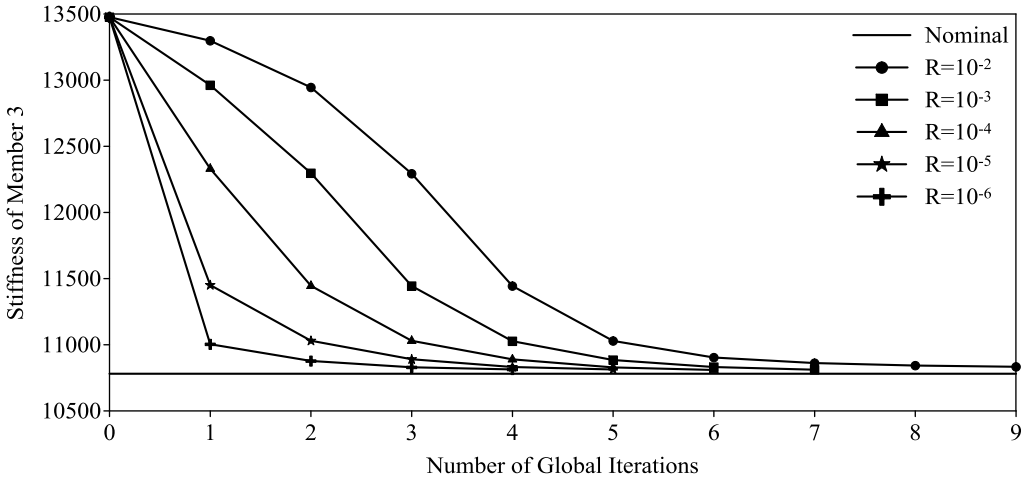

(a) Member 3 of Defect 1

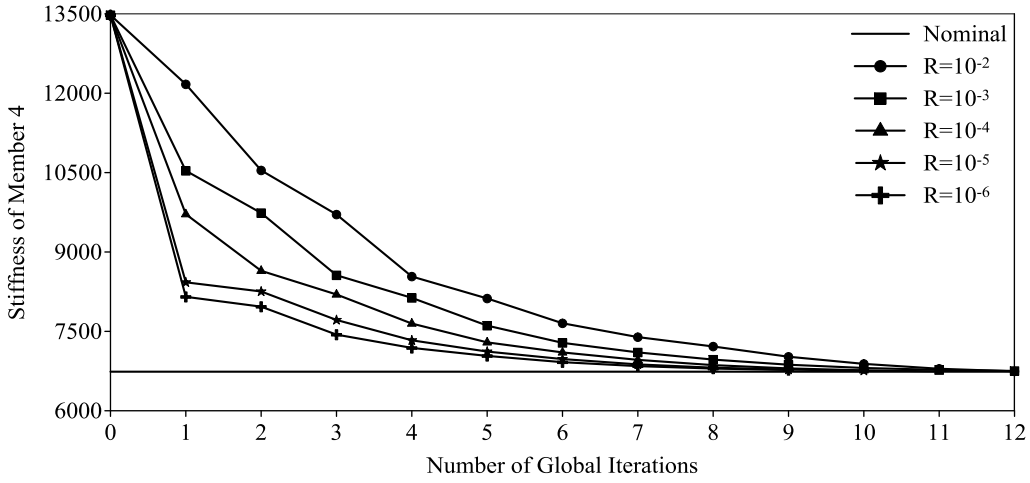

(b) Member 4 of Defect 2

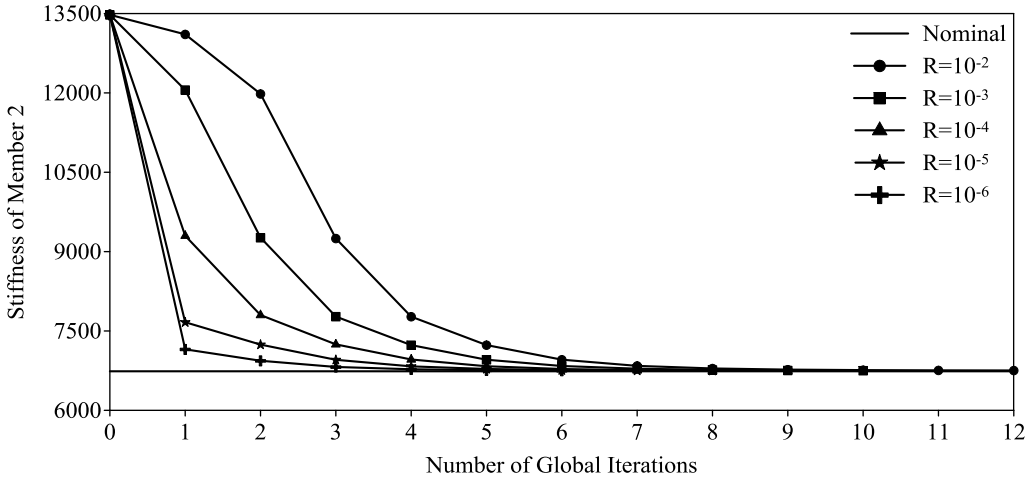

(c) Member 2 of Defect 3

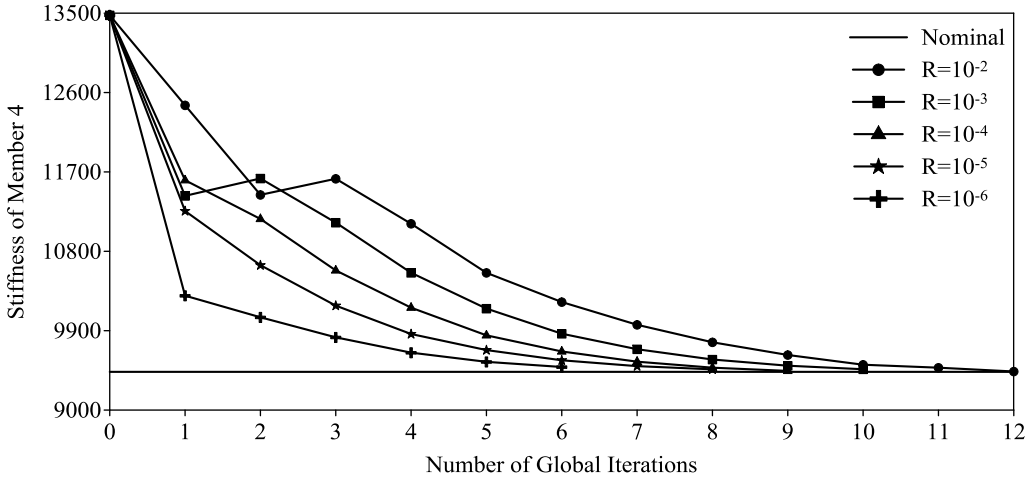

(d) Member 4 of Defect 3

Figure 6.11 Convergence behaviors using different value of measurement noise covariance

6.3 Health Assessment of Three-Bay Three-Story Frame

6.3.1 Description of the Frame

A two-dimensional three-bay three-story frame shown in Figure 6.12 is considered. The frame comprised of 21 members; 9 beams and 12 columns. The width of each bay is 9.14 m and the height of each story is 3.66 m. The beams and columns are made of W21×68 and W14×61 sections, respectively of Grade 50 steel. The frame is represented by the finite element (FE) with 21 elements and 16 nodes. Each node has three DDOFs; two translational and one rotational. The support at the bases is considered to be fixed. Therefore, the total number of DDOFs for the frame is 36. The theoretical stiffness parameters k_i, defined in terms of (E_iI_i/L_i), for the beam and column are estimated to be 13476 kN-m and 14553 kN-m, respectively. The first two natural frequencies of the defect-free frame are estimated to be f_1 = 6.0023 Hz and f_2 = 18.944 Hz. Then, assuming the same damping for the first two significant frequencies, a procedure suggested by Clough and Penzien (2003) is used to calculate the Rayleigh damping coefficients *a* and *b*. They are found to be 2.86393 and 0.00063799, respectively, for the equivalent modal damping of 5%, commonly used in developing design guidelines. The frame is excited by two types of loading; impulsive and seismic excitations.

6.3.2 Frame under Two Impulsive Loadings

In the first example, the capability of UKF-UI-WGI is verified for a structural health assessment problem already available in the literature in order to demonstrate the superiority of the proposed method. Das et al. (2012) assessed health of the frame shown in Figure 6.12 using the GILS-EKF-UI procedure. The frame was excited simultaneously

by two impulsive loadings applied at nodes 1 and 9 in the horizontal direction as shown in Figure 6.13. For the theoretical verification of the method, the information on responses is numerically generated using a commercial software ANSYS (ver. 14.0). After the responses are generated, the information on the excitation force is completely ignored. In this example, the health of the frame is assessed using responses from 0.05 to 0.37s with the time increment of 0.00025s providing a total of 1281 time points

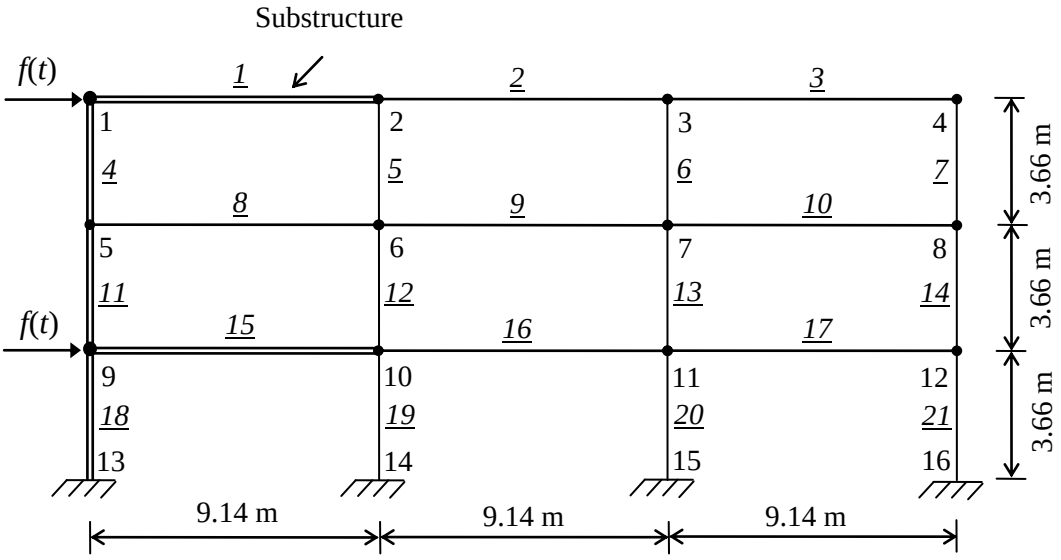

Figure 6.12 A three-bay three-story steel frame under impulse excitation

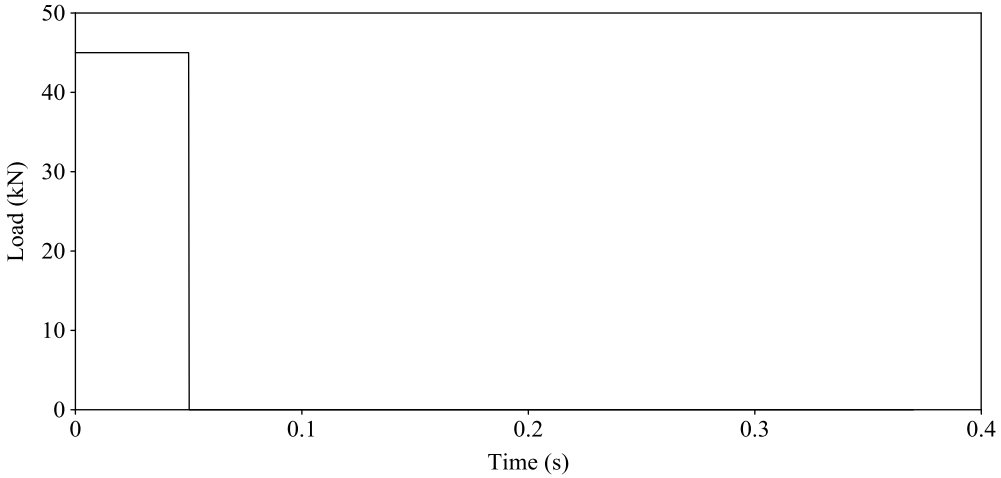

Figure 6.13 Impulse excitation at nodes 1and 9

6.3.2.1 Substructure Selection

The substructure for this example is shown in double lines in Figure 6.12 and the information required about the substructure is summarized in Figure 6.14. At the minimum, responses at 15 DDOFs (nodes 1, 2, 5, 9, and 10) must be available to identify the two input excitations using the ILS-UI procedure. This substructure is used for all cases; defect-free and defective states in the subsequent sections related to this example.

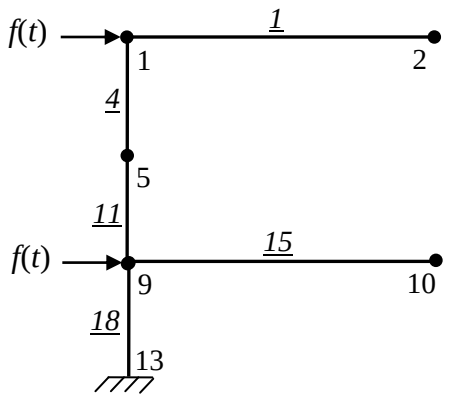

kn = 1, 9
dkn = 6
re = 5
rn = 4
nsub = 6
sc = 3
dsub = 15

Figure 6.14 Substructure needed to implement Stage 1 of UKF-UI-WGI

6.3.2.2 Health Assessment of Defect-Free Frame

The defect-free state of the frame is considered first. In Stage 1, using only responses at 15 DDOFs in the substructure, the stiffness parameters of all 5 elements in the substructure, two Rayleigh damping coefficients and the time-history of two unknown input forces are identified using ILS-UI. The identified stiffness parameters for all 5 elements in the substructure and Rayleigh damping coefficients are given in Table 6.5a. It can be noticed that all the stiffness and damping parameters were identified well. The convergence process of the two Rayleigh damping coefficients is shown in Figure 6.15.

The identified excitation forces at nodes 1 and 9 are shown in Figure 6.16. The accuracy of the identifications can be easily seen from these figures. Using the information from Stage 1, the stiffness parameters for all 21 elements of the whole frame are then identified. The values of all the parameters required to implement UKF-WGI in Stage 2, i.e., R_k, $P_x(0|0)$, $P_s(0|0)$, and w are indicated at the bottom of Table 6.5b. The results of identification are summarized in Table 6.5b, Column 3. The maximum error in the identification is about 0.08% indicating that the frame was identified accurately. Furthermore, the frame can be considered defect-free since the identified stiffness parameters did not differ significantly from the expected values.

The results of identified stiffness parameters reported by Das et al. (2012) using GILS-EKF-UI with assuming responses measured at 15 DDOFs are shown in Table 6.5c, Column 3. As pointed out in Table 6.5c, Column 4, the maximum error in the identification is about 273%. The results indicate that GILS-EKF-UI failed to identify the frame and thus its health cannot be assessed.

This example clearly establishes the superiority of UKF-UI-WGI over GILS-EKF-UI in assessing structural health. The problem was further investigated considering responses measured at a different number of DDOFs in order to explore the minimum number of responses required for the successful identification of the whole frame. The errors in the identified stiffness parameter of all elements of the frame using UKF-UI-WGI with responses available at 18 DDOFs (nodes 1, 2, 3, 5, 9, and 10), 21 DDOFs (nodes 1, 2, 3, 4, 5, 9, and 10), and 24 DDOFs (nodes 1, 2, 3, 4, 5, 9, 10, and 12) are investigated and the results are summarized in Columns 6, 8, and 10, respectively, of Table 6.5b. The maximum error in the identification did not improve significantly with

using additional response information. However, when the whole frame was identified using GILS-EKF-UI and the responses at 18, 21, and 24 DDOFs, the corresponding maximum errors in the identification reported to be 67.7%, 49.7%, and 4.3%, respectively as shown in Table 6.5c. As mentioned earlier, the acceptable error in identification is about 10% as reported in the literature. The optimal number of responses required for the successful identification of the whole frame using GILS-EKF-UI is 24 DDOFs for this example. The maximum error in the identification using UKF-UI-WGI and responses at 15 DDOFs is much smaller than that of GILS-EKF-UI with responses at 24 DDOFs.

It is to be noted that Kalman filter-based algorithms estimate the stiffness parameters of the whole frame by predicting responses at all DDOFs and then correcting the predicted responses and stiffness parameters using available measurements. For the nonlinear SI, the linearization process used in the EKF procedure is not accurate and requires more response information to compensate for the error. Since UKF-based procedures propagate uncertainty more efficiently, they require much smaller response information to assess structural health. For the example considered here, the optimum number of responses required for successful identification of the whole frame is 15 for UKF-UI-WGI and 24 for GILS-EKF-UI.

Table 6.5 Stiffness parameter (*EI/L*) identification for defect-free case using UKF-UI-WGI

(a) Stage 1: Identification of substructure

Member	Theoretical (kN-m)	Identified	Error (%)
k_1	13476	13482	0.04
k_4	14553	14559	0.04
k_{11}	14553	14580	0.18
k_{15}	13476	13501	0.18
k_{18}	14553	14580	0.19
a	2.863935	2.870977	0.25
$b\times10^{-4}$	6.379902	6.245979	-2.10

(b) Stage 2: Identification of whole structure

Member	Theoretical (kN-m)	15 DDOFs		18 DDOFs		21 DDOFs		24 DDOFs	
		Identified	Error (%)	Identified	Error (%)	Identified	Error (%)	Identified	Error (%)
(1)	(2)	(3)	(4)	(5)	(6)	(7)	(8)	(9)	(10)
k_1	13476	13487	0.08	13483	0.05	13485	0.07	13485	0.07
k_2	13476	13466	-0.08	13484	0.06	13484	0.06	13483	0.05
k_3	13476	13486	0.07	13484	0.05	13485	0.07	13484	0.06
k_4	14553	14557	0.03	14557	0.03	14557	0.03	14558	0.03
k_5	14553	14558	0.03	14555	0.02	14556	0.02	14556	0.02
k_6	14553	14560	0.05	14557	0.03	14558	0.03	14560	0.05
k_7	14553	14551	-0.01	14559	0.04	14558	0.03	14559	0.04
k_8	13476	13477	0.00	13475	-0.01	13474	-0.02	13471	-0.03
k_9	13476	13476	0.00	13475	-0.01	13473	-0.03	13472	-0.03
k_{10}	13476	13470	-0.04	13472	-0.03	13471	-0.04	13469	-0.05
k_{11}	14553	14557	0.03	14559	0.04	14559	0.04	14560	0.05
k_{12}	14553	14553	0.00	14558	0.04	14558	0.04	14559	0.04
k_{13}	14553	14563	0.07	14559	0.04	14561	0.06	14561	0.06
k_{14}	14553	14563	0.07	14560	0.05	14561	0.05	14561	0.05
k_{15}	13476	13476	0.00	13474	-0.02	13474	-0.02	13471	-0.04
k_{16}	13476	13471	-0.04	13470	-0.04	13469	-0.05	13474	-0.02
k_{17}	13476	13470	-0.04	13469	-0.05	13469	-0.05	13471	-0.04
k_{18}	14553	14560	0.05	14559	0.04	14559	0.04	14559	0.04
k_{19}	14553	14560	0.05	14557	0.03	14558	0.03	14557	0.02
k_{20}	14553	14549	-0.03	14557	0.02	14557	0.03	14557	0.03
k_{21}	14553	14557	0.03	14559	0.04	14560	0.05	14559	0.04
Note:	$R_k = 10^{-4}$; $P_x(0\|0) = 1.0$; $P_s(0\|0) = 10^3$; $w = 50$								

(c) Identification of (*EI/L*) for defect-free case using GILS-EKF-UI (Das et al. 2012)

Member	Theoretical (kN-m)	15 DDOFs		18 DDOFs		21 DDOFs		24 DDOFs	
		Identified	Error (%)	Identified	Error (%)	Identified	Error (%)	Identified	Error (%)
(1)	(2)	(3)	(4)	(5)	(6)	(7)	(8)	(9)	(10)
k_1	13476	11549	-14.3	14249	5.7	13473	0.0	13545	0.5
k_2	13476	6384	-52.6	15241	13.1	13244	-1.7	13681	1.5
k_3	13476	24229	79.8	8321	-38.3	13779	2.2	13497	0.2
k_4	14553	27805	91.1	16037	10.2	14514	-0.3	14601	0.3
k_5	14553	10595	-27.2	15485	6.4	14410	-1.0	14542	-0.1
k_6	14553	11857	-18.5	12273	-15.7	14693	1.0	14547	0.0
k_7	14553	13325	-8.4	24412	67.7	14333	-1.5	14432	-0.8
k_8	13476	2930	-78.3	10149	-24.7	11680	-13.3	13109	-2.7
k_9	13476	50270	273	15249	13.2	11170	-17.1	13519	0.3
k_{10}	13476	40685	202	17062	26.6	16639	23.5	13458	-0.1
k_{11}	14553	11798	-18.9	10859	-25.4	12672	-12.9	14192	-2.5
k_{12}	14553	9602	-34.0	10497	-27.9	11716	-19.5	14552	0.0
k_{13}	14553	14115	-3.0	18201	25.1	14494	-0.4	14903	2.4
k_{14}	14553	22920	57.5	21218	45.8	21784	49.7	14547	0.0
k_{15}	13476	12047	-10.6	10015	-25.7	11737	-12.9	13153	-2.4
k_{16}	13476	6082	-54.9	10387	-22.9	10303	-23.5	13705	1.7
k_{17}	13476	14577	8.2	17322	28.5	18879	40.1	13808	2.5
k_{18}	14553	17465	20.0	10272	-29.4	12572	-13.6	14375	-1.2
k_{19}	14553	10073	-30.8	11568	-20.5	11671	-19.8	14312	-1.7
k_{20}	14553	9499	-34.7	19770	35.8	13730	-5.7	14351	-1.4
k_{21}	14553	28112	93.2	17496	20.2	20806	43.0	15177	4.3
Note:	$R_k = 10^{-4}$; $P_x(0\|0) = 1.0$; $P_s(0\|0) = 10^3$; $w = 1000$								

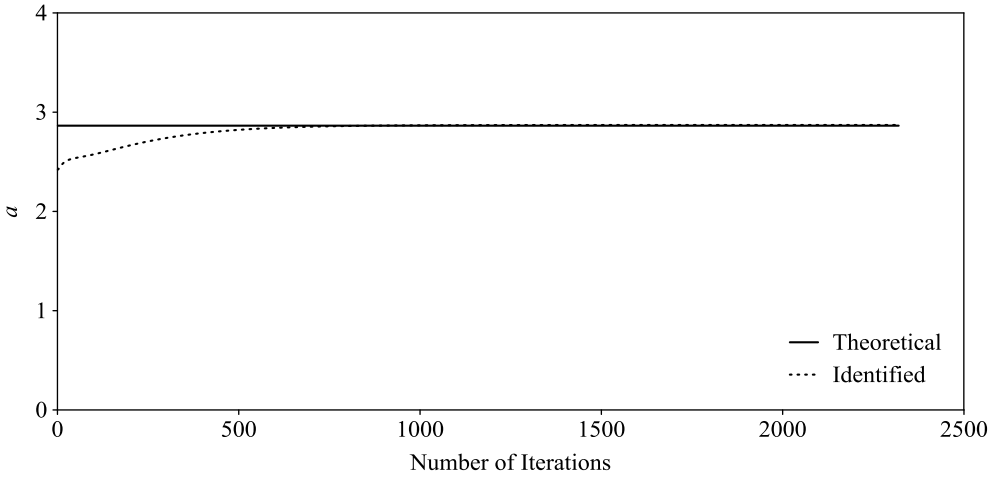

(a) Damping coefficient, *a*

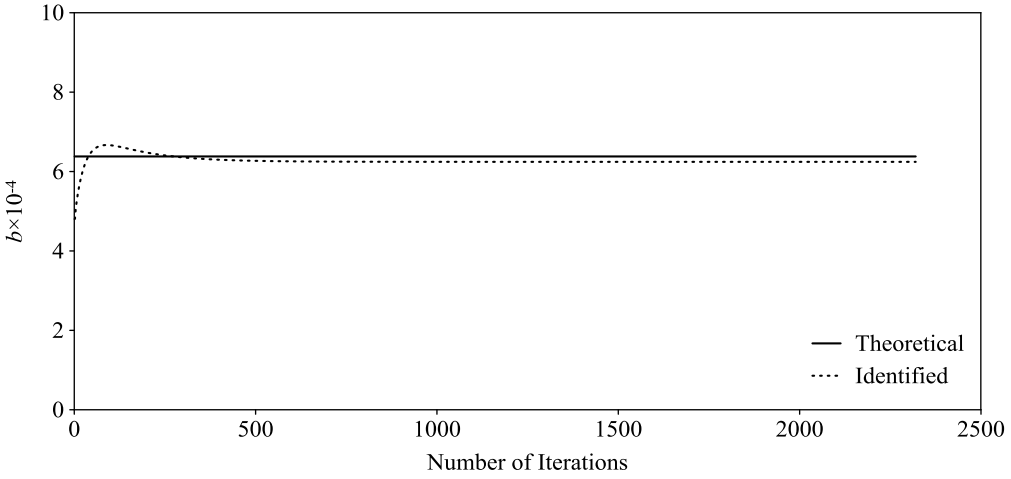

(b) Damping coefficient, *b*

Figure 6.15 Convergence behavior of identified Rayleigh damping cofficients for defect-free case

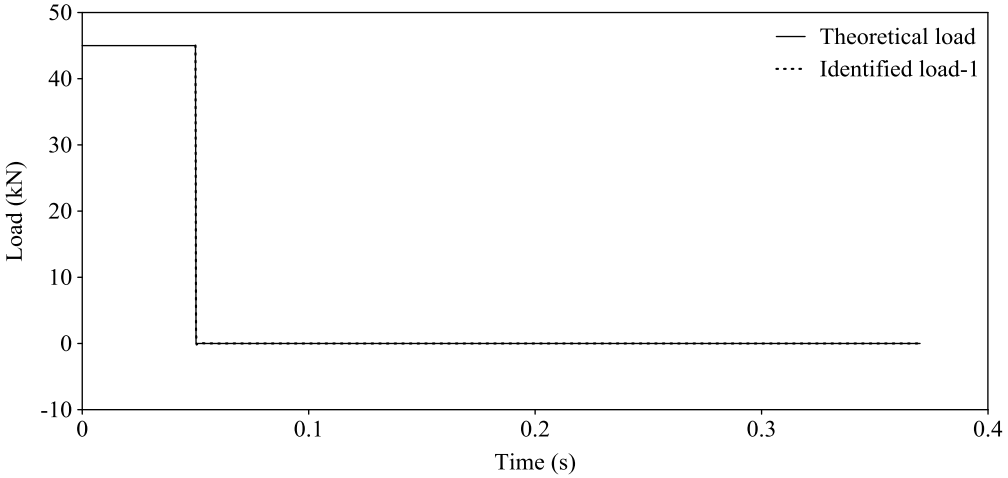

(a) Impulse excitation at node 1

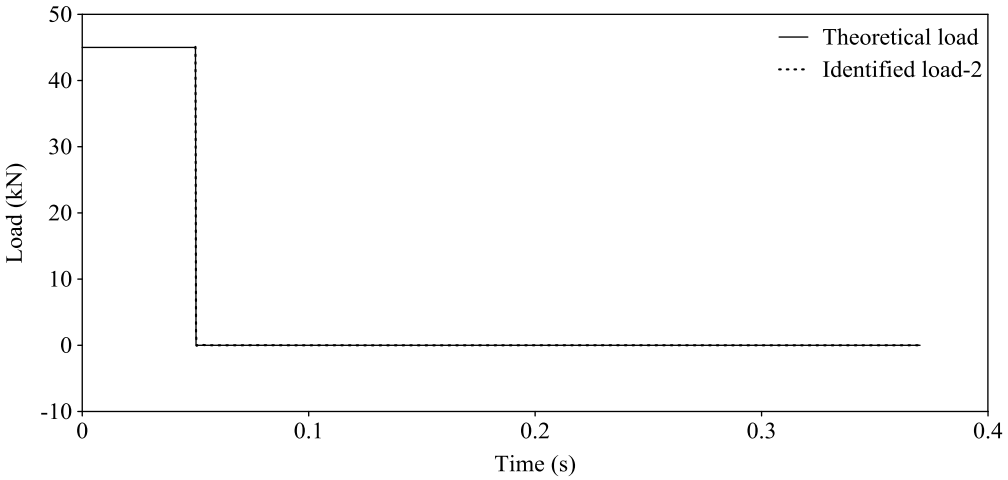

(b) Impulse excitation at node 9

Figure 6.16 Theoretical and identified impulse excitation for defect-free case

6.3.2.3 Health Assessment of Defective Frame

After successfully identifying the defect-free frame, several defective states of the frame are considered. Three defect scenarios, similar to the cases presented by Das et al. (2012), are considered. They are:

(i) Defect 1 - stiffness parameter of one member is reduced by different amounts

(ii) Defect 2 - stiffness parameters of multiple members are reduced by different amounts

(iii) Defect 3 - cross sectional area over a finite length of a member is reduced

In all cases, the capability of UKF-UI-WGI to assess locations and severity of defects is checked using responses measured at 15 DDOFs in the substructure. As mentioned earlier, Das et al. (2012) reported the results of identification using GILS-EKF-UI and responses measured at 24 DDOFs.

(i) Defect 1- Reduction in stiffness of a single member

In this defect scenario, the stiffness parameter of member 15 connecting nodes 9 and 10 is reduced by 15%, 30%, 50%, and 90% of the defect-free value by assuming that the moment of inertia of the member is reduced over the entire length. In all four defective cases, the FE representation of the frame and the substructure required in the first stage are considered to be the same as that of the defect-free case. Using the reduced moment of inertia of the member in ANSYS simulation, the responses at 15 DDOFs (nodes 1, 2, 5, 9, and 10) are generated in all four cases. Then, only response information is used in the first stage to identify the excitation force and the stiffness parameters of the substructure and damping coefficients. It is important to note that the defective member is in the substructure. The identified stiffness parameters of all 5 elements in the

substructure are shown in Table 6.6a. Using information from Stage 1 in UKF-WGI, the whole frame is identified and the results are summarized in Table 6.6b. The reduction in the identified stiffness parameter of member 15 is found to be 14.82%, 29.76%, 49.80%, and 90.02% for the four different defect scenarios, respectively. The reduction in the identified stiffness parameters of member 15 are very similar to the actual reductions introduced in the member. The identified stiffness parameters for all other members change slightly to satisfy the underlying requirements of the FE formulation. Obviously, UKF-UI-WGI successfully identified the location and the severity of the defects. The example also indicates that the proposed UKF-UI-WGI can identify relatively small amount of defects in a member.

The results of stiffness parameters for whole structures using GILS-EKF-UI with 24 DDOFs are shown in Table 6.6c as reported by Das et al. (2012). It can be noticed that the error in identification for all four defective cases using GILS-EKF-UI with responses at 24 DDOFs is higher than that of using UKF-UI-WGI with responses at 15 DDOFs.

Table 6.6 Identification of *EI/L* for defect 1 using UKF-UI-WGI with 15 DDOFs

(a) Stage 1: Identification of substructure

Member	Theoretical (kN-m)	15% Reduction in k_{15}		30% Reduction in k_{15}		50% Reduction in k_{15}		90% Reduction in k_{15}	
		Identified	Change (%)	Identified	Change (%)	Identified	Change (%)	Identified	Change (%)
(1)	(2)	(3)	(4)	(5)	(6)	(7)	(8)	(9)	(10)
k_1	13476	13482	0.04	13482	0.05	13482	0.05	13482	0.05
k_4	14553	14559	0.04	14559	0.04	14559	0.04	14559	0.04
k_{11}	14553	14593	0.27	14606	0.37	14625	0.49	14663	0.75
k_{15}	13476	11486	**-14.77**	9468	**-29.74**	6771	**-49.75**	1358	**-89.92**
k_{18}	14553	14593	0.28	14607	0.37	14626	0.50	14665	0.77

(b) Stage 2: Identification of whole structure

Member	Theoretical (kN-m)	15% Reduction in k_{15}		30% Reduction in k_{15}		50% Reduction in k_{15}		90% Reduction in k_{15}	
		Identified	Change (%)	Identified	Change (%)	Identified	Change (%)	Identified	Change (%)
(1)	(2)	(3)	(4)	(5)	(6)	(7)	(8)	(9)	(10)
k_1	13476	13496	0.14	13505	0.22	13520	0.32	13664	1.40
k_2	13476	13474	-0.02	13478	0.02	13484	0.06	13549	0.54
k_3	13476	13487	0.08	13488	0.09	13491	0.11	13694	1.62
k_4	14553	14588	0.24	14608	0.38	14634	0.56	14499	-0.37
k_5	14553	14583	0.20	14602	0.34	14633	0.55	14682	0.88
k_6	14553	14586	0.23	14605	0.36	14633	0.55	14527	-0.18
k_7	14553	14582	0.20	14602	0.34	14632	0.54	14893	2.34
k_8	13476	13469	-0.05	13463	-0.10	13452	-0.18	13437	-0.29
k_9	13476	13461	-0.12	13446	-0.22	13425	-0.38	13264	-1.58
k_{10}	13476	13450	-0.20	13433	-0.32	13409	-0.50	13557	0.60
k_{11}	14553	14592	0.27	14622	0.47	14666	0.77	14465	-0.61
k_{12}	14553	14581	0.19	14613	0.41	14660	0.74	14783	1.58
k_{13}	14553	14606	0.37	14650	0.67	14710	1.08	15407	5.87
k_{14}	14553	14604	0.35	14639	0.59	14689	0.94	15436	6.07
k_{15}	13476	11479	**-14.82**	9466	**-29.76**	6765	**-49.80**	1345	**-90.02**
k_{16}	13476	13457	-0.14	13448	-0.21	13433	-0.32	13291	-1.37
k_{17}	13476	13459	-0.13	13453	-0.17	13433	-0.32	12047	-10.61
k_{18}	14553	14623	0.48	14675	0.84	14733	1.24	14545	-0.05
k_{19}	14553	14625	0.50	14682	0.89	14746	1.33	14938	2.64
k_{20}	14553	14607	0.37	14660	0.73	14719	1.14	15357	5.53
k_{21}	14553	14616	0.43	14666	0.78	14726	1.19	15447	6.14

Note: $R_k = 10^{-4}$; $P_x(0|0) = 1.0$; $P_s(0|0) = 10^3$; $w = 50$

(c) Identification of (*EI/L*) for Defect 1 using GILS-EKF-UI with 24 DDOFs (Das et al., 2012)

Member	Theoretical (kN-m)	15% Reduction in k_{15}		30% Reduction in k_{15}		50% Reduction in k_{15}		90% Reduction in k_{15}	
		Identified	Change (%)	Identified	Change (%)	Identified	Change (%)	Identified	Change (%)
(1)	(2)	(3)	(4)	(5)	(6)	(7)	(8)	(9)	(10)
k_1	13476	13660	1.36	13800	2.40	14022	4.05	14132	4.87
k_2	13476	13660	1.36	13604	0.95	13516	0.30	14011	3.97
k_3	13476	13403	-0.54	13339	-1.02	13224	-1.87	12015	-10.84
k_4	14553	14850	2.04	15135	4.00	15635	7.44	16068	10.41
k_5	14553	14612	0.41	14657	0.72	14757	1.40	15803	8.59
k_6	14553	14471	-0.56	14366	-1.28	14096	-3.14	13402	-7.91
k_7	14553	14184	-2.54	13952	-4.13	13491	-7.30	12110	-16.79
k_8	13476	13309	-1.24	13545	0.51	13884	3.03	13338	-1.03
k_9	13476	13124	-2.61	12722	-5.60	12037	-10.68	12318	-8.59
k_{10}	13476	13612	1.01	13796	2.37	14257	5.79	15219	12.93
k_{11}	14553	14558	0.03	14985	2.97	15573	7.01	14642	0.61
k_{12}	14553	14706	1.05	14796	1.67	14743	1.31	14370	-1.26
k_{13}	14553	14929	2.58	14924	2.55	15081	3.63	18502	27.14
k_{14}	14553	14292	-1.79	14098	-3.13	13938	-4.23	13103	-9.96
k_{15}	13476	11407	**-15.35**	9610	**-28.69**	7085	**-47.43**	1496	**-88.90**
k_{16}	13476	13343	-0.99	12960	-3.83	12372	-8.19	11843	-12.12
k_{17}	13476	13453	-0.17	13197	-2.07	12958	-3.85	10902	-19.10
k_{18}	14553	14682	0.89	15029	3.27	15415	5.92	14668	0.79
k_{19}	14553	14417	-0.93	14477	-0.52	14466	-0.60	15039	3.34
k_{20}	14553	14651	0.67	14847	2.02	15158	4.16	18497	27.10
k_{21}	14553	14905	2.42	14745	1.32	14660	0.74	12948	-11.03

Note: $R_k = 10^{-4}$; $P_x(0|0) = 1.0$; $P_s(0|0) = 10^3$; $w = 1000$ for all cases except for 90% reduction, w=10

(ii) Defect 2 - Reduction of stiffness of multiple members

In Defect 2, two members in the frame are considered to be defective at the same time. Two different combinations are considered:

(a) Stiffness parameter of members 1 and 17 are reduced by 30% and 20%, respectively

(b) Stiffness parameter of members 15 and 17 are reduced by 30% and 20%, respectively

It is important to point out that in both cases one of the defective members is in the substructure. Using the same substructure as shown in Figure 6.14 and responses at 15 DDOFs, the stiffness parameters of the substructure are identified as shown in Table 6.7a, Columns 3 and 5. Then, using information from Stage 1, the whole structure is identified following the same procedures discussed for Defect 1. The identified stiffness parameters of all members are presented in Table 6.7b, Columns 3 and 5, respectively, for the two defect scenario cases. In both cases, the locations of the defective members are identified properly. This example clearly indicates that the proposed method can identify defects in several members and the defective members need not to be in the substructure. However, the defect detection capability increases significantly if the defective member is in the substructure or close to it. As in the previous example, the detection capability of UKF-UI-WGI is found to be better than that of GILS-EKF-UI even using responses at 24 DDOFs.

(iii)Defect 3 - Reduction of area over a finite length of a member

In Defect 3, a less severe defect is considered. The cross-sectional area of member 16 connecting nodes 10 and 11 is considered to be corroded over a length of 40 cm and located at a distance of 1.2 m from node 10 as shown in Figure 6.17. The reduction of the flange and web thicknesses caused the reduction in the cross-sectional area by 75.23%

and the moment of inertia by 76.40% from the nominal values. A similar defect scenario was considered by a research team member earlier in laboratory investigations. To simulate the defective spot in ANSYS, a new element of length 40 cm with reduced cross-sectional properties is introduced and the responses are analytically generated. Since the presence of defect is unknown before the inspection, the same FE representation of the whole frame and the substructure considered earlier for the defect-free case are used for the defect detection. Using responses at 15 DDOFs and the proposed method, the frame is identified. The identified stiffness parameters for the substructure are shown in Table 6.7a, Column 7 and for the whole frame are summarized in Table 6.7b, Column 7. The stiffness parameter of member 16 is reduced by the maximum amount indicating that it is the defective member. The example clearly indicates that the proposed UKF-UI-WGI procedure can detect less severe defect in a small part of a member.

Considering all the defect-free and defective cases in this example, it can be concluded that the proposed method is robust to detect defects of different levels of severity at different locations in the structure. Defects need not to be in the substructure. It is also established that the proposed UKF-UI-WGI is superior to GILS-EKF-UI for nonlinear SI.

Table 6.7 Identification of *EI/L* for Defects 2 and 3 using UKF-UI-WGI with 15 DDOFs

(a) Stage 1: Identification of substructure

Member	Theoretical (kN-m)	Defect 2				Defect 3	
		Reduction in k_1 and k_{17}		Reduction in k_{15} and k_{17}		Reduction in k_{16}	
		Identified	Change (%)	Identified	Change (%)	Identified	Change (%)
(1)	(2)	(3)	(4)	(5)	(6)	(7)	(8)
k_1	13476	9454	**-29.85**	13482	0.05	13482	0.04
k_4	14553	14582	0.20	14559	0.04	14559	0.04
k_{11}	14553	14580	0.18	14605	0.36	14575	0.15
k_{15}	13476	13501	0.18	9467	**-29.75**	13496	0.15
k_{18}	14553	14580	0.19	14606	0.36	14575	0.15

(b) Stage 2: Identification of whole structure

Member	Theoretical (kN-m)	Defect 2				Defect 3	
		Reduction in k_1 and k_{17}		Reduction in k_{15} and k_{17}		Reduction in k_{16}	
		Identified	Change (%)	Identified	Change (%)	Identified	Change (%)
(1)	(2)	(3)	(4)	(5)	(6)	(7)	(8)
k_1	13476	9524	**-29.32**	13699	1.66	13465	-0.08
k_2	13476	13385	-0.68	13522	0.34	13481	0.04
k_3	13476	13841	2.71	13781	2.26	13834	2.66
k_4	14553	14692	0.96	14760	1.42	14375	-1.22
k_5	14553	14615	0.43	14683	0.89	14661	0.74
k_6	14553	14731	1.22	14629	0.52	14745	1.32
k_7	14553	14879	2.24	14961	2.81	14708	1.07
k_8	13476	13295	-1.34	13328	-1.10	13316	-1.19
k_9	13476	13178	-2.21	13184	-2.17	13673	1.46
k_{10}	13476	12716	-5.64	13054	-3.13	13192	-2.11
k_{11}	14553	14471	-0.56	14541	-0.09	14422	-0.90
k_{12}	14553	14396	-1.08	14379	-1.20	15273	4.95
k_{13}	14553	14459	-0.65	14705	1.05	14318	-1.62
k_{14}	14553	15066	3.52	15105	3.79	13948	-4.15
k_{15}	13476	13239	-1.76	9314	**-30.89**	13190	-2.12
k_{16}	13476	13384	-0.68	13225	-1.86	12391	**-8.05**
k_{17}	13476	11762	**-12.72**	11666	**-13.43**	13074	-2.98
k_{18}	14553	14423	-0.89	14605	0.36	14267	-1.97
k_{19}	14553	14266	-1.97	14403	-1.03	15485	6.40
k_{20}	14553	14319	-1.61	14578	0.17	14124	-2.94
k_{21}	14553	14620	0.46	14911	2.46	14154	-2.74

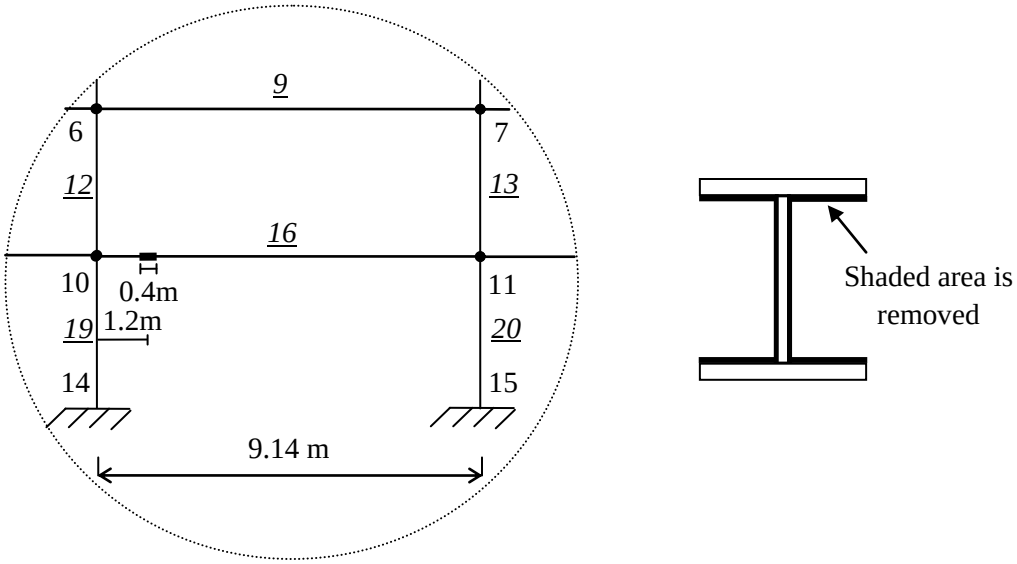

(a) Location of defect (b) Reduction in cross-sectional area

Figure 6.17 Location and details of loss of area for Defect 3

6.3.3 Frame under Seismic Excitation

To demonstrate further the capabilities of UKF-UI-WGI for the SHA, a more complicated form of dynamic loading excitation is considered. The frame shown in Figure 6.12 is considered again; however, it is now excited by seismic instead of impulsive loading. The frame is excited by the N-S component of 1994 El. Centro earthquake ground motion, as shown in Figure 6.18. The information on responses is numerically generated by applying the ground motion at the base using ANSYS. After the responses are generated, the information on the input excitation is completely ignored. In this example, the health of the frame is assessed using responses from 1.52 to 2.37s with the time increment of 0.00025s providing a total of 3401 time points. Defect-free and two defective states (Defect 1 with 15% and 30% reduction in stiffness parameter of member 15) are considered to demonstrate the SHA capabilities of UKF-UI-WGI.

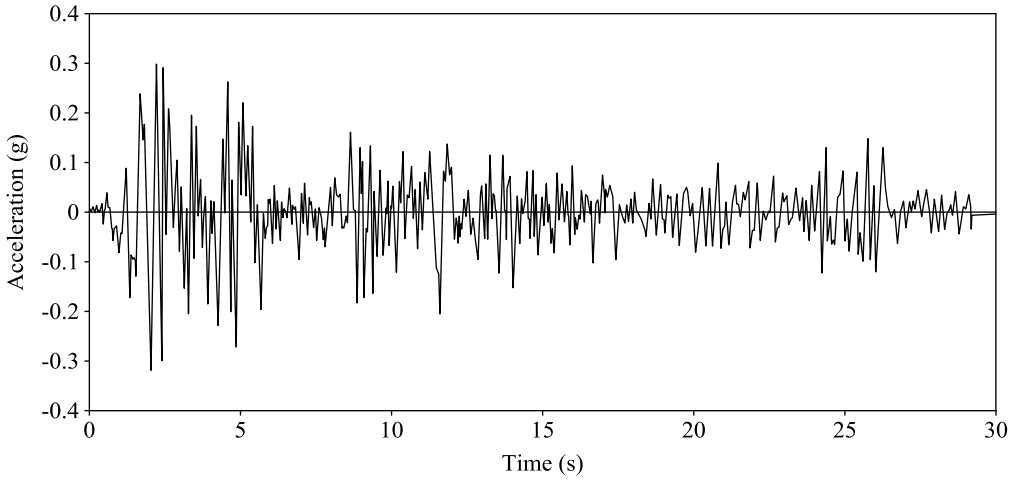

Figure 6.18 N-S component of 1994 El. Centro earthquake acceleration time-history

6.3.3.1 Substructure Selection

The substructure for this example is considered to consist of 2 members (1 and 4) and 3 nodes (1, 2, and 5). The information about the substructure is summarized in Figure 6.19. The responses at 9 DDOFs are required to implement Stage 1 of the UKF-UI-WGI procedure.

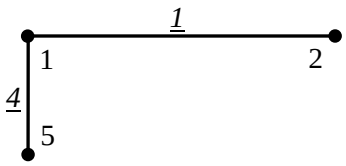

kn = 1
dkn = 3
re = 2
rn = 2
nsub = 3
sc = 0
dsub = 9

Figure 6.19 Substructure needed to implement Stage 1 of UKF-UI-WGI

6.3.3.2 Health Assessment of Defect-Free Frame

The defect-free state of the frame is considered in this section. Using responses at 9 DDOFs in the substructure, the stiffness parameter for the two elements in the substructure, the two Rayleigh damping coefficients, and the ground motion are identified in Stage 1. The identified stiffness parameters and the errors in identification are summarized in Columns 3 and 4, respectively of Table 6.8a. From the results, it can be observed that the errors in identification are very small. The two damping coefficients and the input ground acceleration are also identified accurately. The theoretical and identified ground acceleration time-histories are shown in Figure 6.20.

Then, using information obtained from Stage 1 and responses at 15 DDOFs (nodes 1, 2, 5, 9, and 10), as in the example of impulsive excitation, the whole frame is identified and the results are summarized in Table 6.8b, Columns 3 and 4. The results clearly indicate the defect-free state of the frame.

6.3.3.3 Health Assessment of Defective Frame

Defect 1 with 15% and 30% reduction in stiffness parameter of member 15, as mentioned in details in example of impulsive loads, is considered in this section. In Stage 1, the substructure is identified using responses at 9 DDOFs and then using the information of Stage 1 and 15 DDOFs (nodes 1, 2, 5, 9, and 10), the whole structure is identified. The results of identification of stiffness parameters in Stages 1 and 2 for two defects are shown in Table 6.8a and b, respectively. The convergence process of the stiffness parameter of defective member 15 with 15% reduction is shown in Figure 6.21. The results clearly indicate the defective states of the frame and the location of the defective member and the severity of defects.

Table 6.8 Identification of *EI/L* for seismic excitation using UKF-UI-WGI

(a) Stage 1: Identification of substructure

Member	Theoretical (kN-m)	Defect-free		15% Reduction in k_{15}		30% Reduction in k_{15}	
		Identified	Change (%)	Identified	Change (%)	Identified	Change (%)
(1)	(2)	(3)	(4)	(5)	(6)	(7)	(8)
k_1	13476	13477	0.006	13477	0.006	13477	0.006
k_4	14553	14554	0.006	14554	0.006	14554	0.006

(b) Stage 2: Identification of whole structure

Member	Theoretical (kN-m)	Defect-free		15% Reduction in k_{15}		30% Reduction in k_{15}	
		Identified	Change (%)	Identified	Change (%)	Identified	Change (%)
(1)	(2)	(3)	(4)	(5)	(6)	(7)	(8)
k_1	13476	13481	0.03	13440	-0.27	13380	-0.71
k_2	13476	13475	-0.01	13455	-0.16	13447	-0.22
k_3	13476	13480	0.03	13476	0.00	13487	0.08
k_4	14553	14557	0.03	14518	-0.24	14457	-0.66
k_5	14553	14561	0.05	14545	-0.06	14506	-0.32
k_6	14553	14561	0.06	14471	-0.57	14659	0.73
k_7	14553	14557	0.03	14518	-0.24	14420	-0.91
k_8	13476	13478	0.01	13416	-0.44	13327	-1.10
k_9	13476	13479	0.02	13410	-0.49	13301	-1.30
k_{10}	13476	13478	0.01	13768	2.16	13813	2.50
k_{11}	14553	14554	0.01	14527	-0.18	14405	-1.02
k_{12}	14553	14551	-0.01	14668	0.79	14473	-0.55
k_{13}	14553	14551	-0.01	14869	2.17	15223	4.61
k_{14}	14553	14554	0.01	14001	-3.80	13992	-3.86
k_{15}	13476	13476	0.00	11374	**-15.60**	9228	**-31.52**
k_{16}	13476	13476	0.00	13181	-2.19	12884	-4.40
k_{17}	13476	13470	-0.05	13317	-1.18	13633	1.16
k_{18}	14553	14556	0.02	14387	-1.14	14114	-3.02
k_{19}	14553	14557	0.03	14214	-2.33	13956	-4.10
k_{20}	14553	14557	0.03	14944	2.69	15471	6.31
k_{21}	14553	14558	0.03	15027	3.26	14923	2.54

Note: $R_k = 10^{-4}$; $P_x(0|0) = 1.0$; $P_s(0|0) = 10^3$; $w = 50$

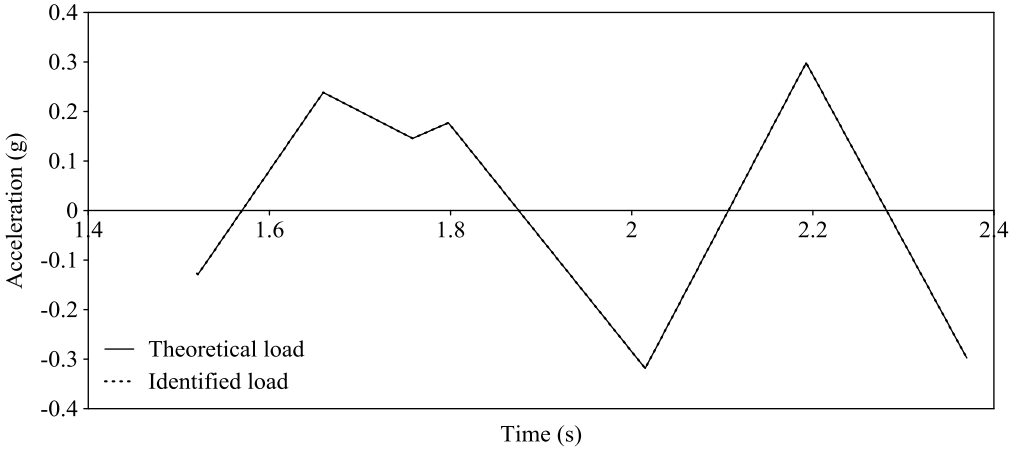

Figure 6.20 Theoretical and identified input ground acceleration

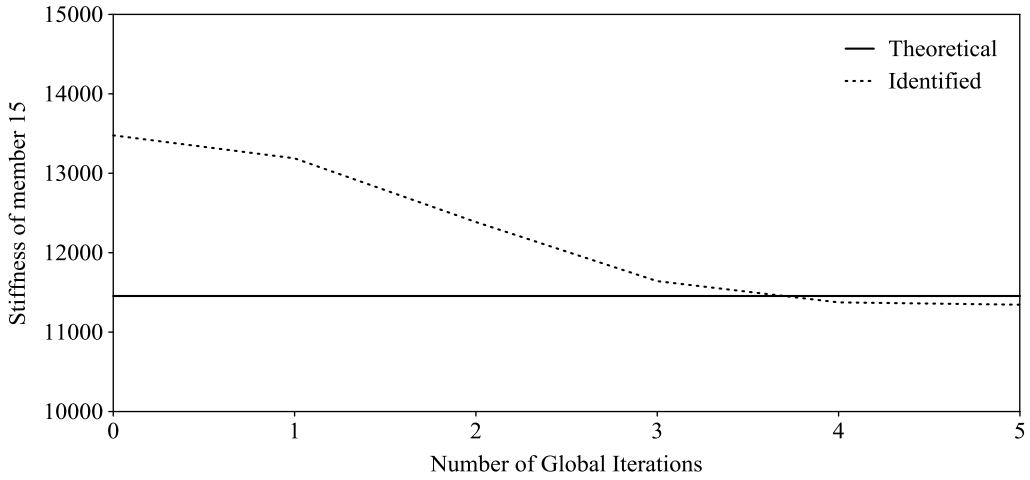

Figure 6.21 Convergence process of stiffness of member 15 in Defect 1-15% reduction

6.4 Health Assessment of Two-Bay Five-Story Frame

The verification of the UKF-UI-WGI procedure to assess defect-free and defective states of a structure at the element level is further studied to a larger structural system, as discussed next.

6.4.1 Description of the Frame

A two-dimensional two-bay five-story frame with a bay width of 9.14 m and a story height of 3.66 m, as shown in Figure 6.22, is considered. The frame has a total of 25 members; 10 beams and 15 columns. The beams and columns are made of W21×68 and W14×61 sections, respectively, of Grade 50 steel. The frame is modeled by 18 nodes in the FE representation. Each node has three dynamic degrees of freedom (DDOFs); two translational and one rotational. The support condition at the base (nodes 16, 17, and 18) of the frame is considered to be fixed. The total number of DDOFs for the frame is 45. The actual theoretical stiffness parameter values k_i evaluated in terms of (E_iI_i/L_i) are calculated to be 13476 kN-m and 14553 kN-m for a typical beam and column, respectively. First two natural frequencies of the defect-free frame are estimated to be f_1 = 3.5981 Hz and f_2 = 11.231 Hz, respectively. Following the procedure described in Clough and Penzien (2003), Rayleigh damping coefficients a and b are calculated to be 1.7122088 and 0.00107326, respectively, for an equivalent modal damping of 5% (commonly used in model codes in the US) of the critical for the first two modes.

The frame is excited by sinusoidal loading, $f(t)$ = 4.5 sin(20t) kN, applied horizontally at node 1, as shown in Figure 6.22. Instead of conducting the experiments and following the general practices, the information on responses are numerically generated using a commercially available software ANSYS (ver. 15.0). The responses are

obtained at 0.0001 s time interval. After the responses are simulated, the information on input excitations is completely ignored. Responses between 0.02 s and 0.32 s providing 3001 time points are used in the subsequent health assessment process.

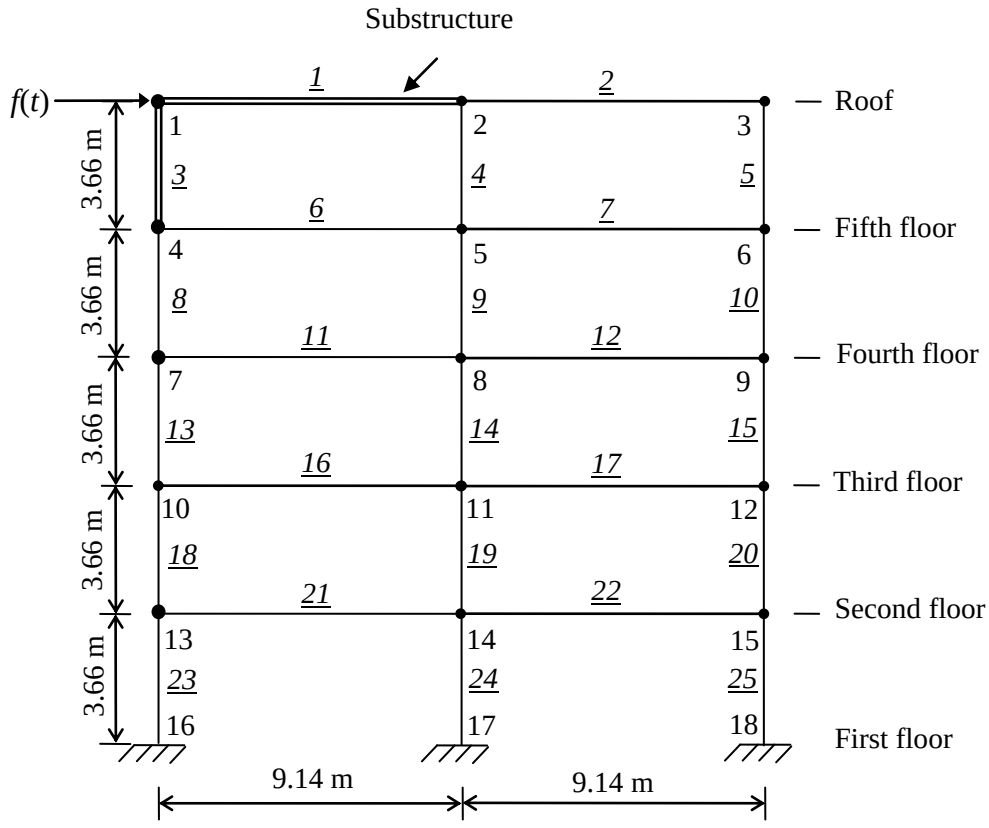

Figure 6.22 Finite element representation of a two-bay five-story frame

6.4.2 Substructure Selection

The information required to select the substructure is summarized in Figure 6.23. The substructure consists of 2 elements (1 and 3) and 3 nodes (1, 2, and 4) as shown in Figure 6.22 with double lines. Accordingly, at least responses at 9 DDOFs are available to identify the input excitation using the ILS-UI procedure.

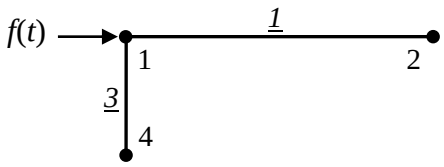

kn = 1
dkn = 3
re = 2
rn = 2
nsub = 3
sc = 0
dsub = 9

Figure 6.23 Substructure needed to implement Stage 1 of UKF-UI-WGI

6.4.3 Structural Health Assessment Using UKF-UI-WGI

To demonstrate the effectiveness of the proposed procedure for large structural systems, the following five cases are considered:

(i) Defect-free frame

(ii) Defect 1 - stiffness of member 22 is reduced by 30%

(iii) Defect 2 - stiffness of member 17 is reduced by 20%

(iv) Defect 3 - stiffness of member 12 is reduced by 50%

(v) Defect 4 - loss of cross sectional area over a finite length of member 22

6.4.3.1 Substructure Identification Using the ILS-UI Procedure

The substructure mentioned above is the same for all five cases. Using only responses at 3 nodes in the substructure, the stiffness and damping parameters and the time-history of unknown input force are identified using the ILS-UI procedure in Stage 1. The errors in identification of the stiffness parameter are shown in Table 6.9 for all cases. From the results, it can be observed that the errors in the identified stiffness parameter of

the two members in the substructure are very small. The excitation time-history was also identified very accurately for all five cases. Figure 6.24 shows the theoretical and identified excitation load for the defect-free case.

Table 6.9 Change (%) in (*EI/L*) identification of substructure using ILS-UI

Member	Theoretical (kN-m)	Defect Free	Defect 1	Defect 2	Defect 3	Defect 4
(1)	(2)	(3)	(4)	(5)	(6)	(7)
k_1	13476	0.0012	0.0012	0.0012	0.0012	0.0012
k_3	14553	0.0012	0.0012	0.0012	0.0012	0.0012

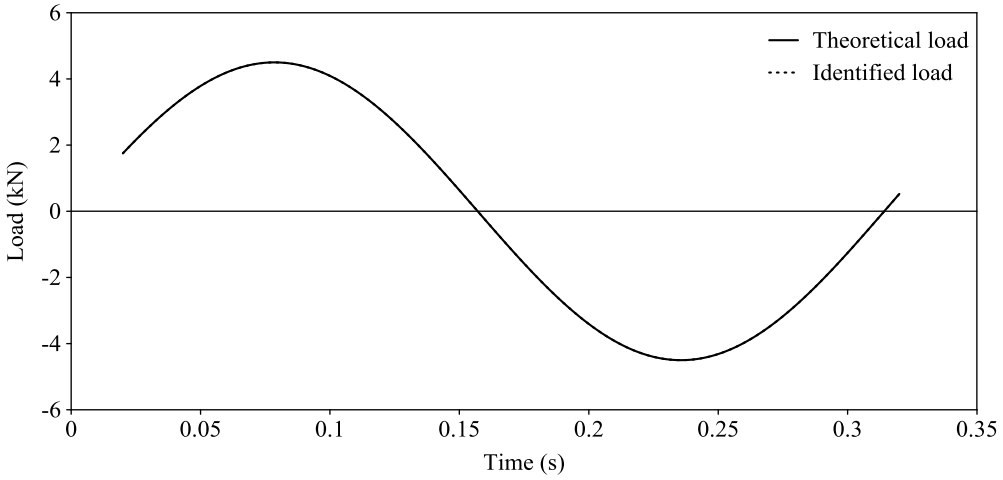

Figure 6.24 Theoretical and identified excitation load for defect-free frame

6.4.3.2 Complete Structure Identification Using the UKF-WGI Procedure

The information of Stage 1 is used to initiate UKF-WGI. Then, the stiffness parameters of all 25 elements of the frame for all five cases are estimated in Stage 2. The values of the parameters required to initiate the procedure, R_k, $P_x(0|0)$, $P_s(0|0)$, and w are

considered to be 10^{-4}, 0.1, 10^{3}, and 10, respectively as summarized at the bottom of the tables.

(i) Defect-free frame

Using only responses at the substructure, i.e., 9 DDOFs (nodes 1, 2, and 4), the whole structure is identified. The errors in the identified stiffness parameters are shown in Column 4 of Table 6.10. The maximum error in the identification is only 0.5%. The frame can be considered as defect-free since the identified stiffness parameters of all the elements did not differ significantly from the expected values. The results also indicate that the responses available at 9 DDOFs are sufficient to identify the defect-free state of the frame.

(ii) Defect 1 - stiffness of member 22 is reduced by 30%

After assessing structural health of the defect-free frame, the defective cases are considered to examine the capability of the proposed procedure if it can identify the location and severity of defects. In Defect 1, member 22 connecting nodes 14 and 15, is considered to be defective. From the figure, it can be observed that the defective beam is located in the second floor and it is furthest from the substructure. The moment of inertia of the member over the entire length is considered to be reduced by 30% of the defect-free value. As mentioned earlier, for this illustrative example, the responses are numerically generated using ANSYS by appropriately modeling the location, nature, and extent of defects. In real inspections, they will be measured. After generating the responses, the information on excitation is completely ignored.

Using responses at 9 DDOFs in the substructure, as used for the defect-free case, the stiffness parameter for all the elements in the frame is identified. The results are summarized in Table 6.11, Column 3. The algorithm correctly identified location of the defective element, member 22; however, its stiffness is reduced by 17.7% not the theoretical value of 30%. Furthermore, the maximum error in the identification for other defect-free members is about 6.4%. The accuracy of identification can be improved as discussed next.

The author observed that to identify defective states with reasonable accuracy will require more number of responses than the defect-free case. The absolute minimum numbers of required responses are still open questions, and since the author is the first to use the concept, it is still unknown. To study the issue comprehensively, the frame is identified using 9 responses at the substructure plus few more responses at other nodes. The results are summarized in Table 6.11, Columns 5, 7, and 9 using responses at 12, 15, and 18 DDOFs, respectively. They represent responses at the substructure plus at nodes (7), (7 and 10), and (7, 10, and 13), respectively. It can be observed that the reduction in the stiffness parameter of member 22 approaches the true value of 30% with the increase in the total number of responses used for the identification. Also, differences in the identified stiffness parameters for the defect-free and defective members get wider with the increased responses making the defect identification relatively simpler. It can be concluded that the proposed algorithm accurately identified the location of the defective element using responses at 9, 12, 15, and 18 DDOFs; however, whenever possible, as many additional responses as practicable beyond that of measured at the substructure should be used for SHA.

Table 6.10 Identification of (EI/L) of whole structure for defect-free using 9 DDOFs

Member	Theoretical (kN-m)	Identified	Change (%)
(1)	(2)	(3)	(4)
k_1	13476	13475	0.0
k_2	13476	13468	-0.1
k_3	14553	14552	0.0
k_4	14553	14548	0.0
k_5	14553	14577	0.2
k_6	13476	13476	0.0
k_7	13476	13479	0.0
k_8	14553	14555	0.0
k_9	14553	14543	-0.1
k_{10}	14553	14575	0.1
k_{11}	13476	13485	0.1
k_{12}	13476	13503	0.2
k_{13}	14553	14535	-0.1
k_{14}	14553	14575	0.2
k_{15}	14553	14575	0.2
k_{16}	13476	13491	0.1
k_{17}	13476	13459	-0.1
k_{18}	14553	14569	0.1
k_{19}	14553	14552	0.0
k_{20}	14553	14628	0.5
k_{21}	13476	13481	0.0
k_{22}	13476	13459	-0.1
k_{23}	14553	14550	0.0
k_{24}	14553	14536	-0.1
k_{25}	14553	14503	-0.3

Note: $R_k = 10^{-4}$; $P_x(0|0) = 0.1$; $P_s(0|0) = 10^3$; $w = 10$

Table 6.11 Identification of (EI/L) of whole structure for Defect 1

Member	Theoretical (kN-m)	Available responses at substructure (nodes 1, 2, 4) and at nodes							
		-		7		7, 10		7, 10, 13	
		9DDOFs		12DDOFs		15DDOFs		18DDOFs	
		Identified	Change (%)	Identified	Change (%)	Identified	Change (%)	Identified	Change (%)
(1)	(2)	(3)	(4)	(5)	(6)	(7)	(8)	(9)	(10)
k_1	13476	13439	-0.3	13465	-0.1	13475	0.0	13466	-0.1
k_2	13476	13555	0.6	13734	1.9	13991	3.8	14132	4.9
k_3	14553	14507	-0.3	14538	-0.1	14552	0.0	14546	0.0
k_4	14553	14562	0.1	14571	0.1	14669	0.8	14698	1.0
k_5	14553	14678	0.9	14293	-1.8	13845	-4.9	13669	-6.1
k_6	13476	13507	0.2	13461	-0.1	13488	0.1	13429	-0.4
k_7	13476	13374	-0.8	13494	0.1	13377	-0.7	13425	-0.4
k_8	14553	14423	-0.9	14507	-0.3	14616	0.4	14520	-0.2
k_9	14553	14368	-1.3	14468	-0.6	14559	0.0	14652	0.7
k_{10}	14553	14309	-1.7	14769	1.5	14437	-0.8	14519	-0.2
k_{11}	13476	13705	1.7	13526	0.4	13642	1.2	13484	0.1
k_{12}	13476	13532	0.4	13440	-0.3	13424	-0.4	13386	-0.7
k_{13}	14553	15169	4.2	14719	1.1	14751	1.4	14678	0.9
k_{14}	14553	15186	4.4	14739	1.3	14347	-1.4	14692	1.0
k_{15}	14553	14932	2.6	14111	-3.0	14550	0.0	13971	-4.0
k_{16}	13476	13374	-0.8	13936	3.4	13693	1.6	13621	1.1
k_{17}	13476	12611	-6.4	13162	-2.3	13372	-0.8	13511	0.3
k_{18}	14553	14214	-2.3	14703	1.0	15248	4.8	14534	-0.1
k_{19}	14553	14145	-2.8	13770	-5.4	14555	0.0	13630	-6.3
k_{20}	14553	14695	1.0	14213	-2.3	14359	-1.3	15998	9.9
k_{21}	13476	13079	-3.0	12861	-4.6	12484	-7.4	13644	1.2
k_{22}	13476	11085	**-17.7**	10519	**-21.9**	10127	**-24.9**	9734	**-27.8**
k_{23}	14553	14563	0.1	14395	-1.1	14005	-3.8	14547	0.0
k_{24}	14553	13857	-4.8	14624	0.5	14864	2.1	14258	-2.0
k_{25}	14553	13977	-4.0	14324	-1.6	14701	1.0	14568	0.1
Note:	$R_k = 10^{-4}$; $P_x(0\|0) = 0.1$; $P_s(0\|0) = 10^3$; $w = 10$								

6.4.3.3 Locations of Additional Responses

Suppose that the inspector has resources to collect responses at 18 DDOFs; 3 nodes in the substructure (1, 2, and 4) plus 3 additional nodes. For the clarity of the presentation, let us consider that responses at 18 DDOFs have two parts; 9 responses are at substructure and the other 9 responses are not in the substructure. The responses at the substructure are fundamental to implement the procedure and their locations are known. However, the locations of responses not in substructure conceptually can be anywhere in the structure. The most desirable locations of 3 additional nodes in order to detect the defective beam 22 are explored using five different locations for them. It is important to note that the responses at the substructure are at fifth and roof level and they are the farthest from the defective beam 22 at the second floor level. The locations of 3 additional nodes are considered to be:

Case 1: Fifth floor and roof level (nodes 3, 5, and 6)

Case 2: Fourth floor level (nodes 7, 8, and 9)

Case 3: Third to fifth floor levels at right hand exterior column (nodes 6, 9, and 12)

Case 4: Second to fourth floor levels at left hand exterior column (nodes 7, 10, and 13)

Case 5: Second to fourth floor levels at right hand exterior column (nodes 9, 12, and 15)

The whole frame is identified using response information for all five cases mentioned above and the results are summarized in Table 6.12. In all cases, the defective member is identified but with various levels of accuracy. In Case 1, since the locations of measured responses are the furthest from the defective member, the accuracy is the worst, as expected. Case 5 is found to be the best. In this case, one measured node point is connected to the defective element. It can be concluded that the capability of the

proposed algorithm to detect defect location and its severity will be the best if it is closer to the measurement points. The other three cases are between these two limit cases based on the proximity of the defective element. The results indicate that the proposed algorithm will identify the health of a structure even when the defect spot is away from the measurement points; however, attempts should be made to measure responses at different locations in a structure so that at least one of them will be closer to defective spot. For SHA in the presence of other defect scenarios, only results for Case 5 are given.

Table 6.12 Change (%) in *EI/L* identification using different locations of measured additional nodes for Defect 1

Member	Theoretical (kN-m)	3 additional nodes				
		3, 5, 6	7, 8, 9	6, 9, 12	7, 10, 13	9, 12, 15
		Case 1	Case 2	Case 3	Case 4	Case 5
(1)	(2)	(3)	(4)	(5)	(6)	(7)
k_1	13476	0.0	-0.1	0.0	-0.1	0.0
k_2	13476	0.0	3.4	1.5	4.9	2.8
k_3	14553	0.0	-0.1	0.0	0.0	0.0
k_4	14553	0.0	0.8	0.5	1.0	0.6
k_5	14553	0.0	-4.2	-1.8	-6.1	-4.0
k_6	13476	-0.1	-0.4	-0.2	-0.4	-0.1
k_7	13476	0.2	-0.4	-0.6	-0.4	-0.2
k_8	14553	-0.7	-0.2	-1.1	-0.2	-0.2
k_9	14553	0.0	0.7	1.4	0.7	0.6
k_{10}	14553	-0.4	-0.4	-0.4	-0.2	-1.0
k_{11}	13476	-1.4	-0.1	0.2	0.1	0.2
k_{12}	13476	0.9	0.0	-0.9	-0.7	-0.2
k_{13}	14553	-2.0	0.1	-3.4	0.9	-1.8
k_{14}	14553	2.8	-0.9	2.3	1.0	0.6
k_{15}	14553	6.9	2.0	-0.3	-4.0	0.3
k_{16}	13476	5.9	4.2	0.8	1.1	-0.3
k_{17}	13476	-8.1	-1.8	-1.0	0.3	0.4
k_{18}	14553	6.6	4.9	13.6	-0.1	2.4
k_{19}	14553	-2.9	-5.0	-2.6	-6.3	-1.4
k_{20}	14553	-8.2	-4.8	-3.4	9.9	0.2
k_{21}	13476	-8.4	-5.3	-5.1	1.2	0.5
k_{22}	13476	**-18.9**	**-23.6**	**-26.0**	**-27.8**	**-29.7**
k_{23}	14553	-3.4	-3.3	-6.4	0.0	-0.7
k_{24}	14553	-2.4	0.4	2.0	-2.0	-0.1
k_{25}	14553	4.1	3.1	3.1	0.1	0.0
Note:	$R_k = 10^{-4}$; $P_x(0\|0) = 0.1$; $P_s(0\|0) = 10^3$; $w = 10$					

(iii) Defect 2: reduction in the stiffness of member 17 by 20%

In Defect 2, member 17 connecting nodes 11 and 12, is considered to be defective. The moment of inertia of the member over the entire length is considered to be reduced by 20% of the defect-free value. This defect is less severe than Defect 1. Using responses at 18 DDOFs with their location as in Case 5 mentioned above, the whole frame is identified using UKF-UI-WGI. The identification results are presented in Table 6.13, Columns 3 and 4. The maximum reduction in the identified stiffness parameter is found to be about 19.7% for member 17. The results clearly indicate that the UKF-UI-WGI procedure is capable of identifying the location and relatively less severe defect.

(iv) Defect 3: reduction in the stiffness of member 12 by 50%

In this example, the capability of the proposed procedure is checked if it can identify a relatively severe defect. In Defect 3, the moment of inertia of member 12 is reduced by 50% of the defect-free value over the entire length. Following the similar procedures discussed earlier, using responses at 18 DDOFs with their location as in Case 5, the frame is identified and the results are presented in Table 6.13, Columns 5 and 6. All the observations made earlier for the two defective states are also applicable here.

Table 6.13 Stiffness parameter (*EI/L*) identification of whole structure for Defects 2 and 3

Member	Theoretical (kN-m)	Defect 2		Defect 3	
		Identified	Change %	Identified	Change %
(1)	(2)	(3)	(4)	(5)	(6)
k_1	13476	13464	-0.1	13483	0.1
k_2	13476	13820	2.6	14073	4.4
k_3	14553	14546	0.0	14569	0.1
k_4	14553	14613	0.4	14679	0.9
k_5	14553	14082	-3.2	13704	-5.8
k_6	13476	13527	0.4	13484	0.1
k_7	13476	13423	-0.4	13393	-0.6
k_8	14553	14658	0.7	14553	0.0
k_9	14553	14481	-0.5	14496	-0.4
k_{10}	14553	14441	-0.8	14494	-0.4
k_{11}	13476	13577	0.7	13527	0.4
k_{12}	13476	13488	0.1	6789	**-49.6**
k_{13}	14553	14584	0.2	14377	-1.2
k_{14}	14553	14473	-0.6	14396	-1.1
k_{15}	14553	14571	0.1	14702	1.0
k_{16}	13476	13423	-0.4	13513	0.3
k_{17}	13476	10817	**-19.7**	13610	1.0
k_{18}	14553	14095	-3.1	15019	3.2
k_{19}	14553	14766	1.5	14285	-1.8
k_{20}	14553	14657	0.7	14569	0.1
k_{21}	13476	13343	-1.0	13441	-0.3
k_{22}	13476	13503	0.2	13498	0.2
k_{23}	14553	14879	2.2	14295	-1.8
k_{24}	14553	14413	-1.0	14748	1.3
k_{25}	14553	14528	-0.2	14564	0.1
Note:	$R_k = 10^{-4}$; $P_x(0\|0) = 0.1$; $P_s(0\|0) = 10^3$; $w = 10$				

(v) Defect 4: loss of cross sectional area over a finite length

The capability of the UKF-UI-WGI procedure is further examined if it can identify defect spot in a defective member. For this defect, the cross-sectional area of member 22, a beam at the second floor level, is considered to be corroded over a length of 20 cm, located at a distance of 0.5 m from node 15, as shown in Figure 6.25. The web and flange thicknesses are considered to be reduced to one fourth of their original values. The loss of thicknesses will result in the reduction of the cross-sectional area by 74.44% and the moment of inertia by 73.20% from the nominal values. The identification of stiffness parameter of the whole frame using UKF-UI-WGI with responses at 18 DDOFs and their location as in Case 5 is shown in Column 3 of Table 6.14 and the error in the identification is shown in Column 4 of Table 6.14. The stiffness parameter for member 22 is reduced by the maximum amount of 16.6%, significantly more than other members, indicating that it is defective. To locate the defective spot more accurately within the defective member, the defective member can be represented by more number of finite elements and then identify the segment of the defective element with the largest reduction in the stiffness parameter. This procedure can be implemented without conducting any new experiment. To implement the concept, defective member 22 can be represented by two elements. Suppose, at first, a new node is introduced at the mid-span of member 22; a new node 19 is located at 4.57 m from node 14. In the FE representation, the two elements are denoted as 22a and 22b, as shown in Figure 6.25. The identified stiffness parameter of the whole frame using responses at 18 DDOFs is shown in Column 6 of Table 6.14. The stiffness parameter for element 22b is reduced by the maximum amount of 19.5%, significantly more than other members. It is clear that element 22b contains the

defect. To locate the defect more accurately, the length of element 22b can be reduced by moving the new node. Suppose, the new node is located at 6.0 m from node 14. Thus, the lengths of the two elements 22a and 22b are 6.0 m and 3.14 m, respectively. The identified stiffness parameters for this case are shown in Column 9 of Table 6.14. The results confirm that element 22b is defective. The process can be continued until the desired length of the segment is obtained. It can also be observed that the reduction in the identified stiffness parameter of the modified segment containing the defect increases with the reduction of its length. This example confirms that UKF-UI-WGI can detect defect spot accurately in a defective element.

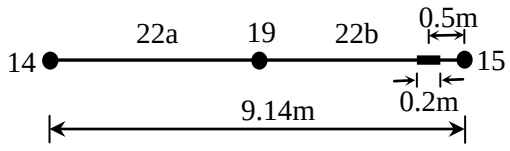

Figure 6.25 Defect 4 representation

Table 6.14 Stiffness parameter (*EI/L*) identification for Defect 4

Member	Locating the defective member			Additional node at mid-span of member 22			Additional node at a distance 6m from node 14		
	Theoretical (kN-m)	Identified (kN-m)	Change %	Theoretical (kN-m)	Identified (kN-m)	Change %	Theoretical (kN-m)	Identified (kN-m)	Change %
(1)	(2)	(3)	(4)	(5)	(6)	(7)	(8)	(9)	(10)
k_1	13476	13487	0.1	13476	13475	0.0	13476	13484	0.1
k_2	13476	13877	3.0	13476	13812	2.5	13476	14154	5.0
k_3	14553	14572	0.1	14553	14557	0.0	14553	14569	0.1
k_4	14553	14638	0.6	14553	14648	0.7	14553	14687	0.9
k_5	14553	13927	-4.3	14553	14025	-3.6	14553	13602	-6.5
k_6	13476	13463	-0.1	13476	13459	-0.1	13476	13454	-0.2
k_7	13476	13455	-0.2	13476	13446	-0.2	13476	13427	-0.4
k_8	14553	14511	-0.3	14553	14489	-0.4	14553	14539	-0.1
k_9	14553	14577	0.2	14553	14736	1.3	14553	14515	-0.3
k_{10}	14553	14521	-0.2	14553	14332	-1.5	14553	14589	0.2
k_{11}	13476	13438	-0.3	13476	13512	0.3	13476	13418	-0.4
k_{12}	13476	13547	0.5	13476	13360	-0.9	13476	13638	1.2
k_{13}	14553	14260	-2.0	14553	14278	-1.9	14553	14239	-2.2
k_{14}	14553	14573	0.1	14553	14750	1.4	14553	14490	-0.4
k_{15}	14553	14701	1.0	14553	14532	-0.1	14553	14780	1.6
k_{16}	13476	13357	-0.9	13476	13395	-0.6	13476	13383	-0.7
k_{17}	13476	13645	1.3	13476	13538	0.5	13476	13621	1.1
k_{18}	14553	14689	0.9	14553	15081	3.6	14553	14186	-2.5
k_{19}	14553	14403	-1.0	14553	14104	-3.1	14553	14865	2.1
k_{20}	14553	14692	1.0	14553	14633	0.5	14553	14656	0.7
k_{21}	13476	13913	3.2	13476	13573	0.7	13476	13861	2.9
k_{22a}	13476	11243	**-16.6**	26952	27258	1.1	20529	20786	1.3
k_{22b}				26952	21702	**-19.5**	39227	22664	**-42.2**
k_{23}	14553	14614	0.4	14553	14341	-1.5	14553	14994	3.0
k_{24}	14553	14593	0.3	14553	14521	-0.2	14553	14510	-0.3
k_{25}	14553	14434	-0.8	14553	14545	-0.1	14553	14424	-0.9
Note:	$R_k = 10^{-4}$; $P_x(0\|0) = 0.1$; $P_s(0\|0) = 10^3$; $w = 10$								

6.4.4 Structural Health Assessment Using GILS-EKF-UI Procedure

To demonstrate the superiority of the proposed procedure, its performance is compared with the GILS-EKF-UI procedure developed by the team members earlier. The results of the GILS-EKF-UI procedure for the defect-free and four defective cases, considered earlier, are summarized in Table 6.15. For the defect-free case, responses at 9 DDOFs are used to identify the structure. The results indicate that the maximum error in the identification is about 76.3% using GILS-EKF-UI. It is only 0.5% for UKF-UI-WGI. Obviously, the EKF-based procedure failed to assess the defect-free state of the frame.

For four defective cases, the EKF-based procedure identified the defect locations and their severity reasonably well. However, for SHA, its use may not be straightforward. For Defect 1, the stiffness parameter of the defective member 22 reduced by 29.8%; however, it reduced for member 5 by 14.8%, incorrectly indicating that they may also be defective. In addition, it increased for member 2 by 13.9%. Therefore, it can be concluded that the EKF-based procedure failed to assess the health of the frame. Results in Tables 6.13 and 6.14 indicate that there is no such assessment problem when UKF-UI-WGI is used, establishing its superiority. Similar conclusions can be made when other defect scenarios are considered. To avoid any similar problems in structural health assessment, the author recommends using UKF-UI-WGI instead of GILS-EKF-UI procedures developed by the team earlier.

Table 6.15 Change (%) in *EI/L* identification of whole structure using GILS-EKF-UI procedure

Member	Theoretical (kN-m)	Defect-Free	Defect 1	Defect 2	Defect 3	Defect 4
		9DDOFs	18DDOFs	18DDOFs	18DDOFs	18DDOFs
(1)	(2)	(3)	(4)	(5)	(6)	(7)
k_1	13476	-1.4	-0.3	-0.4	-0.5	-0.2
k_2	13476	-8.9	13.9	13.6	22.7	13.3
k_3	14553	-1.6	-0.3	-0.4	-0.5	-0.2
k_4	14553	-1.5	3.1	3.0	4.8	2.9
k_5	14553	24.7	-14.8	-14.2	-21.2	-14.2
k_6	13476	0.6	-1.7	-1.5	-2.3	-1.6
k_7	13476	-3.1	-1.0	-1.1	-1.5	-1.0
k_8	14553	-1.9	-2.1	-1.6	-2.5	-2.0
k_9	14553	-5.1	2.9	2.2	2.8	2.4
k_{10}	14553	0.1	-1.7	-1.6	-1.9	-1.0
k_{11}	13476	13.4	0.4	0.9	1.0	0.1
k_{12}	13476	-0.4	-0.6	-0.4	**-49.9**	0.1
k_{13}	14553	4.8	-2.4	-0.8	-1.7	-2.5
k_{14}	14553	-5.1	0.6	-0.2	-0.9	0.3
k_{15}	14553	-9.8	0.4	0.2	0.8	1.0
k_{16}	13476	-5.5	0.1	0.0	0.4	-0.9
k_{17}	13476	1.4	0.6	**-19.6**	1.1	1.5
k_{18}	14553	3.1	8.1	3.5	8.2	5.1
k_{19}	14553	-9.0	-4.2	-2.1	-4.6	-3.5
k_{20}	14553	76.3	-0.3	0.1	-0.1	0.7
k_{21}	13476	-3.9	1.3	0.5	1.2	4.6
k_{22}	13476	0.5	**-29.8**	0.3	0.4	**-16.4**
k_{23}	14553	-3.5	-3.5	-1.6	-4.1	-1.7
k_{24}	14553	2.1	1.6	0.9	2.1	1.1
k_{25}	14553	-3.7	0.1	0.0	0.1	-0.8
Note:	$R_k = 10^{-4}$; $P_x(0\|0) = 0.1$; $P_s(0\|0) = 10^3$; $w = 10$					

6.4.5 Optimum Number of Measured Responses

In this section, the absolute minimum of measured responses required to identify the frame is further explored considering the location of the defective member known. First, the responses are assumed to be available at the substructure and a node connecting to the defective member, i.e., at 12 DDOFs. Then, they are assumed to be available at the substructure and 2 additional nodes, i.e., at 15 DDOFs, where one of them is connecting to the defective member. The results of identification using UKF-UI-WGI with 12 and 15 DDOFs for Defects 1-3 are shown in Table 6.16. The results show that in all cases, the UKF-UI-WGI is able to identify the locations of the defects and their severity reasonably well using responses only at 12 DDOFs. However, the results also show that the reductions are not only in the defective member but also in some other members incorrectly indicating that they may also be defective. To improve the capability of defect detection, the responses at 15 DDOFs should be used. The results of 15 DDOFs for all cases show that the location and severity of defect are identified accurately.

Therefore, it can be concluded here that if the location of defect is known, responses at 15 DDOFs, including responses at a node connecting to defective member, are sufficient to identify the structure. However, if the location of defect is not known, responses at 18 DDOFs are required to identify the structure and it is preferred to be measured at all floor levels.

Table 6.16 Change (%) in (*EI/L*) identification using UKF-UI-WGI with 12 and 15DDOFs

Member	Theoretical (kN-m)	Defect 1		Defect 2		Defect 3	
		12DDOFs	15DDOFs	12DDOFs	15DDOFs	12DDOFs	15DDOFs
		Available responses at substructure (nodes 1, 2, 4) and at nodes					
		15	9, 15	12	9, 12	9	9, 12
(1)	(2)	(3)	(4)	(5)	(6)	(7)	(8)
k_1	13476	0.3	0.0	-0.2	0.0	0.0	0.2
k_2	13476	-1.3	-0.4	1.6	1.2	11.3	0.6
k_3	14553	0.4	0.0	-0.2	0.1	0.0	0.2
k_4	14553	-0.6	0.1	0.9	0.3	2.7	0.1
k_5	14553	0.2	0.7	0.9	-2.1	-12.6	-1.5
k_6	13476	0.8	-0.1	0.9	0.2	-0.6	0.4
k_7	13476	1.2	-0.1	-3.9	-0.1	-1.9	-0.2
k_8	14553	0.0	0.0	4.3	0.1	-0.5	0.3
k_9	14553	0.6	0.6	-1.3	0.8	1.3	-0.3
k_{10}	14553	-1.5	-0.7	-6.5	-1.2	-2.4	-0.3
k_{11}	13476	0.8	0.6	1.0	-0.1	1.9	-0.1
k_{12}	13476	-3.6	-0.8	8.0	-0.5	**-50.3**	**-49.8**
k_{13}	14553	9.7	2.9	-2.6	-1.9	2.2	-1.2
k_{14}	14553	5.9	0.2	-6.2	1.1	0.2	-0.3
k_{15}	14553	-7.4	-1.2	-5.5	0.3	-3.7	0.7
k_{16}	13476	-9.7	-1.8	6.1	-0.4	-5.6	0.4
k_{17}	13476	7.8	1.9	**-21.0**	**-19.6**	3.8	0.7
k_{18}	14553	0.9	0.9	-3.8	2.1	2.3	5.7
k_{19}	14553	2.7	-1.9	2.8	-1.0	3.7	-1.5
k_{20}	14553	-11.4	-1.0	-9.3	1.1	4.2	0.6
k_{21}	13476	4.7	1.6	-12.6	0.0	3.1	-1.0
k_{22}	13476	**-31.4**	**-29.2**	3.4	0.4	-7.1	0.0
k_{23}	14553	-4.4	-1.9	3.1	-0.6	-2.2	-3.4
k_{24}	14553	0.9	-1.0	3.7	0.1	2.8	2.4
k_{25}	14553	0.2	0.9	7.0	-0.6	-1.4	-0.4
Note:	$R_k = 10^{-4}$; $P_x(0\|0) = 0.1$; $P_s(0\|0) = 10^3$; $w = 10$						

6.5 Observations and Discussions

The proposed UKF-UI-WGI procedure is verified to identify the health of large structural systems. Three different size and configuration of structures are considered. The structures are excited by different types of loadings including impulsive, sinusoidal, and seismic loading. One and multiple input excitation(s) are considered. Small and relatively severe damages are numerically simulated in single and multiple members in the structure. Different damage scenarios are also considered in terms of reduction in the stiffness parameters or cross-sectional areas. Different number of measured responses and their locations with respect to the location of defect is also studied in order to show their effects on the identification accuracy.

Several important observations can be made from the numerical examples. The proposed method is capable of identifying the location and severity of defects at the local element level using only a limited number of noise-contaminated responses and without using input excitation information. Moreover, it can detect defect spot accurately in a defective element. The procedure can identify the defect even if the measured responses are not close to the defective member; however, the accuracy of identification improves as the measured responses become closer to the defective member. One of the advantages of the integrated procedure is that it does not need to guess the initial values of the unknown stiffness parameters; it can be generated from the first stage of the procedure. The substructure approach is important to identify the input excitation time-history using only a limited number of measured responses.

The global weighted iteration with an objective function, introduced in the traditional UKF algorithm, plays an important role in the stability and convergency of the

algorithm. It also improves the UKF algorithm to identify a large structural systems using only a short duration of measured responses. The robustness of the proposed procedure is also demonstrated by conducting parametric studies. They showed that the procedure is able to identify the structure also if the values of the parameters, required to implement the procedure, are not close to the true values.

The comparative study between the proposed UKF-UI-WGI and the GILS-EKF-UI procedure developed earlier by the research team shows the superiority of the proposed procedure for structural health assessment. Moreover, the measured responses required to identify the structural systems using UKF-UI-WGI procedure is smaller than that of GILS-EKF-UI.

CHAPTER 7

SUMMARY AND CONCLUSIONS

7.1 Summary

A novel robust structural health assessment (SHA) procedure is developed in two stages. The procedure is vibration-based nonlinear system identification (SI) technique. The structure is represented by finite element. The basic premise of SI-based SHA methods is that structural defect will alter the parameters of the structural elements, i.e., stiffness, mass, and/or energy dissipation, which in turn change global structural responses. Thus, by tracking the signature embedded in the structural responses, the information on the locations of defects and their severities can be obtained.

The unscented Kalman filter with weighted global iteration (UKF-WGI) procedure is developed first. In this procedure, a weighted global iteration (WGI) with an objective function is incorporated with the traditional UKF algorithm in order to obtain stable, convergent, and optimal solution. In addition, it improves the UKF algorithm in order to be able to identify a large structural system using short response time-histories measured at a limited number of dynamic degrees of freedom (DDOFs). The UKF-WGI procedure is extensively verified for several SHA problems including linear and nonlinear structural systems; considering small and severe defects in single and multiple members, and using noise free and noisy dynamic responses. The comparative study between the results of UKF-WGI and extended Kalman filter with weighted global iteration (EKF-WGI) procedure is also conducted to demonstrate the superiority of the UKF-WGI procedure.

Then, the unscented Kalman filter with unknown input and weighted global iteration (UKF-UI-WGI) procedure is developed. It is integration of iterative least-squares with

unknown input (ILS-UI) and the UKF-WGI procedures. The substructure concept is also incorporated in the approach. The procedure is implemented in two stages. In the first stage, based on the location of input excitation(s), the substructure is selected. Then, using only the responses at all DDOFs of substructure, the ILS-UI procedure is implemented to identify the input excitation time-histories, the stiffness parameters of all the elements in the substructure and the two Rayleigh damping coefficients. The information extracted from the first stage satisfies all the requirements to implement UKF-WGI in the second stage. After implementing the UKF-WGI procedure, the stiffness parameters of all the elements in the structure are identified. By comparing the identified stiffness properties with the expected values; reference values obtained from the design drawings; or previous values if inspections are carried out periodically, the location(s), number, and severity of defects can be established.

The effectiveness of UKF-UI-WGI procedure is verified with the help of several numerical SHA problems. The health assessment of relatively large real structural systems under various types of excitation, i.e., harmonic, impulsive, and earthquake, is studied. Small and severe defects in single and multiple members are considered. The optimum number and location of measured responses required to identify the structure are explored. The effects of various parameters on the SHA are also investigated. With the help of these studies, it is documented that the proposed method is robust, accurate, and stable in assessing health of large structural systems using only a limited number of responses and without using input excitation information.

Finally, two comparative studies are considered to demonstrate the superiority of the proposed procedure. First, it is between UKF-WGI and the traditional UKF procedure

and then between UKF-UI-WGI and the generalized iterative least-squares extended Kalman filter with unknown input (GILS-EKF-UI) procedure, developed earlier by the research team.

7.2 Conclusions

Based on this study, several important conclusions can be made. They are:

1. The proposed UKF-UI-WGI procedure is a nondestructive SHA procedure. It can identify the structure using only limited response information and without using input excitation information and it is capable of identifying:
   a. location of the defect at the local element level and also severity of the defect accurately,
   b. single and multiple defects in the structure,
   c. small and severe defects considering different kinds of defect simulation such as reduction in stiffness parameter or reduction in the thickness or cross section of the member,
   d. a defect spot within a defective member, and
   e. the state of structures excited by any type of loadings such as harmonic, impulsive, and earthquake loadings, applied at any location.
2. The weighted global iteration with an objective function incorporated with the UKF algorithm plays important role in the identification as follows:
   a. obtain stable, convergent, and optimal solution,
   b. improve the UKF procedure to identify a large structural system, and
   c. use only a limited number of responses with short time-histories, often fractions of a second.

3. The integration of the ILS-UI procedure with the UKF-WGI procedure, producing a two-stage approach, has significant impact on the latter as follows:
   a. The input excitation time-histories, required to implement UKF-WGI, are identified using ILS-UI.
   b. The identified stiffness parameters of all the members in the substructure using ILS-UI help to generate the initial stiffness parameters of the whole structure, required to initiate the UKF-WGI procedure.
   c. The identified damping coefficients using ILS-UI is used as known parameters in the UKF-WGI procedure.
4. The substructure approach is useful in order to identify the input excitation time-histories using only responses measured at the substructure.
5. The finite element representation of the structure is important in order to identify the structure at the local element level.
6. The accuracy of identification of the defective member in the structure improves when the responses at a node connected to the defective member are measured.
7. A large value of weight factor accelerates the convergency of the UKF-WGI algorithm; however, it must not be so large that the stability might be compromised.
8. A large value of initial stiffness covariance matrix is desirable to accelerate the UKF-WGI processing. However, its value should not be very large so that the stability might be compromised.
9. The proposed procedure correctly identified the locations and the severity of defects, even when the quality of the measured responses is not good.

10. The comparative study between the proposed UKF-based procedure and the EKF-based procedure showed that:
    a. The UKF-based procedure is superior to the EKF-based procedure for identification of nonlinear structural systems.
    b. The UKF-based procedure is more robust to structural identification in the presence of measurement noises than the EKF-based procedure.
    c. The number of measured responses required to identify the structure using the UKF-based procedure is much less than that using the EKF-based procedure.
    d. In general, the errors in identification using the UKF-based procedure are much smaller than that using the EKF-based procedure.

7.3 Recommendations for Future Work

Although significant improvements have been achieved in this study toward the ultimate goal of developing robust method for SHA to real large structural systems, there are still several issues which need further investigation. The following topics can be addressed in the future:

1. The method needs to be extended for three dimensional structures.
2. The method needs to be extended further to identify highly nonlinear hysteretic structural systems.
3. The method needs to be verified using experimental responses obtained from full scale real structures.
4. The method needs to be extended to framed structure with semi-rigid connections.

APPENDIX A

NOTATIONS AND SYMBOLS

The following symbols are used in this dissertation:

$\mathbf{A}_{kn}(t)$ = matrix resulting from multiplication of global stiffness coefficient matrix related to key nodes and measured displacement and velocity in substructure at time *t*

$\mathbf{A}_{sub}(t)$ = matrix resulting from multiplication of global stiffness coefficient matrix and measured displacement and velocity in substructure at time *t*

a = mass proportional damping coefficient

b = stiffness proportional damping coefficient

B = total number of measured acceleration responses

$\mathbf{C}$ = global viscous damping matrix for whole structure

$\mathbf{C}_{col.i}$ = i^{th} column in square root of the error covariance matrix of the state

dkn = total number of dynamic degrees of freedom of key nodes in substructure

dsub = total number of dynamic degrees of freedom in substructure

E_i = Young's modulus of elasticity of i^{th} element

$esub$ = total number of elements in substructure

$\mathbf{f}(t)$ = excitation force vector for whole structure at time *t*

$\mathbf{f}_{kn}(t)$ = excitation force vector applied at key nodes at time *t*

$\mathbf{F}_{kn}(t)$ = vector of unknown input excitations and inertia forces for key nodes at time *t*

$\mathbf{f}_{kn}^{i}$ = identified excitation force at i^{th} iteration

$f(\ \ )$ = nonlinear function of the state vector

f_1, f_2 = first two natural frequencies of the structure

$h(\ \ )$ = nonlinear function relating state to measurement vector

$\mathbf{H}$ = measurement matrix relating state to measurement vector

$\mathbf{I}$ = unit matrix

I_i = moment of inertia of i^{th} element

$\mathbf{K}$ = global stiffness matrix for whole structure

$\mathbf{K}_{sub}$ = global stiffness matrix for substructure

$\mathbf{K}_{kn,sub}$ = stiffness matrix containing all rows related to the key nodes extracted from the global stiffness matrix of the substructure

$\mathbf{K}_i$ = stiffness matrix of i^{th} element in the global coordinate system

$\bar{\mathbf{K}}_i$ = stiffness matrix for i^{th} element in the local coordinate system

$\widetilde{\mathbf{K}}$ = vector of unknown stiffness parameters of whole structure

$\widetilde{\mathbf{K}}(0|0)$ = initial mean of unknown stiffness parameters of whole structure

$\mathbf{K}_{k+1}$ = Kalman gain matrix at discrete time k+1

$\mathrm{K}_{q|q}^{(i)}$ = identified stiffness parameter at the end of i^{th} global iteration

k_i = stiffness parameter of i^{th} element

kn = total number of key nodes in substructure

L = total number of unknown stiffness parameters of whole structure

L_i = length of i^{th} element

$\mathbf{M}$ = global mass matrix for whole structure

$\mathbf{M}_{sub}$ = global mass matrix for substructure

$\mathbf{M}_{kn,sub}$ = mass matrix containing all rows related to the key nodes extracted from the global mass matrix of the substructure

$\mathbf{M}_i$ = mass matrix for i^{th} element in the global coordinate system

$\bar{\mathbf{M}}_i$ = mass matrix for i^{th} element in the local coordinate system

$\bar{m}_i$ = mass per unit length for i^{th} element

N = total number of dynamic degrees of freedom in whole structure

n = dimension of the state vector

nsub = total number of nodes in substructure

$\mathbf{P}_{sub}$ = vector of unknown system parameters in substructure

$\mathbf{P}_{0|0}$ = initial error covariance matrix of the state

$\mathbf{P}_s(0|0)$ = initial error covariance matrix of the stiffness parameters of whole structure

$\mathbf{P}_x(0|0)$ = initial error covariance matrix of the displacement and velocity responses

$\mathbf{P}_{k+1|k}$ = predicted error covariance matrix at discrete time k+1 given measurements up to discrete time k

$\mathbf{P}_{k+1|k+1}$ = updated error covariance matrix at discrete time k+1 by incorporating measurements at discrete time k+1

$\mathbf{P}_{k+1|k}^{YY}$ = predicted measurement error covariance matrix at discrete time k+1 given measurements up to discrete time k

$\mathbf{P}_{k+1|k}^{ZY}$ = predicted cross correlation matrix at discrete time k+1 given measurements up to discrete time k

q = total number of measurement time points

$\mathbf{R}_k$ = measurement noise covariance matrix at discrete time k

re = total number of related elements in substructure

rn = total number of related nodes in substructure

sc = total number of constraints to dynamic degrees of freedom in substructure at support

$\mathbf{S}_i$ = global stiffness coefficient matrix of i^{th} element in the global coordinate system

$\bar{\mathbf{S}}_i$ = stiffness coefficient matrix of i^{th} element in the local coordinate system

$\mathbf{T}_i$ = transformation matrix for i^{th} element

usub = total number of unknown parameters in substructure

$\mathbf{V}_k$ = zero mean white measurement noise vector at discrete time *k*

W_i = weighted factor for sigma points and their error covariance

w = weight factor

$x_i(t), \dot{x}_i(t), \ddot{x}_i(t)$ = horizontal displacement, velocity, and acceleration of i^{th} node

$\mathbf{X}(t)$ = displacement response vector for whole structure at time *t*

$\dot{\mathbf{X}}(t)$ = velocity response vector for whole structure at time *t*

$\ddot{\mathbf{X}}(t)$ = acceleration response vector for whole structure at time *t*

$\mathbf{X}_{sub}(t)$ = displacement response vector for substructure at time *t*

$\dot{\mathbf{X}}_{\mathrm{sub}}(t)$ = velocity response vector for substructure at time *t*

$\ddot{\mathbf{X}}_{sub}(t)$ = acceleration response vector for substructure at time *t*

$\widehat{\mathbf{X}}(0|0)$ = initial mean of displacement vector for all dynamic degrees of freedom in the structure

$\widehat{\dot{\mathbf{X}}}(0|0)$ = initial mean of velocity vector for all dynamic degrees of freedom in the structure

X, Y = global coordinate system

$\overline{\mathrm{X}}, \overline{\mathrm{Y}}$ = local coordinate system

$y_i(t), \dot{y}_i(t), \ddot{y}_i(t)$ = vertical displacement, velocity, and acceleration of i^{th} node

$\mathrm{y}_{i,k}$ = i^{th} measured response at discrete time *k*

$\mathbf{Y}_k$ = measurement vector at discrete time *k*

$\mathbf{Y}_{k+1}$ = measurement vector at discrete time *k*+1

$\hat{\mathbf{Y}}_{k+1|k}$ = predicted measurement vector at discrete time k+1 given measurements up to discrete time k

$\mathbf{Z}_t$ = state vector at time t containing displacement, velocity, and unknown stiffness parameter of whole structure

$\dot{\mathbf{Z}}_t$ = time derivative of state vector at time t

$\mathbf{Z}_k$ = state vector at discrete time k

$\hat{\mathbf{Z}}_{0|0}$ = initial mean of state vector

$\hat{\mathbf{Z}}_{k|k}$ = mean values of the state vector at discrete time k given measurements up to discrete time k

$\hat{\mathbf{Z}}_{k+1|k}$ = predicted mean values of the state vector at discrete time k+1 given measurements up to discrete time k

$\hat{\mathbf{Z}}_{k+1|k+1}$ = updated state vector at discrete time k+1 by incorporating measurements at discrete time k+1

$\boldsymbol{\chi}_{i,k|k}$ = i^{th} sigma points generated around the state vector at discrete time k given measurements up to discrete time k

$\boldsymbol{\chi}_{i,k+1|k}$ = i^{th} predicted sigma points at discrete time k+1 given measurements up to discrete time k

λ = scaling parameter

α = scaling factor determining the extent of the spread of the sigma points around the prior mean

κ = secondary scaling factor and is usually set to 0

β = scaling factor used to emphasize the weighting on the zeroth sigma point for the posterior covariance calculation

δ_{ik} = difference between measured and corresponding estimated response for i^{th} element in measurement vector at discrete time k

γ_i = normalized mean-square of the difference between i^{th} measurement and corresponding estimated response

$\bar{\beta}$ = average of normalized mean-square of the difference between i^{th} measurement and corresponding estimated response

$\bar{\theta}$ = objective function showing the scatterness in the root mean-square γ from the central value $\bar{\beta}$

$\theta_i(t), \dot{\theta}_i(t), \ddot{\theta}_i(t)$ = rotational displacement, velocity, and acceleration of i^{th} node

Δt = time increment

$\mathbf{\Phi}_{k+1|k}$ = Jacobian matrix of the state transition of the system from discrete time k to k+1

ε_f = predetermined convergence criterion for force excitation

ε_s = predetermined convergence criterion for stiffness parameter identification

ω_m, ω_n = first two natural circular frequencies of the structure

ξ = damping ratio

REFERENCES

Abdul Wahab, M. M. and De Roeck, G. (1999), "Damage Detection in Bridges Using Modal Curvatures: Applications to a Real Damage Scenario," Journal of Sound and Vibration, Vol. 226, No. 2, pp. 217−235.

Adams, R. D., Cawley, P., Pye, C. J., and Stone, B. J. (1978), "A Vibration Technique for Non-Destructively Assessing the Integrity of Structures," Journal of Mechanical Engineering Science, Vol. 20, No. 2, pp. 93-100.

Adams, R. D., Walton, D., Flitcroft, J. E., and Short, D. (1975), "Vibration Testing as a Nondestructive Test Tool for Composite Materials," Composite Reliability, ASTM STP 580, American Society for Testing and Materials, pp.159-175.

Aditya, G. and Chakraborty, S. (2008), "Sensitivity Based Health Monitoring of Structures with Static Responses," Scientia Iranica, Vol. 15, No. 3, pp. 267-274.

Agbabian, M. S., Masri, S. F., Miller, R. K., and Caughey, T. K. (1991), "System Identification Approach to Detection of Structural Changes," Journal of Engineering Mechanics, ASCE, Vol. 117, No. 2, pp. 370-390.

Al-Hussein, A. and Haldar, A. (2014), "A New Extension of Unscented Kalman Filter for Structural Health Assessment with Unknown Input," Proceedings of SPIE 9061, Sensors and Smart Structures Technologies for Civil, Mechanical, and Aerospace Systems, pp. 90612Y.

Al-Hussein, A. and Haldar, A. (2015a), "A Comparison of Unscented and Extended Kalman Filtering for Nonlinear System Identification," Proceedings of the 12th International Conference on Applications of Statistics and Probability in Civil Engineering (ICASP12), Vancouver, Canada, July 12-15.

Al-Hussein, A. and Haldar, A. (2015b), "Health Assessment of Nonlinear Structural Systems," International Journal of Life Cycle Reliability and Safety Engineering, Vol. 4, No. 1, pp. 25-34.

Al-Hussein, A. and Haldar, A. (2015c), "Novel Unscented Kalman Filter for Health Assessment of Structural Systems with Unknown Input," Journal of Engineering Mechanics, ASCE, Vol. 141, No. 7, pp. 04015012.

Al-Hussein, A. and Haldar, A. (2015d), "Structural Health Assessment at a Local Level Using Minimum Information," Engineering Structures, Vol. 88, pp. 100-110.

Al-Hussein, A. and Haldar, A. (2015e), "Unscented Kalman Filter with Unknown Input and Weighted Global Iteration for Health Assessment of Large Structural Systems," Structural Control and Health Monitoring, DOI: 10.1002/stc.1764.

Al-Hussein, A. and Haldar, A. (2015f), "Structural Health Assessment using Extended and Unscented Kalman Filters," International Journal of Sustainable Materials and Structural Systems, (Under Review).

Al-Hussein, A. and Haldar, A. (2015g), "Nonlinear System Identification from Uncertain Measurements," Mechanical Systems and Signal Processing, (Under Review).

Al-Hussein, A. and Haldar, A. (2015h), "Computational Intelligence for Structural Identifications," 2015 IEEE Symposium on Computational Intelligence for Engineering Solutions, (Under Review).

Al-Hussein, A., Das, A. K., and Haldar, A. (2013), "A New Approach for Structural Health Assessment using Unscented Kalman Filter," 11th International Conference on Structural Safety and Reliability (ICOSSAR'13), Columbia University, New York, N.Y., pp. 1579-1585.

Allemang, R. J. and Brown, D. L. (1982), "Correlation Coefficient for Modal Vector Analysis," Proceedings of the 1st International Modal Analysis Conference, pp. 110−116.

Anh, T. V. (2009), "Enhancements to the Damage Locating Vector Method for Structural Health Monitoring," PhD Dissertation, National University of Singapore, Singapore.

ANSYS version 14.0 (2011), The Engineering Solutions Company.

ANSYS version 15.0 (2013), The Engineering Solutions Company.

Avitabile, P. and Pechinsky, F. (1994), "Coordinate Orthogonality Check (CORTHOG)," Proceedings of International Modal Analysis Conference of Sound and Vibration, pp. 753−760.

Balis Crema, L., Castellani, A., and Coppotelli, G. (1995), "Generalization of Non Destructive Damage Evaluation Using Modal Parameters," Proceedings of the 13th International Modal Analysis Conference, pp. 428–431.

Banan, M. R., Banan, M. R., and Hjelmstad, K. D. (1994a), "Parameter Estimation of Structures from Static Response I: Computational Aspects," Journal of Structural Engineering, ASCE, Vol. 120, No. 11, pp. 3243-3258.

Banan, M. R., Banan, M. R., and Hjelmstad, K. D. (1994b), "Parameter Estimation of Structures from Static Response II: Numerical Simulation Studies," Journal of Structural Engineering, ASCE, Vol. 120, No. 11, pp. 3259-3283.

Bandara, R. P. (2013), "Damage Identification and Condition Assessment of Building Structures Using Frequency Response Functions and Neural Networks," PhD Dissertation, School of Civil Engineering and Built Environment, Queensland University of Technology, Australia.

Beck, J. L. and Yuen, K. V. (2004), "Model Selection Using Response Measurements: Bayesian Probabilistic Approach," Journal of Engineering Mechanics, ASCE, Vol. 130, No. 2, pp. 192-203.

Berman, A. and Flannelly, W. G. (1971), "Theory of Incomplete Models of Dynamic Structures," AIAA Journal, Vol. 9, No. 8, pp. 1481-1487.

Bisby, L. A. and Briglio, M. B. (2004), "ISIS Canada Educational Module No. 5: An Introduction to Structural Health Monitoring," Prepared by ISIS Canada, A Canadian Network of Centers of Excellence, pp. 1-37

Brechlin, E., Bendel, K., and Keiper, W. (1998), "A New Scaled Modal Assurance Criterion for Eigenmodes Containing Rotational Degrees of Freedom," Proceedings of International Seminar on Modal Analysis, Vol. 3, pp. 197−206.

Brincker, R., Kirkegaard, P. H., Anderson, P., and Martinez, M. E. (1995), "Damage Detection in an Offshore Structure," Proceedings of the 13th International Modal Analysis Conference (IMAC XIII), Nashville, Tennessee, pp. 661–667.

Caravani, P., Watson, M. L., and Thomson, W. T. (1977), "Recursive Least Squares Time Domain Identification of Structural Parameters," Journal of Applied Mechanics, ASME, Vol. 44, No. 1, pp. 135-40.

Carden, E. P. and Fanning, P. (2004), "Vibration Based Condition Monitoring: A Review," Structural Health Monitoring, Vol. 3, No. 4, pp. 355-377.

Carmichael, D. G. (1979), "The State Estimation Problem in Experimental Structural Mechanics," International Conference on Application of Statistics and Probability in Soil and Structural Engineering, Third Edition, Sydney, Australia, pp. 802-815.

Catbas, F. N., Aktan, A. E., Allemang, R. J., and Brown, D. L. (1998), "A Correlation Function for Spatial Locations of Scaled Mode Shapes: Coordinate Modal Error Function (COMEF)," Proceedings of the 16th International Modal Analysis Conference, Santa Barbara, California, , pp. 1550- 1555.

Cawley, P. and Adams, R. D. (1979), "The Location of Defects in Structures from Measurements of Natural Frequencies," Journal of Strain Analysis for Engineering Design, Vol. 14, No. 2, pp. 49−57.

Chang, P. C. and Liu, S. C. (2003), "Recent Research in Nondestructive Evaluation of Civil infrastructure," Journal of Materials of Civil Engineering, Vol. 15, No. 3, pp. 298−304.

Chatzi, E. N. and Smyth, A. W. (2009), "The Unscented Kalman Filter and Particle Filter Methods for Nonlinear Structural System Identification with Non-Collocated Heterogeneous Sensing," Structural Control and Health Monitoring, Vol.16, No. 1, pp. 99-123.

Chatzi, E. N. and Smyth, A. W. (2013), "Particle Filter Scheme with Mutation for the Estimation of Time-Invariant Parameters in Structural Health Monitoring Applications," Structural Control and Health Monitoring, Vol. 20, No. 7, pp. 1081–1095.

Chatzi, E. N., Smyth, A. W., and Masri, S. F. (2010), "Experimental Application of On-Line Parametric Identification for Nonlinear Hysteretic Systems with Model Uncertainty," Journal of Structural Safety, Vol. 32, No. 5, pp. 326–337.

Chen, J. and Li, J. (2004), "Simultaneous Identification of Structural Parameters and Input Time History from Output-Only Measurements," Journal of Computational Mechanics, Vol. 33, No. 5, pp. 365-374.

Chen, L., Seereeram, S., and Mehra, R. K. (2003), "Unscented Kalman Filter for Multiple Spacecraft Formation Flying," Proceedings of the American Control Conference, Vol. 2, Denver, CO, pp. 1752–1757.

Chen, T., Morris, J., and Martin, E. (2005), "Particle Filters for State and Parameter Estimation in Batch Processes," Journal of Process Control, Vol. 15, No. 6, pp. 665–673.

Choi, J., Lima, A. C., and Haykin, S. (2005), "Kalman Filter-Trained Recurrent Neural Equalizers for Time-Varying Channels," IEEE Transactions on Communications, Vol. 53, No. 3, pp. 472–480.

Choi, J., Yeap, T. H., and Bouchard, M. (2004), "Nonlinear State-Space Modelling Using Recurrent Multilayer Perceptrons with Unscented Kalman Filter," IEEE International Conference on Systems, Man and Cybernetics, Vol. 4. The Hague, Netherlands, pp. 3427–3432.

Clough, R. W. and Penzien, J. (2003), "Dynamics of Structures," Third Edition, Computers and Structures, CA, USA.

Cook, R. D., Malkus, D. S., Plesha, M. E., and Witt, R. J. (2002), "Concepts and Applications of Finite Element Analysis," Fourth Edition, John Wiley & Sons, Inc., NJ.

Crassidis, J. L. and Markley, F. L. (2003), "Unscented Filtering for Spacecraft Attitude Estimation," Journal of Guidance, Control, and Dynamics, Vol. 26, No. 4, pp. 536–542.

Das, A. K. (2012), "Health Assessment of Three Dimensional Large Structural Systems Using Limited Uncertain Dynamic Response Information," PhD Dissertation, Department of Civil Engineering and Engineering Mechanics, University of Arizona, Tucson, Arizona.

Das, A. K. and Haldar, A. (2010a), "Structural Integrity Assessment under Uncertainty for Three Dimensional Offshore Structures," International Journal of Terraspace Science and Engineering (IJTSE), Vol. 2, No. 2, pp. 101-111.

Das, A. K. and Haldar, A. (2010b), "Structural Health Assessment of Truss Bridges using Noise-contaminated Uncertain Dynamic Response Information," International Journal of

Engineering under Uncertainty: Hazards, Assessment, and Mitigation, Vol. 2, No. 3-4, pp. 75-87.

Das, A. K. and Haldar, A. (2011a), "Health Assessment of Structures Exposed to Seismic Excitation," ISET Journal of Earthquake Technology, Vol. 48, No.1, 514.

Das, A. K. and Haldar, A. (2011b), "Structural Health Assessment using only Noise-Contaminated Responses," International Conference on Vulnerability and Risk Analysis and Management (ICVRAM), ASCE, April 11-13.

Das, A. K. and Haldar, A. (2012a), "Health Assessment of Three Dimensional Large Structural Systems - A Novel Approach," International Journal of Life Cycle Reliability and Safety Engineering, Vol. 1, No. 1, pp. 1-14.

Das, A. K. and Haldar, A. (2012b), "Health Assessment with only Limited Noise Contaminated Response Information," Health Assessment of Engineered Structures: Bridges, Buildings and Other Infrastructures, Edited by Achintya Haldar, World Scientific Publishing Co., Inc., New York.

Das, A. K. and Haldar, A. (2012c), "Health Prognosis of Large Engineering Structures using Minimum Information," Joint Conference of the Engineering Mechanics Institute and 11th ASCE Joint Specialty Conference on Probabilistic Mechanics and Structural Reliability (EMI/PMC), University of Notre Dame, Indiana, USA, June 17-20.

Das, A. K., Haldar, A., and Chakraborty, S. (2012), "Health Assessment of Large Two Dimensional Structures using Minimum Information – Recent Advances," Advances in Civil Engineering, 2012, Article ID 582472, doi:10.1155/2012/582472.

Das, K. A., Al-Hussein, A., and Haldar, A. (2013), "Algorithmic and Computing Technologies for Health Assessment of Real Structures in the Presence of Large Nonlinearity," 2013 ASCE International Workshop on Computing in Civil Engineering, University of Southern California, June 23-25.

DiPasquale, E. and Cakmak, A.S. (1988), "Identification of the Severity Limit State and Direction of Seismic Structural Damage," Tech. Report NCEER-88-0022. National Center for Earthquake Engineering Research, Buffalo, N.Y.

Doebling, S. W., Farrar, C. E., and Prime, M. B. (1998), "A Summary Review of Vibration-Based Damage Identification Methods," The Shock and Vibration Digest, Vol. 30, No. 2, pp. 91-105.

Doebling, S. W., Farrar, C. R., Prime, M. B., and Shevits, D. W. (1996), "Damage Identification and Health Monitoring of Structural and Mechanical Systems from Changes in their Vibration Characteristics: A Literature Review," Los Alamos National Laboratory, Report LA-13070-MS.

Dutta, A. and Talukdar, S. (2004), "Damage Detection in Bridges Using Accurate Modal Parameters," Finite Elements in Analysis and Design, Vol. 40, No. 3, pp. 287-304.

Evensen, G. (1994), "Sequential Data Assimilation with a Nonlinear Quasi-Geostrophic Model Using Monte Carlo Methods to Forecast Error Statistics," Journal of Geophysical Research, Vol. 99, No. C5, pp. 10143–10162.

Eykhofif, P. (1982), "On the Coherence among the Multitude of System Identification Methods," IFAC System Identification and System Parameter Estimation, International Federation of Automatic Control (IFAC), Washington, D.C., pp. 31-42.

Fan, W. and Qiao, P. (2011), "Vibration-Based Damage Identification Methods: A Review and Comparative Study," Structural Health Monitoring, Vol. 10, No. 1, pp. 83-111.

Farrar, C. R. and Worden, K. (2011), "An Introduction to Structural Health Monitoring," New Trends in Vibration Based Structural Health Monitoring, Springer Vienna, pp. 1-17.

Farrar, C. R., Baker, W. E., Bell, T. M., Cone, K.M., Darling, T. W., Duffey, T. A., Eklund, A., and Migliori, A. (1994), "Dynamic Characterization and Damage Detection in the I-40 Bridge over the Rio Grande," Los Alamos National Laboratory report, LA-12767-MS.

Farrar, C. R., Doebling, S. W., and Nix, D. A. (2001), "Vibration-Based Structural Damage Identification," Philosophical Transactions: Mathematical, Physical and Engineering Sciences, Vol. 359, No. 1778, pp. 131−149.

Fotsch, D. and Ewins, D. J. (2001), "Further Applications of the FMAC," Proceedings of International Modal Analysis Conference, pp. 635-639.

Friswell, M. I., Penny, J. E. T., and Wilson, D. A. L. (1994), "Using Vibration Data and Statistical Measures to Locate Damage in Structures," The International Journal of Analytical and Experimental Modal Analysis, Vol. 9, pp. 239-254.

Ghanem, R. and Ferro, G. (2006), "Health Monitoring for Strongly Non-Linear Systems Using the Ensemble Kalman Filter," Structural Control and Health Monitoring, Vol. 13, No. 1, pp. 245–259.

Haldar, A. and Al-Hussein, A. (2014), "Structural Health Assessment: Challenges," International Conference on Disaster Mitigation, ICDM'14, Chennai, India, pp. K7-1 to K7-10, January 23-24.

Haldar, A. and Al-Hussein, A. (2015), "Prognostics and Structuring Health Assessment Using Uncertain Measured Response Information," International Conference of Advances in Reliability, Maintenance, and Safety, ICRESH-ARMS 2015, Sweden, June 1-4.

Haldar, A. and Das, A. K. (2010), "Prognosis of Structural Health - Nondestructive Methods," International Journal of Performability Engineering, Special Issue on Prognostics and Health Management (PHM), Vol. 6, No. 5, pp. 487-498.

Haldar, A. and Das, A. K. (2012a), "Past, Present, and Future of Structural Health Assessment," Proceedings of International Symposium on Engineering under Uncertainty: Safety Assessment and Management (ISEUSAM), Shibpur, India.

Haldar, A. and Das, A. K. (2012b), "Past, Present, and Future of Structural Health Assessment," International Journal of Life Cycle Reliability and Safety Engineering, Vol. 1, No. 4, pp. 33-43.

Haldar, A., Das, A. K., and Al-Hussein, A. (2013), "Data Analysis Challenges in Structural Health Assessment using Measured Dynamic Responses," Advances in Adaptive Data Analysis, Vol. 5, No. 4, pp. 1350017-1 to 1350017-22.

Haldar, A., Ling, X., and Wang, D. (1998), "Use of SI for Damage Evaluation at the Element Level," Structural Engineering World Congress, San Francisco, California, paper (CD-ROM) reference: T216-1.

Hao, Y., Xiong, Z., Sun, F., and Wang, X. (2007), "Comparison of Unscented Kalman Filters," Proceedings of IEEE International Conference on Mechatronics and Automation 2007, Harbin, China, pp. 895-899.

Hearn, G. and Testa, R. B. (1991), "Modal Analysis for Damage Detection in Structures," Journal of Structural Engineering, ASCE, Vol. 117, No. 10, pp. 3042–3063.

Heylen, W. and Janter, T. (1990), "Extensions of the Modal Assurance Criterion," Journal of Vibrations and Acoustics, Vol. 112, No. 4, pp. 468−472.

Heylen, W. and Lammens, S. (1996), "FRAC: A Consistent Way of Comparing Frequency Response Functions," Proceedings of International Conference on Identification in Engineering Systems, Swansea, UK, pp. 48−57.

Hjelmstad, K. D. and Shin, S. (1997), "Damage Detection and Assessment of Structures from Static Response," Journal of Engineering Mechanics, ASCE, Vol. 123, No. 6, pp. 568-576.

Hoshiya, M. and Maruyama, O. (1987), "Identification of Running Load and Beam System," Journal of Engineering Mechanics, Vol. 113, No. 6, pp. 813-824.

Hoshiya, M. and Saito, E. (1984), "Structural Identification by Extended Kalman Filter," Journal of Engineering Mechanics, ASCE, Vol. 110, No. 12, pp. 1757–1772.

Hu, N., Wang, X., Fukunaga, H., Yao, Z. H., Zhang, H. X., and Wu, Z. S. (2001), "Damage Assessment of Structures Using Modal Test Data," International Journal of Solids and Structures, Vol. 38, No. 18, pp. 3111-3126.

Hua, X. G. (2006), "Structural Health Monitoring and Condition Assessment of Bridge Structures," PhD Dissertation, Department of Civil Engineering and Structural Engineering, the Hong Kong Polytechnic University, Hong Kong.

Huth, O., Feltrin, G., Maeck, J., Kilic, N., and Motavalli, M. (2005), "Damage Identification Using Modal Data: Experiences on a Prestressed Concrete Bridge," Journal of Structural Engineering, ASCE, Vol. 131, No. 12, pp. 1898-1910.

Imai, H., Yun, C. B., Maruyama, O., and Shinozuka, M. (1989), "Fundamentals of System Identification in Structural Dynamics," Probabilistic Engineering Mechanics, Vol. 4, No.4, pp. 162-173

Jazwinski, A. H. (1970), "Stochastic Process and Filtering Theory," Academic Press, Inc. New York.

Julier, S. J. (2002), "The Scaled Unscented Transformation," Proceedings of the American Control Conference, Vol. 6, pp. 4555-4559.

Julier, S. J. (2003), "The Spherical Simplex Unscented Transformation," Proceedings of American Control Conference, Vol. 3, pp. 2430-2434.

Julier, S. J. and Uhlmann, J. K. (1997), "New Extension of the Kalman Filter to Nonlinear Systems," Proceedings of SPIE 3068, Signal Processing, Sensor Fusion, and Target Recognition VI, 182, pp. 182–193.

Julier, S. J. and Uhlmann, J. K. (2002), "Reduced Sigma Point Filters for the Propagation of Means and Covariances through Nonlinear Transformations," Proceedings of American Control Conference, Vol. 2, pp. 887-892.

Julier, S. J. and Uhlmann, J. K. (2004), "Unscented Filtering and Nonlinear Estimation," Proceedings of the IEEE, Vol. 92, No. 3, pp. 401-422.

Julier, S. J., Uhlmann, J. K., and Durrant-Whyte, H. F. (1995), "A New Approach for Filtering Nonlinear Systems," Proceedings of the American Control Conference, Seattle, Washington, Vol. 3, pp. 1628-1632.

Julier, S., Uhlmann, J., and Durrant-Whyte, H. F. (2000), "A New Method for the Nonlinear Transformation of Means and Covariances in Filters and Estimators," IEEE Transactions on Automatic Control, Vol. 45, No. 3, pp. 477-482.

Kalman, R. E. (1960), "A New Approach to Linear Filtering and Prediction Problems," Transactions of the ASME-Journal of Basic Engineering, Vol. 82, pp. 35-45.

Kalman, R. E. and Bucy, R. S. (1961), "New Results in Linear Filtering and Prediction Theory," Journal of Fluids Engineering, Vol. 83, No. 1, pp. 95-108.

Katkhuda, H. (2004), "In-service Health Assessment of Real Structures at the Element Level with Unknown Input and Limited Global Responses," PhD Dissertation, Department of Civil Engineering and Engineering Mechanics, University of Arizona, Tucson, Arizona.

Katkhuda, H. and Haldar, A. (2006), "Defect Identification under Uncertain Blast Loading," Journal of Optimization and Engineering, Vol. 7, No. 3, pp. 277–296.

Katkhuda, H. and Haldar, A. (2008), "A Novel Health Assessment Technique with Minimum Information," Structural Control and Health Monitoring, Vol. 15, No. 6, pp. 821-838.

Katkhuda, H., Martinez-Flores, R., and Haldar, A. (2005), "Health Assessment at Local Level with Unknown Input Excitation," Journal of Structural Engineering, ASCE, Vol. 131, No. 6, pp. 956-965.

Kerschen, G., Worden, K., Vakakis, A. F., and Golinval, J. C. (2006), "Past, Present and Future of Nonlinear System Identification in Structural Dynamics," Mechanical Systems and Signal Processing, Vol. 20, No. 3, pp. 505-592.

Khalil, M., Sarkar, A., and Adhikari, S. (2007), "Data Assimilation in Structural Dynamics: Extended-, Ensemble Kalman and Particle Filters," Proceedings of the 1st International Conference on Uncertainty in Structural Dynamics, University of Sheffield, Sheffield, UK.

Kim, J. T. and Stubbs, N. (1995), "Model Uncertainty Impact and Damage-Detection Accuracy in Plate Girder," Journal of Structural Engineering, ASCE, Vol. 121, No. 10, pp. 1409-1417.

Ko, J. M., Wong, C. W., and Lam, H. F. (1994), "Damage Detection in Steel Framed Structures by Vibration Measurement Approach," Proceedings of the 12th International Modal Analysis Conference, pp. 280-286.

Koh, C. G., Chen, Y. F., and Liaw, C.-Y. (2003), "A Hybrid Computational Strategy for Identification of Structural Parameters," Journal of Computers and Structures, Vol. 81, No. 2, pp. 107-117.

Koh, C. G., Hong, B., and Liaw, C.-Y. (2000), "Parameter Identification of Large Structural Systems in Time Domain," Journal of Structural Engineering, ASCE, Vol. 126, No. 8, pp. 957-963.

Koh, C. G., Liaw, C.-Y., and Hong, B. (1999), "Structural Monitoring by System Identification in Time Domain," Proceedings of SPIE 3671, Smart Systems for Bridges, Structures, and Highways, Newport Beach, California.

Koh, C. G., See, L. M., and Balendra, T. (1991), "Estimation of Structural Parameters in Time Domain: A Substructural Approach," Earthquake Engineering and Structural Dynamics, Vol. 20, No. 8, pp. 787-801.

Law, S.S. and Yong, D. (2011), "Substructure Methods for Structural Condition Assessment," Journal of Sound and Vibration, Vol. 330, No. 15, pp. 3606–3619.

Lee, D.-J. and Alfriend, K. T. (2004), "Adaptive Sigma Point Filtering for State and Parameter Estimation," Collection of Technical Papers-AIAA/AAS Astrodynamics Specialist Conference, Vol. 2. Providence, RI, pp. 897–916.

Li, H., Yang, H., and Hu, S.-L. J. (2006), "Modal Strain Energy Decomposition Method for Damage Localization in 3D Frame Structures," Journal of Engineering Mechanics, ASCE, Vol. 132, No. 9, pp. 941-951.

Li, P., Zhang, T., and Ma, B. (2004), "Unscented Kalman Filter for Visual Curve Tracking," Image and Vision Computing, Vol. 22, No. 2, pp. 157–164.

Lieven, N. A. J. and Ewins, D. J. (1988), "Spatial Correlation of Mode Spaces: The Coordinate Modal Assurance Criterion (COMAC)," Proceedings of the 6th International Modal Analysis Conference, pp. 690‑695.

Lifshitz, J. M. and Rotem, A. (1969), "Determination of Reinforcement Unbonding of Composites by a Vibration Technique," Journal of Composite Materials, Vol. 3, pp. 412-423.

Lin, J.-S. and Zhang, Y. (1994), "Nonlinear Structural Identification using Extended Kalman Filter," Journal of Computers and Structures, Vol. 52, No. 4, pp. 757-764.

Ling, X. (2000), "Linear and Nonlinear Time Domain System Identification at Element Level for Structural Systems with Unknown Excitations," PhD Dissertation, Department of Civil Engineering and Engineering Mechanics, University of Arizona, Tucson, Arizona.

Ling, X. and Haldar, A. (2004), "Element Level System Identification with Unknown Input with Rayleigh Damping," Journal of Engineering Mechanics, ASCE, Vol. 130, No. 8, pp. 877-885.

Liu, P.-L. (1995), "Identification and Damage Detection of Trusses Using Modal Data," Journal of Structural Engineering, ASCE, Vol. 121, No. 4, pp. 599–608.

Liu, P.-L. and Chian, C.-C. (1997), "Parametric Identification of Truss Structures Using Static Strains," Journal of Structural Engineering, ASCE, Vol. 123, No. 7, pp. 927-933.

Logan, D. L. (2007), "A First Course in the Finite Element Method," Fourth Edition, Thomson.

Loh, C.-H. and Tsaur, Y.-H. (1988), "Time Domain Estimation of Structural Parameters," Engineering Structures, Vol. 10, No. 2, pp. 95–105.

Lourens, E., Papadimitriou, C., Gillijns, S., Reynders, E., De Roeck, G., and Lombaert, G. (2012), "Joint Input-Response Estimation for Structural Systems Based on Reduced-Order Models and Vibration Data from a Limited Number of Sensors," Mechanical Systems and Signal Processing, Vol. 29, pp. 310-327.

Ma, C.-K. and Ho C.-C. (2004), "An Inverse Method for the Estimation of Input Forces Acting on Non-Linear Structural Systems", Journal of Sound and Vibration, Vol. 275, No. 3-5, pp. 953-971.

Maeck, J. and De Roeck, G. (2002), "Damage Assessment of a Gradually Damaged RC Beam Using Dynamic System Identification," Proceedings of the 20th International Modal Analysis Conference, Society for Experimental Mechanics, Los Angeles, CA, pp. 1560-1566.

Mariani, S. and Ghisi, A. (2007), "Unscented Kalman Filtering for Nonlinear Structural Dynamics," Journal of Nonlinear Dynamics, Vol. 49, No. 1-2, pp. 131-150.

Martinez-Flores, R. (2005), "Damage Assessment Potential of a Novel System Identification Technique - Experimental Verification," PhD Dissertation, Department of Civil Engineering and Engineering Mechanics, University of Arizona, Tucson, Arizona.

Martinez-Flores, R. and Haldar, A. (2007), "Experimental Verification of a Structural Health Assessment Method without Excitation Information," Journal of Structural Engineering, Vol. 34, No. 1, pp. 33-39.

Martinez-Flores, R., Katkhuda, H., and Haldar, A. (2008), "A Novel Health Assessment Technique with Minimum Information: Verification," International Journal of Performability Engineering, Vol. 4, No. 2, pp. 121-140.

Maybeck, P. S. (1979), "Stochastic Models, Estimation, and Control Theory," Academic Press, Inc., UK.

Mehrabi, A. B., Tabatabai, H., and Lotfi, H. R. (1998), "Damage Detection in Structures Using Precursor Transformation Method," Journal of Intelligent Material Systems and Structures, Vol. 9, No. 10, pp. 808-817.

Modena, C., Sonda, D., and Zonta, D. (1999), "Damage Localization in Reinforced Concrete Structures by Using Damping Measurements," Proceedings of the International Conference on Damage Assessment of Structures (DAMAS 99), Dublin, Ireland, pp. 132–141.

Montalvão, D., Maia, N. M. M., and Ribeiro, A. M. R. (2006), "A Review of Vibration-Based Structural Health Monitoring with Special Emphasis on Composite Materials," The Shock and Vibration Digest, Vo. 38, No. 4, pp. 295–324.

Narkis, Y. (1994), "Identification of Crack Location in Vibrating Simply Supported Beams," Journal of Sound and Vibration, Vol. 172, No. 4, pp. 549–558.

Nasrellah, H. A. (2009), "Dynamic State Estimation Techniques for Identification of Parameters of Finite Element Structural Models," PhD Dissertation, IISc, Bangalore, India.

Nasrellah, H. A. and Manohar, C. S. (2011), "Particle Filters for Structural System Identification Using Multiple Test and Sensor Data: A Combined Computational and Experimental Study," Structural Control and Health Monitoring, Vol. 18, No. 1, pp. 99-120.

Oh, B. H. and Jung, B. S. (1998), "Structural Damage Assessment with Combined Data of Static and Modal Tests," Journal of Structural Engineering, ASCE, Vol. 124, No.8, pp. 956-965.

Oreta, A. W. C. and Tanabe, T. (1993), "Localized Identification of Structures by Kalman Filter," Journal of Structural Engineering/Earthquake Engineering, Vol. 9, No. 4, pp. 217-225.

Oreta, A. W. C. and Tanabe, T. (1994), "Element Identification of Member Properties of Framed Structures," Journal of Structural Engineering, ASCE, Vol. 120, No. 7, pp. 1961-1976.

Pandey, A. K. and Biswas, M. (1994), "Damage Detection in Structures Using Changes in Flexibility," Journal of Sound and Vibration, Vol. 169, No. 1, pp. 3–17.

Pandey, A. K. and Biswas, M. (1995), "Damage Diagnosis of Truss Structures by Estimation of Flexibility Change," Modal Analysis - The International Journal of Analytical and Experimental Modal Analysis, Vol. 10, No. 2, pp. 104-117.

Pandey, A. K., Biswas, M., and Samman, M. M. (1991), "Damage Detection from Changes in Curvature Mode Shapes," Journal of Sound and Vibration, Vol. 145, No. 2, pp. 321-332.

Pandit, S. K. and Wu, S.-M. (1993), "Time Series and System Analysis with Applications," Krieger Publishing Company.

Panteliou, S., Chondros, T., Chondros, V., Argyrakis, V., and Dimarogonas, A. (2001), "Damping Factor as an Indicator of Crack Severity," Journal of Sound and Vibration, Vol. 241, No. 2, pp. 235–245.

Penny, J. E. T., Wilson, D. A. L., and Friswell, M. I. (1993), "Damage Location in Structures Using Vibration Data", Proceedings of the 11th International Modal Analysis Conference, Society for Experimental Mechanics, Bethel, pp. 861-867.

Perry, M. J., Koh, C. G., and Choo, Y. S. (2006), "Modified Genetic Algorithm Strategy for Structural Identification," Journal of Computers and Structures, Vol. 84, No. 8-9, pp. 529-540.

Popescu, C. and Wong, Y. S. (2003), "The Unscented and Extended Kalman Filter for Systems with Polynomial Restoring Forces," Collection of Technical Papers-44th AIAA/ASME/ASCE/AHS/ASC Structures, Structural Dynamics and Materials Conference, Vol. 1. Norfolk, VA, pp. 100–110.

Raghavendrachar, M. and Aktan, A. E. (1992), "Flexibility of Multi Reference Impact Testing for Bridge Diagnostics," Journal of Structural Engineering, ASCE, Vol. 118, No. 8, pp. 2186-2203.

Richardson, M. H. and Mannan, M. A. (1992), "Remote Detection and Location of Structural Faults Using Modal Parameters," Proceedings of the 10th International Modal Analysis Conference, Vol. 1, Stockholm, Sweden, pp. 502–507.

Romanenko, A. and Castro, J. A. A. M. (2004), "The Unscented Filter as an Alternative to the EKF for Nonlinear State Estimation: A Simulation Case Study," Journal of Computers and Chemical Engineering, Vol. 28, No. 3, pp. 347–355.

Romanenko, A., Santos, L. O., and Afonso, P. A. F. N. A. (2004), "Unscented Kalman Filtering of a Simulated pH System," Industrial and Engineering Chemistry Research, Vol. 43, No. 23, pp. 7531–7538.

Rytter, A. (1993), "Vibration Based Inspection of Civil Engineering Structures," PhD Dissertation, Department of Building Technology and Structural Engineering, University of Aalborg, Denmark.

Salawu, O. S. (1997), "Detection of Structural Damage through Changes in Frequency: A Review," Engineering Structures, Vol. 19, No. 9, pp. 718-723.

Salawu, O. S. and Williams C. (1994), "Damage Location Using Vibration Mode Shapes," Proceedings of 12 International Modal Analysis Conference, pp. 933-939.

Salawu, O. S. and Williams, C. (1995), "Bridge Assessment Using Forced-Vibration Testing", Journal of Structural Engineering, ASCE, Vol. 121, No. 2, pp. 161-173.

Salehi, M., Rad, S. Z., Ghayour, M., and Vaziry, M. A. (2011), "A Non Model-Based Damage Detection Technique Using Dynamically Measured Flexibility Matrix," Iranian IJSTM, Transactions of Mechanical Engineering, Vol. 35, No. 1, pp. 137-149.

Sanayei, M. and Onipede, O. (1991), "Damage Assessment of Structures Using Static Test Data," AIAA Journal, Vol. 29, No. 7, pp. 1174-1179.

Sanayei, M. and Saletnik, M. J. (1996a), "Parameter Estimation of Structures from Static Strain Measurements I: Formulation," Journal of Structural Engineering, ASCE, Vol. 122, No. 5, pp. 555-562.

Sanayei, M. and Saletnik, M. J. (1996b), "Parameter Estimation of Structures from Static Strain Measurements II: Error Sensitivity Analysis," Journal of Structural Engineering, ASCE, Vol. 122, No. 5, pp. 563-572.

Sanders, D. R., Kim, Y. I., and Stubbs, R. N. (1992), "Nondestructive Evaluation of Damage in Composite Structures Using Modal Parameters," Experimental Mechanics, Vol. 32, No. 3, pp. 240–251.

Sato, T. and Qi, K. (1998), "Adaptive H_∞ Filter: Its Application to Structural Identification," Journal of Engineering Mechanics, ASCE, Vol. 124, No. 11, pp.1233-1240.

Sato, T. and Qi, K. (1999), "Nonlinear Structural Identification Based on H_∞ Filter Algorithm," Proceedings of SPIE 3667, Smart Structures and Materials: Mathematics and Control in Smart Structures, pp. 394-405.

Shao, C. X., Liu, H., and Huang, W. H. (1985), "Identification of Vibrating System Parameters by Maximum Likelihood Method," In ASME Design Engineering Technical Conference, Cincinnati, OH, England. Sponsored by ASME, NewYork, NY, USA. Paper 85-DET- 112.

Shinozuka, M., Yun, C.-B., and Imai, H. (1982), "Identification of Linear Structural Dynamics Systems," Journal of the Engineering Mechanics, ASCE, Vol. 108, No. 6, 1371−1390.

Sitz, A., Schwarz, U., Kurths, J., and Voss, H. U. (2002), "Estimation of Parameters and Unobserved Components for Nonlinear Systems from Noisy Time Series," Physical Review E, Vol. 66, No. 1, pp. 1–9.

Skjaerbaek, P. S., Nielsen, S. R. K., and Cakmak, A. S. (1996), "Assessment of Damage in Seismically Excited RC-Structures from a Single Measured Response," Proceedings of the 14th International Modal Analysis Conference, pp. 133–139.

Smyth, A. W., Masri, S. F., Chassiakos, A. G., and Caughey, T. K. (1999), "On-Line Parametric Identification of MDOF Nonlinear Hysteretic Systems," Journal of Engineering Mechanics, ASCE, Vol. 125, No. 2, pp.133–142.

Sohn, H., Farrar, C. R., Hemez, F. M., Shunk, D. D., Stinemates, D. W., Nadler, B. R., and Czarnecki, J. J. (2004), "A Review of Structural Health Monitoring Literature: 1996-2001," Los Alamos National Laboratory, LA-13976-MS.

Srinivasan, M. G. and Kot, C. A. (1992), "Effects of Damage on the Modal Parameters of a Cylindrical Shell," Proceedings of the 10th International Modal Analysis Conference, San Diego, CA, pp. 529-535.

Stubbs, N. and Osegueda, R. (1990a), "Global Non-Destructive Damage Evaluation in Solids," Modal Analysis: The International Journal of Analytical and Experimental Modal Analysis, Vol. 5, No. 2, pp. 67-79,

Stubbs, N. and Osegueda, R. (1990b), "Global Damage Detection in Solids-Experimental Verification," Modal Analysis: The International Journal of Analytical and Experimental Modal Analysis, Vol. 5, No. 2, pp. 81–97.

Stubbs, N., Broome, T. H., and Osegueda, R. (1990), "Nondestructive Construction Error Detection in Large Space Structures," AIAA Journal, Vol. 28, No. 1, pp. 146–152.

Stubbs, N., Kim, J. T., and Topple, K. (1992), "An Effect and Robust Algorithm for Damage Localization in Offshore Platforms," Proceedings of ASCE 10th Structural Congress, San Antonio, Texas, pp. 543-546.

Tenne, D. and Singh, T. (2003), "The Higher Order Unscented Filter," Proceedings of the American Control Conference, Vol. 3, Denver, CO., pp. 2441-2446.

Teughels, A. and De Roeck, G. (2005), "Damage Detection and Parameter Identification by Finite Element Model Updating," Archives of Computational Methods in Engineering., Vol. 12, No. 2, pp. 123-164

Toki, K., Sato, T., and Kiyono, J. (1989), "Identification of Structural Parameters and Input Ground Motion from Response Time Histories," Journal of Structural Engineering/Earthquake Engineering, Vol. 6, No. 2, pp. 413-421.

Torkamani, M. A. M. and Ahmadi, A. K. (1988a), "Stiffness Identification of Two and Three Dimensional Frames," International Journal of Earthquake Engineering and Structural Dynamics, Vol. 16, pp. 1157-1176.

Torkamani, M. A. M. and Ahmadi, A. K. (1988b), "Stiffness Identification of Tall Buildings during Construction Period Using Ambient Tests," International Journal of Earthquake Engineering and Structural Dynamics, Vol. 16, pp. 1177-1188.

Torkamani, M. A. M. and Ahmadi, A. K. (1988c), "Stiffness Identification of Frames using Simulated Ground Motion," Journal of Engineering Mechanics, ASCE, Vol. 114, No. 5, pp. 753-776.

Udwadia, F. E. and Proskurowski, W. (1998), "A Memory-Matrix-Based Identification Methodology for Structural and Mechanical Systems," Earthquake Engineering and Structural Dynamics, Vol. 27, No. 12, pp. 1465-1481.

van der Merwe, R. and Wan, E. A. (2001a), "The Square-Root Unscented Kalman Filter for State and Parameter-Estimation," Processing of the IEEE International Conference on Acoustics, Speech and Signal Processing (ICASSP'01), Vol. 6, Salt Lake City, UT, pp. 3461-3464.

van der Merwe, R. and Wan, E. A. (2001b), "Efficient Derivative-Free Kalman Filters for Online Learning," Proceedings of the European Symposium on Artificial Neural Networks (ESANN), Bruges, Belgium, pp. 205-210.

van der Merwe, R., Wan, E. A., and Julier, S. (2004), "Sigma-Point Kalman Filters for Nonlinear Estimation and Sensor-Fusion: Applications to Integrated Navigation," Proceedings of the AIAA Guidance, Navigation and Control Conference, RI.

van Zandt, J. R. (2001), "A More Robust Unscented Transform," Proceedings of SPIE 4473, Signal and Data Processing of Small Targets, San Diego, pp. 371–380.

Vo, P. (2003), "Experimental Study of the Time Domain Damage Identification," PhD Dissertation, Department of Civil Engineering and Engineering Mechanics, University of Arizona, Tucson, Arizona.

Vo, P. H. and Haldar, A. (2003), "Post-Processing of Linear Accelerometer Data in Structural Identification," Journal of Structural Engineering, Vol. 30, No. 2, pp. 123-130.

Vo, P. H. and Haldar, A. (2004), "Health Assessment of Beams - Experimental Investigations," Journal of Structural Engineering, Special issue on Advances in Health Monitoring/Assessment of Structures including Heritage and Monument Structures, Vol. 31, No. 1, pp. 23-30.

Vo, P. H. and Haldar, A. (2008), "Health Assessment of Beams – Experimental Verification," Structure and Infrastructure Engineering, Vol. 4, No. 1, pp. 45-56.

Voss, H. U., Timmer, J., and Kurths J. (2004), "Nonlinear Dynamical System Identification from Uncertain and Indirect Measurements," International Journal of Bifurcation and Chaos, Vol. 14, No. 6, pp. 1905–1933.

Wan, E.A. and van der Merwe, R. (2000), "The Unscented Kalman Filter for Nonlinear Estimation," Proceedings of Adaptive Systems for Signal Processing, Communications, Control Symposium, Lake Louise, Alberta, Canada.

Wang, D. (1995), "Element Level Time Domain System Identification Techniques with Unknown Input Information," PhD Dissertation, Department of Civil Engineering and Engineering Mechanics, University of Arizona, Tucson, Arizona.

Wang, D. and Haldar, A. (1994), "Element-Level System Identification with Unknown Input Information," Journal of Engineering Mechanics, ASCE, Vol. 120, No. 1, pp. 159-176.

Wang, D. and Haldar, A. (1997), "System Identification with Limited Observations and without Input," Journal of Engineering Mechanics, ASCE, Vol. 123, No. 5, pp. 504-511.

Wang, L., Chan, T. H. T., Thambiratnam, D. P., and Tan, A. C. C. (2010), "Improved Correlation-Based Modal Strain Energy Method for Global Damage Detection of Truss Bridge Structures," Proceedings of the International Symposium on Life-Cycle Performance of Bridge and Structures, Science Press, Changsha, China, pp. 145-154.

Wang, W. and Zhang, A. (1987), "Sensitivity Analysis in Fault Vibration Diagnosis of Structures," Proceedings of 5th International Modal Analysis Conference, London, England, pp. 496–501.

Wei, J. C., Wang, W., and Allemang, R. J. (1990), "Model Correlation and Orthogonality Criteria Based on Reciprocal Modal Vectors," Proceedings of SAE Noise and Vibration Conference, pp. 607−616.

West, W. M. (1984), "Illustration of the Use of Modal Assurance Criterion to Detect Structural Changes in an Orbiter Test Specimen," Proceeding of Air Force Conference on Aircraft Structural Integrity, pp. 1–6.

Wu, M. and Smyth, A.W. (2007), "Application of the Unscented Kalman Filter for Real-Time Nonlinear Structural System Identification," Structural Control and Health Monitoring, Vol. 14, No. 7, pp. 971-990.

Xu, B., He, J., Rovekamp, R., and Dyke, S. J. (2012), "Structural Parameters and Dynamic Loading Identification from Incomplete Measurements: Approach and Validation," Mechanical Systems and Signal Processing, Vol. 28, pp. 244-257.

Yamaguchi, H., Matsumoto, Y., Kawarai, K., Dammika, A. J., Shahzad, S., and Takanami, R. (2013), "Damage Detection Based on Modal Damping Change in Bridges,"

Yang, J. N. and Lin, S. (2005), "Identification of Parametric Variations of Structures Based on Least Squares Estimation and Adaptive Tracking Technique," Journal of Engineering Mechanics, ASCE, Vol. 131, No. 3, pp. 290-298.

Yang, J. N., Lin, S., Huang, H., and Zhou, L. (2006), "An Adaptive Extended Kalman Filter for Structural Damage Identification," Structural Control and Health Monitoring, Vol. 13, No. 4, pp. 849–867.

Yang, J. N., Pan, S., and Huang, H. (2007), "An Adaptive Extended Kalman Filter for Structural Damage Identification II: Unknown Inputs," Structural Control and Health Monitoring, Vol. 14, No. 3, pp. 497-521.

Yang, J. N., Pan, S., and Lin, S. (2007), "Least Square Estimation with Unknown Excitations for Damage Identification of Structures," ASCE Journal of Engineering Mechanics, ASCE, Vol. 133, No. 1, pp. 12-21.

Yeo, I., Shin, S., Lee, H. S., and Chang, S.-P. (2000), "Statistical Damage Assessment of Framed Structures from Static Responses," Journal of Engineering Mechanics, ASCE, Vol. 126, No. 4, pp. 414-421.

Yoshida, I. and Sato, T. (2002), "Health Monitoring Algorithm by The Monte Carlo Filter Based on Non-Gaussian Noise," Journal of Natural Disaster Science, Vol. 24, No. 2, pp. 101–107.

Yun, C.-B. and Shinozuka, M. (1980),"Identification of Nonlinear Structural Dynamic Systems," Journal of Structural Mechanics, Vol. 8, No. 2, pp. 187-203.

Zhang, D. (2010), "Controlled Substructure Identification for Shear Structures," PhD Dissertation, Department of Civil Engineering, University of Southern California, California.

Zhao, J. and Dewolf, J. T. (1999), "Sensitivity Study for Vibrational Parameters Used in Damage Detection," Journal of Structural Engineering, ASCE, Vol. 125, No. 4, pp. 410-416.